Radiobiological Modeling and Experimental Quantification of Radiobiological Parameters used in Cervical Cancer Brachytherapy Dose Calculation

by

Braden Chow

A thesis submitted in partial fulfillment of the requirements for the degree of

Doctor of Philosophy

in

Medical Physics

Department of Oncology
University of Alberta

ABSTRACT

Cervical cancer is the fourth most common cancer worldwide, with an estimated 604,000 cases identified in 2020. The standard care for locally advanced cervical cancers is concurrent chemotherapy and external beam radiotherapy (EBRT) with a brachytherapy (BT) boost. Current guidelines recommend that the combined EBRT and BT doses be prescribed in units of radiobiological dose, which is calculated using radiobiological parameters α/β and $T_{1/2}$. Though dose calculations are performed with conventional values of α/β (10 Gy for tumor and 3 Gy for organs at risk) and $T_{1/2}$ (1.5 hours for both), a wide range of values have been reported in literature and their potential implications on current dose prescriptions have not been thoroughly investigated.

This work presents the potential uncertainty that arises from the current body of reported parameter values and highlights pitfalls in estimating the clinical equivalency between two types of BT boosts: high-dose-rate (HDR) and pulsed-dose-rate (PDR). Variance in the α/β ratio and $T_{1/2}$, within the ranges of values reported in the literature, can introduce over 10% variance in the calculated radiobiological tumor dose for PDR treatments, while changes in the α/β ratio can result in over 13% variance for HDR treatments. These significant variances highlight the need for further efforts to establish definitive radiobiological parameter values.

Compared to the different radiation sources and treatment schedules used in previous experiments reported in literature, the *in vitro* experiments with cervical cancer cell lines performed in this study utilized clinical BT sources and clinically relevant treatment schedules. To do so, a first-in-kind **b**rachytherapy **a**fterloader ***in vitro*** **r**adiation **d**elivery **a**pparatus

(BAIRDA) was developed to deliver radiation to tissue culture plates. Parameter values (both α/β and $T_{1/2}$) for seven cervical cancer cell lines (four squamous cell carcinoma and three adenocarcinoma) were determined using BAIRDA through single acute and fractionated hourly radiation schedules. Confirmatory experiments with a traditional irradiator yielded similar results for all cell lines, providing support for the novel BAIRDA methodology.

Uncertainties influencing *in vitro* experiments using both irradiator and BAIRDA configurations, including those associated with measurements of cell survival and dose, were evaluated to refine the radiobiological parameters. Of the two, the dominant uncertainty was from cell survival measurements. The experimentally determined α/β and $T_{1/2}$ values varied by a maximum of 0.5 Gy and 0.4 hours, respectively, when considering either all experimental uncertainties or limiting the analysis to including only the variance in the surviving fraction for an experiment triplicate, which has been the common approach. BAIRDA experiments had a larger overall uncertainty than those using established irradiator methodology, but it could be reduced to a comparable level with further refinements of the experimental setup. Regardless, a complete uncertainty analysis did not affect the study's findings, and the radiobiological parameters estimated with BAIRDA and traditional irradiators remained similar. Therefore, the uncertainty investigation provides greater confidence in the BAIRDA methodology and findings utilizing it.

The radiobiological parameters reported in this study indicate that α/β for both squamous cell carcinoma and adenocarcinoma may be lower than the current conventional assumption (10 Gy) for tumor, while $T_{1/2}$ may be higher than the conventional assumption (1.5 hours) for squamous cell carcinoma and lower for adenocarcinoma. These results suggest the potential for

personalizing BT boosts based on cancer type; a PDR BT boost might deliver a greater radiobiological dose than the conventionally equivalent HDR BT boost for squamous cells and vice versa for adenocarcinoma. Further research building upon the findings of this thesis is needed to translate the results to the improvements of cervical cancer BT. To determine if they hold clinically, further investigation of cervical cancer radiobiological parameter values is needed in more clinically relevant formats (e.g. *in vivo* or through patient outcomes studies).

PREFACE

The entirety of this thesis represents original research that was motivated by the objectives of my Ph.D. project and was supervised by Drs. G. Menon and B. Warkentin. The work presented is a multidisciplinary collaborative effort, with a summary of the contributions provided below.

Chapter 3 was published as: Chow B, Warkentin B, Menon G. "Radiobiological dose calculation parameters for cervix cancer brachytherapy: A systematic review", *Brachytherapy* 2019;18(4):546-558. I was responsible for the literature review and parameter analysis. G. Menon and B. Warkentin provided recommendations in parameter analysis, general guidance, and assisted with manuscript composition.

Chapter 4 was published as: *Physics in Medicine and Biology* as: Chow B, Warkentin B, Nanda K, Ghosh S, Huang F, Gamper AM, Menon G. "BAIRDA: a novel in vitro setup to quantify radiobiological parameters for cervical cancer brachytherapy dose estimations", *Physics in Medicine and Biology* 2022;67(4):045012. I conducted the *in vitro* experiments in the Gamper Lab (University of Alberta, Edmonton, AB) and was responsible for tissue culturing, experimental measurements, and analysis of the experimental results. Dr. A.M. Gamper provided expertise with experiment methodology and interpretation of experimental results. Ms. K. Nanda provided training with tissue cultures. Dr. S. Ghosh advised on the statistical analysis. F. Huang assisted with manuscript composition. A.M. Gamper and G. Menon oversaw project conceptualization, general guidance, and assisted with manuscript composition. B. Warkentin provided data interpretation, general guidance, and assisted with manuscript composition. Design of the novel apparatus (BAIRDA) received input from an interdisciplinary team, including myself, A.M. Gamper, G. Menon, and B. Warkentin.

Chapter 5 is being published as Chow B, Warkentin B, McEwen M, Huang F, Nanda K, Gamper AM, Menon G. "Uncertainties associated with clonogenic assays using a Cs-137 irradiator and Ir-192 afterloader: A comprehensive compilation for radiation researchers", *Radiation Research* In press 2022. I was responsible for all measurements and data analysis. Dr. M. McEwen calibrated the ion chamber used for Cs-137 irradiator measurements at the National Research Council of Canada. Dr. F. Huang provided editorial comments. K. Nanda analyzed clonogenic

assays to allow for comparisons of inter-operator subjectivity. Drs. A.M. Gamper, B. Warkentin, and G. Menon provided general guidance and assisted with manuscript composition.

ACKNOWLEDGEMENTS

I would like to thank my supervisors, Dr. Geetha Menon and Dr. Brad Warkentin, for their encouragement and patience. Their support, expertise, and passion for research provided me the opportunity for learning throughout the program. The research would not have been possible without their support.

The research project has included contributions from an interdisciplinary team and I am grateful for the assistance from everyone. Thanks to Dr. Armin Gamper for his supervision and advice throughout the project. His expertise in radiation biology, support throughout research, and input on experiment design have been invaluable. I would also like to thank Drs. Sunita Ghosh, Fleur Huang, and Malcolm McEwen for their advice and input throughout the project.

This research has been funded by the Alberta Women's Health Foundation through the Women and Children's Health Research Institute. It is through their generosity that this research is possible. In addition, I am grateful for the sponsorship and awards from the Association of Medical Physicists in Alberta, the Graduate Students' Association, Brian and Gail Heidecker, TD Bank Financial Group, the University of Alberta, and the Women and Children's Health Research Institute. Their backing has allowed me to focus on my research and share my findings at the international level.

I am thankful to my supervisory committee, including Dr. Gino Fallone and Dr. Ron Sloboda, for their advice and insight. I also want to thank Dr. Lesley Baldwin and Dr. Don Robinson for participating in my candidacy exam. Finally, thanks to Dr. Don Robinson and Dr. Deidre Batchelar for participating in my thesis defence and providing valuable feedback on my thesis.

Thanks to Curtis Osinchuk and Lance Spiridon, who helped with the design and manufacture of components for my project. Whether it was cutting simple blocks or designing novel structures, there was nothing that could not be made.

Throughout my project, I have been fortunate to spend time with many fellow students and lab members. I want to thank Clara Fallone, Gawon Han, Aaron Purchase, Hongwei Sun, and Amanda Swan for many fond memories. I also want to thank current and former members of Gamper Lab, including Amirali Bukhari, Dr. Wen-Hsin Hsu, Sean Malia, Dr. Daise Matthew, Kareena Nanda, Keenan Ramji, and Min-Hsuan Wu, for their support and lively conversation (even if it was not necessarily on research!). I would also like to thank the medical physicists at the Cross Cancer Institute for their instruction, support, and contributions to an excellent student environment.

As a graduate student, I had the opportunity to participate in many extracurricular activities. I want to thank Dr. Amr Heikal, Dr. Michael Reynolds, Mr. David Sinn, and Mrs. Heather Warkentin for guidance throughout my time as a Quality Assurance Technician. I would also like to thank the fellow founding members of the Oncology Graduate Students' Association, in particular Andrew Locke, Shayla Mosley, and Kirby Zeigler, for their efforts in establishing a space for all oncology students to socialize and for the creation of a welcoming environment for current and future students.

Finally, I want to thank my family for their constant support and kind words. Thanks to my parents, Kin and Jo-Anne Chow, and brother, Kelton, for their steadfast love and patience. Thanks as well to my extended family, in particular my grandparents, Joseph Quan, Grace Quan, Yee Mon Chow, and Mei Wah Chow, for venturing across the Pacific Ocean to Canada.

TABLE OF CONTENTS

LIST OF FIGURES

LIST OF TABLES

LIST OF ABBREVIATIONS

AAPM TG	American Association of Physicists in Medicine Task Group
AC	Adenocarcinoma
ACE	Advanced collapsed cone engine
ASC	Adenosquamous carcinoma
ATCC	American Type Culture Collection
BAIRDA	**B**rachytherapy **a**fterloader ***in vitro*** **r**adiation **d**elivery **a**pparatus
BED	Biologically effective dose
BrdUrd	Bromodeoxyuridine
BT	Brachytherapy
Co-60	Cobalt-60
Cs-137	Cesium-137
CC	Collapsed cone
COMS	Collaborative ocular melanoma study
CRE	Cumulative radiation effect
CT	Computed tomography
CTV	Clinical target volume
D_{2cc}	Dose delivered to 2 cm^3 of the organ at risk
D90	Dose delivered to 90% of the tumor
DRF	Dose reduction factor
EBRT	External beam radiotherapy
EMBRACE	Image guided intensity modulated **E**xternal beam radiochemotherapy and **M**RI based adaptive **bra**chytherapy in locally advanced **ce**rvical cancer
EQD2	Equieffective Dose in 2 Gy Fractions
ESGO	European Society of Gynaecological Oncology
ESP	European Society of Pathology
ESTRO	European SocieTy for Radiotherapy and Oncology
FDG	Fluorodeoxyglucose
FIGO	Federation Internationale de Gynecologie et d'Obstetrique
GBBS	Grid-based Boltzmann solver
GEC	The Groupe Européen de Curiethérapie
GTV	Gross tumor volume
HDI	Human development index
HDR	High dose rate
HPV	Human papilloma virus
HPV(-)	Human papilloma virus (negative)
HPV(+)	Human papilloma virus (positive)
HR	High risk
IMRT	Intensity modulated radiation therapy
IR	Intermediate risk
Ir-192	Iridium-192
LACC	Locally advanced cervical cancer
LBTE	Linear Boltzmann transport equation
LCR	Long control region
LDR	Low dose rate

LD_{50}	Lethal dose 50%
LKB	Lyman-Kutcher-Burman
LPL	Lethal-potentially lethal
LQ	Linear-quadratic
LQL	Linear-quadratic-linear
LR	Low risk
MBDCA	Model based dose calculation algorithm
MRI	Magnetic resonance imaging
NHEJ	Non-homologous end joining
NSD	Nominal standard dose
OAR	Organs at risk
OcB	Oncentra Brachy
OD	Optical density
Os-192	Osmium-192
OTT	Overall treatment time
PDR	Pulsed dose rate
PET	Positron emission tomography
PLA	Poly(lactic acid)
Pt-192	Platinum-192
PTV	Planning target volume
PV	Pixel value
Ra-226	Radium-226
SBRT	Stereotactic body radiation therapy
SAT	Single acute exposure
SCC	Squamous cell carcinoma
SF	Surviving fraction
SIB	Simultaneous integrated boost
T&O	Tandem and ovoids
T&R	Tandem and ring
.tif	Tagged image file format
TPR	Tissue phantom ratio
TRS	Technical report series
TDF	Time dose fractionation
USC	Universal survival curve
VMAT	Volumetric modulated arc therapy

CHAPTER 1
INTRODUCTION

1.1 Cervical Cancer Prevalence

Cervical cancer is the fourth most common cancer in women worldwide with an estimated 604,127 cases identified in 2020 and 1,350 expected to be diagnosed in Canada in the same year (1,2). While the incidence of cervical cancer has decreased in developed countries in the last 50 years due to increased screening, many developing countries have seen rapid increases in cervical cancer mortality; it is the second most common cancer for women in countries with a low or medium Human Development Index (HDI; a measure of social and economic development) (1,3). Similar trends exist for cervical cancer related-mortality, where a lower HDI correlates to an increase in cervical cancer mortality by a factor of 2 to 4 (4,5,6,7).

1.2 Cervical Cancer Etiology

Cervical cancer is strongly associated with human papillomavirus (HPV) infection (8,9). Two strains, HPV-16 and HPV-18, are correlated with greater carcinogenic risks in the HPV positive (HPV(+)) population, contributing to about 70% of cervical cancers (10). Both strains operate similarly, with continued expression of the E6 and E7 proteins that inactivate the tumor suppressing proteins pRB and p53 (11,12). HPV-18 has been indicated to have a more active Long Control Region (LCR)-E6-E7 region than HPV-16, which may lead to a more aggressive tumor (13). In a systemic review of 13 studies, cervical cancer patients with HPV-18 had a worse 3-year overall survival than those with HPV-16 (14).

Tumor formation is a multi-step process, including the development of genetic variation (15). While a high risk factor, HPV infection alone is unlikely to cause cancer (15,16). Additional cofactors that may contribute to cervical cancer include smoking, chlamydia trachomatis infection, and multiparity (17,18). Cervical cancers may also occur without HPV infection (HPV negative; HPV(-)) and account for 10% to 15% of all cervical cancers (19,20,21). HPV(-) cervical cancer patients have been found to have a poorer prognosis than HPV(+) (19,21,22). Both Rodriguez-Carunchio *et al* and Nicolas *et al* identified a lower mean overall survival (67.7

and 77.0 months, respectively) in HPV(-) compared to HPV(+) (108.9 and 153.8 months, respectively) cervical cancer patients (19,21).

1.3 Types of Cervical Cancer

The vast majority of cervical cancers are squamous cell carcinoma (SCC), forming on the surface of the ectocervix, which is the inferior aspect of the cervix that faces the vagina (Figure 1.1) (23). The most common non-SCC cervical cancer is adenocarcinoma (AC), forming in the glandular tissue of the endocervix that connects the vagina to the uterus (24,25). Less common cervical cancers include adenosquamous (ASC; containing both squamous cells and glandular cells) and endometrioid (a subset of adenocarcinoma cells defined based on tumor morphology) carcinoma (22,26). Compared to SCC, the other types are associated with a poorer prognosis in both overall survival and disease-free survival (24,25). For example, patients with AC and ASC cervical cancers experienced lower 5-year progression free survival (30.0 vs 47.6%) and 5-year overall survival (41.3 vs 58.1%) than the SCC subgroup (25).

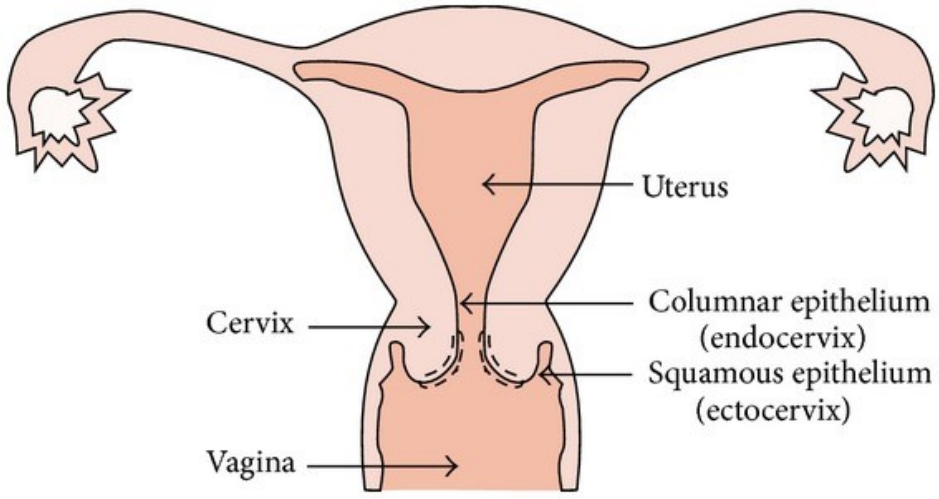

Figure 1.1: Coronal view of the uterus. Squamous cell carcinoma originates in the ectocervix while adenocarcinoma is formed in the endocervix. [Reprinted with permission from: Bengtsson E, Malm P. Screening for cervical cancer using automated analysis of PAP-smears. *Comput Math Method M* 2014;2914:842037].

1.4 Cervical Cancer Imaging

Magnetic resonance imaging (MRI), computed tomography (CT), and positron emission tomography (PET) are used in developed countries for staging cervical cancers and planning treatments. A T2-weighted MRI is ideal for providing an accurate evaluation of the primary tumor, spread into the parametrium, and the detection of surrounding normal tissue involvement (27,28,29,30,31). These aspects allow for accurate tumor staging by delineating operable and advanced cancers in 75% to 96% of cases (32). PET and CT imaging may be performed for the evaluation of distant metastatic sites (27,29). The PET imaging process uses fluorodeoxyglucose (FDG) as a tracer to track the uptake of glucose in rapidly metabolizing cells (e.g. primary tumor and metastatic sites) (27). The use of CT imaging along with PET addresses the limited spatial resolution of the latter (27).

1.5 Staging of Cervical Cancer

Two classification systems, TNM and Federation Internationale de Gynecologie et d'Obstetrique (FIGO), are used for assessing the progression of tumors (27,29,33). TNM staging classifies cancers based on the progression of the primary tumor (T) on a scale of 0 to 4 (with substaging represented by letters a and b), regional lymph node involvement (N) on a scale of 0 to 3 (only stages 0 and 1 are used in cervical cancer to represent regional lymph node metastasis), and distant metastatic spread (M) on a scale of 0 to 1 (34). FIGO classifies tumors based on disease progression from stage I to IV (33,35). Table 1.1 presents the equivalent stages of TNM and FIGO (36).

Both classification systems are widely used for cervical cancer staging. For example, the European Society of Gynaecological Oncology/European SocieTy for Radiotherapy and Oncology/European Society of Pathology (ESGO/ESTRO/ESP) recommends the use of TNM staging for cervical cancers while the use of FIGO staging has been recommended by the American Brachytherapy Society (37,38). For the remainder of the chapter, the TNM staging will be utilized with the comparable FIGO stage listed by Brierley *et al* provided in brackets (36).

Table 1.1: Stage equivalencies of TNM and FIGO structures [Reprinted with permission from: Brierley J, Gospodarowicz MK, Wittekind C. Cervix Uteri. *TNM Online* 2017:166-170].

Primary Tumor (TNM - T)		**Lymph Nodes (TNM - N)**		**Metastatic (TNM - M)**	
TNM	**FIGO**	**TNM**	**FIGO**	**TNM**	**FIGO**
T1	I	N0		M0	
T1a	IA	N1	IIIB	M1	IVB
T1a1	IA1				
T1a2	IA2				
T1b	1B				
T1b1	IB1				
Tb12	IB2				
T2	II				
T2a	IIA				
T2a1	IIA1				
T2a2	IIA2				
T2b	IIB				
T3a	IIIA				
T3b	IIIB				
T4	IVA				

1.6 Treatment of Cervical Cancer

Management of cervical cancer depends on the tumor stage. For early stage patients (stage T1a (IA)), the standard treatment is surgery (simple or radical hysterectomy). While radiation therapy is a potential alternative when surgery is not possible, previous clinical outcomes have shown that it results in lower patient survival and disease-free survival when compared to a radical hysterectomy (39). In a study of over 4,800 cervical cancer patients, hysterectomies decreased the 5-year mortality rate 62% (to approximately 20% from 52%) when compared to radiation treatment alone for lesions <4 cm in diameter (39).

If there is lymph node or parametrial involvement, the treatment includes concurrent radiation therapy and chemotherapy (chemoradiotherapy) (37). The radiation therapy arm includes both

external beam radiotherapy (EBRT; the delivery of treatment using a radiation source that is external to the patient and directed or focussed to target the tumor) and brachytherapy (BT; the placement of a radiation source inside or near the tumor). EBRT is mostly delivered using modulated techniques like intensity modulated radiation therapy (IMRT) or volumetric modulated arc therapy (VMAT) to treat the tumor bed and lymph nodes (35,37). BT treatments may be delivered using a variety of applicators (devices inserted into the patient to guide the radiation source) and through different delivery techniques (more details provided in Section 1.7).

Patients with locally advanced cervical cancer (LACC; stage T1b (IB1) to T4 (IVA)) are typically treated with chemoradiotherapy, with a BT boost (29). Cisplatin, a radiosensitizing drug that enhances the tumor killing capability of EBRT, is the most commonly used chemotherapy drug for cervical cancer treatment; other drugs include 5- fluorouracil and alternate platinum compounds (35,40,41). The use of chemoradiotherapy has been associated with improved treatment outcomes. A randomized trial of stage T3b (IIIB) patients, treated with cisplatin-based chemoradiotherapy showed 8% higher overall survival and disease-free survival after 5 years compared to patients treated with radiation alone (42). Current guidelines recommend curative intent RT doses of 85 to 95 Gy EQD2 (EQuieffective Dose in 2 Gy fractions; details in the next chapter) to be delivered via EBRT and a BT boost (31). The image guided intensity modulated **E**xternal beam radiochemotherapy and **M**RI based adaptive **BRA**chytherapy in locally advanced **CE**rvical cancer (EMBRACE) II study highlights common EBRT requirements, including 45 Gy in 25 fractions delivered by IMRT or VMAT to the primary tumor and a simultaneous integrated boost (SIB) dose to 60 Gy EQD2 (after EBRT and BT) to the pelvic and para-aortic lymph nodes (31).

1.7 Brachytherapy

Through the precise placement of the radiation source and making use of the sharp dose falloff with distance from the source, BT facilitates delivery of highly localized boost doses to the residual tumor following EBRT or inbetween EBRT fractions (typically towards the end of EBRT), with the additional advantage of reducing doses to the surrounding normal tissue (Figure 1.2). The use of BT is seen as a superior treatment option that provides better clinical outcomes

in patient survival in comparison to boosting with EBRT (an alternative for delivering localized radiation) (29,43,44). In addition, the shorter overall treatment times in BT limits tumor repopulation, a significant factor in the loss of tumor control, potentially improving treatment outcomes (45). Complex EBRT techniques, like SBRT (stereotactic body radiation therapy), have been evaluated as a boost option following chemoradiation when BT is not possible, though their efficacy remains to be proven (46).

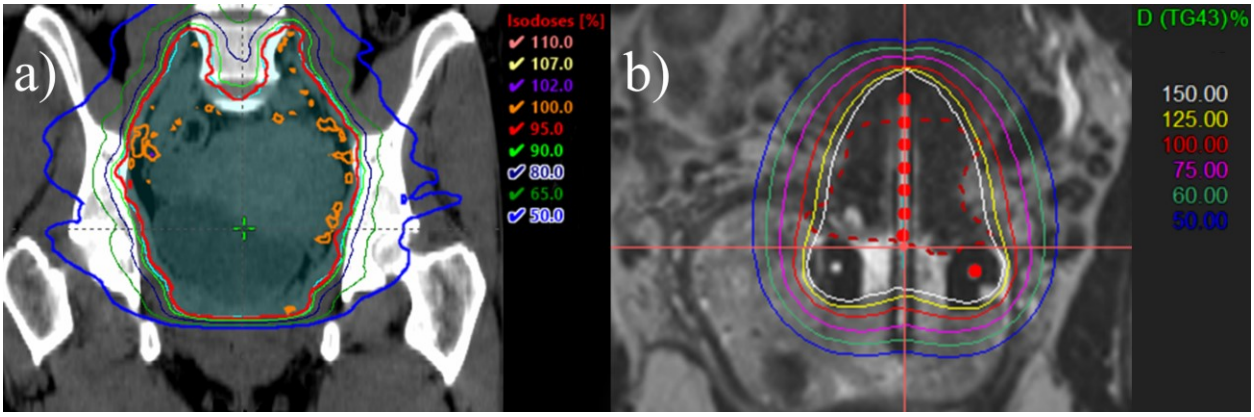

Figure 1.2: (a) Coronal view of a VMAT EBRT treatment for cervical cancer showing the target volume in blue (planning target volume; PTV) (b) Coronal view of the BT plan for the same patient. The red dashed line represents the high risk clinical target volume (HR-CTV; defined in Section 1.9).

1.7.1 Brachytherapy Sources

Radium-226 (Ra-226) was the first radioactive source to be used in the BT treatment of cervical cancer (29,47). However, the use of Ra-226 features multiple drawbacks, including low specific activity and potential leakage of radon-222. The use of Ra-226 was thus replaced with cesium-137 (Cs-137) (29). Cs-137 also has low specific activity and its current use is primarily limited to low or middle income countries (48,49). Newer BT sources have a high specific activity, which allows for smaller sources and applicators, increasing patient comfort. The most commonly used BT source for cervical cancer is iridium-192 (Ir-192), which has a specific activity over 100 times that of Cs-137 (Table 1.2). However, Ir-192 requires frequent source exchanges due to its short half-life of 74 days. Cobalt-60 (Co-60) BT sources are also used for treating cervical cancer (50).

Table 1.2: Properties of BT sources [Reprinted with permission from: Grupen C, Werthenbach U, Stroh T. Introduction to radiation protection. Berlin: Springer; 2010].

Property	**Ra-226**	**Co-60**	**Cs-137**	**Ir-192**
Specific activity (GBq/mg)	0.037	41.9	3.2	341
Half-life (years)	1600	5.3	30.2	0.20
Average γ ray energy (MeV)	0.083	1.25	0.662	0.380

The decay scheme of Ir-192 is complex and has multiple decay pathways (51). The decay is predominantly via β^- to form metastable platinum-192 (Pt-192). Ir-192 may also undergo electron capture to form metastable osmium-192 (Os-192). Both metastable isotopes release γ rays when forming a stable isotope; the average γ ray energy from the decay is 0.380 MeV (Figure 1.3).

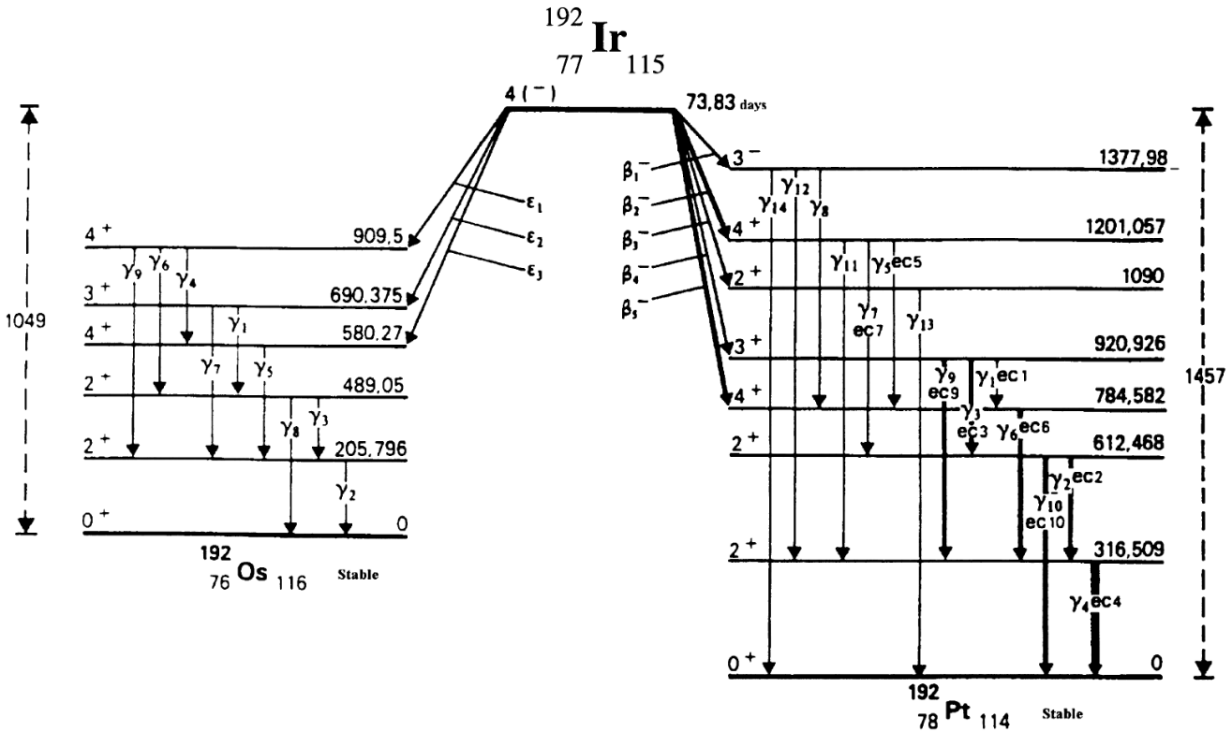

Figure 1.3: Decay scheme of Ir-192. The black vertical arrows represent γ rays emitted from metastable states while horizontal black lines represent energy levels of Ir-192, Os-192, or Pt-192 [Reprinted with permission from: Fonseca KA, Koskinas MF, Dias MS. Disintegration rate measurement of a 192Ir solution. *Appl Radiat Isotopes* 2001;54(1):141-145].

1.7.2 Brachytherapy Delivery Techniques

In modern times, BT treatments for cervical cancer are delivered using remote afterloading devices ("afterloaders"), which remotely move the source into an applicator inserted in the patient via a transfer tube. Based on the dose rate delivered, afterloaders are divided into low-dose-rate (LDR), high-dose-rate (HDR), and pulsed-dose-rate (PDR). Details of the technique and the commonly used radioactive sources in these treatment types are discussed below.

1.7.2.1 Low Dose Rate (LDR) BT

LDR BT (0.4 to 2 Gy/hr), used Cs-137 sources to deliver dose continuously over an extended period (e.g. 1 to 3 days per insertion with 1 to 2 total insertions for cervical cancer BT), and was planned using orthogonal films (29,52,53). Each insertion used multiple spherical sources (typically 20 to 24 for three channel Selectron LDR afterloaders (Nucletron, The Netherlands)) interspaced with steel spacers loaded into the patient, forming a "source train" (54,55). Figure 1.4 illustrates an example of sources loaded inside BT applicators for treatment (56).

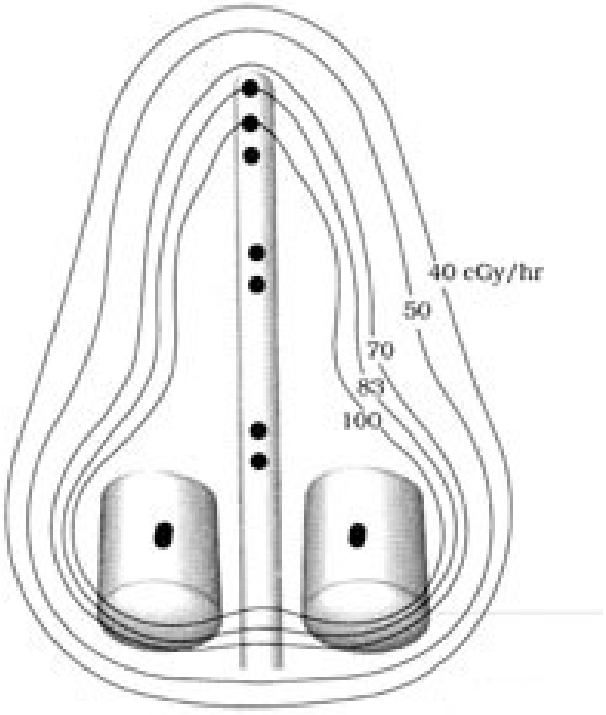

Figure 1.4: Example of a source loading for an LDR treatment. The black dots represent Cs-137 sources. Solid spherical spacers occupy spaces between the sources (not shown) to fix the position of the loaded sources. [Reprinted with permission from: Jhingran A, Eifel P. Radiation therapy for cervical carcinoma. *Glob Libr Women Med* 2009].

The disadvantages of using Cs-137 sources arise due to its low specific activity, resulting in longer treatments and large sources (and, therefore, bigger applicators). In addition, the fixed position of sources during treatment limits the potential for dose optimization (57). Compared to modern techniques, fixed source positions make tumor dose escalation difficult without also increasing the dose to the surrounding organs at risk (OAR).

1.7.2.2 High Dose Rate (HDR) BT

HDR BT (> 12 Gy/hr) commonly uses Ir-192 (though Co-60 is also in use) to deliver fractionated treatments that are spread over multiple days (58). The single source in an HDR afterloader, described as a "stepping source", moves through a series of preplanned source positions (dwell positions) for prescribed lengths of time (dwell times) to deliver the desired dose (59,60).

The use of HDR BT over LDR BT provides clinical, patient care, and economic advantages. Since it is believed that both HDR and LDR BT can provide similar clinical outcomes (both local control of the tumor and survival), these advantages make HDR BT an attractive alternative to LDR BT (61,62,63). For example, the use of the stepping source allows for superior dose optimization (59). If additional dose is desired locally near a given source position, this can be achieved by increasing the dwell time at that specific position. This enables "almost limitless" options for achieving a better dose distribution (57). Both LDR and HDR BT treatments can be delivered by remote afterloading, allowing for the reduction of unnecessary exposure. However, HDR afterloaders provide an economic advantage as they allow for a higher throughput of patients due to the shorter treatment times (few minutes per day). Furthermore, HDR BT treatments can be delivered on an outpatient basis and do not require a hospital stay for the patient (59).

In Canada, BT treatments are delivered almost exclusively using HDR. In 2017, 93% of institutes in Canada reported using HDR BT (64). Similar trends are seen internationally, with one survey identifying approximately 85% of centers in Asia, Europe, Australia, New Zealand, and North America using HDR BT for cervical cancer treatment (65).

1.7.2.3 Pulsed Dose Rate (PDR) BT

PDR BT is a hybrid treatment that delivers radiation through small hourly fractions (or "pulses") for a prolonged period (2 to 3 days) (Figure 1.5) (53). PDR afterloaders use an Ir-192 stepping source in the same manner as HDR.

PDR BT's capacity for dose optimization allows it to retain one of HDR BT's main advantages. In addition, it is believed that the lower hourly dose rate in PDR BT may reduce OAR toxicity compared to HDR BT (66). This will be further discussed in Chapter 2. However, this reduction in OAR toxicity has not been definitively identified in patient outcome data (67,68,69). Kumar *et al* reported the first prospective randomized study comparing HDR BT and PDR BT patients, noting lower radiation toxicity with PDR BT, though the improvement was not statistically significant (70). Unlike LDR BT, where treatments are delivered continuously, nursing care can be provided to the patient in between pulses without increasing the overall treatment time. However, like LDR BT, patient throughput is lower, which has limited the popularity of PDR BT in the United States and Canada (71). In 2020, only one of 37 centers in Canada reported use of PDR BT (72).

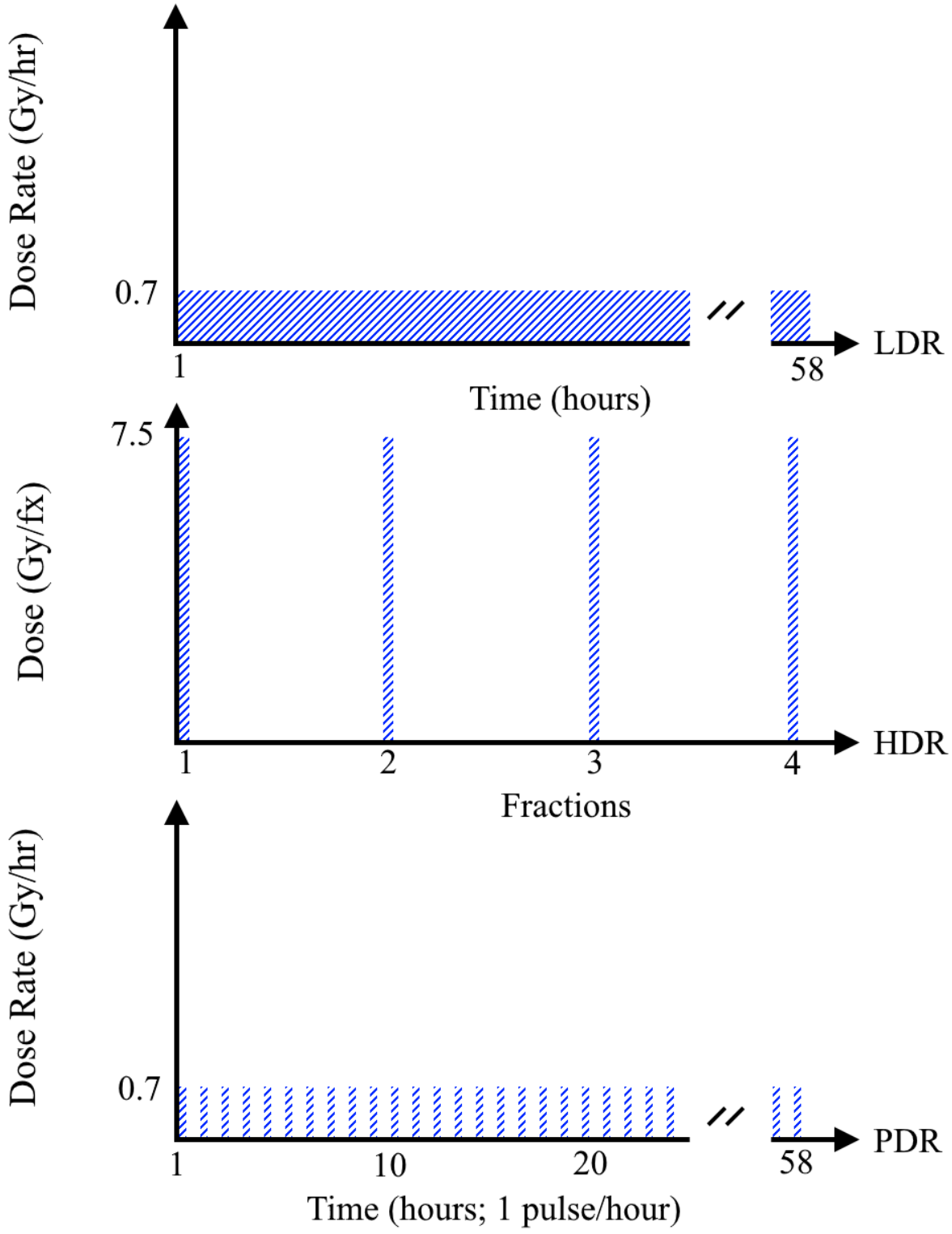

Figure 1.5: Examples of (a) LDR, (b) HDR, and (c) PDR treatments aiming at delivering a similar brachytherapy boost dose of ~44 Gy EQD2.

1.7.3 Applicators for Cervical Cancer

Intracavitary (placement of applicators in a cavity) BT, the common technique for delivering cervical cancer treatments, mostly uses the tandem and ring (T&R, Figure 1.6(a)) or tandem and ovoids (T&O, Figure 1.6(b)) applicators (29). The tandem is inserted through the cervix and into the uterus while the ring/ovoids sit(s) inferior to the ectocervix. The tandem treats the uterine portion of the tumor while the ring or ovoids treat(s) the upper portion of the vagina. Other vaginal components include the cylinder and split ring, with ongoing studies regarding the advantages of each applicator type (29,73). The selection of the vaginal component depends on the patient's anatomy and the extension of the tumor.

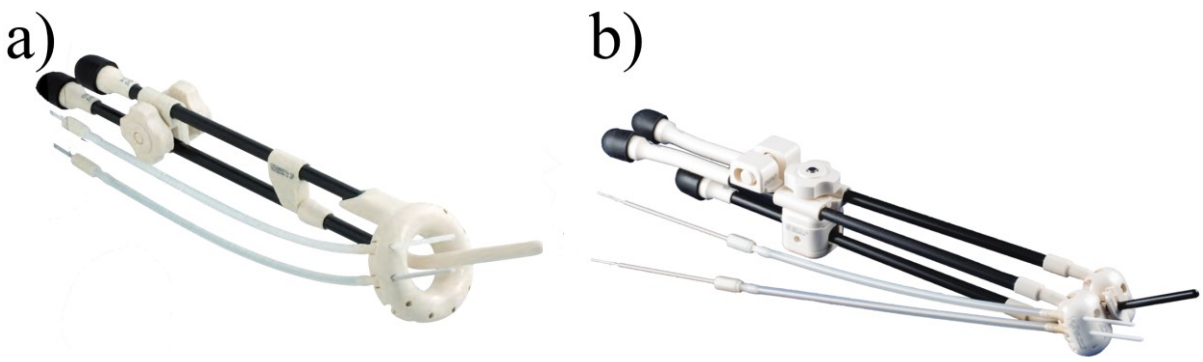

Figure 1.6: Intracavitary applicators used for cervical cancer BT: (a) tandem and ring and (b) tandem and ovoids, including interstitial needles. [Reprinted with permission from: Viswanathan AN, Beriwal S, De Los Santos JF, Demanes DJ, Gaffney D, Hansen J, *et al*. American Brachytherapy Society consensus guidelines for locally advanced carcinoma of the cervix. Part II: High-dose-rate brachytherapy. *Brachytherapy* 2012;11(1):47-52].

The addition of an interstitial (applicators placed inside the tissue) component to the intracavitary applicator (intracavitary/interstitial) facilitates delivery of more lateral dose and helps treat wide tumors that cannot otherwise be treated using an intracavitary technique alone (Figure 1.7(a)). The use of interstitial needles, as shown in Figure 1.7(b), allows for increased dose sculpting. Interstitial only treatments for cervical cancer are rare and account for 1% of cervical cancer treatments (67). Intracavitary/interstitial treatments are used in half of the Canadian centers (64).

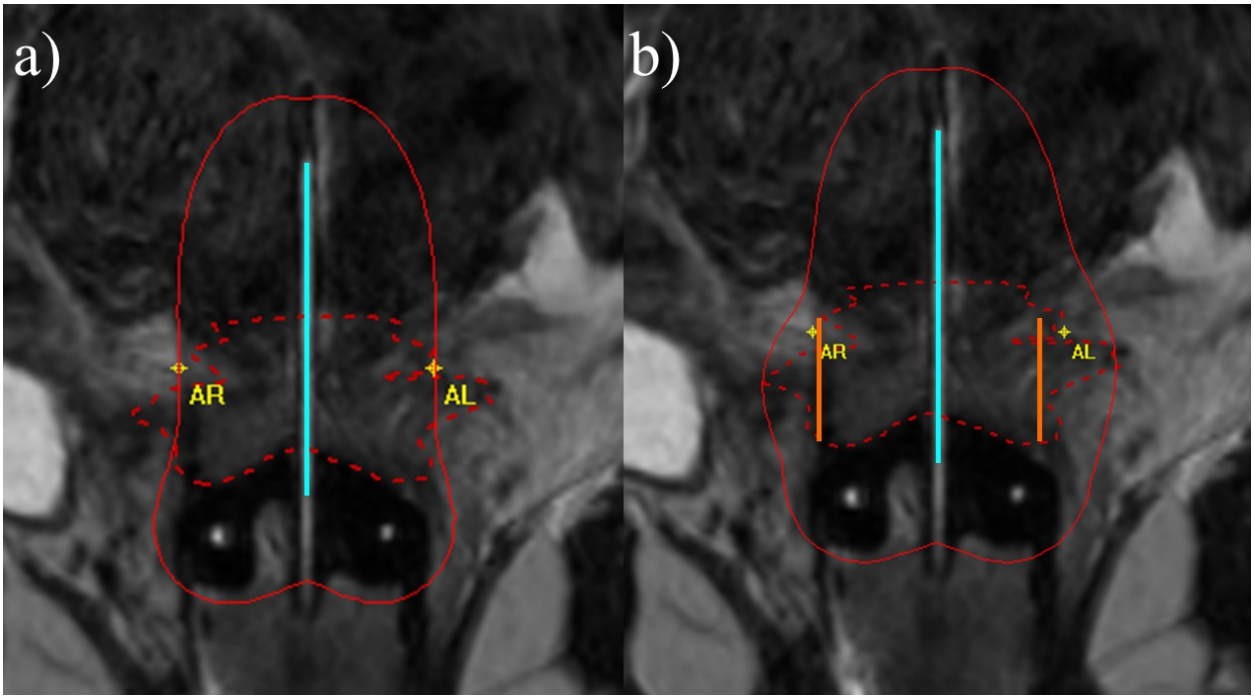

Figure 1.7: (a) Isodose profile for an intracavitary only treatment (tandem shown in light blue) normalized to the A points (see Section 1.8). The dashed and solid red lines represent the HR-CTV and the 100% isodose line, respectively. (b) Isodose profile for an intracavitary and interstitial treatment of the same tumor. The interstitial needles (in orange) provide increased lateral coverage of the HR-CTV.

1.8 Point-Based Prescriptions

The Manchester system is the most extensively used dose prescription system in the world and is characterized by dose to four points: Point A, Point B, bladder point, and rectum point (74). The location of these points was historically identified using orthogonal radiographs and provides limited information on patient anatomy:

- Point A is defined 2 cm superior to the cervical os and 2 cm lateral from the cervical canal on both sides (A_{right} and A_{left}) when viewed in the coronal plane (Figure 1.8) (75).
- Point B is located 2 cm up the midline and 5 cm away laterally at the level of Point A on both sides (B_{right} and B_{left}) and provides an estimate of the absorbed dose to the adjacent internal iliac and obturator lymph nodes (29).
- The bladder point acts as a reference for the bladder dose. It is defined after the insertion of a Foley balloon filled with 7 cm^3 of radio-opaque fluid into the bladder and is the posterior-most point of the balloon's surface (29).

- The reference point for rectal and upper vaginal dose is the recto-vaginal point, defined as 5 mm posterior to the vaginal posterior wall (29).

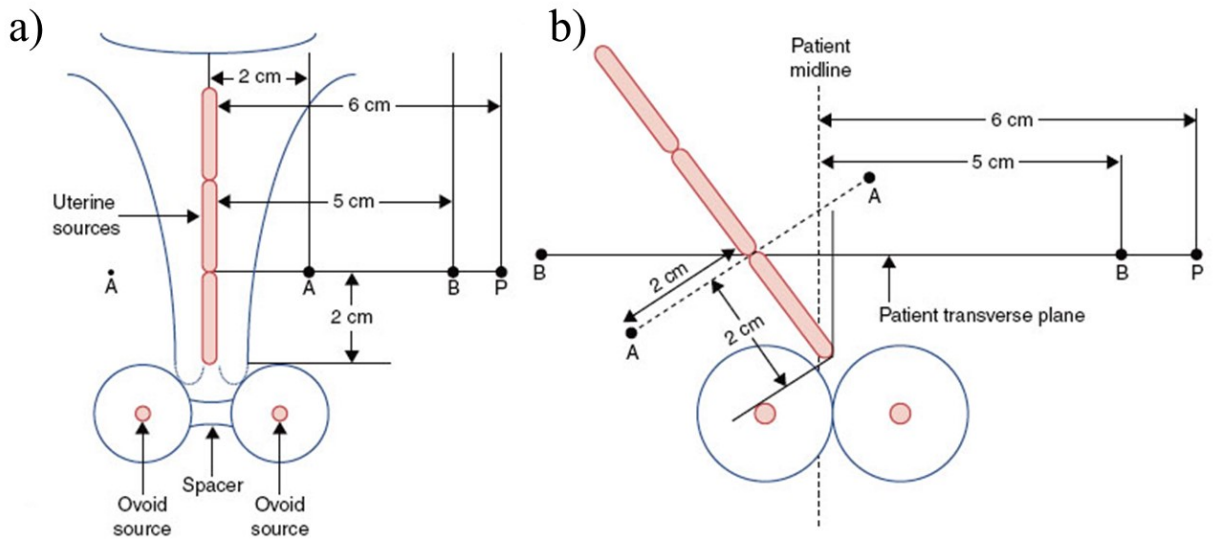

Figure 1.8: Example of the Manchester system treatment geometry and the position of Points A and B in the coronal plane for (a) an ideal patient configuration and (b) a distorted configuration. [Reprinted with permission from: Halperin E, Perez C, Brady L. Perez and Brady's Principles and Practice of Radiation Oncology. Philadelphia: Wolters Kluwer Lippincott Williams & Wilkins; 2013].

Further research into point-based anatomical definitions suggests that the use of point-based prescriptions is not accurate (76,77). This is due to variations in the tumor and cervix sizes and anatomical locations of the surrounding OARs, which can result in tumor overdosing or underdosing, potentially affecting patient outcomes (Figure 1.9). Despite these concerns, point-based prescriptions are often utilized as a starting point for treatment prescriptions (77).

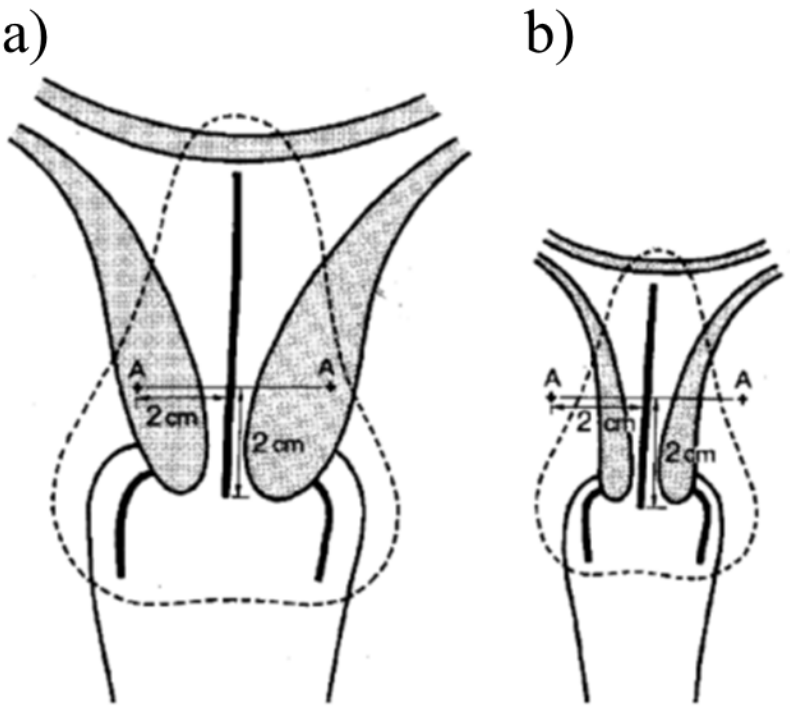

Figure 1.9: Anterior-posterior representation of the cervix and Point A for variations in cervix size. (a) Point A in a large cervix that can lead to underdosing of the tumor. (b) Point A in a small cervix that may lead to overdosing, including the organs at risk [Reprinted with permission from Khan F. The physics of radiation therapy. Philadelphia: Lippincott Williams & Wilkins; 2010].

1.9 Volume-Based Prescriptions

The limitations of point-based prescriptions can be overcome with volume-based planning, where prescriptions are made based on contoured regions. However, this requires 3D imaging of the patient and has led to the replacement of films with CT and later with MRI. Current guidelines (e.g. GEC-ESTRO) recommend use of MR images for contouring and planning (29). The residual gross tumor volume (GTV-T_{res}) is defined as the tumor volume that remains at the time of BT. The treated clinical target volumes (CTV) are described as high-risk (HR-CTV), intermediate-risk (IR-CTV), and low-risk (LR-CTV) (Figure 1.10) (29,31,38,78). The HR-CTV represents the macroscopic tumor load and includes the cervix, GTV-T_{Res}, and residual pathologic tissue (29). The HR-CTV is the volume with the highest risk of recurrence. The IR-CTV includes the primary GTV (GTV-T_{init}) and margins around the HR-CTV to represent the macroscopic disease. Finally, the LR-CTV defines the microscopic spread of the tumor and includes the parametria, uterus, and upper vagina. The use of multiple definitions allows for

multiple prescription targets based on the risk/benefit of escalating dose prescriptions to each CTV. Common dose metrics include the lowest dose delivered to 90% of the tumor (D90) and the highest dose delivered to a 2 cm^3 region of a contoured OAR ($D2_{cc}$; mainly bladder, rectum, sigmoid, and small bowel). Optimization of dwell positions and dwell times is performed to achieve the desired prescription doses to the targets while limiting OAR doses. The use of volume-based prescriptions has seen widespread adoption in the treatment of cervical cancer and has led to improved patient outcomes, such as overall and local survival compared to the point-based prescriptions (79,80,81,82).

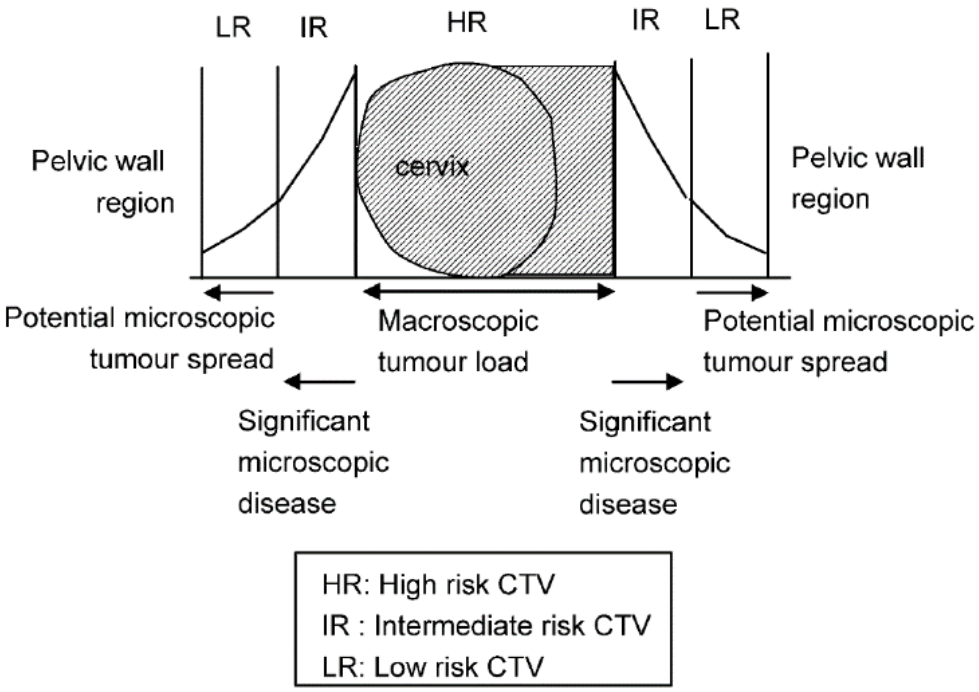

Figure 1.10: Definition of high risk (HR), intermediate risk (IR), and low risk (LR) CTV, which delineates the tumor into multiple regions based on macroscopic loading and potential for microscopic spread. [Reprinted with permission from: Haie-Meder C, Pötter R, Van Limbergen E, Briot E, De Brabandere M, Dimopoulos J, *et al*. Recommendations from gynaecological (GYN) GEC-ESTRO working group (I): concepts and terms in 3D image based 3D treatment planning in cervix cancer brachytherapy with emphasis on MRI assessment of GTV and CTV. *Radiother Oncol* 2005;74(3):235-245].

1.10 Dose Calculation Algorithm

1.10.1 AAPM TG-43 Formalism

Remote afterloaders from all vendors are accompanied by dedicated treatment planning software. For example, Elekta (Stockholm, Sweden) and Varian (Palo Alto, CA) offer Oncentra Brachy (OcB) and BrachyVision, respectively. The American Association of Physicists in Medicine's Task Group Number 43 (AAPM TG-43) formalism is the most commonly used approach for calculating the physical dose delivered for cervical cancer BT. This water-based formalism calculates the dose to a point-of-interest utilizing the known dose at a reference point and several other factors as described below.

The geometric setup for TG-43 calculation is shown in Figure 1.11. Positions are defined in polar coordinates, with r referring to the distance away from the center of the active source and θ being the angle off the longitudinal axis with the origin (r = 0) located at the center of the source (83,84). The reference point is defined along the perpendicular axis at r_0 = 1 cm and $\theta_0 = 90°$. The active source length (L) and angle subtended (β) by the source from the dose calculation point are also included in the dose calculation.

According to the TG-43 formalism, the dose rate ($\dot{D}$) from a source at a distance r and angle θ is given by (84):

$$\dot{D}(r,\theta) = S_k \cdot \Lambda \cdot \frac{G_X(r,\theta)}{G_X(r_0,\theta_0)} \cdot g_X(r) \cdot F(r,\theta) \quad (1.1)$$

S_k, the air-kerma strength, is a measure of the source strength (units of U, or cGy cm^2/hr). It is obtained from the air-kerma rate ($\dot{K}_\delta(d)$) in vacuum for a given cutoff energy (δ) at a distance d along the transverse axis (θ = 90°) of the source. The cutoff energy is typically selected as 5 keV as photons below this energy do not contribute to tissue dose more than 1 mm away from the source (84). Measurement of $\dot{K}_\delta(d)$ typically occurs 1 meter away from the source. S_k is calculated as:

$$S_k = \dot{K}_\delta(d) \cdot d^2 \quad (1.2)$$

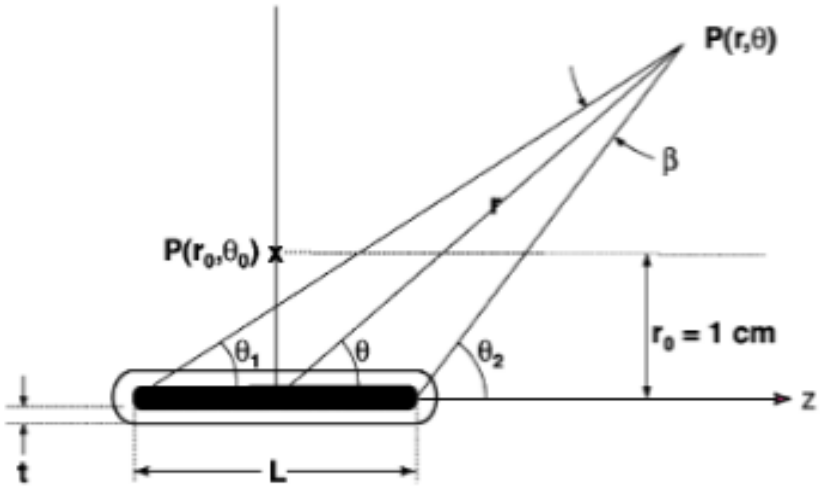

Figure 1.11: Definition of polar coordinates used in TG-43 formalism to calculate the dose rate at a calculation point P(r, θ) from a source of active length L. The reference dose rate is defined at the reference point (r_0 = 1 cm, θ_0 = 90°) along the transverse axis of the source. Calculation of the dose rate requires the angle subtended (β) by the source and the distance (r) from the center of the source to the calculation point. [Reprinted with permission from: Rivard MJ, Coursey BM, DeWerd LA, Hanson WF, Huq S, Ibbott GS, *et al*. Update of AAPM Task Group No. 43 Report: A revised AAPM protocol for brachytherapy dose calculations. *Med Phys* 2004;31(3):633-674].

Λ is the dose-rate constant in water at 1 cm along the transverse axis (at the reference point) of a unit air kerma strength source (S_k = 1 U) and has units of cGy/h/U. It converts the air-kerma strength to absorbed dose in water and is given by (84):

$$\Lambda = \frac{\dot{D}(r_0,\theta_0)}{S_k} \tag{1.3}$$

where $\dot{D}(r_0, \theta_0)$ is the dose rate at the reference point. The value of Λ is dependent on the radionuclide and the source model. Λ accounts for the spatial distribution of the radioactive material inside the source, the source encapsulation, self-filtration of the source, and source geometry (83).

G_X is the geometry function that provides an estimate of the falloff in photon fluence based on the spatial distribution of radioactivity in the active length neglecting absorption or scattering. The value of G_X is dependent on the distribution of activity within the source. For a point source approximation (denoted by subscript P), the value of the geometry function (G_P) is given by r^{-2}. For a line source approximation, the value of G_L is (84):

$$G_L(r,\theta) = \begin{cases} \frac{\beta}{L\, r \sin(\theta)}, \text{if } \theta \neq 0 \\ (r^2 - L^2/4)^{-1} \text{ if } \theta = 0 \end{cases} \quad (1.4)$$

where β is the angle subtended ends of the active length of the source at the calculation point (Figure 1.11) and L is the active length of the source.

g_x, the radial dose function, accounts for dose falloff in the transverse plane, excluding the falloff that is already considered in the geometric function, including photon scattering and attenuation. g_x is defined by (84):

$$g_X(r) = \frac{\dot{D}(r,\theta_0)}{\dot{D}(r_0,\theta_0)} \frac{G_X(r_0,\theta_0)}{G_X(r,\theta_0)} \quad (1.5)$$

F is the anisotropy function and accounts for variations in dose rate as a function of the polar angle relative to the transverse plane. The value of F in the transverse plane is unity but decreases as r decreases, θ approaches 0° or 180°, source encapsulation increases, and photon energy decreases (84). It is defined as (84):

$$F(r,\theta) = \frac{\dot{D}(r,\theta)}{\dot{D}(r,\theta_0)} \frac{G_L(r,\theta_0)}{G_L(r,\theta)} \quad (1.6)$$

Use of the TG-43 formalism allows for a simplification of complex dose calculations and the characterization of dose rate through the use of a handful of parameters, many of which are tabulated in published literature as they are source and model dependent (e.g. Perez-Calatayud *et al* provide values of Λ, g_L, and F for multiple HDR Ir-192 sources) (85). S_k is obtained from the source calibration certificate and G_X can be calculated based on the position of the source and calculation point of interest.

1.10.2 Model Based Dose Calculation Algorithms (MBDCA)

The underlying assumptions of the water-based dose calculation algorithm (TG-43) introduce uncertainties in dose calculations, in particular for treatments with significant tissue and material heterogeneities (86,87). To overcome this issue, the AAPM TG-186 report recommends the implementation of model-based dose calculation algorithms (MBDCA). MBDCAs calculate the actual dose delivered to the patient by modeling radiation transport in non-water media with the

consideration of tissue, air-tissue interface, and applicator heterogeneities (88). Three major MBDCA methods are briefly discussed below.

One method is to solve the governing equation that describes the behavior of radiation particles as they interact with matter: the Boltzmann transport equation (89). It is commonly assumed that the particles only interact with matter (no interactions with each other), an assumption that will hold in the absence of external magnetic fields (89). The assumption allows the particle behavior to be described by the linear Boltzmann transport equation (LBTE) (89). LBTE solvers calculate an approximate solution through a deterministic approach. Energy, spatial, and angular variables are discretized, which results in a linear system of equations that are subsequently solved iteratively (88). The use of discretized phase-space has led to these methods being categorized as grid-based Boltzmann solvers (GBBS). Acuros BV in BrachyVision (Varian, Palo Alto, California) is an example of a GBBS implemented in treatment planning software for Ir-192 sources (90).

The LBTE can also be solved stochastically with a Monte Carlo method. In this case, a series of input parameters (radiation geometry, materials, and interaction cross sections) and a random number generator are used to simulate physical interactions and dose deposition. Monte Carlo methods rely on the law of large numbers and the central limit theorem to determine the solution of the LBTE; running the simulation a large number of times will result in convergence to the solution for energy deposition in the specified materials. There is currently no commercially available Monte Carlo BT treatment planning software as the long calculation times associated with Monte Carlo calculations have prevented their use in routine clinical practice (91).

A third methodology, superposition/convolution, calculates the dose by superimposing dose deposition kernels around sites of interaction. Dose deposition kernels, generated using Monte Carlo method in water medium, are used in conjunction with ray tracing to calculate radiation transport along a photon's path to points of interest. The calculation of the convolution at every position is computationally taxing. As a result, a "collapsed cone" (CC) algorithm is used to improve the computational speed by angular discretization of energy: cones of the kernel's energy transport are collapsed along its axis. The CC algorithm is utilized in Oncentra Brachy as

the Advanced Collapsed cone Engine (ACE) (92). A feature of ACE is the use of "HU based" definitions, which assign material properties to voxels based on measured HU values and a CT calibration curve instead of predefined densities and materials (93).

As reported in several studies, the difference between doses calculated by TG-43 and MBDCAs for cervical cancer BT treatments is <5% (87,94,95,96). Mikell *et al* showed that dose to Points A and B as well as the OAR D_{2cc}s (bladder, rectum, and sigmoid) calculated using Acuros BV differed from TG-43 values by up to 5% (94). This represents larger deviations compared to other publications. A retrospective study of eight cervical cancer BT plans by Hyer *et al* showed <2.6% difference in the Point A and OAR D_{2cc} doses between Acuros BV and TG-43 calculated doses (95). Similarly, Hofbauer *et al* showed <2% changes between Acuros BV and TG-43 in target D90 and OAR D_{2cc} and $D_{0.1cc}$ (96). Abe *et al* noted the importance of proper material selection for each calculation; when recalculating seven Ir-192 BT treatments, the difference between TG-43 and OcB ACE for rectum D_{2cc} was 11.9% when the rectum was assigned the properties of air instead of water (97).

An explanation for the limited differences between TG-43 and MBDCA-calculated dose in cervical cancer BT is found in the photon energy of the sources, composition of tissues irradiated, and current applicator types. The γ energy of sources used in cervical cancer BT is in the Compton range (380 keV for Ir-192 and 1.25 MeV for Co-60). The Compton effect is directly proportional to the electron density of the material (98). In cervical cancer BT, the electron densities of the irradiated soft tissues are similar (approximately 1.05 times that of water) (99). In addition, current BT applicators are mostly plastic, which reduces material heterogeneity compared to higher density metallic applicators. These factors result in similar doses with water-based dose calculation and MBDCAs in gynecological BT.

1.11 Radiobiological Dose Prescriptions

The combined dose from EBRT and BT in cervical cancer treatments is specified in terms of radiobiological dose (29). Radiobiological dose contrasts with physical dose (the energy deposited in matter by ionizing radiation per unit mass) by incorporating the relationship between cell response factors and dose delivery parameters to better predict a treatment's outcome (66,100). The radiobiological dose is calculated using the α/β ratio and halftime of repair ($T_{1/2}$), parameters that characterize the irradiated tissue's response to radiation. Conventionally, α/β ratios of 10 Gy and 3 Gy are assumed for the tumor and for all other tissues, respectively, while the $T_{1/2}$ of all tissues is assumed to be 1.5 hours (29,31,60). A detailed explanation of these parameters and their use in radiobiological dose calculations is given in Chapter 2.

While not considered in current radiobiological dose calculations, recent guidelines stress the importance of the overall treatment time (OTT; time from the start of EBRT to the end of BT). For example, the EMBRACE II guidelines highlight the need to limit the overall treatment time (OTT) to less than 50 days (31). The retroEMBRACE study notes that the extension of OTT by 1 week was equivalent to a decrease in the HR-CTV D90 of 5 Gy EQD2 (101).

Several groups have recommended radiobiological dose prescriptions for the tumor and tolerance limits for the OARs. Currently, the most commonly used target dose prescriptions (in Gy_{10}) and OAR dose limits (in Gy_3) follow the EMBRACE II guidelines; shown in Table 1.3 (31):

Table 1.3: Planning aims and limits for prescribed dose in cervical cancer treatment suggested by the EMBRACE II study (31). Dose values are in units of EQD2, the calculation of which is discussed in Chapter 2.

Dose (Units)	**Planning aim**	**Dose limit**
D90 HR-CTV (Gy_{10})	90 - 95	>85
D98 HR-CTV (Gy_{10})	>75	-
D2cc Bladder (Gy_3)	<80	<90
D2cc Rectum (Gy_3)	<65	<70
D2cc Sigmoid Colon (Gy_3)	<70	<75
D2cc Bowel (Gy_3)	<70	<75

1.12 Thesis Overview

The transition to volume-based prescriptions has resulted in the adoption of multiple conventions to allow comparison of prior clinical experience with LDR BT to that of HDR BT and, to a lesser extent, PDR BT. This includes the assumption of values for the radiobiological parameters α/β and $T_{1/2}$. However, a wide range of values for α/β and $T_{1/2}$ have been reported for cervical cancer tumors and OARs. This research highlights the potential implications of the variance in the radiobiological parameter values, investigates use of *in vitro* experiments to determine α/β and $T_{1/2}$ of cervical cancer cell lines through the use of a novel radiation delivery apparatus, performs a comprehensive uncertainty analysis to better determine the accuracy and precision of the reported α/β and $T_{1/2}$ values and discusses the potential clinical implications of the findings.

Chapter 1 provides an overview of cervical cancer and its treatment with emphasis on the BT component. Chapter 2 introduces the fundamentals of radiobiology and radiobiological dose prescriptions. In addition, it discusses the theory and calculation of radiobiological dose and provides details of clinical prescription uncertainties identified through published literature. The objective of this work is also presented. Chapter 3 explores the previously reported values of radiobiological parameters and their potential clinical implications. The range of radiobiological dose that may be delivered by cervical cancer BT is presented using the previously reported parameter values to highlight the need for accurate radiobiological parameter determination. Chapter 4 presents the findings from *in vitro* experiments conducted using cervical cancer cell lines to quantify radiobiological parameters, α/β and $T_{1/2}$, that better reflect clinical practice than prior approaches. This includes the use of established techniques in radiation biology (clonogenic assays, irradiation using a Cs-137 irradiator) as well as a novel technique for *in vitro* irradiation using a clinical Ir-192 brachytherapy afterloader (brachytherapy afterloader *in vitro* radiation delivery apparatus; BAIRDA). The potential clinical implications of the parameters established in this research for brachytherapy treatment calculations will also be presented. Chapter 5 provides a thorough investigation of uncertainties associated with cell irradiation using a Cs-137 irradiator and Ir-192 afterloaders. In addition, a comprehensive study of the impact of combining several uncertainties in the measurement of cell survival using these two irradiation techniques is presented. Chapter 6 is a summary chapter that also identifies areas of further research.

1.13 References

(1) Sung H, Ferlay J, Siegel RL, Laversanne M, Soerjomataram I, Jemal A, *et al*. Global cancer statistics 2020: GLOBOCAN estimates of incidence and mortality worldwide for 36 cancers in 185 countries. *CA Cancer J Clin* 2021;71(3):209-249.

(2) Brenner DR, Weir HK, Demers AA, Ellison LF, Louzado C, Shaw A, et al. Projected estimates of cancer in Canada in 2020. *CMAJ* 2020;192(9):E199-E205.

(3) Bray F, Lortet-Tieulent J, Znaor A, Brotons M, Poljak M, Arbyn M. Patterns and trends in Human Papillomavirus-related diseases in central and eastern Europe and central Asia. *Vaccine* 2013;31:H32-H45.

(4) Singh GK, Azuine RE, Siapush M. Global inequalities in cervical cancer incidence and mortality are linked to deprivation, low socioeconomic status, and human development. *Int J MCH AIDS* 2012;1(1);17-30.

(5) Momenimovahed Z, Ghoncheh M, Pakzad R, Hasanpour H, Salehiniya H. Incidence and mortality of uterine cancer and relationship with Human Development Index in the world. *Cukurova Med J* 2017;42:233-233.

(6) Khazaei Z, Sohrabivafa M, Mansori K, Naemi H, Goodarzi E. Incidence and mortality of cervix cancer and their relationship with the human development index in 185 countries in the world: An ecology study in 2018. *Adv Hum Biol* 2019;9(3):222-227.

(7) Arbyn M, Weiderpass E, Bruni L, de Sanjosé Sm Saraiya M, Ferlay J, et al. Estimates of incidence and mortality of cervical cancer in 2018: a worldwide analysis. *Lancet Glob Health* 2020;8(2):e191-e203.

(8) Bosch FX, Lorincz A, Muñoz N, Meijer CJLM, Shah KV. The causal relation between human papillomavirus and cervical cancer. *J Clin Pathol* 2002;55(4):244-265.

(9) Ghim SJ, Basu PS, Jenson AB. Cervical cancer: Etiology, pathogenesis, treatment, and future vaccines. *Asian Pac J Cancer Prev* 2002;3(3):207-214.

(10) Schiffman M, Castle PE, Jeronimo J, Rodriguez AC, Wacholder S. Human papillomavirus and cervical cancer. *Lancet* 2007;370(9590):890-907.

(11) Narisawa-Saito M, Kiyono T. Basic mechanisms of high-risk human papillomavirus-induced carcinogenesis: roles of E6 and E7 proteins. *Cancer Sci 2007;*98(10):1505-1511.

(12) Zhu L, Lu Z, Zhao H. Antitumor mechanisms when pRb and p53 are genetically inactivated. *Oncogene* 2015;34(35);4547-4557.

(13) Villa LL, Schlegel R. Differences in transformation activity between HPV-18 and HPV-16 map to the viral LCR-E6-E7 region. *Virology* 1991;181(1):374-377.

(14) Xu Y, Qiu Y, Yan S, Wang H. Prognostic implication of human papillomavirus types in cervical cancer patients: a systemic review and meta-analysis. *Infect Agent Cancer* 2020;15(1):66.

(15) Subramanya D, Grivas PD. HPV and cervical cancer: updates on an established relationship. *Postgrad Med* 2008;120(4):7-13.

(16) Roden RBS, Stern PL. Opportunities and challenges for human papillomavirus vaccination in cancer. *Nat Rev Cancer* 2018;18(4):240-254.

(17) Koskela P, Anttila T, Bjørge T, Brunsvig A, Dillner J, Hakama M, et al. Chlamydia trachomatis infection as a risk factor for invasive cervical cancer. *Int J Cancer* 2000;85(1):35-39.

(18) Muñoz N, Castellsagué X, de González AB, Gissmann L. Chapter 1: HPV in the etiology of human cancer. *Vaccine* 2006;24 Suppl 3:1-10.

(19) Rodriguez-Carunchio L, Soveral I, Steenbergen RDM, Torné A, Martinez S, Fusté P, *et al*. HPV-negative carcinoma of the uterine cervix: a distinct type of cervical cancer with poor prognosis. *BJOG* 2015;112(1):119-127.

(20) Tjalma WAA. HPV negative cervical cancers and primary HPV screening. *Facts Views Vis Obgyn* 2018;10(2):107-113.

(21) Nicolás I, Marimon L, Barnadas E, Saco A, Rodríguez-Carunchio L, Fusté P, *et al*. HPV-negative tumors of the uterine cervix. *Mod Pathol* 2019;32(8):1189-1196.

(22) Arezzo F, Cormio G, Loizzi V, Cazzato G, Cataldo V, Lombardi C, *et al*. HPV-negative cervical cancer: A narrative review. *Diagnostics (Basel)* 2021;11(6):952.

(23) van der Horst J, Siebers AG, Bulten J, Massuger LF, de Kok IMCM. Increasing incidence of invasive and in situ cervical adenocarcinoma in the Netherlands during 2004-2013. *Cancer Med* 2017;6(2):416-423.

(24) Lee YY, Choi CH, Kim TJ, Lee JW, Kim BG, Lee JH, *et al*. A comparison of pure adenocarcinoma and squamous cell carcinoma of the cervix after radical hysterectomy in stage IB-IIA. *Gynecol Oncol* 2011;120(3):439-443.

(25) Chen JLY, Huang CY, Huang YS, Chen RJ, Wang CW, Chen YH, *et al*. Differential clinical characteristics, treatment response and prognosis of locally advanced adenocarcinoma/adenosquamous carcinoma and squamous cell carcinoma of cervix treated with definitive radiotherapy. *Acta Obstet Gynecol Scand* 2014;93(7):661-668.

(26) Pavithra V, Sai Shalini CN, Priya S, Rani U, Rajendiran S, Joseph LD. Small cell neuroendocrine carcinoma of the cervix: A rare entity. *J Clin Diagn Res* 2014;8(2):147-148.

(27) Lee SI, Atri M. 2018 FIGO staging system for uterine cervical cancer: Enter cross-sectional imaging. *Radiology* 2019;292(1):15-24.

(28) Follen M, Levenback CF, Iyer RB, Grigsby PW, Boss EA, Delpassand ES, *et al*. Imaging in cervical cancer. Cancer 2003;98(9 Suppl):2028-2038.

(29) International commission on radiation units & measurements. Report 89: Prescribing, recording, and reporting brachytherapy for cancer of the cervix. *J of the ICRU* 2013; 13:1-258.

(30) Viswanathan A, Dimopoulos J, Kirisits C, Berger D, Pötter R. Computed tomography versus magnetic resonance imaging-based contouring in cervical cancer brachytherapy: results of a prospective trial and preliminary guidelines for standardized contours. *Int J Radiat Oncol Biol Phys* 2007; 68(2):491-498.

(31) Pötter R, Tanderup K, Kirisits C, de Leeuw A, Kirchheiner K, Nout R, *et al* The EMBRACE II study: The outcome and prospect of two decades of evolution within the GEC-ESTRO GYN working group and the EMBRACE studies. *Clin Transl Radiat Oncol* 2018;9:48-60.

(32) Bourgioti C, Chatoupis K, Moulopous LA. Current imaging strategies for the evaluation of uterine cervical cancer. *World J Radiol* 2016;8(4):342-354.

(33) Bhatla N, Berek JS, Fredes MC, Denny LA, Grenman S, Karunaratne K, *et al*. Revised FIGO staging for carcinoma of the cervix uteri. *Int J Gynecol Obstet* 2019;145(1):129-135.

(34) Rosen R, Sapra A. TNM Classification. NCBI 2021.

(35) Bhatla N, Aoki D, Sharma DN, Sankaranarayanan R. Cancer of the cervix uteri. *Int J Gynaecol Obstet* 2018;143 Supple 2:22-36.

(36) Brierley J, Gospodarowicz MK, Wittekind C. Cervix Uteri. *TNM Online* 2017:166-170.

(37) Cibula D, Pötter R, Planchamp F, Avall-Lundqvist E, Fischerova D, Haie-Meder C, *et al*. The European Society of Gynaecological Oncology/European Society for Radiotherapy and Oncology/European Society of Pathology guidelines for the management of patients with cervical cancer. *Virchows Arch* 2018;472(6):919-936.

(38) Viswanathan AN, Thomadsen B. American Brachytherapy Society consensus guidelines for locally advanced carcinoma of the cervix. Part I: General principles. Brachytherapy 2012;11(1):33-46.

(39) Bansal N, Herzog TJ, Shaw RE, Burke WM, Deutsch I, Wright JD. Primary therapy for early-stage cervical cancer: radical hysterectomy vs radiation. *Am J Obstet Gynecol* 2009;201(5):485.e1-9.

(40) McNeil C. New standard of care for cervical cancer sets stage for next questions. *J Natl Cancer* Inst 1999;91(6):500-501.

(41) Candelaria M, Garcia-Arais A, Centina L, Cetina L, Dueñas-Gonzalez A. Radiosensitizers in cervical cancer. Cisplatin and beyond. *Radiat Oncol* 2006;1:15.

(42) Shrivastava S, Mahantshetty U, Engineer R, Chopra S, Hawaldar R, Handre V, *et al*. Cisplatin chemostherapy vs radiotherapy in RIGO stage IIIB squamous cell carcinoma of the uterine cervix: A randomized clinical trial. *JAMA Oncol* 2018;4(4):506-513.

(43) Georg D, Kirisits C, Hillbrand M, Dimopoulos J, Pötter R. Image-guided radiotherapy for cervix cancer: High-tech external beam therapy versus high-tech brachytherapy. *Int J Radiat Oncol Biol Phys* 2008;71(4):1272-1278.

(44) Han K, Milosevic M, Fyles A, Pintilie M, Viswanathan AN. Trends in the utilization of brachytherapy in cervical cancer in the United States. *Int J Radiat Oncol Biol Phys* 2013;87(1):111-119.

(45) Brenner DJ. Radiation biology in brachytherapy. *J Surg Oncol* 1997;65(1):66-70.

(46) Cheng HY, Liang JA, Hung YC, Yeh LS, Chang WC, Lin WC, *et al*. Stereotactic body radiotherapy for pelvic boost in gynecological cancer patients with local recurrence or unsuitable for intracavitary brachytherapy. *Taiwan J Obstet Gynecol* 2021;60(1):111-118.

(47) Kemikler, G. History of brachytherapy. *Turk J Oncol* 2019;34(Supp 1):1-10.

(48) Banahene JO, Darko EO, Awuah B. Low dose rate caesium-137 implant time of intracavitary brachytherapy source of a selected oncology center in Ghana. *Clin Cancer Investig J* 2015;4(2):158-164.

(49) Grover S, Longo J, Einck J, Pri P, Brown D, Chino J, *et al*. The unique issues with brachytherapy in low- and middle-income countries. *Semin Radiat Oncol* 2019;27(2):136-142.

(50) Shukla AK, Jangid PK, Rajpurohit VS, Verma A, Dangayach SK, Gagrani V, *et al*. Dosimetric comparison of 60Co and 192Ir high dose rate source used in brachytherapy treatment of cervical cancer. *J Cancer Res Ther* 2019;15(6):1212-1215.

(51) Fonseca KA, Koskinas MF, Dias MS. Disintegration rate measurement of a 192Ir solution. *Appl Radiat Isotopes* 2001;54(1):141-145.

(52) Chassagne D, Dutreix A, Almond P, Burgers HMV, Busch M, Joslin CA. Report 38: Dose and volume specification for reporting intracavitary therapy in gynecology. *J of the ICRU* 1985;1(1):1-23.

(53) Banerjee R, Kamrava M. Brachytherapy in the treatment of cervical cancer: a review. *Int J Women's Health* 2014;6:555-564.

(54) Grigsby PW,Williamson JF, Perez CA. Source configuration and dose rates for the Selectron Afterloading equipment for gynecologic applicators. *Int J Radiat Oncol Biol Phys* 1992;24(2):321-327.

(55) Bidmead M, Briot E, Burger J, Ferreira I, Grusell E, Kirisits C, *et al*. A practical guide to quality control of brachytherapy equipment [booklet]. Brussels: The European SocieTy for Radiotherapy and Oncology; 2004.

(56) Jhingran A, Eifel P. Radiation therapy for cervical carcinoma. *Glob Libr Women Med* 2009.

(57) Meadows JL, Bichay TJ. Low dose-rate brachytherapy for the treatment of cervix cancer is outdated and should be discontinued. *Med Phys* 2016;43(9):4963.

(58) Tantivatana T, Rongsriyam K. Treatment outcomes of high-dose-rate intracavitary brachytherapy for cervical cancer: a comparison of Ir-192 vs Co-60 sources. *J Gynecol Oncol* 2018;29(5):e86.

(59) Stewart AJ, Viswanathan AN. Current controversies in high-dose-rate versus low-dose-rate brachytherapy for cervical cancer. *Cancer* 2006;107(5):908-915.

(60) Viswanathan AN, Beriwal S, De Los Santos JF, Demanes DJ, Gaffney D, Hansen J, *et al*. American Brachytherapy Society consensus guidelines for locally advanced carcinoma of the cervix. Part II: High-dose-rate brachytherapy. *Brachytherapy* 2012;11(1):47-52.

(61) Orton CG. High and low dose-rate brachytherapy for cervical cancer. *Acta Oncol* 1998;37(2):117-125.

(62) Wang X, Liu R, Ma B, Yang K, Tian J, Jiang L, *et al*. High dose rate versus low dose rate intracavity brachytherapy for locally advanced uterine cervix cancer. *Cochrane Database Syst Rev*;2014;7(7):CD007563.

(63) Patankar SS, Tergas AI, Deutsch I, Burke WM, Hou JY, Ananth CV, *et al*. High verse low-dose rate brachytherapy for cervical cancer. *Gynecol Oncol* 2015;136(3):534-541.

(64) Taggar AS, Phan T, Traptow L, Banerjee R, Doll CM. Cervical cancer brachytherapy in Canada: A focus on interstitial brachytherapy utilization. *Brachytherapy* 2017;16(1):161-166.

(65) Viswanathan AN, Creutzberg CL, Craighead P, McCormack M, Toita T, Narayan K, *et al*. International brachytherapy practice patterns: A survey of the gynecologic cancer intergroup (GCIC). *Int J Radiat Oncol Biol Phys* 2012;82(1):250-255.

(66) Brenner DJ, Hall EJ. Conditions for the equivalence of continuous to pulsed low dose rate brachytherapy. *Int J Radiat Oncol Biol Phys* 1991;20(1):181-190.

(67) Skowronek J, Malicki J, Piotrowski T. Values of biologically equivalent doses in healthy tissues: Comparison of PDR and HDR brachytherapy techniques. *Brachytherapy* 2010;9(2):165-170.

(68) Sharma BA, Signh TT, Singh LJ, Singh YI, Devi YS. Biological effective doses in the intracavitary high dose rate brachytherapy of cervical cancer. *J Contemp Brachytherapy* 2011;3(4):188-192.

(69) Balgobind BV, Koedooder K, Ordonez Zuniga DO, Fajardo RD, Rasch CRN, Pieters BR. A review of the clinical experience in pulsed dose rate brachytherapy. *Br J Radiol* 2015;88(1055):20150310.

(70) Kumar P, Sharma DN, Kumar S, Gandhi AK, Rath GK, Julka PK. Pulsed-dose-rate vs. high-dose-rate intracavitary radiotherapy for locally advanced carcinoma of cervix: A prospective randomized study. *Brachytherapy* 2016;15(3):327-332.

(71) Phan T, Mula-Hussain L, Pavamani S, Pearce A, D'Souza D, Patil NG, *et al*. The changing landscape of brachytherapy for cervical cancer: a Canadian practice survey. *Curr Oncol* 2015;22(5):356-360.

(72) Taggar AS, Martell K, Leung E, Banerjee R, Fortin I, Doll CM. Changing landscape of radiation therapy for advanced cervical cance with a focus on interstitial brachytherapy: A Canadian practice patterns survey. *Pract Radiat Oncol* 2021;S1879-8500(21)00283-6.

(73) Levin D, Menhel J, Rabin T, Pfeffer R, Symon Z. Dosimetric comparison of tandem and ovoids vs tandem and ring for intracavitary gynecologic applications. *Med Dosim* 2008;33(4):315-320.

(74) Khan F. The physics of radiation therapy. Philadelphia: Lippincott Williams & Wilkins; 2010.

(75) Tod M, Meredith WJ. Treatment of cancer of the cervix uteri, a revised Manchester method. *Br J Radiol* 1953;26(305):252-257.

(76) Wang Y, Ye WJ, Du LH, Li AJ, Ren YF, Cao XP. Dose-volume parameters and clinical outcome of CT-guided free-hand high-dose-rate interstitial brachytherapy for cervical cancer. *Chin J Cancer* 2012;31(12):598-604.

(77) Srivastava A, Datta NR. Brachytherapy in cervical cancer: Time to move ahead from point A? *World J Clin Oncol* 2014;5(4):764-774.

(78) Haie-Meder C, Pötter R, Van Limbergen E, Briot E, De Brabandere M, Dimopoulos J, *et al*. Recommendations from gynaecological (GYN) GEC-ESTRO working group (I): concepts and terms in 3D image based 3D treatment planning in cervix cancer brachytherapy with emphasis on MRI assessment of GTV and CTV. *Radiother Oncol* 2005;74(3):235-245.

(79) Marchant KJ, Sadikov E. The evolving practice of intrauterine cervix brachytherapy in Canada: A medical physics perspective. *Brachytherapy* 2013;12(4):324-330.

(80) Kim YJ, Kang HC, Kim YS. Impact of intracavitary brachytherapy technique (2D vs 3D) on outcomes of cervical cancer: a systematic review and meta-analysis. *Strahlenther Onkol* 2020;196(11):973-982.

(81) Cho O, Chun M. Management for locally advanced cervical cancer: new trends and controversial issues. *Radiat Oncol J* 2018;36(4):254–264.

(82) Derks K, Steenhuijsen JLG, van den Berg HA, Houterman S, Cnossen J, van Haaren P, *et al*. Impact of brachytherapy technique (2D versus 3D) on outcome following radiotherapy of cervical cancer. *J Contemp Brachytherapy* 2018;10(1):17-25.

(83) Nath R, Anderson LL, Luxton G, Weaver KA, Williamson JF, Meigooni AS. Dosimetry of interstitial brachytherapy sources: Recommendations of the AAPM Radiation Therapy Committee Task Group No. 43. *Med Phys* 1995:22(2),209–234.

(84) Rivard MJ, Coursey BM, DeWerd LA, Hanson WF, Huq S, Ibbott GS, *et al*. Update of AAPM Task Group No. 43 Report: A revised AAPM protocol for brachytherapy dose calculations. *Med Phys* 2004;31(3):633-674.

(85) Perez-Calatyud J, Ballester F, Das RK, Dewerd LA, Ibbott GS, Meigooni AS, *et al*. Dose calculation for photon-emitting brachytherapy sources with average energy higher than 50 keV: report of the AAPM and ESTRO. *Med Phys* 2012;39(5):2904-2929.

(86) Ghorbani M, Salahshour F, Haghparast A, Moghaddas TA, Knaup C. Effect of tissue composition on dose distribution in brachytherapy with various photon emitting sources. *J Contemp Brachytherapy* 2014;6(1):54-67.

(87) Sloboda RS, Morrison H, Cawston-Grant B, Menon GV. A brief look at model-based dose calculation principles, practicalities, and promise. *J Contemp Brachytherapy* 2017;9(1):79-88.

(88) Beaulieu L, Tedgren AC, Carrier J-F, Davis SD, Mourtada F, Rivard MJ, *et al*. Report of the Task Group 186 on model-based dose calculation methods in brachytherapy beyond the TG-43 formalism: Current status and recommendations for clinical implementation. *Med Phys* 2012;39(10):6208-6236.

(89) Akpochafor MO, Aweda MA, Durosinmi-Etti FA, Adeneye SO, Omojola AD. Simulation of the Linear Boltzmann transport equation in modelling of photon beam data. *IOSR J Appl Phys* 2014;5(6):72-86.

(90) Yousif YAM, Osman AFI, Halato MA. A review of dosimetric impact of implementation of model-based dose calculation algorithms (MBDCAs) for HDR brachytherapy. *Phys Eng Sci Med* 2021;44(3):871-886.

(91) Enger SA, Vijande J, Rivard MJ. Model-based dose algorithms for brachytherapy dosimetry. *Semin Radiat Oncol* 2020;30(1):77-86.

(92) Morrison H, Menon G, Larocque MP, van Veelen B, Niatsetski Y, Weis E, *et al*. Initial evaluation of Advanced Collapsed cone Engine dose calculations in water medium for I-125 seeds and COMS eye plaques. *Med Phys* 2018;45(3):1276-1286.

(93) Pappas EP, Peppa V, Hourdakis CJ, Karaiskos P, Papagiannis P. On the use of a novel Ferrous Xylenol-orange gelatin dosimeter for HDR brachytherapy commissioning and quality assurance testing. *Phys Medica* 2018;45(1):162-169.

(94) Mikkel JK, Klopp AH, Gonzalez GMN, Kisling KD, Price MJ, Berner PA, *et al*. Impact of heterogeneity-based dose calculation using a deterministic grid-based Boltzmann equation solver for intracavitary brachytherapy. *Int J Radiat Oncol Biol Phys* 2012;83(3):e417-422.

(95) Hyer DE, Sheybani A, Jacobson GM, Kim Y. The dosimetric impact of heterogeneity corrections in high-dose-rate 192Ir brachytherapy for cervical cancer: Investigation of both conventional Point-A and volume-optimized plans. *Brachytherapy* 2012;11(6):515-520.

(96) Hofbauer J, Kirisits C, Resch A, Xu Y, Sturdza A, Pötter R, *et al*. Impact of heterogeneity-corrected dose calculation using a grid-based Boltzmann solver on breast and cervix cancer brachytherapy. *J Contemp Brachytherapy* 2016;8(2):143-149.

(97) Abe K, Kadoya N, Sato S, Hashimoto S, Nakajima Y, Miyasaka Y, *et al*. Impact of a commercially available model-based dose calculation algorithm on treatment planning of high-dose-rate brachytherapy in patients with cervical cancer. *J Radiat Res* 2018;59(2):198-206.

(98) Devlin PM, Cormack RA, Holloway CL, Stewart AJ. Brachytherapy: Applications and techniques. Springer Publishing Company; 2015.

(99) Sudhyadhom A. On the molecular relationship between Hounsfield unit (HU), mass density, and electron density in computed tomography (CT). *PLoS One* 2020;15(12): e0244861.

(100) Barendsen GW. Dose fractionation, dose rate and iso-effect relationships for normal tissue responses. *Int J Radiat Oncol Biol Phys* 1982;8(11):1981-1997.

(101) Tanderup K, Fokdal LU, Sturdza A, Haie-Meder C, Nazeron R, van Limbergen E, *et al*. Effect of tumor dose, volume and overall treatment time on local control after radiochemotherapy including MRI guided brachytherapy of locally advanced cervical cancer. *Radiother Oncol* 2016;120(3):441-446.

CHAPTER 2
RADIOBIOLOGY AND RADIOBIOLOGICAL PARAMETERS

A portion of this chapter has been published as: Chow B, Warkentin B, Menon G. Radiobiological dose calculation parameters for cervix cancer brachytherapy: A systematic review. Brachytherapy 2019;18(4):546-558.

2.1 Introduction

A summary of the recommended combined EBRT and BT prescription doses used in locally advanced cervical cancer was provided in Chapter 1. The dose prescription to the tumors and dose limits to the organs at risk (bladder, rectum, sigmoid, small bowel) were given in units of radiobiological dose. This chapter will go into detail about the derivation of radiobiological dose, the importance of the α/β ratio and $T_{1/2}$, and recently published findings of these parameter values.

2.2 Radiobiological Dose

The use of physical dose (the energy deposited per unit mass, units of Gy) does not fully characterize the response of cells to radiation. In a study by Tarbell *et al*, mice irradiated at LDR (5 cGy/min) had a higher median lethal dose (dose that is expected to kill 50% of those exposed; LD_{50}) 180 days after upper body half irradiation than mice irradiated at HDR (80 cGy/min) for the same physical dose (1). The LD_{50} after 180 days for twice-daily 2 Gy fractions (separated by 6 hours) was 28.42 Gy for LDR vs 24.10 Gy for HDR. In addition, Tarbell *et al* determined that increasing the time separation between dose fractions increased LD_{50} after 180 days. If the LDR twice-daily 2 Gy fractions were instead delivered daily, the LD_{50} after 180 days increased from 28.42 Gy to 32.66 Gy.

As there are large variances in the dose rate and dose fractionation size between LDR, HDR, and PDR BT, calculation of equivalencies between different BT schedules requires the use of a prescription metric that considers physical dose, dose fractionation, and dose rate. Historical attempts at bridging these different techniques include the use of "dose reduction factors" (DRF) to convert HDR BT doses to an LDR equivalent (2). In order to

produce the same lethality in mice 26 weeks after irradiation, Lockhart *et al* showed that the total dose of an HDR exposure (at 110 cGy/min) had to be reduced by a factor of 1.8 compared to that of an LDR exposure (at 5 cGy/min) (3). A limitation of the DRF method is its dependence on the treatment schedule and dose fraction size. In the example above from Tarbell *et al*, the DRF for the twice daily 2 Gy fractions at HDR exposures compared to LDR was approximately 1.3. However, in the same study, it was identified that the LD_{50} values after 180 days of single fraction HDR (1 Gy increments delivering dose up to 18 Gy) and LDR treatments were 12.99 Gy and 22.47 Gy, respectively (DRF of 1.7) (1). In addition, decreasing the fraction size from 2 to 1.2 Gy resulted in a much smaller DRF of 1.02 between HDR and LDR exposures (LD_{50} of 28.17 Gy vs 28.60 Gy, respectively). Therefore, comparison of two different dose schedules must have DRFs calculated for each treatment schedule and fraction size.

An important dosimetric change in cervical cancer treatment planning has been the adoption of the more robust radiobiological dose prescription. Radiobiological dose contrasts with physical dose by incorporating the relationship between cellular response factors and dose delivery parameters to better predict treatment outcome (4,5).

2.3 Linear-Quadratic (LQ) Model

The basis for radiobiological dose calculation for cervical cancer radiation is the Linear-Quadratic (LQ) model (6,7). The LQ model was initially developed by both Chadwick and Leenhouts as well as Kellerer and Rossi independently (8,9). It correlates the fraction of cells that survive irradiation (surviving fraction; SF, range of 1 to 0) to the total dose delivered (D). When dose is delivered in a single fraction of radiation, the LQ model is (10):

$$SF = e^{-(\alpha D + \beta D^2)} \tag{2.1}$$

In this equation, SF is the surviving fraction, D is the dose, and the parameters α and β characterize the irradiated cells' radiosensitivity and have units of Gy^{-1} and Gy^{-2}, respectively (10). The values of both α and β are dependent on the cell type and are often combined into the "α/β ratio" (11). Plotting SF against D on a semilogarithmic scale generates a cell survival curve (Figure 2.1). The loss of cells due to the αD component is

called “α damage”, while the quadratic βD^2 term produces additional “β damage”. It can be shown that the amount of α damage equates to the amount of β damage when D equals the α/β ratio. If D is greater than the α/β ratio, then there is more β damage than α damage (and vice versa).

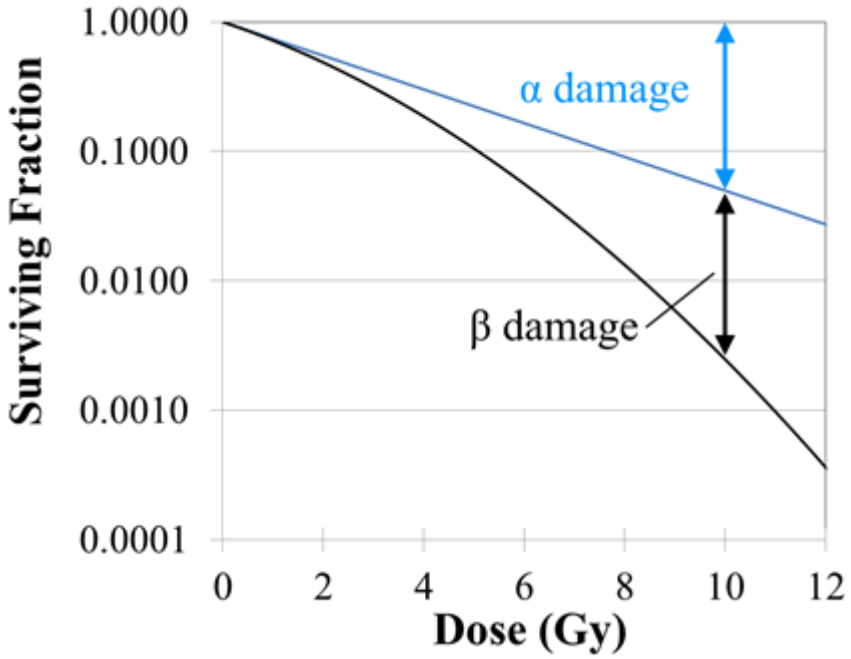

Figure 2.1: Example of surviving fraction in tissue with $\alpha = 0.3\ Gy^{-1}$ and $\alpha/\beta = 10$ Gy. The blue curve represents α damage and blue arrow represents the α damage at 10 Gy. The black curve represents the combined α and β damage while the black arrow represents only β damage at 10 Gy. At 10 Gy, the α and β damages are equal.

2.3.1 Interpretation of the LQ Model

The LQ model uses few parameters and is reasonably well validated for fraction sizes up to 10 Gy (12). This makes the model suitable for the typical dose fraction sizes used in HDR BT for cervical cancer. However, the use of this model requires a discussion of the rationale for the linear and quadratic elements. Chadwick and Leenhouts proposed that the cause of cell death is due to the accumulation of damage in the DNA double helix. Based on this assumption, two causes emerge for a double-strand break: (a) formation in a single radiation event (α damage) and (b) formation through the interaction of two different events where each event creates a single-strand break in the DNA (β damage). Both scenarios are shown in Figure 2.2 below.

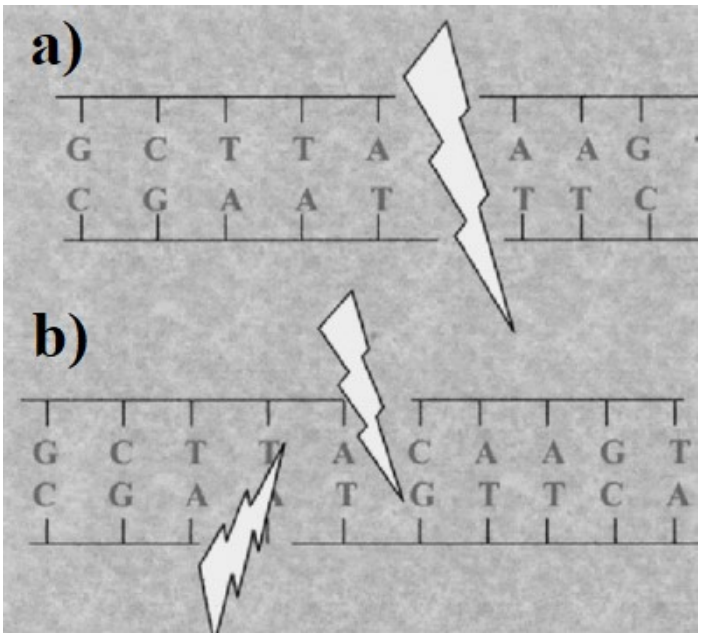

Figure 2.2: Visual representation of theoretical double-strand breaks caused by (a) single radiation events and (b) interaction of multiple single-strand breaks. Each lightning bolt represents a different radiation event. [Reprinted with permission from: Dale R. Use of the linear-quadratic radiobiological model for quantifying kidney response in targeted radiotherapy. *Cancer Biother Radiopharm* 2004;19(3):363-370].

Because a single-strand break is repairable before the formation of a double-strand break, it can be thought of as sublethal damage. By comparison, α damage would describe the formation of lethal damage as a double-strand break that is irreparable.

It should be noted that, while this model assumes that the cause of cell death is the accumulation of double-strand breaks, it is not a complete reflection of the DNA damage process. Chadwick and Leenhouts noted that, at the time of publication, there were no known mechanisms for repairing DNA double-strand breaks (8). However, it has since been determined that double-strand breaks in the DNA can be repaired by the cell through non-homologous end joining (NHEJ) and homologous recombination (13,14,15). Hence, a more general interpretation of the LQ model associates α damage with lethal lesion generation and β damage with the formation of lethal lesions from sublethal lesion interaction.

2.3.2 Modified LQ Model

The calculation of SF in Equation (2.1) assumes a situation where all radiation is delivered in a single acute fraction. However, many radiation schedules are not delivered acutely (e.g. LDR BT) or are fractionated. Both will increase cell survival compared to a single fraction of the same physical dose. Brenner and Hall found a large increase in survival of CHL-F (Chinese hamster) cells *in vitro* when exposed to 20 Gy at a dose rate of 0.36 cGy/min (approximately 4% survival) compared to 107 cGy/min (approximately 0.002%) (4). A method of addressing this limitation in the LQ model is to introduce the generalized Lea-Catcheside time factor, G (a dimensionless value), forming the modified LQ model (12,16):

$$SF = e^{-(\alpha D + \beta G D^2)} \tag{2.2}$$

This modified equation enumerates the impact of dose rate and dose fractionation due to cellular repair of sublethal damage during irradiation through G (12,17). Unlike the α damage, the β damage interactions are modulated by the G factor (17). G, therefore, corresponds to the potential sparing that can occur due to dose fractionation and repair mechanisms for sublethal damage and ranges from 0 to 1; these values are explored in the next section.

2.3.3 Derivation of the Generalized Lea-Catcheside Time Factor

The value of G is essential for analyzing the impact of dose fractionation. Therefore, its derivation is briefly covered in this section.

The number of lethal lesions, N_L, is given by the sum of the lesions formed by a single radiation event, N_α, and the number of interactions between sublethal lesions (N_β) (9):

$$N_L = N_\alpha + N_\beta = \alpha D + \beta G D^2 \tag{2.3}$$

G can therefore be determined by finding N_α and N_β.

The rate of formation of lethal lesions from single radiation events is proportional to the amount of radiation delivered (K_α). Therefore, $dN_\alpha/dt = K_\alpha \dot{D}(t)$, where $\dot{D}(t)$ is the dose rate as a function of time (t). Integrating both sides with respect to time and using the initial condition of 0 lethal lesions formed at time t = 0, $N_\alpha(T) = K_\alpha D$.

The increase in N_β at a given point in time can be taken as the product of the number of sublethal lesions that have been formed at time t ($\dot{N}_{SLL,new}$(t)), the number of previously formed sublethal lesions that remain at time t, $N_{SLL,previous}$(t), and the probability of interaction between sublethal lesions to form a lethal lesion (ε):

$$dN_\beta/dt = \varepsilon \dot{N}_{SLL,new}(\mathrm{t}) N_{SLL,previous}(\mathrm{t}) \tag{2.4}$$

To fully characterize Equation (2.4), functions describing $\dot{N}_{SLL,new}$(t) and $N_{SLL,previous}$(t) must be identified. It is assumed that the number of sublethal lesions formed is proportional to the dose rate. Therefore:

$$\dot{N}_{SLL,new}(\mathrm{t}) = \mathrm{K}_\beta \dot{D}(t) \tag{2.5}$$

where K_β represents the number of sublethal lesions formed per unit of radiation. While $\dot{N}_{SLL,new}$(t) only defines the formation of new sublethal lesions, the value of $N_{SLL,previous}$(t) depends on two factors: the sublethal lesions that have formed previously and the number that have been repaired. Based on this definition, the change in the number of previously generated sublethal lesions at any point in time is given by:

$$dN_{SLL,previous}/dt = \mathrm{K}_\beta \dot{D}(t) - \mu N_{SLL,previous} \tag{2.6}$$

This equation describes two factors influencing the number of sublethal lesions: a formation rate proportional to the dose rate and a first-order repair rate. μ, the time repair constant, has units of hr^{-1} and describes the rate of repair of sublethal lesions. The differential equation may be solved to yield (9):

$$N_{SLL,previous}(t) = \mathrm{K}_\beta e^{-\mu t} \int_{s=0}^{t} ds \dot{D}(s) e^{\mu s} \tag{2.7}$$

where the integral over s represents a summation from time t = 0 to the time t of interest. Substituting Equations (2.5) and (2.7) in Equation (2.4) gives:

$$dN_\beta/dt = \varepsilon \mathrm{K}_\beta \dot{D}(t) \mathrm{K}_\beta e^{-\mu t} \int_{s=0}^{t} ds \dot{D}(s) e^{\mu s} \tag{2.8}$$

Integrating Equation (2.8) with respect to t allows calculation of the total number of lethal lesions produced by β damage (9),

$$N_\beta = \varepsilon \mathrm{K}_\beta{}^2 \int_{t=0}^{T} dt \dot{D}(t) \int_{s=0}^{t} ds \dot{D}(s) e^{\mu(s-t)} \tag{2.9}$$

with T being the time of irradiation. Substitution of N_β in Equation (2.3) yields:

$$\alpha D + \beta G D^2 = \mathrm{K}_\alpha D + \frac{\varepsilon \mathrm{K}_\beta{}^2}{2} \left(\frac{2}{D^2} \int_{t=0}^{T} dt \dot{D}(t) \int_{s=0}^{t} ds \dot{D}(s) e^{\mu(s-t)} \right) D^2 \tag{2.10}$$

If $\alpha = K_\alpha$ and $\beta = \varepsilon K_\beta{}^2/2$, then:

$$G = \frac{2}{D^2}\int_{t=0}^{T} dt\dot{D}(t)\int_{s=0}^{t} ds\dot{D}(s)e^{\mu(s-t)} \quad (2.11)$$

The integral $\int_{s=0}^{t} ds\dot{D}(s)e^{\mu(s-t)}$ in Equation (2.11) represents the sublethal lesion that is formed first and the potential repair it may undergo between time t = s (when it forms) and t (when the second sublethal lesion forms) (17). $dt\dot{D}(t)$ represents the second sublethal lesion that interacts with the first to form a lethal lesion.

The value of the Lea-Catcheside time factor ranges from 0 to 1. The value of 1 represents the scenario of a single acute fraction of radiation, where no repair can occur before all the radiation is delivered, maximizing the β damage that occurs (17). A value of G < 1 represents a reduction in cell killing due to the repair of sublethal lesions. A value of G = 0 represents the unique scenario where no β damage occurs and all cell death occurs by α damage.

2.3.4 Radiobiological Parameters of the Modified LQ Model

The modified LQ model with the generalized Lea-Catcheside time factor calculates SF using the dose rate as a function of time ($\dot{D}(t)$), α, β, and μ. The latter three parameters (α, β, and μ) characterize the response of the irradiated cells to radiation and are dependent on the cell type (5). The calculation of radiobiological dose uses the α/β ratio and $T_{1/2}$ and will be further discussed in this section.

The α/β ratio determines the sensitivity of tissue to dose rate and fractionation: a low α/β ratio corresponds to a potential for significantly less damage when the dose rate or dose fraction size is reduced (18). This is illustrated in Figure 2.3, where the SF for a single acute treatment is plotted against dose for α damage (corresponding to an infinitely large α/β ratio) only, α/β = 10 Gy and α/β = ratio of 3 Gy, assuming α = 0.3 Gy^{-1}. For the same α value, the β damage increases if the α/β ratio decreases. For example, at 10 Gy, the α damage alone results in an SF of approximately 0.05 when α = 0.3 Gy^{-1}. For α/β = 10 and 3 Gy, the β damage would further decrease SF to 0.0025 (5% survival for the cells surviving the α damage) and 2 x 10^{-6} (0.005%), respectively. Therefore, the modified LQ

model suggests that tissues with a lower α/β ratio have greater sparing potential as G decreases.

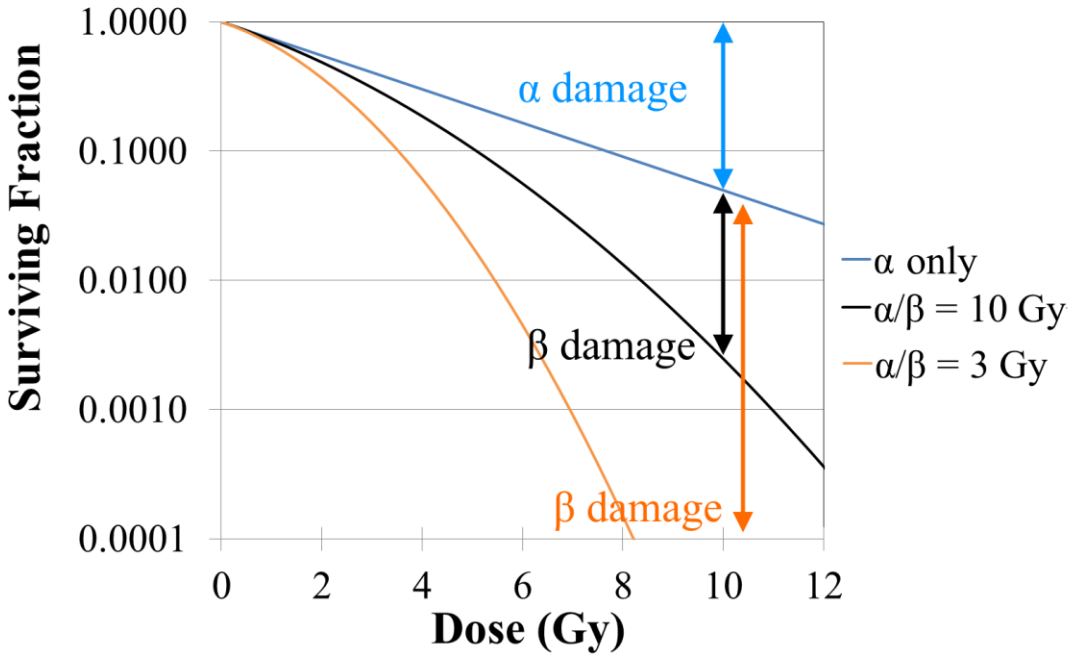

Figure 2.3: Illustration of surviving fraction curves in tissue with only α damage (*i.e.* β = 0), α/β = 10 Gy, and α/β = 3 Gy (with α = 0.3 Gy^{-1} in all three cases). For α/β = 3 Gy, the α and β damage are equivalent at 3 Gy and the β damage is dominant at >3 Gy.

The rate of repair of sublethal lesions is described by μ, which can be expressed in terms of the time required to repair half of the sublethal damage in the tissue assuming a single exponential rate of repair (halftime of repair, $T_{1/2}$) (18,19):

$$\mu = \ln(2) / T_{1/2} \tag{2.12}$$

2.3.5 Limitations of the Modified LQ Model

The modified LQ model has been widely used in radiation therapy and remains the basis of most radiobiological dose calculations. However, there are deviations between experimental and expected results using the model. This section will provide a brief summary of the common criticisms against the modified LQ model.

2.3.5.1 Overestimation of Cell Death at High Doses

The LQ model predicts that response to higher doses of radiation will be dominated by the quadratic component (the β damage). However, it has been previously noted that the LQ model overestimates cell killing at high doses. Park *et al* showed that SF data of irradiated non-small-cell lung cancer (H460), fitted using the LQ model (with data up to 8 Gy; dashed line in Figure 2.4) underestimated survival by an order of magnitude at 18 Gy (20). Furthermore, it was determined that improved survival projections were provided by an alternative survival model that hybridizes the LQ model with the multitarget model to better fit survival at high doses (projection shown in solid black on Figure 2.4; further discussed in Section 2.3.6) (20)

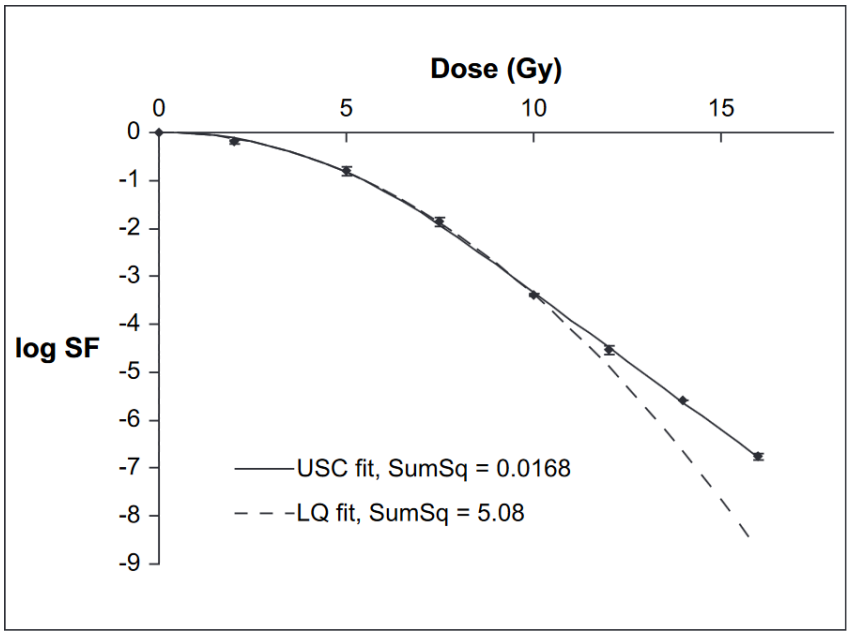

Figure 2.4: Comparison of experimental results and LQ model. The data points are shown as circles and the LQ model fit (performed with data ≤8 Gy) is the dashed line. The solid line shows the fit with the Universal Survival Curve (USC; see Section 2.3.6). [Reprinted with permission from: Park C, Papiez L, Zhang S, Story MM, Timmerman RD. Universal survival curve and single fraction equivalent dose: useful tools in understanding potency of ablative radiotherapy. *Int J Radiat Oncol Biol Phys* 2008;70(3):847-852].

2.3.5.2 Non-Monoexponential Repair Kinetics

The repair rate of sublethal damage in the LQ model is assumed to be monoexponential. However, the possibility of biexponential repair has previously been raised due to

growing evidence of a second repair process in animal studies (18,21). Both Millar *et al* and Pop *et al* have found a biexponential repair rate with a "fast" and a "slow" component of repair when exposing animal cells (mouse kidney cells *in vitro* and rat spinal cord *in vivo*, respectively) (22,23). The discrepancy between the two repair rates may affect calculated SFs in prolonged treatments, such as PDR BT.

2.3.5.3 Reoxygenation

Previous investigation of advanced cervical cancers has shown that patients with progression-free survival had higher hemoglobin levels during treatment than patients who developed a local recurrence (24). Despite this understanding of the effect of hypoxia on treatment outcome, no clinically implemented dose model considers hypoxia or reoxygenation (25). Therefore, the current use of the modified LQ model may overestimate the amount of cell killing that occurs in hypoxic tumors.

2.3.5.4 Cellular Proliferation

It has been long established that, after irradiation, there is an onset of enhanced proliferation (cellular repopulation) in the tumor (26). Denekamp noted that, two weeks after exposure to 3 Gy per day for a week, proliferation of mouse skin cells increased by a factor of 2 (26). The enhanced proliferation results in the reduction in the SF (and therefore treatment effectiveness). In addition, Barendsen conducted a review of multiple single acute and fractionated radiation exposures delivered to mice and rats which reported an LD_{50} (after 21 to 365 days) (5). While a wide range of responses was reported, an average additional 0.5 Gy per day would be required to compensate for proliferation in order to achieve the same LD_{50} in the irradiated tissue (e.g. foot, leg, lung) (5).

The importance of the proliferation effect can also be seen in historical radiobiological dose models. Models such as the Nominal Standard Dose (NSD), Time, Dose, and Fractionation (TDF), and Cumulative Radiation Effect (CRE) correct for the length of treatment (11,27). While modifications may be incorporated in the LQ model and its

associated radiobiological doses (see Section 2.4.3.4), a method of accounting for proliferation is not utilized in the base or modified LQ model (Equations (2.1) and (2.2)).

2.3.6 Alternatives to the LQ Model

More complex cell survival models have been proposed, including the repair-misrepair model (RMR), the lethal-potential lethal model (LPL), the two-lesion kinetics model (TLK), and the linear-quadratic-linear (LQL) (28,29,30,31). Although these more complex models typically reduce to a linear-quadratic form under certain limiting conditions, their predictions often deviate from those of the LQ model at higher doses per fraction, where their accuracy has been contested (32,33). Phenomenological models such as the universal survival curve (USC) have also been developed to better describe the shape of the high dose region of the cell survival relationship (20). Brenner states that the LQ model has been "reasonably well validated" for doses up to 10 Gy per fraction, and is "reasonable for use up to about 18 Gy" (12). As typical EBRT and BT fractions for cervical cancer treatment do not reach these high doses per fraction, it is unclear whether the more complex models will provide further improvements to the calculated radiobiological dose.

2.4 Radiobiological Dose in the LQ Model

The LQ model is the basis for radiobiological dose calculations. The units of radiobiological dose associated with the LQ model are the biologically effective dose (BED) and equieffective dose in 2 Gy fractions (EQD2), radiobiological doses derived from the LQ model. This section will summarize BED, EQD2, and the calculation of BED for HDR, LDR, and PDR BT.

2.4.1 Biologically Effective Dose (BED)

BED is described as the theoretical total dose required to cause the same amount of cell death if the dose was delivered at an infinitesimally low dose rate and in infinitesimally small fractions separated far apart in time (11,34). As these conditions prevent any accumulation and integration of sublethal damage, it may also be considered as the dose required for having the same effect as a given treatment if G equals 0 (and also represents

the maximum possible dose required for the specified biological effect). The equivalency between a physical dose and the BED (D_{BED}) can be obtained by equating the SF for both conditions:

$$SF = e^{-(\alpha D+\beta G D^2)} = e^{-(\alpha D_{BED}+\beta(0) {D_{BED}}^2)} \tag{2.13}$$

D_{BED} is hence determined to be:

$$D_{BED} = D\left(1+\frac{GD}{\alpha/\beta}\right) \tag{2.14}$$

As G is unitless, the units for D_{BED} are the same as D (Gy). To distinguish BED from physical dose, all quantities of BED will be described as "Gy BED". Another interpretation of the relationship between BED and the physical dose is to consider the BED as a product of physical dose and a "relative effectiveness" (RE) factor (5):

$$D_{BED} = D(RE) \tag{2.15}$$

where RE is defined as (10):

$$RE = 1+\frac{\beta \text{ damage}}{\alpha \text{ damage}} = \left(1+\frac{\beta G D^2}{\alpha D}\right) \tag{2.16}$$

In this regard, RE can be considered as the ratio of Gy BED to physical Gy and ranges from 1 (when G = 0) to $1 + D/(\alpha/\beta)$ (when G = 1).

2.4.2 Equieffective Dose in 2 Gy Fractions (EQD2)

While the BED provides a useful metric to compare different treatments, it does not provide an intuitive understanding of the amount of physical radiation required to deliver the radiobiological dose as "infinitesimally low dose rate" treatments in "infinitesimally small fractions" do not exist in radiation oncology. A conversion to 2 Gy fractions, the conventional EBRT fraction size, provides a common ground for comparison with clinical experience (27). The EQD2 provides this translation by converting the BED (dose delivered in infinitesimally small fractions) to the dose required to have the same effect when dose is delivered in 2 Gy well separated fractions (35).

The relationship between EQD2 (D_{EQD2}) and BED is (10,35):

$$D_{EQD2} = D_{BED}/\left(1+(2/(\alpha/\beta))\right) = \frac{D(1+GD/(\alpha/\beta))}{(1+(2/(\alpha/\beta)))} \tag{2.17}$$

All references to units of EQD2 will be in the form of "Gy EDQ2".

2.4.3 BED Equations for Cervical Cancer BT

As shown in Equation (2.14), the calculation of BED for radiation treatments requires determination of the associated G factor. As HDR, LDR, and PDR BT all deliver radiation in widely different treatment schedules, each requires its own derivation of BED.

2.4.3.1 EBRT and HDR BT

EBRT and HDR BT are both high dose rate treatments with fractions well separated in time. Therefore, their BED is calculated in the same manner (6,7). Based on the currently accepted values for $T_{1/2}$ and the sufficiently separated fractionation schedules of EBRT (typically one fraction a day) and HDR (typically, one fraction a day), dose calculations for both treatments assume complete sublethal damage repair in between fractions (36). As a result, the SF following fractionated EBRT or HDR BT could be considered as the product of survival after multiple separate single acute fractions. For a single acute fraction of dose d, $SF = e^{-(\alpha d+\beta d^2)}$, as shown in Equation (2.1). If the second fraction of dose d was delivered after all sublethal damage from the first fraction was repaired, then the SF after 2 fractions ($SF_{2\ fr}$) would be:

$$SF_{2\ \mathrm{fr}} = SF^2 = e^{-2(\alpha d+\beta d^2)} \tag{2.18}$$

If this process was repeated for N fractions, the SF ($SF_{N\ fr}$) would be

$$SF_{N\ \mathrm{fr}} = e^{-N(\alpha d+\beta d^2)} \tag{2.19}$$

By substituting $SF_{N\ fr}$ into Equation (2.13) (11,34):

$$D_{BED} = Nd\left(1+\frac{d}{\alpha/\beta}\right) \tag{2.20}$$

This method of calculating BED applies for both HDR BT ($D_{BED,HDR}$) and EBRT ($D_{BED,EBRT}$). By comparison to Equation (2.14), G for these fractionated treatments equals 1/N. Therefore, the greater the fractionation, the greater the sparing compared to the delivery of a single acute fraction of radiation.

Equation (2.20) assumes a complete repair of sublethal damage between fractions. This may not be true when the time between fractions decreases. If this time is shortened to the point that not all previously generated sublethal lesions are fully repaired before a

new fraction is delivered, sublethal lesions created by two different fractions can interact to form lethal lesions (18).

Two models have been developed to quantify incomplete repair for acute fractions of radiation. The first is the Thames model, which has been previously used in cervical cancer studies (37,38). It introduces the factor H_N to represent the amount of incomplete repair remaining at the start of each fraction assuming monoexponential repair and is based on a generalization of the split dose SF model presented by Oliver (39,40):

$$H_N = \left(\frac{2}{N}\right)\left(\frac{k}{1-k}\right)\left(\frac{N-\left(1-k^N\right)}{1-k}\right) \tag{2.21}$$

where N is the number of fractions and k is a function of the repair rate that depends on the time interval between fractions (x) (39):

$$k = e^{-\mu x} \tag{2.22}$$

The value of H_N is positive and approaches 0 if sufficient time is provided between fractions. The BED formula, including H_N, for an N fraction treatment delivering equal dose d per fraction, is given as (39):

$$D_{BED} = Nd\left(1 + \frac{d(1+H_N)}{\alpha/\beta}\right) \tag{2.23}$$

For fractionated treatments that are sufficiently separated, where complete sublethal damage repair occurs and the value of H_N decreases to 0, Equation (2.23) simplifies to (2.20).

Dale reported an alternative method for quantifying the relative effectiveness for multiple acute fractions of radiation (utilizing Equation (2.16)) (41):

$$RE = 1 + \left(\frac{1}{\alpha/\beta}\right)\left(\frac{d}{N}\right)\left(\frac{N\left(1-k^2\right)-2k\left(1-k^N\right)}{(1-k)^2}\right) \tag{2.24}$$

This value is equivalent to the method of calculating BED derived by Thames (39). If Dale's definition of RE is equated to Equation (2.23) with Equation (2.15), then:

$$D\left(1 + \left(\frac{1}{\alpha/\beta}\right)\left(\frac{d}{N}\right)\left(\frac{N\left(1-k^2\right)-2k\left(1-k^N\right)}{(1-k)^2}\right)\right) = Nd\left(1 + \frac{d(1+H_N)}{\alpha/\beta}\right) \tag{2.25}$$

which can be simplified to:

$$\left(\frac{1}{N}\right)\left(\frac{N\left(1-k^2\right)-2k\left(1-k^N\right)}{(1-k)^2}\right) = 1 + H_N \tag{2.26}$$

When H_N is isolated in Equation (2.26), the value of H_N matches the form in Equation (2.21), validating that both equations are equivalent.

2.4.3.2 LDR BT

Though LDR BT for cervical cancer is not widely used currently, the calculation of BED for LDR BT can provide insight into the derivation of BED for PDR BT.

LDR BT is considered a single continuous irradiation that starts at time t = 0, has a duration period of T, and delivers radiation at a constant dose rate of R. From Equation (2.11), the value of the generalized Lea-Catcheside time factor becomes:

$$\mathrm{G} = 2\frac{R^2}{D^2}\int_{t=0}^{T} dt \int_{s=0}^{t} ds e^{\mu(s-t)} \tag{2.27}$$

Solving the second integration yields:

$$\mathrm{G} = 2\frac{R^2}{D^2}\int_{t=0}^{T} dt \frac{1-e^{-\mu t}}{\mu} \tag{2.28}$$

The final form of G, on solving the integration in Equation (2.28), is:

$$\mathrm{G} = 2\frac{R^2}{D^2}\frac{\mu T + e^{-\mu T} - 1}{\mu^2} \tag{2.29}$$

The BED for LDR ($D_{BED,LDR}$) is obtained by substituting this value of G in Equation (2.14):

$$D_{BED,LDR} = D\left(1 + 2\frac{R\mu T + Re^{-\mu T} - R}{D\mu^2}\frac{R}{\alpha/\beta}\right) \tag{2.30}$$

which simplifies to (through substitution of $R = D/T$):

$$D_{BED,LDR} = D\left(1 + \frac{2}{\mu T}\left(\mathrm{T} - \frac{1}{\mu T}[1 - e^{-\mu T}]\right)\frac{D}{\alpha/\beta}\right) \tag{2.31}$$

2.4.3.3 PDR BT

In PDR BT, multiple characteristics of the treatment delivery must be considered, such as the number of pulses (N), length of each pulse (T), dose rate during the pulse (R), and time between the end of one pulse to the start of the next (pulse interval; x). This derivation will follow the one detailed by Dale *et al,* which calculates the amount of β damage and α damage that occurred, and then substitutes the results into Equation (2.16) (42). It is assumed that multiple equal pulses are delivered regularly (e.g. hourly) and that the dose rate during a pulse is constant.

The β damage generated during each pulse is determined in the same manner as for a protracted fraction of radiation (41). All potential lethal β damage is characterized as a series of paired sites for radiation to "hit". The damage depends on the number of targets hit after irradiation: no damage occurs if neither target is hit (Figure 2.5(a)), sublethal damage occurs only if one site is hit (Figure 2.5(b)), while damage to both sites results in lethal damage (Figure 2.5(c)).

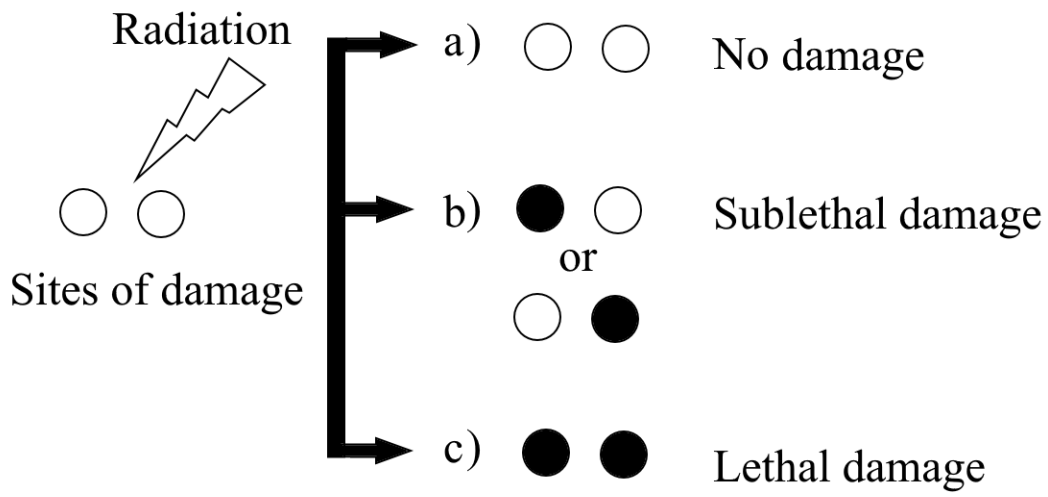

Figure 2.5: Sites of sublethal damage during irradiation appearing in the derivation of relative effectiveness by Dale *et al* (42). Radiation hits on two potential sites (open circles) may result in (a) no damage if neither site is hit, (b) sublethal damage if one site is hit, and (c) lethal damage if both sites are hit. Lethal damage on a site is indicated by the filled black circles.

In a short time dt, the probability of sublethal damage in either site ($P_{sublethal}$) is given by $P_{sublethal} = 2pRdt$, where p is the probability that a sublethal event occurs per unit dose (assumed to be small) (41). However, the repair is monoexponential (sublethal repair decays with respect to time at a rate of $e^{-\mu t}$). Therefore, the probability that the sublethal damage forms but does not get repaired by time t is given by:

$$P_{sublethal}(t) = 2pRe^{-\mu t}dt \tag{2.32}$$

While this characterizes the damage after irradiation for a short time, pulses are usually prolonged. Therefore, the probability that sublethal damage has occurred and is not

repaired after continuous irradiation for a length of time T is given by the integration of Equation (2.32) in t (41):

$$P_{sublethal}(T) = \int_{t=0}^{T} 2pRe^{-\mu t}dt = \frac{2pR}{\mu}(1 - e^{-\mu t}) \quad (2.33)$$

In PDR BT, sublethal damage repair continues during the interval between pulses, x, when no radiation is delivered. Therefore, the probability that the radiation damage remains is $\frac{2pR}{\mu}YK$, where $K = e^{-\mu x}$ and $Y = 1 - e^{-\mu T}$. After the second pulse of radiation, the probability of sublethal damage (again, assuming that p is small) is approximately the sum of the probability of sublethal damage forming from the first pulse and the second pulse:

$$P_{sublethal}(t) = \frac{2pR}{\mu}YKe^{-\mu t} + \frac{2pR}{\mu}(1 - e^{-\mu t}) \quad (2.34)$$

At any point in time, the second target may also be inflicted a sublethal damage, which occurs with a possibility of pRdt. Therefore, the probability of lethal damage in a single potential lethal lesion site, P_{lethal}, during the second pulse is:

$$P_{lethal}(t) = \varepsilon\left[\frac{2pR}{\mu}YKe^{-\mu t} + \frac{2pR}{\mu}(1 - e^{-\mu t})\right]pRdt \quad (2.35)$$

where ε is the probability of interaction. If there are n sites for interaction, then the number of interactions during the second pulse (β damage; B(2)) is given by:

$$B(2) = \varepsilon n\frac{2p^2R^2}{\mu}\int_{t=0}^{T}[YKe^{-\mu t} + 1 - e^{-\mu t}]dt = \frac{2\beta R^2}{\mu}\left[T - \frac{1}{\mu}(Y - KY^2)\right] \quad (2.36)$$

where t = 0 is defined as the beginning of the second pulse and $\beta = n\varepsilon p^2$. If additional pulses are added and $z = e^{-\mu T}$, B(N) for the N^{th} pulse has the following results:

$$B(1) = \frac{2\beta R^2}{\mu}\left[T - \frac{1}{\mu}(Y)\right] \quad (2.37)$$

$$B(2) = \frac{2\beta R^2}{\mu}\left[T - \frac{1}{\mu}(Y - KY^2)\right] \quad (2.38)$$

$$B(3) = \frac{2\beta R^2}{\mu}\left[T - \frac{1}{\mu}(Y - KY^2 - K^2zY^2)\right] \quad (2.39)$$

Therefore, for N pulses:

$$B(N) = \frac{2\beta R^2}{\mu}\left[T - \frac{1}{\mu}(Y - KY^2 - K^2zY^2 - \cdots - K^{N-1}z^{N-2}Y^2)\right] \quad (2.40)$$

The sum of all β damage from all N pulses (TB) is then given as the sum of B(1) to B(N):

$$TB(N) = \frac{2\beta R^2}{\mu}\left[NT - \frac{1}{\mu}(NY - (N-1)KY^2 - (N-2)K^2zY^2 - \cdots - K^{N-1}z^{N-2}Y^2)\right] \tag{2.41}$$

This may be simplified to (42):

$$B(N) = \frac{2\beta R^2}{\mu}\left[NT - \frac{1}{\mu}(NY - SY^2)\right] \tag{2.42}$$

where S is given by (42):

$$S = \frac{NK - K - NK^2z + K^{N+1}z^N}{(1-Kz)^2} \tag{2.43}$$

To calculate RE, the α damage must be determined as well, which is proportional to the total dose, and is thus given by αNRT (42). Substituting the α and β damages into Equation (2.16), the BED for PDR, $D_{BED,PDR}$, can be calculated using Equation (2.15):

$$D_{BED,PDR} = NRT\left(1 + \frac{\frac{2\beta R^2}{\mu}\left[NT - \frac{1}{\mu}(NY - SY^2)\right]}{\alpha NRT}\right) = Nd_p\left(1 + \frac{d_p\left(\frac{2}{\mu T}\right)\left[1 - \frac{1}{N\mu T}(NY - SY^2)\right]}{(\alpha/\beta)}\right) \tag{2.44}$$

where d_p is the dose per pulse (R/T). Following the definition in Equation (2.14), the value of G for PDR can be given as:

$$G = \frac{2\left[1 - \frac{1}{N\mu T}(NY - SY^2)\right]}{N\mu T} \tag{2.45}$$

2.4.3.4 Proposed Proliferation Correction for BED Calculations

It has been previously demonstrated that after irradiation, there is an onset of enhanced tumor proliferation (26). This proliferation can replace cells lost to radiation and reduce the effectiveness of a radiation treatment. As Fowler notes, lack of consideration for the OTT in the base form of the LQ model is a major criticism as longer treatments may have to contend with a greater amount of proliferation (27). An example was shown in Chapter 1, where the extension of OTT by 1 week correlated to a decrease in the HR-CTV D90 of 5 Gy EQD2 (43).

Fowler introduced a simple modification to the LQ model to include OTT by introducing an exponential factor into the LQ model that "works in the reverse direction to the killing effect of radiation", $e^{\gamma\Delta T}$ (11). γ represents the rate of enhanced proliferation of the tumor after radiation and ΔT represents the duration the tumor undergoes accelerated proliferation (11). When applied to Equation (2.2):

$$SF = e^{-(\alpha D+\beta G D^2)} e^{\gamma \Delta T} \tag{2.46}$$

γ is defined similarly to $T_{1/2}$, assuming monoexponential growth in the tumor after irradiation:

$$\gamma = \ln(2) / T_{pot} \tag{2.47}$$

where T_{pot} is the "potential doubling time", the time required to double the number of proliferating cells in the absence of spontaneous cell loss (44).

The value of ΔT was given by Fowler as (11):

$$\Delta T = \begin{cases} OTT - T_{kickoff}, OTT > T_{kickoff} \\ 0, \ OTT \leq T_{kickoff} \end{cases} \tag{2.48}$$

where $T_{kickoff}$ is the "kickoff time", the length of time between radiation delivery and the start of increased tumor proliferation. It is assumed that there is no proliferation prior to this time.

The impact of the proliferation on BED can be determined by redefining D_{BED} (Equation (2.13)) with the inclusion of the proliferation correction factor:

$$SF = e^{-(\alpha D+\beta G D^2-\gamma \Delta T)} = e^{-(\alpha D_{BED}+\beta(0) {D_{BED}}^2)} \tag{2.49}$$

Once again isolating for D_{BED} yields (11):

$$D_{BED} = D\left(1 + \frac{GD}{\alpha/\beta}\right) - \frac{\ln(2)\Delta T}{T_{pot}\alpha} = D_{BED,0} - \frac{\ln(2)\Delta T}{T_{pot}\alpha} \tag{2.50}$$

where $D_{BED,0}$ represents the dose without proliferation correction. Typically, cervical cancer treatments including EBRT and the BT boost can be completed within 7 – 8 weeks (6). It should be noted that the OTT used in Equation (2.48) is simply the time interval between the first and final fractions of radiation treatment. Thus, for a given OTT, any differences in how the treatments are scheduled or delivered are ignored in the calculation of the proliferation correction. In other words, a delay towards the start of treatment would be treated as equivalent to the same length of delay towards the end of treatment. Underlying this is the assumption of simple exponential repopulation dynamics (after $T_{kickoff}$) that produce the commonly reported linear reduction in radiobiological dose as a function of OTT (e.g. a given dose per day) (5,11,45).

The direct application of a proliferation factor in clinical prescription is not common and is instead provided in terms of OTT limits. The EMBRACE II guidelines highlight the need to limit the OTT to less than 50 days (7).

2.5 Application of Radiobiological Dose in Cervical Cancer

Section 2.4 provides a framework to calculate radiobiological dose for a single component of treatment. However, the sole use of EBRT or BT alone is uncommon outside of radical BT for locally advanced cervical cancer (6). The use of radiobiological dose, in particular BED and EQD2, allows for the summation of both radiation techniques. This section will summarize the application of radiobiological dose to cervical cancer radiation treatments.

2.5.1 Conventional Parameter Assumptions

The calculation of radiobiological dose requires the α/β ratio and, for all situations outside of well separated fractions, $T_{1/2}$. A wide range of values, for both tumor and normal tissue, have been identified in the literature for these parameters (46,47,48). Kelland and Steel irradiated multiple cervical cancer cells, acquired via biopsy, *in vitro*. By fitting the results to the modified LQ model, α/β ratios were found to be in the range of 6.0 to 16.5 Gy and $T_{1/2}$ values from 0.26 to 5.7 hours. A similar wide range was found for surrounding normal tissue. By fitting the Lyman-Kutcher-Burman model to normal tissue complications of rectal damage (grade 2 or higher toxicity), Marzi *et al* and Tucker *et al* found α/β ratios of 2.3 and 4.8 Gy, respectively (47,48). In addition, Fowler reported the most likely $T_{1/2}$ of rectal and bladder tissue ranged between 1.5 to 2.5 hours when assuming an α/β ratio of 2 to 4 Gy (49). However, Roberts *et al*, found a most likely value of normal tissue $T_{1/2}$ to be 0.5 hours assuming an α/β ratio of 3 Gy (50).

The conventionally assumed values for α/β are 10 Gy for the tumor and 3 Gy for the OARs, while $T_{1/2}$ is taken as 1.5 hours for both tissues (6,7). The gynecological GEC-ESTRO working group also uses these values (51). Fowler noted that the selection of $T_{1/2}$ = 1.5 hours has been assumed for many years without precise justification beyond a lack of contradicting clinical evidence (49).

2.5.2 Sample Dose Calculation

As noted in Chapter 1, current dose prescriptions for targets and tolerance dose limits for OARs are given in units of Gy EQD2 for a combined course of EBRT and BT boost. An example (dose to the HR-CTV) is given in this section to highlight the application of Section 2.4. Consider a radiation treatment including EBRT and BT delivered to the HR-CTV. The EBRT dose of 45 Gy in 1.8 Gy daily fractions is delivered over 5 weeks. This is followed by a PDR BT boost delivered in 58 hourly pulses of 0.73 Gy/pulse to the HR-CTV D90. Let the pulse delivery period be 15 min/pulse. Assuming the conventional radiobiological parameters for tumor (α/β = 10 Gy, $T_{1/2}$ = 1.5 hours), the EBRT delivers 44.2 Gy EQD2 while the PDR delivers 46.1 Gy EQD2. The combined dose from EBRT and BT to the HR-CTV D90 is thus 90.3 Gy EQD2, which meets the dose recommendations of the EMBRACE II study (7). Assuming no interruptions, the overall treatment can be completed in 38 days (5 weeks of EBRT delivered on weekdays, followed by BT as soon as possible in week 6) which is less than the recommended OTT of 50 days (7).

2.5.3 Calculation of Equivalency Between BT Treatments

The definition of BED (and therefore EQD2) in Equation (2.14) states that two treatments that have the same radiobiological dose will have the same SF in the irradiated tissue. This would suggest that the two treatments would also have equivalent radiobiological outcomes, allowing for the conversion of one treatment to another. For example, the radiobiological dose delivered by a four fraction HDR BT treatment of 7.75 Gy each to the HR-CTV D90 would be similar to a 58 pulse PDR BT delivering 0.73 Gy/pulse (45.9 vs 46.1 Gy EQD2, respectively).

2.5.3.1 Theoretical Advantage of PDR over HDR BT

As noted in Chapter 1, PDR BT's lower hourly dose rate could reduce OAR toxicity compared to HDR BT (52). This can be seen by comparing the radiobiological dose delivered during a BT boost.

Consider the two BT boosts discussed in Section 2.5.3. Assuming the conventional radiobiological parameter values, the radiobiological dose to the tumor is approximately the same for these two treatments. However, if the same BT boost dose was received by an OAR (conventional $\alpha/\beta = 3$ Gy), a higher radiobiological dose would be delivered by HDR (66.7 Gy EQD2) than by PDR (51.4 Gy EQD2). This suggests that, when delivering the same tumor dose, PDR BT may reduce the dose delivered to the OARs, thereby reducing the potential radiation damage to normal tissue.

While the discussion involved the OAR receiving the same dose as the HR-CTV D90, the same trend in the results occurs when the OAR dose is reduced. Guerrero and Li introduced a "sparing factor", the reduction of dose that an OARs receives compared to the tumor dose, in order to explain inconsistencies in the reported OAR $T_{1/2}$ (53). If a sparing factor of 0.7 was used (i.e. physical dose to the OAR was 70% of the tumor), as determined by Guerrero and Li to yield a consistent $T_{1/2}$ in their analysis of previous studies, the same theoretical advantages of PDR remain, i.e. HDR (36.6 Gy EQD2) still delivers a higher radiobiological dose than PDR (30.5 Gy EQD2).

2.6 Thesis Objective

There is currently a wide range of radiobiological parameter values reported for cervical cancer and OARs (further discussed in Chapter 3). However, the conventionally selected parameter values have been primarily assumed for many years despite a lack of direct supporting evidence (49). Yet there have been minimal studies exploring the impacts of these parameter variances. The use of radiobiologically-oriented dose prescriptions demands a mature understanding of the underlying radiobiological model and its limitations. Appreciating how the dose modeling process can lead to misestimation of cellular dose effects, and in turn, treatment outcomes, can help clinical teams design more robust radiation treatment regimens for curing locally advanced cervical cancer.

This research aims to generate a theoretical and practical correlation between the radiobiological parameters used in radiotherapy dose prescription and cervical cancer treatment outcomes. A comprehensive evaluation of radiobiological dose calculation and

the associated parameters was conducted, a study that has not been performed previously. Additionally, the lack of justification for recommended radiobiological parameter values was addressed through a series of radiation experiments on cervical cancer cell lines in conditions closely replicating clinical treatments using HDR and PDR BT. This produced data to derive radiobiological parameters and was conducted in three parts to address the concerns identified above:

A. **Radiobiological dose modeling and dosimetry study:** Evaluate the effect of radiobiological parameter uncertainties on the estimated efficacy of different cervical cancer BT treatment regimens (varying dose rates, fractionation schemes, and OTT).
B. **Experimental investigation of biological parameters:** Evaluate biological responses of cervical cancer tumor tissue when treated with different doses and dose rates in order to reduce uncertainties identified in the radiobiological modeling and dosimetry study.
C. **Comprehensive estimation of uncertainties associated with cell survival experiments:** Identify and determine the uncertainties involved in the preparation of the cells, irradiation of the cells, and counting of the cell colonies after irradiation.

2.7 References

(1) Tarbell NJ, Amato DA, Down JD, Mauch P, Hellman S. Fractionation and dose rate effects in mice: a model for bone marrow transplantation in man. *Int J Radiat Oncol Biol Phys* 1987;13(7):1065-1069.

(2) Nag S. High dose rate brachytherapy: Its clinical applications and treatment guidelines. *Technol Cancer Res Treat* 2004;3(3):269-287.

(3) Lockhart SP, Down JD, Steel GG. The effect of low dose-rate and cyclophosphamide on the radiation tolerance of the mouse lung. *Int J Radiat Oncol Biol Phys* 1986;12(8):1437-1440.

(4) Hall EJ, Brenner DJ. The dose-rate effect revisited: Radiobiological considerations of importance in radiotherapy. *Int J Radiat Oncol Biol Phys* 1991;21(6):1403-1414.

(5) Barendsen GW. Dose fractionation, dose rate and iso-effect relationships for normal tissue responses. *Int J Radiat Oncol Biol Phys* 1982;8(11):1981-1997.

(6) International commission on radiation units & measurements. Report 89: Prescribing, recording, and reporting brachytherapy for cancer of the cervix. *J of the ICRU* 2013; 13:1-258.

(7) Pötter R, Tanderup K, Kirisits C, de Leeuw A, Kirchheiner K, Nout R, *et al* The EMBRACE II study: The outcome and prospect of two decades of evolution within the GEC-ESTRO GYN working group and the EMBRACE studies. *Clin Transl Radiat Oncol* 2018;9:48-60.

(8) Chadwick KH, Leenhouts HP. A molecular theory of cell survival. *Phys Med Biol* 1973;18(1):78-87.

(9) Kellerer AM, Rossi HH. RBE and the primary mechanism of radiation action. *Radiat Res* 1971;47(1):15-34.

(10) Dale RG. The application of the linear-quadratic dose-effect equation to fractionated and protracted radiotherapy. *Br J Radiol* 1985;58(690):515-528.

(11) Fowler JF. The linear-quadratic formula and progress in fractionated radiotherapy. *Br J Radiol* 1989;62(740):679-694.

(12) Brenner DJ. The linear-quadratic model is an appropriate methodology for determining isoeffective doses at large doses per fraction. *Semin Radiat Oncol* 2008;18(4):234-239.

(13) Szostak JW, Orr-Weaver TL, Rothstein RJ, Stahl FW. The double-strand-break repair model for recombination. *Cell* 1983;33(1):25-35.

(14) Li X, Heyer WD. Homologous recombination in DNA repair and DNA damage tolerance. *Cell Res* 2008;18(1):99-113.

(15) Chang HHY, Pannuzio NR, Adachi N, Lieber MR. Non-homologous DNA end joining and alternative pathways to double-strand break repair. *Nat Rev Mol Cell Biol* 2017;18(8):495-406.

(16) Lea DE, Catcheside DG. The mechanism of the induction by radiation of chromosome aberrations inTradescantia. *J Genet* 1942;44:216-245.

(17) Brenner DJ, Hlatky LR, Hahnfeldt PJ, Huang Y, Sachs RK. The linear-quadratic model and most other common radiobiological models result in similar predictions of time-dose relationships. *Radiat Res* 1998;150(1):83-91.

(18) Dale RG, Jones B. The clinical radiobiology of brachytherapy. *Br J Radiol* 1998;71(845):465-483.

(19) Thames HD, Bentzen SM, Turesson I, Overgaard M, Van den Bogaert W. Time-dose factors in radiotherapy: A review of the human data. *Radiother Oncol* 1990;19(3):219-235 .

(20) Park C, Papiez L, Zhang S, Story MM, Timmerman RD. Universal survival curve and single fraction equivalent dose: useful tools in understanding potency of ablative radiotherapy. *Int J Radiat Oncol Biol Phys* 2008;70(3):847-852.

(21) Fowler JF. Repair between dose fractions: A simpler method of analyzing and reporting apparently biexponential repair. *Radiat Res* 2002;158(2):141-151.

(22) Millar WT, Jen YM, Hendry JH, Canney PA. Two components of repair in irradiated kidney colony-forming cells. *Int J Radiat Biol* 1994;66(2):189-196.

(23) Pop LA, Millar WT, van der Plas M, van der Kogel AJl. Radiation tolerance of rat spinal cord to pulsed dose rate (PDR) brachytherapy: the impact of differences in temporal dose distribution. *Radiother Oncol* 2000;55(3):301-315.

(24) Winter 3rd WE, Maxwell GL, Tian CC, Sobel E, Rose GS, Thomas G, *et al*. Association of hemoglobin level with survival in cervical carcinoma patients treated with concurrent cisplatin and radiotherapy: a gynecologic oncology group study. *Gynecol Oncol* 2004;94(2):495-501.

(25) Guerrero M, Carlson DJ. A radiobiological model of reoxygenation and fractionation effects. *Med Phys* 2017;44(5):2002-2010.

(26) Denekamp J. Cell kinetics and radiation biology. *Int J Radiat Biol Relat Stud Phys Chem Med* 1986;49(2):357-380.

(27) Fowler JF. 21 years of biologically effective dose. *Br J Radiol* 2010;83(991):554-568.

(28) Tobias CA. The Repair-misrepair model in radiobiology: comparison to other models. *Radiat Res Suppl* 1985;8:S77-95.

(29) Curtis SB. Lethal and potentially lethal lesions induced by radiation--a unified repair model. *Radiat Res* 1986;106(2):252-270.

(30) Stewart RD. Two-lesion kinetic model of double-strand break rejoining and cell killing. *Radiat Res* 2001;156(4):365-378.

(31) Carlone M, Wilkins D, Raaphorst P. The modified linear-quadratic model of Guerrero and Li can be derived from a mechanistic basis and exhibits linear-quadratic-linear behaviour. *Phys Med Biol* 2005;50(10):L9-L13.

(32) Kirkpatrick JP, Meyer JH, Marks LB. The linear-quadratic model is inappropriate to model high dose per fraction effects in radiosurgery. *Semin Radiat Oncol* 2008;18(4):240-243.

(33) Song CW, Cho LC, Yuan J, Dusenbery KE, Griffin RJ, Levitt SH. Radiobiology of stereotactic body radiation therapy/stereotactic radiosurgery and the linear-quadratic model. *Int J Radiat Oncol Biol Phys* 2013;87(1):18-19.

(34) Joiner M, Kogel A. Basic clinical radiobiology. 4th ed. Boca Raton: CRC Press/Taylor & Francis Group; 2009.

(35) Withers HR, Thames Jr HD, Peters LJ. A new isoeffect curve for change in dose per fraction. *Radiother Oncol* 1983;1(2):187-191.

(36) Banerjee R, Kamrava M. Brachytherapy in the treatment of cervical cancer: a review. *Int J Women's Health* 2014;6:555-564.

(37) Lindblom E, Dasu A, Beskow C, Toma-Dasu I. High brachytherapy doses can counteract hypoxia in cervical cancer—a modelling study. *Phys Med Biol* 2016;62(2):560-572.

(38) Skowronek J, Malicki J, Piotrowski T. Values of biologically equivalent doses in healthy tissues: Comparison of PDR and HDR brachytherapy techniques. *Brachytherapy* 2010;9(2):165-170.

(39) Thames HD. An 'incomplete-repair' model for survival after fractionated and continuous irradiations. *Int J Radiat Biol Relat Stud Phys Chem Med* 1985;47(3):319-339.

(40) Oliver R. A comparison of the effects of acute and protracted gamma-radiation on the growth of seedlings of Vicia Faba. Part II Theroetical Calcualtions. *Int J Radiat Biol Relat Stud Phys Chem Med* 1964;8:475-499.

(41) Dale RG. The application of the linear-quadratic model to fractionated radiotherapy where there is incomplete normal tissue recovery between fractions, and possible implications for treatments involving multiple fractions per day. *Br J Radiol* 1986;59(705):919-927.

(42) Dale RG, Huczkowski J, Trott KR. Possible dose rate dependence of recovery kinetics as deduced from a preliminary analysis of the effects of fractionated irradiations at varying dose rates. *Br J Radiol* 1988;61(722):153-157.

(43) Tanderup K, Fokdal LU, Sturdza A, Haie-Meder C, Nazeron R, van Limbergen E, *et al*. Effect of tumor dose, volume and overall treatment time on local control after radiochemotherapy including MRI guided brachytherapy of locally advanced cervical cancer. *Radiother Oncol* 2016;120(3):441-446.

(44) Brady L, Yaeger T. Encyclopedia of radiation oncology. Springer, Heidelberg, Dordrecht London, New York: Springer-Verlag Berlin, Heidelberg; 2013.

(45) Travis EL, Tucker SL. Isoeffect models and fractionated radiation therapy. *Int J Radiat Oncol Biol Phys* 1987;13(2):283-287.

(46) Kelland LR, Steel GG. Differences in radiation response among human cervix carcinoma cell lines. *Radiother Oncol* 1988;13(2):225-232.

(47) Marzi S, Saracino B, Perongari MG, Arcangeli S, Gomellini S, Arcangeli G, *et al*. Modeling of alpha/beta for late rectal toxicity from a randomized phase II study: conventional versus hypofractionated scheme for localized prostate cancer. *J Exp Clin Cancer Res* 2009;28(1):117.

(48) Tucker SL, Thames HD, Michalski JM, Bosch WR, Mohan R, Winter K, *et al*. Estimation of α/β for late rectal toxicity based on RTOG 94-06. *Int J Radiat Oncol Biol Phys* 2011;81(2):600-605.

(49) Fowler JF. Dose reduction factors when increasing dose rate in LDR or MDR brachytherapy of carcinoma of the cervix. *Radiother Oncol* 1997;45(1):49-54.

(50) Roberts SA, Hendry JH, Swindell R, Wilkinson JM, Hunter RD. Compensation for changes in dose-rate in radical low-dose-rate brachytherapy: A radiobiological analysis of a randomised clinical trial. *Radiother Oncol* 2004;70(1):63-74.

(51) Pötter R, Haie-Meder C, Van Limbergen E, Barillot I, De Brabandere M, Dimopoulos J, *et al*. Recommendations from gynaecological (GYN) GEC ESTRO working group (II): concepts and terms in 3D image-based treatment planning in cervix cancer brachytherapy-3D dose volume parameters and aspects of 3D image-based anatomy, radiation physics, radiobiology. *Radiother Oncol* 2006;78(1):67-77.

(52) Brenner DJ, Hall EJ. Conditions for the equivalence of continuous to pulsed low dose rate brachytherapy. *Int J Radiat Oncol Biol Phys* 1991;20(1):181-190.

(53) Guerrero M, Li XA. Halftime for repair of sublethal damage in normal bladder and rectum: an analysis of clinical data from cervix brachytherapy. *Phys Med Biol* 2006;51(16):4063-4071.

CHAPTER 3
PREVIOUSLY REPORTED PARAMETER VALUES AND THEIR IMPACT ON RADIOBIOLOGICAL DOSE

A version of this chapter has been published as: Chow B, Warkentin B, Menon G. Radiobiological dose calculation parameters for cervix cancer brachytherapy: A systematic review. Brachytherapy 2019;18(4):546-558.

3.1 Introduction

The use of radiobiological dose prescriptions in cervical cancer treatment planning represents an important dosimetric change as it incorporates the relationship between cellular response factors and dose delivery parameters to better predict treatment outcomes (1,2). Clinical outcomes data suggest that such factors play a significant role in cervical cancer patient outcomes (3,4,5). Therefore, their incorporation combined with accurate parameter selection is essential for meaningful dosimetry comparisons of different BT treatments.

The calculation of radiobiological dose, either BED or EQD2, requires the use of several parameters. This includes parameters characterizing the treatment (e.g. pulse time of PDR BT, overall treatment time) and radiobiological parameters characterizing the dose response of irradiated tissue (e.g. α, β, $T_{1/2}$). While there are recommended parameter values, they are not definitive (6,7).

An increasing reliance on radiobiological dose, and therefore on the assumed radiobiological parameter values, highlights the necessity of a full understanding of the underlying radiobiological models; variances in the assumed radiobiological parameter values can strongly affect the calculated dose (8,9). Uncertainties in radiobiological parameters and discrepancies between the conventionally assumed values and experimentally determined results (as seen in Tables 3.1 to 3.5) could affect the equivalency in delivered radiobiological dose between treatments and, therefore, clinical outcome. Despite this, there has been no comprehensive evaluation of all the radiobiological parameters associated with cervical cancer BT. As such, a detailed review of the published values of radiobiological parameters and their potential impact

on calculated radiobiological dose is necessary. This chapter provides context to the radiobiological parameter values shown in Tables 3.1 to 3.5, summarizes the potential variance in radiobiological dose that may occur in clinical dose calculations when using the parameter values reported, and highlights potential pitfalls in the current approach to dose calculation.

3.2 Estimation of Parameters Used in Dose Calculation

3.2.1 α and β

Estimation of the α/β ratio of cervical cancers generally includes the estimation of the two parameters α and β. Multiple groups have investigated values of α and β for cervical cancer tumors with more studies focused on α estimation as it is important for radiobiological dose calculations when proliferation is considered. For five cervical cancer strains tested *in vitro*, Kelland and Steel found a median [min - max] α value of 0.33 [0.18 - 0.61] Gy^{-1} and a median β value of 0.026 [0.020 - 0.069] Gy^{-2} (10). Chapman and Nahum used West *et al*'s experimental data on surviving fractions to get an α value of 0.35 ± 0.21 Gy^{-1} and a β value of 0.06 Gy^{-2} (no standard deviation provided) for cervical cancer tissue (11,12). Similarly, Roberts *et al*, in a clinical outcomes study, estimated the α value of cervical cancer tumors to be 0.13 [95% confidence interval (CI) of 0.06 - 0.20] Gy^{-1} when assuming a $T_{1/2}$ of 1.5 hr (13). Hall and Giaccia have stated that an α value of 0.3 ± 0.1 Gy^{-1} was reasonable for all tissue when used in the LQ model (14). Similar values were referenced by Gasinska *et al*, who assumed an α value of 0.2 Gy^{-1} for radioresistant tissues and 0.3 - 0.4 Gy^{-1} for radiosensitive tissue (15).

The value of the α/β ratio can vary widely depending on the type of tissue (16). Late responding normal tissue is associated with an α/β ratio of 1 to 6 Gy and early responding normal tissue has been found to have an α/β ratio ranging from 7 to 10 Gy (6). Tumors typically have α/β ratios similar to early responding normal tissue and are often within the range of 7 to 20 Gy (6). As noted previously, Kelland and Steel determined the values of α and β for a series of *in vitro* experiments of human cervical cancer cell lines using LDR treatment to establish a median α/β ratio of 11.5 [6.0 - 16.5] Gy (10). Conventionally, including the values recommended in the ICRU 89 report, α/β ratios of 3 and 10 Gy are used for late and early responding tissue (including tumors), respectively (6,7).

3.2.2 $T_{1/2}$

The conventional value of 1.5 hours for $T_{1/2}$ is recommended by GEC-ESTRO (6). According to Fowler, this has been assumed for many years "with no precise justification except its failure to contradict clinical information" (17). There is a significant discrepancy between the experimental and recommended values for $T_{1/2}$ for tumor cells. The previously mentioned study by Kelland and Steel determined a median $T_{1/2}$ of 1.9 [0.26 - 5.7] hours (10). Based on clinical outcomes, Roberts *et al* determined the highest likelihood of $T_{1/2}$ for tumor cells to be 0.25 hours if the conventional α/β ratio of 10 Gy was assumed, while a $T_{1/2}$ of 1.5 hours was likely only if the α/β ratio was over 50 Gy (13).

The $T_{1/2}$ for normal tissue is similarly contested. Considering the increase in reported complications in the vagina, urinary tract, and bowel in a clinical outcomes study involving different LDR BT treatments for cervical cancer, Fowler estimated $T_{1/2}$ to likely range from 1.5 to 2.5 hours (17). However, Roberts *et al* indicated that, assuming an α/β ratio of 3 Gy, the most likely range of $T_{1/2}$ values for normal tissue was 0.32 to 1.11 hours (13). Guerrero and Li bridged this inconsistency in results through the introduction of a sparing factor (see Section 2.5.3.1), the reduction of physical dose received in normal tissue compared to the tumor, into Fowler's calculations (18). Based on their investigation, they estimated the halftime of repair for normal bladder and rectum tissue to be in the range of 0.20 to 0.40 hours, assuming an α/β ratio of 3 Gy.

3.2.3 Proliferation Parameters ($T_{kickoff}$, T_{pot})

The OTT has been correlated to treatment outcomes in several studies. Chen *et al* found that prolonging HDR treatments in cervical cancer patients with an OTT equal to or exceeding 63 days resulted in a significantly lower 5-year cause-specific survival compared to patients with an OTT shorter than 63 days (65% and 83%**,** respectively) (19). Also, Gasinska *et al*, Song *et al*, Tanderup *et al*, and Tergas *et al* found that cervical cancer patient outcomes improved for treatments with an OTT of less than 60, 56, 49, and 70 days, respectively (15,20,21,22). ICRU 89 recommends that the OTT not exceed 55 days (6).

$T_{kickoff}$ and T_{pot} are parameters used to incorporate cellular proliferation in dose calculations (see Section 2.4.3.4). To determine the influence of OTT on BED in cervical cancer, Gasinska *et al*

assumed a range of $T_{kickoff}$ values (21, 28, and 35 days) (15). Later studies have used the lower value of 21 days, which was considered a conservative option in the calculation of radiobiological dose (15,23,24). Huang *et al*, based on outcomes data, estimated $T_{kickoff}$ to be approximately 19 [95% CI of 11 - 22] days (25).

Two groups have put considerable effort into calculating possible values of T_{pot} for cervical cancers (26,27). Using a cohort of 66 patients, Tsang *et al* found a median T_{pot} of 5.0 [1.2 - 42.1] days using bromodeoxyuridine (BrdUrd) labeling of cervical cancer biopsies (26). Using the same method, Bolger *et al* in two different studies with over 120 cervical cancer patients in each study, determined median T_{pot} values of 4.4 [3.1 - 6.4, interquartile range] days and 4.0 [3.1 - 6.3, interquartile range] days, respectively (27,28). Gasinska *et al* also conducted BrdUrd labeling in 229 patients and determined a mean T_{pot} of 6.8 ± 7.4 days with a full range of 1.4 to 75 days (15). A possible reason for these variances could be the large amount of interlaboratory deviation caused by systematic differences in operator reporting patterns between laboratories during BrdUrd labeling of cervical tumor biopsies (29). Further deviation may be caused by differences in the sample population; Symonds *et al* notes that T_{pot} may decrease with disease progression (30).

3.2.4 Summary of Conventional Recommendations and Other Reported Values

Tables 3.1 to 3.4 provide a summary of both the conventional recommendations and other published values for the α/β ratio and $T_{1/2}$, and the methodology of the estimation. There are no conventionally recommended values for α, $T_{kickoff,}$ and T_{pot}. Instead of calculating the effects of proliferation, limitations are typically recommended for the maximum OTT. Table 3.5 provides a summary of reported values for parameters used when considering proliferation effects.

Table 3.1: Reported α/β ratios for tumor tissue.

	Conventional recommendation (6,7)	Other reported values (references in brackets)	Methodology of estimation
α/β ratio for tumor (Gy)	10	20.8 - ∞ (13) [a]	Review of reported patient outcomes using Kaplan-Meier survival curves and Cox regression analysis of 5-year follow up data of patients who received LDR BT. This range of values (95% CI) was determined as most likely assuming a tumor $T_{1/2}$ of 1.5 hours.
		6.0 - 16.5 (10)	Calculation of survival curves of human cervical cancer lines (acquired via biopsy) at three different dose rates (0.016, 0.032, and 1.5 Gy/min) for a total physical dose up to 16 Gy. Values of α, β, and $T_{1/2}$ were estimated from the survival curves.
		5.9 - 20.9 (31)	Analysis of previously published data by Kelland and Steel (10). Maximum likelihood method was used as opposed to a best-fit from a covariance matrix as used in the original study. Values of α, β, and $T_{1/2}$ were estimated.
		6 - 14 (32)	Review of data from a variety of human tumors from different sites irradiated *in situ*, including sarcomas and melanomas. While citing multiple technical issues with measurement results, it was suggested that the vast majority of previous research supported that tumors have an α/β ratio above 8 Gy.

[a] Roberts *et al* report a β/α 95% confidence range of -0.018 to 0.048 Gy^{-1}. A β/α approaching 0 would correspond to an infinitely large value for α/β.

Table 3.2: Reported α/β ratios for late responding normal tissue.

	Conventional recommendation (6,7)	Other reported values (references in brackets)	Methodology of estimation
α/β ratio for late responding normal tissue (Gy)	3	4.3 (Rectum only, 33)	Logistic regression analysis of 327 cases of stage IIb and III cervical carcinoma patients treated with EBRT and intracavitary BT between 1971 and 1980. Complications were determined based on organ morbidity at the time of death.
		4.8 (Rectum only, 34)	Utilized the Lyman-Kutcher-Burman (LKB) model for normal tissue complication probability (NTCP) to fit data from patients in the RTOG 94-06 database with grade 2 or higher late rectal toxicity (35). A likelihood ratio test was used to determine whether an LQ-corrected LKB model fit the data better than the LKB model based on physical dose alone.
		5.4 (Rectum only, 36)	Analysis of multiple publications reporting late rectal toxicity of grade 2 or higher. Rectal toxicity was plotted against the EQD2 for the rectum; the data was best fit when using an α/β ratio of 5.4 Gy.
		2.3 (Rectum only, 37)	Utilized the LKB model for NTCP to fit data from 162 prostate cancer patients treated in a randomized trial. Patients with a grade 2 or higher rectal toxicity were considered to have organ morbidity and results were fit using the maximum likelihood method.
		2.5 (5)	Review of data published from in vivo irradiation of skin, lung, spinal cord, brain, kidney, and bone marrow tissue from mice, rabbits, and humans. Two distinct groups of tissue were found with approximate α/β ratios of 10 Gy and 2.5 Gy. The latter group was later associated with late responding normal tissue.
		3.4 - 4.5 (38)	No rationale provided.

Table 3.3: Reported $T_{1/2}$ values for tumor tissue.

	Conventional recommendation (6,7)	Other reported values (references in brackets)	Methodology of estimation
$T_{1/2}$ for tumor (hr)	1.5	0.0 - 0.64 (13)	Review of reported patient outcomes using Kaplan-Meier survival curves and Cox regression analysis of 5-year follow up data of patients who received LDR BT. This range of values (95% CI) was determined as most likely assuming a tumor α/β ratio of 10 Gy.
		1.9 [0.26 - 5.7] (10)	Calculation of survival curves of human cervical cancer lines (acquired via biopsy) at three different dose rates (0.016, 0.032, and 1.5 Gy/min) for a total physical dose up to 16 Gy. Values of α, β, and $T_{1/2}$ were estimated from the survival curves.
		0.37 [0.15 - 2.15] (31)	Analysis of previously published data by Kelland and Steel (10). Maximum likelihood method was used as opposed to a best-fit from a covariance matrix as used in the original study. Values of α, β, and $T_{1/2}$ were estimated.

Table 3.4: Reported $T_{1/2}$ values for late responding normal tissue.

	Conventional recommendation (6,7)	Other reported values (references in brackets)	Methodology of estimation
$T_{1/2}$ for late responding normal tissue (hr)	1.5	0.32 - 1.11 (13)	Review of reported patient outcomes using Kaplan-Meier survival curves and Cox regression analysis of 5-year follow up data of patients who received LDR BT. This range of values (95% CI) was determined as most likely assuming a normal tissue α/β ratio of 3 Gy.
		1.5 - 2.5 (17)	Review of reported late effects in patients receiving LDR BT. The $T_{1/2}$ that caused a difference in late patient complication was estimated to be 1.5 to 2.5 hours, assuming an α/β ratio in normal tissue of 2-4 Gy.
		0.20 - 0.40 (18)	Review of three studies in which LDR BT delivered with different dose rates caused statistically equivalent late patient complication.

Table 3.5: Reported values for proliferation.

	Reported values (references in brackets)	Estimation methodology
$T_{kickoff}$ (days)	11 - 22 (25)	Least χ^2 fit of TCP estimations to report patient outcome was conducted while varying $T_{kickoff}$ alone. All assumed parameter values required for calculating $T_{kickoff}$ were adopted from literature.
	21 - 35 (15)	Values assumed. No rationale was provided for the selected range.
T_{pot} (days)	6.8 ± 7.4 (15) [a]	BrdUrd labelling of biopsy samples of 229 patients with stage IB to IIIB carcinoma of the cervix treated from 1987 to 1999.
	5.0 [1.2 - 42.1] (29) [b]	BrdUrd labelling of biopsy samples of 84 patients with stage IB to IV carcinoma of the cervix from 1991 to 1996.
	4.4 (27) [b]	BrdUrd labelling of biopsy samples of 138 patients with stage I to IV carcinoma of the cervix from 1991 to 1992. An interquartile range of 3.1 to 6.4 was reported.
	4.0 (28) [b]	BrdUrd labelling of biopsy samples of 121 patients with stage I to IV carcinoma of the cervix. An interquartile range of 3.1 to 6.3 days was reported.
α (Gy^{-1})	0.06 - 0.20 (13)	Review of reported patient outcomes using Kaplan-Meier survival curves and Cox regression analysis of 5-year follow up data of patients who received LDR BT. This range of values (95% CI) was determined as most likely assuming a tumor $T_{1/2}$ of 1.5 hours.
	0.18 - 0.61 (10)	Calculation of survival curves of human cervical cancer lines (acquired via biopsy) at three different dose rates (0.016, 0.032, and 1.5 Gy/min) for a total physical dose up to 16 Gy. Values of α, β, and $T_{1/2}$ were estimated from the survival curves.
	0.29 - 0.74 (31)	Analysis of previously published data by Kelland and Steel (10). Maximum likelihood method was used as opposed to a best-fit from a covariance matrix as used in the original study. Values of α, β, and $T_{1/2}$ were estimated.
	0.35 ± 0.21 (11,12) [a]	Analysis of surviving fraction of cervical cancer biopsy samples irradiated at 3.8 to 4.2 Gy/min with 2 Gy.
	0.20 - 0.40 (14)	No rationale provided.

[a] Reported value is a mean.
[b] Reported value is a median.

3.3 Effect of Parameter Uncertainties

3.3.1 Uncertainty in Conventional Radiobiological Parameter Recommendations

While conventional recommendations have been provided for the α/β ratio and $T_{1/2}$, the values cited in Tables 3.1 to 3.4 highlight a fair degree of uncertainty. Deviation of both parameters from conventional values (for tumor or critical structures) could result in non-equivalent radiobiological doses being delivered by the PDR and HDR BT boosts that are otherwise assumed to be dosimetrically equivalent through Equations (2.20) and (2.44). These differences in the radiobiological dose could result in different patient outcomes depending on which BT boost was utilized. Table 3.6 illustrates this by presenting the radiobiological doses to the tumor when calculated using the conventional values and the different combinations of α/β and $T_{1/2}$ values based on maximum likelihood calculations published by Roberts *et al* (13). The calculations are done for an EBRT treatment delivering 25 fractions of 1.8 Gy each followed by a BT boost of (i) PDR1: 2 insertions with 37 pulses of 0.60 Gy/pulse per insertion; or (ii) HDR1: 5 fractions of 6.6 Gy each. Both schedules are designed to deliver a tumor dose of approximately 90 Gy EQD2 (combined EBRT and BT) when assuming an α/β ratio of 10 Gy and a $T_{1/2}$ of 1.5 hours. PDR pulse times are based on an Ir-192 activity of 0.5 Ci. EQD2 values calculated in Table 3.6 show the variation in doses when considering different combinations of the parameter values. Larger values of α/β result in a minimal decrease in EQD2 of about 1.0 Gy for PDR1 while a difference of 12.0 Gy occurs for HDR1. Conversely, lower values of $T_{1/2}$ reduced the dose by over 9.0 Gy EQD2 for PDR1, but did not have an effect on HDR1.

Table 3.6: Radiobiological tumor dose calculated for an EBRT treatment delivering 25 fractions of 1.8 Gy followed by a BT boost (either PDR1: PDR BT boost of 2 insertions with 37 pulses of 0.60 Gy/pulse per insertion or HDR1: HDR BT boost of 5 fractions of 6.6 Gy each) using different combinations of α/β ratios and $T_{1/2}$. Radiobiological dose was calculated using the conventionally recommended values (α/β ratio = 10 Gy and $T_{1/2}$ = 1.5 hr) and those within the 95% confidence interval reported by Roberts *et al* (13).

α/β (Gy)	**$T_{1/2}$ (hr)**	**Methodology**	**Gy EQD2**	
			PDR1	HDR1
10	1.5	Conventional parameters	90.4	89.9
10	0.25	Conventional α/β, most likely $T_{1/2}$	83.5	89.9
10	0.00	Conventional α/β, lowest likely $T_{1/2}$	81.3	89.9
10	0.64	Conventional α/β, highest likely $T_{1/2}$	85.6	89.9
52.6	1.5	Conventional $T_{1/2}$, most likely α/β	89.6	80.6
20.8	1.5	Conventional $T_{1/2}$, lowest likely α/β	89.9	84.3
Infinitely large value [a]	1.5	Conventional $T_{1/2}$, highest likely α/β	89.4	78.0

[a] Roberts *et al* reported a β/α 95% confidence range of -0.018 Gy^{-1} to 0.048 Gy^{-1}. A β/α approaching 0 would correspond to an infinitely large value for α/β.

Table 3.6 highlights the potential variance in HDR and PDR BT boosts using α/β ratios and $T_{1/2}$ values from a single study. However, a large range of radiobiological parameters have been reported in Tables 3.1 to 3.5. The impact of the full range parameters reported will be explored in the following sections.

3.3.1.1 α/β Ratio Uncertainties

Table 3.7 highlights the change in PDR and HDR treatment doses when the α/β ratio of the tumor and critical structure are varied from their conventional values of 10 and 3 Gy, respectively. The table shows the EQD2 doses when calculated with different α/β ratios (corresponding to the range given in Table 3.1) for four different potential BT boosts following an EBRT treatment delivering 25 fractions of 1.8 Gy each: (i) PDR1: 2 insertions with 37 pulses of 0.60 Gy/pulse per insertion; (ii) PDR2: 58 pulses of 0.73 Gy/pulse; (iii) HDR1: 5 fractions of 6.6 Gy each; (iv) HDR2: 4 fractions of 7.75 Gy each; and (v) HDR3: 3 fractions of 9.5 Gy each. PDR treatments are commonly delivered in one or two insertions, while the choice of the number of HDR fractions is adopted from the American Brachytherapy Society's consensus guidelines for locally advanced carcinoma of the cervix (39). All five treatment schedules are designed to

deliver a tumor dose of approximately 90 Gy EQD2 (combined EBRT and BT) when using conventional α/β and $T_{1/2}$ values and not taking proliferation corrections into account. Without proliferation, the radiobiological doses are independent of the relative timing of the EBRT and BT treatments. For example, if BT sequentially follows EBRT as opposed to beginning BT prior to EBRT completion, the combined (EBRT + BT) dose is unchanged; this is provided the treatment fractions are separated such that no sublethal damage from a BT fraction remains at the next EBRT fraction or vice versa, as would generally be the case with typical separations of at least one day. The calculations shown in Table 3.7 also assume that $T_{1/2}$ is 1.5 hours, and PDR pulse times are based on an Ir-192 activity of 0.5 Ci.

As seen from the estimated doses in Table 3.7, variations in the α/β ratio have a greater effect on HDR doses than PDR doses. Consequently, as the α/β ratio deviates more from the originally assumed conventional value of 10 Gy, the difference in the total dose for the two delivery methods will also increase. For a tumor with an α/β ratio less than 10 Gy, HDR BT delivers a higher radiobiological dose than PDR BT**.** For example, assuming an α/β ratio of 6 Gy, the total radiobiological dose to the tumor from a HDR3 BT boost would be 7.1 Gy EQD2 (7.7%) greater than from a PDR2 BT boost. However, the opposite is true if the α/β ratio is 20 Gy as a treatment with a PDR2 BT boost would deliver 6.2 Gy EQD2 (7.0%) more than the HDR3 BT boost. Table 3.7 also presents an example of the variation in an assumed tolerance dose of 65 Gy EQD2 received by a critical structure for the five different treatment schedules and two alternative assumptions for the α/β ratio, and with the same assumed $T_{1/2}$ value of 1.5 hours.

Table 3.7: Variation in the radiobiological dose to tumor and critical structures assuming a $T_{1/2}$ = 1.5 hours and different α/β ratios.

BT Treatment	Dose to Tumor [a] (Gy EQD2)				Dose to OAR per pulse/fraction (% of tumor dose) [c]	Dose to critical structure tissue [a] (Gy EQD2)		
	α/β ratio (Gy)					α /β ratio (Gy)		
	6	10[b]	14	20		2.5	3 [d]	5
PDR1, 37 p x 0.60 Gy, x 2 insertions	91.0	90.4	90.2	90.0	0.34 Gy (56%)	64.5	65.0	66.4
PDR2, 58 p x 0.73 Gy	92.0	90.4	89.6	89.0	0.40 Gy (55%)	64.7	65.0	65.9
HDR1, 5 fr x 6.6 Gy	95.8	89.9	86.9	84.5	3.41 Gy (52%)	65.3	65.0	64.2
HDR2, 4 fr x 7.75 Gy	97.2	90.1	86.6	83.7	3.93 Gy (51%)	65.5	65.0	63.8
HDR3, 3 fr x 9.5 Gy	99.1	90.6	86.3	82.8	4.71 Gy (50%)	65.7	65.0	63.3

[a] Includes EBRT of 25 fractions of 1.8 Gy each.
[b] Conventional recommendation for α/β ratio of tumor tissue.
[c] The critical structure dose assumes: 1) the full EBRT dose was delivered to the structure (45 Gy in 25 fractions); 2) the BT brings the EQD2 to a tolerance dose of 65 Gy EQD2.
[d] Conventional recommendation for α/β ratio of critical structure tissue (e.g. rectum).

Treatments with large doses per fraction/pulse are most strongly affected by a change in the α/β ratio. This can be seen in Figure 3.1, which plots the change in radiobiological dose with the α/β ratio for the five BT boosts discussed in Table 3.7. HDR3, which utilized the largest dose per fraction (9.5 Gy) experienced the greatest change in radiobiological dose delivered; the radiobiological dose decreased by approximately 7.8 Gy EQD2 when the α/β ratio increased from 10 to 20 Gy and increased by 8.5 Gy EQD2 when the α/β ratio decreased from 10 to 6 Gy. Though the trend was similar to HDR, the overall change in radiobiological doses for PDR1 and PDR2 over the 6 to 20 Gy α/β ratio range was small (1 and 2 Gy EQD2, respectively).

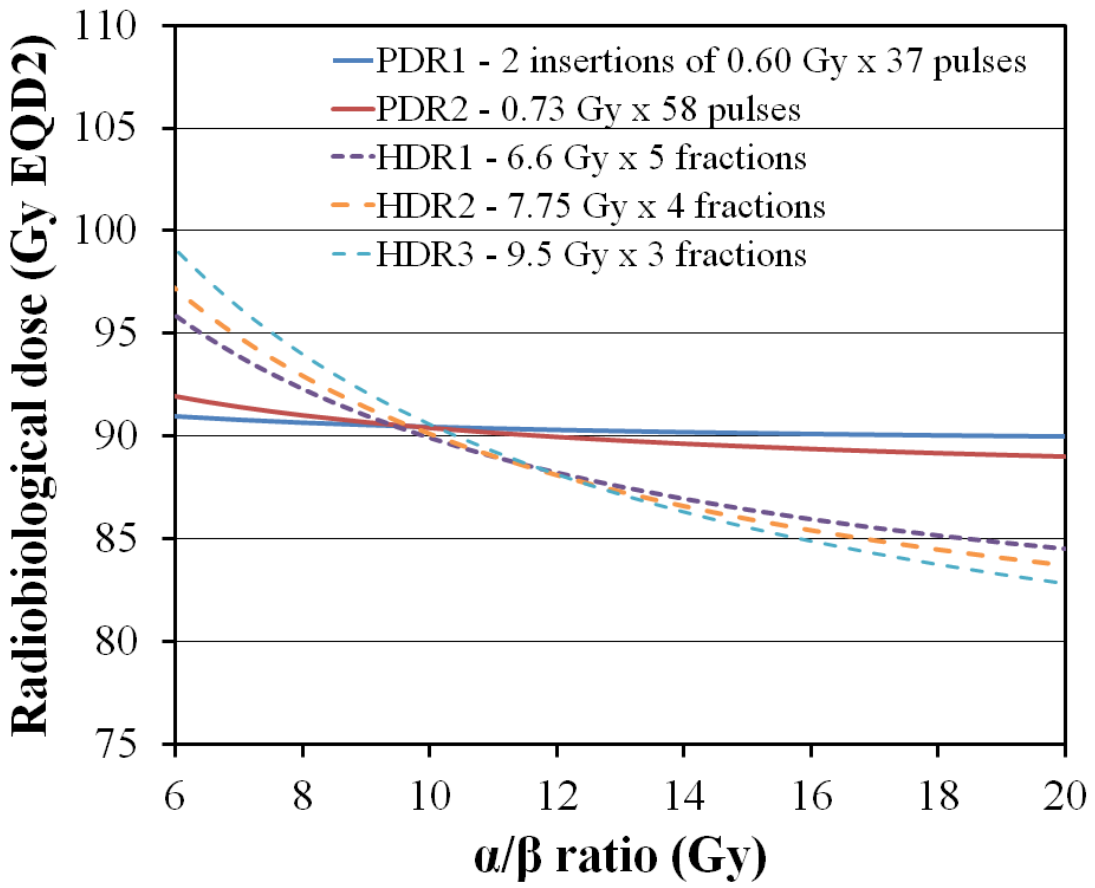

Figure 3.1: Change in tumor EQD2 with α/β for different PDR and HDR BT regimens after EBRT (25 fr x 1.8 Gy) and assuming $T_{1/2}$ = 1.5 hr.

3.3.1.2 $T_{1/2}$ Uncertainties

Since $T_{1/2}$ is not included in Equation (2.20) (which assumes complete repair between fractions), any variation in $T_{1/2}$ does not affect fractionated HDR BT dose calculations. However, changes in $T_{1/2}$ have a strong impact on the radiobiological dose calculated for PDR BT, where the treatment pulses are usually delivered hourly and there is insufficient time for the complete repair of sublethal lesions (Table 3.6). De Leeuw *et al* supports this conclusion; changes in the $T_{1/2}$ had minimal effect on the calculated EQD2 for HDR BT for 2 insertions of 2 fractions each separated by 17 hours but resulted in significant variation in calculated EQD2 values for a PDR BT treatment of 2 insertions of 32 pulses each (40).

A lower $T_{1/2}$ would result in a smaller biological effect (tumor control or critical organ toxicity) for PDR treatments. This effect can be seen in Figure 3.2, which plots radiobiological dose

against $T_{1/2}$ for four different BT boosts following an EBRT treatment delivering 25 fractions of 1.8 Gy each: (i) PDR1: 2 insertions with 37 pulses of 0.60 Gy/pulse per insertion, (ii) PDR2: 58 pulses of 0.73 Gy/pulse, (iii) PDR3: 39 pulses of 1.0 Gy/pulse, and (iv) HDR1: 5 fractions of 6.6 Gy each. The time per pulse for the PDR treatments was calculated with a 0.5 Ci Ir-192 source. All four treatments deliver a tumor dose of approximately 90 Gy EQD2 when assuming the conventional $T_{1/2}$ of 1.5 hours and an α/β ratio of 10 Gy. An increase in $T_{1/2}$ will result in a higher dose being delivered by any PDR BT schedule and vice versa, while the HDR BT boost delivers the same radiobiological dose regardless of any changes to $T_{1/2}$. This effect can be quite significant. For example, if the $T_{1/2}$ of the tumor was 0.4 hours instead of 1.5 hours, consistent with one of the reported tumor values in Table 3.3, PDR3 would deliver approximately 9.1 Gy EQD2 (10.1%) less dose than expected.

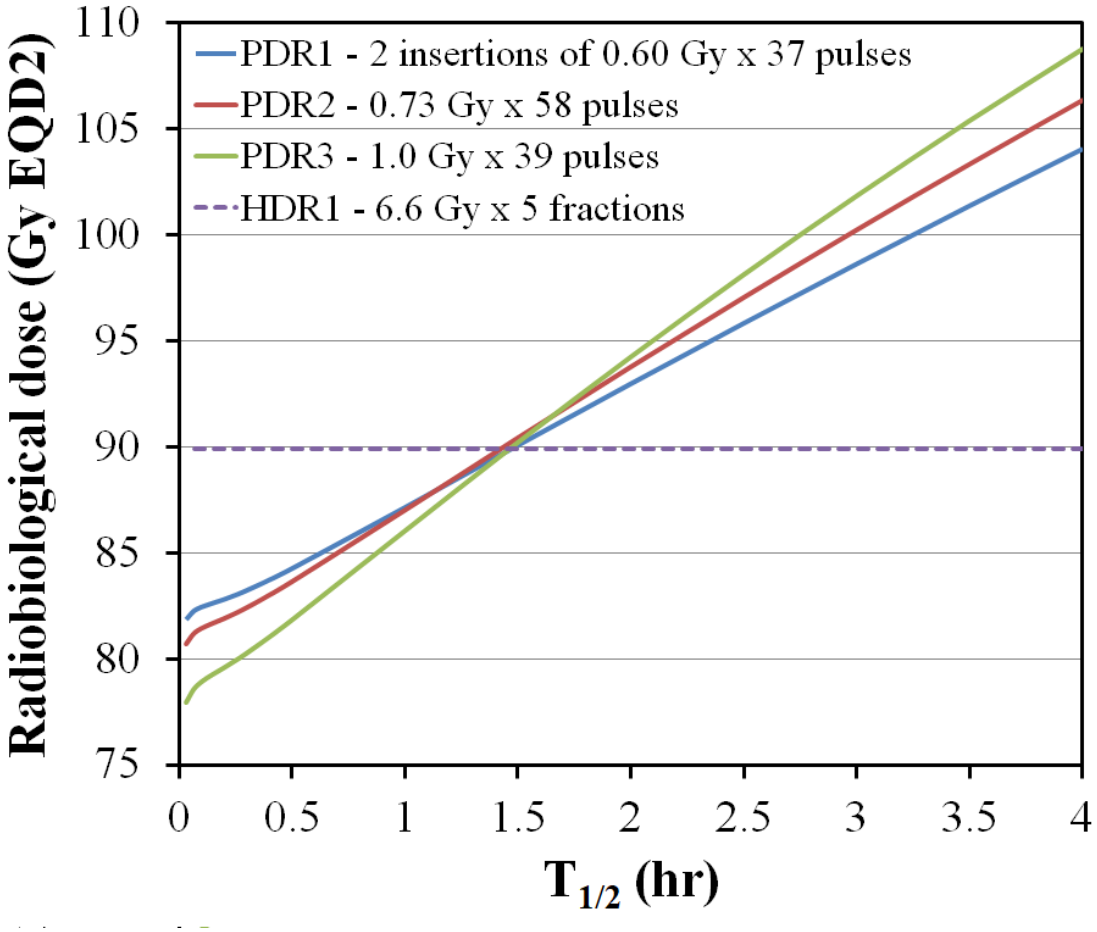

Figure 3.2: Change in tumor EQD2 with $T_{1/2}$ for different PDR and HDR BT regimens after EBRT (25 fr x 1.8 Gy) and assuming α/β = 10 Gy.

3.3.2 Number and Frequency of Pulses in PDR BT

In addition to α/β and $T_{1/2}$, the BED equation for PDR (Equation (2.44)) contains dependencies on several parameters, including pulse delivery time, pulse interval, and number of pulses. To better understand the trends in the PDR BT data seen in Figure 3.2, it is useful to define a parameter q:

$$q = \left(\frac{2}{\mu T}\right)\left(1 - \frac{1}{N\mu T}[NY - SY^2]\right) \tag{3.1}$$

such that Equation (2.44) can be expressed as $D_{BED,PDR} = Nd(1 + d_p q/(\alpha/\beta))$, a form more directly comparable to the BED expression used for HDR. Larger q values represent more radiobiological dose being delivered per unit of physical dose. Figure 3.3 plots q against $T_{1/2}$ for six different PDR BT boosts: (i) PDR1: 58 hourly pulses, (ii) PDR2: 73 hourly pulses, (iii) PDR3: 40 hourly pulses, (iv) PDR4: 58 bihourly pulses (one pulse every two hours), (v) PDR5: 58 semihourly pulses (one pulse every 30 minutes), and (vi) PDR6: 58 hourly pulses with a lower dose rate. All six treatments are assumed to deliver 0.73 Gy/pulse. PDR1 to PDR5 have an assumed time per pulse of 10 minutes while PDR6 has an assumed time per pulse of 30 minutes. Compared to PDR1, PDR2 and PDR3 reflect changes in the value of q due to the number of pulses while PDR4 and PDR5 demonstrate changes in q due to the time between pulses. As illustrated, by comparing PDR1 and PDR6, q is dependent on the duration of each pulse (which is a function of the dose per pulse and instantaneous dose rate), though the dependence only becomes appreciable for values of $T_{1/2}$ small enough to approach the pulse duration. The repetition time (i.e. - hourly, semihourly, or bihourly pulses) and the halftime of repair both strongly affect q. However, since pulses are conventionally delivered hourly, the most relevant dependence affecting q is $T_{1/2}$. For example, when assuming an α/β ratio of 10 Gy and $T_{1/2}$ of 1.5 hours, the value of q for PDR1 is 4.22, resulting in a tumor dose of 46.2 Gy EQD2 from BT (and a total dose of 90.4 Gy EQD2 with an EBRT treatment of 25 fractions of 1.8 Gy). However, a $T_{1/2}$ of 0.4 hours would result in a q value of 1.33 and would significantly decrease the BT tumor dose to 38.7 Gy EQD2 (total dose of 83.0 Gy EQD2 including EBRT). In comparison, an increase in pulse duration (PDR6) changes the q value from 4.22 to 4.19, assuming a $T_{1/2}$ of 1.5 hours. This would only result in a small decrease in the dose delivered (0.1 Gy EQD2).

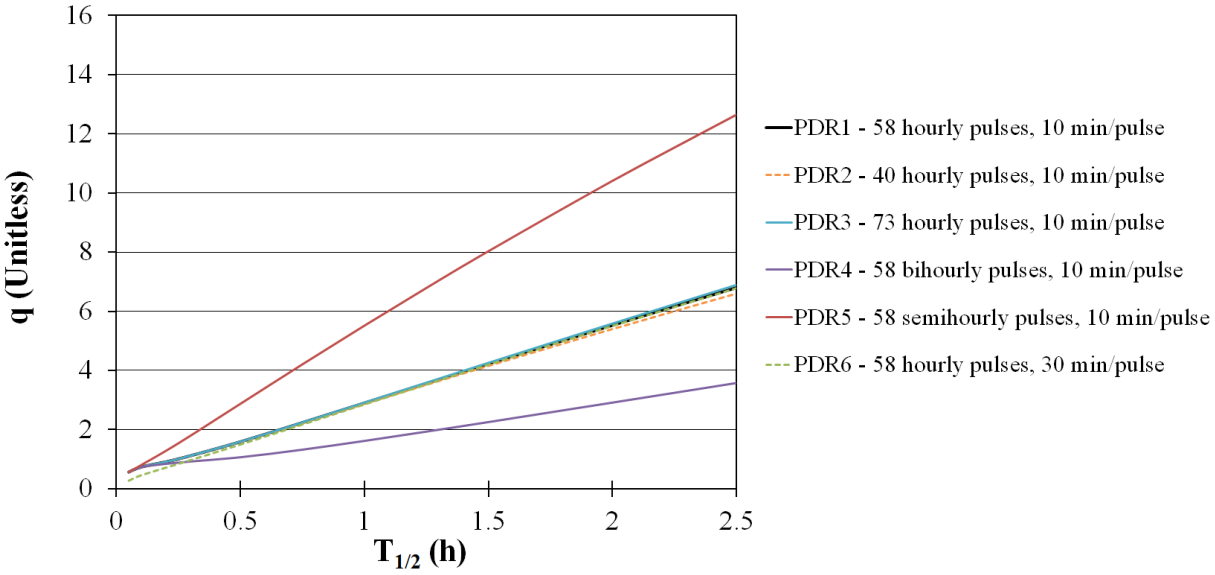

Figure 3.3: Value of parameter q plotted against $T_{1/2}$ for different pulse repetition times, pulse durations, and number of pulses.

3.3.3 Source Strength in PDR BT

When considering parameter ranges, it is important to recognize that multiple combinations of α/β ratios and $T_{1/2}$ may satisfy a given radiobiological equivalency. Consider two PDR treatments: (i) PDR1: 2 insertions with 37 pulses of 0.60 Gy/pulse per insertion and (ii) PDR2: 58 pulses of 0.73 Gy/pulse. If PDR1 and PDR2 were found to be radiobiologically equivalent, the α/β ratio and $T_{1/2}$ of the tissue cannot be determined from this result alone; one of the two parameters must be assumed. Figure 3.4 plots combinations of $T_{1/2}$ and α/β ratios which result in the two PDR treatments (PDR1 and PDR2) having the same radiobiological dose (according to Equation (2.44) for 4 different Ir-192 source air kerma strengths (and hence pulse times and dose rates): (i) Activity 1: 0.25 Ci, (ii) Activity 2: 0.5 Ci, (iii) Activity 3: 1 Ci, and (iv) Activity 4: 2 Ci. Activity 1 corresponds to a 0.5 Ci source that has decayed by one half-life. Instead of providing a single solution, the equivalence suggests an infinite number of solutions for different combinations of the α/β ratio and $T_{1/2}$ values. This correlation introduces another aspect of uncertainty into the published values of the α/β ratio and $T_{1/2}$: *a priori* assumptions of α/β will influence the calculated $T_{1/2}$ and vice versa. It is important to note that the correlations shown in Figure 3.4 are derived from an assumed hypothetical equivalency between two clinically used PDR schedules; since this radiobiological equivalency may not necessarily exist, the specific equivalent combinations of α/β and $T_{1/2}$ shown in Figure 3.4 may not be correct. A similar

correlation between extracted values of the α/β ratio and $T_{1/2}$ was demonstrated by Roberts *et al* (13). Their analysis excludes a $T_{1/2}$ of 1.5 hours from its 95% confidence interval when assuming an α/β ratio of 10 Gy, one of the combinations illustrated in Figure 3.4.

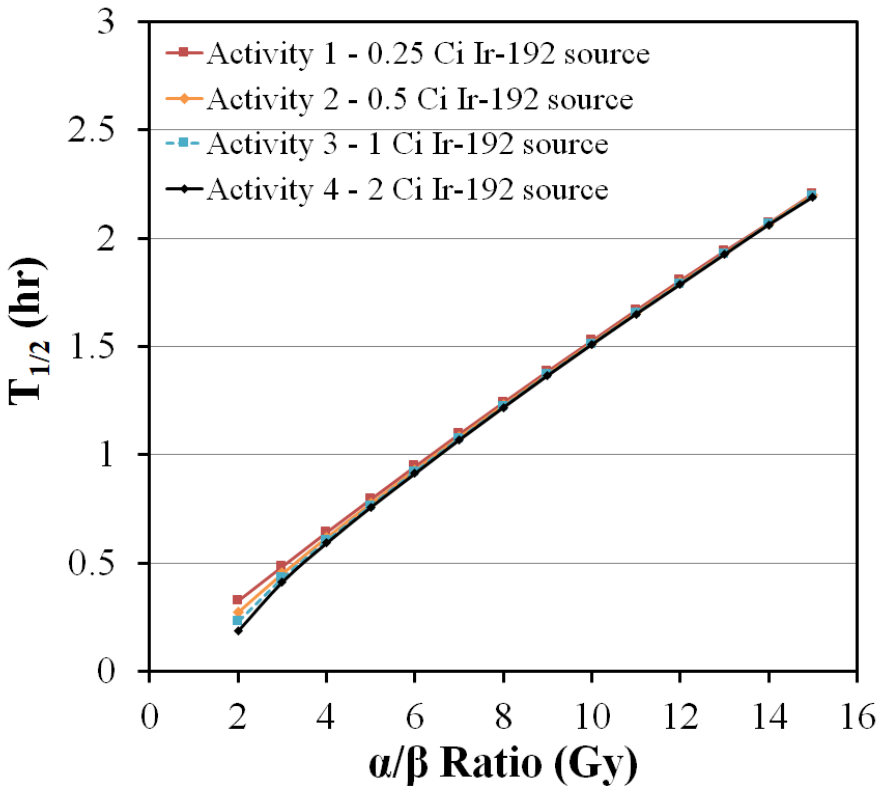

Figure 3.4: Plot of combinations of $T_{1/2}$ and α/β ratios which result in the same radiobiological dose for two PDR treatments (PDR1 (2 insertions with 37 pulses of 0.60 Gy/pulse per insertion) and PDR2 (58 hourly pulses of 0.73 Gy/pulse)) for four different instantaneous dose rates. The equivalency of the two treatments is assumed.

3.3.4 Proliferation Parameters

Conventional treatment recommendations, which suggest a maximum OTT based on outcomes data, do not fully consider the radiobiological impact of proliferation. Currently, no correction is implemented for treatments that deliver the same radiobiological dose (before proliferation is considered) but have different OTTs. Treatments considered equivalent could therefore potentially correspond to different radiobiological doses and different outcomes. In the retroEMBRACE study, a loss of 1% to 3% in local control/week was reported for prolonged OTT (21). ICRU 89 recommends that the OTT be within 55 days, which is made possible by using a simultaneously integrated nodal boost (when necessary) within the EBRT course;

reducing treatment interruptions; and planning ahead the timing of the BT treatment (6,41). An even shorter time frame is often possible – e.g. an EBRT followed by a single insertion PDR boost could be completed within 40 days if there are no treatment interruptions.

The difference in radiobiological dose due to increased tumor proliferation over an additional 15 days in the 55-day treatment can be calculated using Equation (2.50). Let:

$$\Delta BED = BED_1 - BED_2 \tag{3.2}$$

where ΔBED represents the difference in radiobiological dose after proliferation is considered and BED_1 and BED_2 represent the radiobiological dose delivered with an OTT of OTT_1 and OTT_2**,** respectively. Assuming that all parameters (α, T_{pot}, $T_{kickoff}$, and $D_{BED,0}$) except for OTT are the same and the OTT values for both cases are longer than $T_{kickoff}$ ($\Delta T = OTT - T_{kickoff}$), then:

$$\Delta BED = \frac{\ln(2)\,(OTT_2 - T_{kickoff})}{T_{pot}\alpha} - \frac{\ln(2)\,(OTT_1 - T_{kickoff})}{T_{pot}\alpha} \tag{3.3}$$

$$\Delta BED = \frac{\ln(2) OTT_{diff}}{T_{pot}\alpha} \tag{3.4}$$

where OTT_{diff} is the difference between the two OTTs (OTT_1 and OTT_2). For example, assuming T_{pot} = 4.5 days and α = 0.3 Gy^{-1}, a treatment lasting 55 days will deliver 6.4 Gy EQD2 less than if it had an OTT of 40 days (T_{diff} = 15 days). As suggested by Equation (3.4), smaller values of T_{pot} and α for the tumor will increase ΔBED, resulting in a larger variation in tumor dose due to differences in OTT. Figure 3.5(a) highlights this effect where the radiobiological dose from a 90 Gy EQD2 prescription (after consideration of proliferation) is plotted against OTT for four combinations of T_{pot} and α with an assumed $T_{kickoff}$ of 21 days. Consider a BT treatment that is prolonged by 15 days. The radiobiological dose delivered by the treatment will decrease due to the increase in OTT (ΔD). For larger values of T_{pot} and α (such as 5.0 days and 0.5 Gy^{-1}, respectively), there would be a loss of 3.5 Gy EQD2 (ΔD_1); however, for smaller T_{pot} and α values (such as 4.0 days and 0.2 Gy^{-1}, respectively), the dose loss of 10.8 Gy EQD2 (ΔD_2) would potentially be much more concerning. It is worth noting that, much like how multiple combinations of the α/β ratio and $T_{1/2}$ can correspond to a radiobiological equivalency, multiple combinations of T_{pot} and α can predict equal amounts of proliferation-based radiobiological dose reduction. Recent recommendations by Tanderup *et al* suggest that the commonly cited values for T_{pot} and α may not accurately estimate the effects of proliferation (21). They found that an

increase of one week to a 7-week OTT was comparable to a tumor dose de-escalation of 5 Gy EQD2. An example of a combination of T_{pot} and α values that mathematically replicate this rate of dose loss is 4.0 days and 0.2 Gy^{-1}, which represents the lower end of values reported in Table 3.5. In comparison, since more commonly cited values of T_{pot} and α for the tumor are 4.5 days and 0.3 Gy^{-1}, current dose calculations incorporating proliferation may still underestimate its effect.

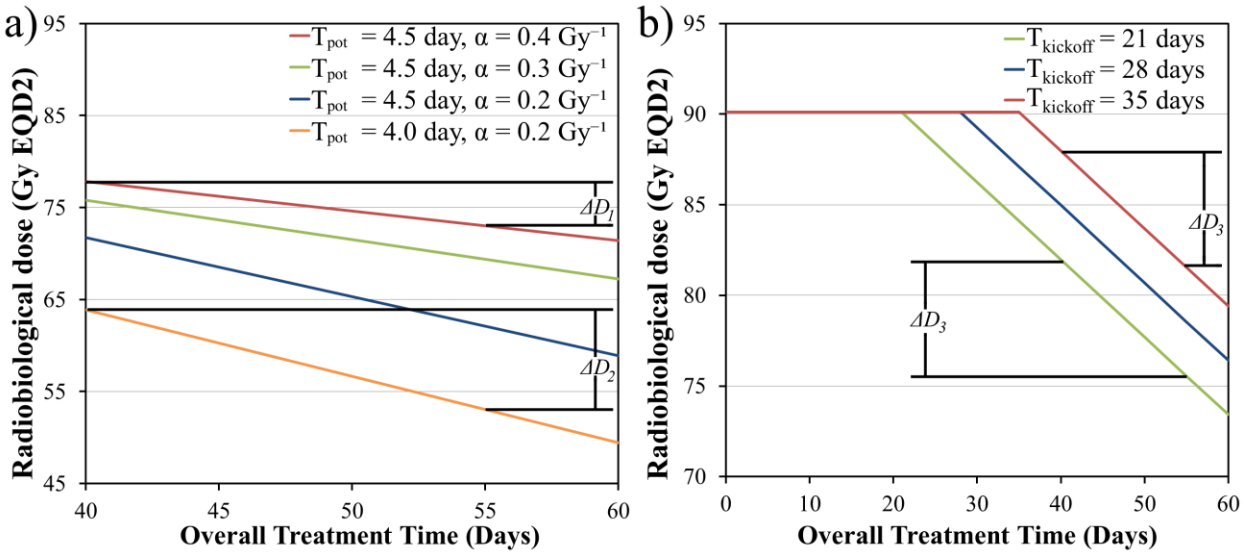

Figure 3.5: Radiobiological dose, considering proliferation, after a 90 Gy EQD2 prescription for (a) different potential doubling times (T_{pot}) and α values and (b) different kickoff times ($T_{kickoff}$). ΔD represents the difference in dose between treatments of overall treatment times 40 days and 55 days: ΔD_1 assumes T_{pot} = 4.5 days and α = 0.4 Gy^{-1}, ΔD_2 assumes T_{pot} = 4.0 days and α = 0.2 Gy^{-1}, and ΔD_3 assumes T_{pot} = 4.5 days and α = 0.3 Gy^{-1}. Changing the value of $T_{kickoff}$ did not affect the value of ΔD_3.

$T_{kickoff}$ variance is not expected to affect the calculated proliferation dose loss between two treatments since the shortest OTTs currently considered are longer than the maximum value of $T_{kickoff}$ given in Table 3.5. In this case, Equation (3.4) is sufficient to describe differences in radiobiological dose delivered by different OTTs. This can be seen in Figure 3.5(b) where the radiobiological dose from a 90 Gy EQD2 prescription (after proliferation is considered) is plotted against OTT for three values of $T_{kickoff}$. The T_{pot} is assumed to be 4.5 days and α is 0.3 Gy^{-1}. The difference in dose of 6.5 Gy EQD2 between treatments delivered over 40 days and 55 days (ΔD_3) is not impacted by the value of $T_{kickoff}$. Similar results were found by Gasinska *et al*. They estimated that the amount of radiobiological dose lost daily due to proliferation was the same regardless of the assumed kickoff time (varied from 21, 28, and 35 days) (15).

3.4 Conclusion

The use of radiobiological dose is recommended to compare treatments and outcomes from different treatment techniques used in cervical cancer brachytherapy. However, possible variance in parameter values used in these calculations and the inconsistent consideration of proliferation introduces significant additional uncertainty into dose calculation. Variance in the α/β ratio and $T_{1/2}$, within the range of values reported in the literature, can introduce over 10% variance in the calculated radiobiological tumor dose for PDR treatments, while changes in the α/β ratio can result in over 13% variance in HDR treatments (with $T_{1/2}$ not having any significant effect). Similarly, the extension of OTT can introduce a variance of over 5 Gy EQD2 due to differences in reported values of α and T_{pot}. This highlights the need for further efforts to establish more definitive parameter values. Improved radiobiological parameters, potentially combined with refinements to current radiobiological dose models, could increase the accuracy of treatment planning and consequently lead to better outcomes for cervical cancer patients. Therefore, additional research into the identification of α/β ratio and $T_{1/2}$ values for cervical cancer cells is warranted.

3.5 References

(1) Barendsen GW. Dose fractionation, dose rate and iso-effect relationships for normal tissue responses. *Int J Radiat Oncol Biol Phys* 1982;8(11):1981-1997.

(2) Hall EJ, Brenner DJ. The dose-rate effect revisited: Radiobiological considerations of importance in radiotherapy. *Int J Radiat Oncol Biol Phys* 1991;21(6):1403-1414.

(3) Kirchheiner K, Nout RA, Lindegaard JC, Haie-Meder C, Mahantshetty U, Segedin B, *et al.* Dose–effect relationship and risk factors for vaginal stenosis after definitive radio(chemo)therapy with image-guided brachytherapy for locally advanced cervical cancer in the EMBRACE study. *Radiother Oncol* 2016;118(1):160-166.

(4) Mazeron R, Fokdal LU, Kirchheiner K, Georg P, Jastaniyah N, Šegedin B, *et al*. Dose–volume effect relationships for late rectal morbidity in patients treated with chemoradiation and MRI-guided adaptive brachytherapy for locally advanced cervical cancer: Results from the prospective multicenter EMBRACE study. *Radiother Oncol* 2016;120(3):412-419.

(5) Sturdza A, Pötter R, Fokdal LU, Haie-Meder C, Tan LT, Mazeron R, *et al*. Image guided brachytherapy in locally advanced cervical cancer: Improved pelvic control and survival in RetroEMBRACE, a multicenter cohort study. *Radiother Oncol* 2016;120(3):428-433.

(6) International commission on radiation units & measurements. Report 89: Prescribing, recording, and reporting brachytherapy for cancer of the cervix. *J of the ICRU* 2013; 13:1-258.

(7) Lang S, Nulens A, Briot E, Kirisits C, De Brabandere M, Dumas I, *et al*, Intercomparison of treatment concepts for MR image assisted brachytherapy of cervical carcinoma based on GYN GEC-ESTRO recommendations. *Radiother Oncol* 2006;78(2):185-193.

(8) Fowler JF. Sensitivity analysis of parameters in linear-quadratic radiobiologic modeling. *Int J Radiat Oncol Biol Phys* 2009;73(5):1532-1537.

(9) Nath R, Bice WS, Butler WM, Chen Z, Meigoni AS, Narayana V, *et al* AAPM recommendations on dose prescription and reporting methods for permanent interstitial brachytherapy for prostate cancer: Report of Task Group 137. *Med Phys* 2009;36(11):5310-5322.

(10) Kelland LR, Steel GG. Differences in radiation response among human cervix carcinoma cell lines. *Radiother Oncol* 1988;13(2):225-232.

(11) West CM, Davidson SE, Roberts SA, Hunter RD. Intrinsic radiosensitivity and prediction of patient response to radiotherapy for carcinoma of the cervix. *Br J Cancer* 1993;68(4):819-823.

(12) Chapman JD, Nahum AE. Radiotherapy treatment planning. Baton Rouge: CRC Press; 2016.

(13) Roberts SA, Hendry JH, Swindell R, Wilkinson JM, Hunter RD. Compensation for changes in dose-rate in radical low-dose-rate brachytherapy: A radiobiological analysis of a randomised clinical trial. *Radiother Oncol* 2004;70(1):63-74.

(14) Hall E, Giaccia A. Radiobiology for the radiologist. 7th ed. Philadelphia PA: Williams & Wilkins; 2012.

(15) Gasinska A, Fowler JF, Lind BK, Urbanski K. Influence of overall treatment time and radiobiological parameters on biologically effective doses in cervical cancer patients treated with radiation therapy alone. *Acta Oncol* 2004;43(7):657-666.

(16) Joiner M, Kogel A. *Basic clinical radiobiology*. 4th ed. Boca Raton: CRC Press/Taylor & Francis Group; 2009.

(17) Fowler JF. Dose reduction factors when increasing dose rate in LDR or MDR brachytherapy of carcinoma of the cervix. *Radiother Oncol* 1997;45(1):49-54

(18) Guerrero M, Li XA. Halftime for repair of sublethal damage in normal bladder and rectum: an analysis of clinical data from cervix brachytherapy. *Phys Med Biol* 2006;51(16):4063-4071.

(19) Chen SW, Liang JA, Yang SN, Ko HL, Lin FJ. The adverse effect of treatment prolongation in cervical cancer by high-dose-rate intracavitary brachytherapy. *Radiother Oncol* 2003;67(1):69-76.

(20) Song S, Rudra S, Hasselle MD, Dorn PL, Mell LK, Mundt AJ, *et al*. The effect of treatment time in locally advanced cervical cancer in the era of concurrent chemoradiotherapy. *Cancer* 2013;119(2):325-331.

(21) Tanderup K, Fokdal LU, Sturdza A, Haie-Meder C, Nazeron R, van Limbergen E, *et al*. Effect of tumor dose, volume and overall treatment time on local control after radiochemotherapy including MRI guided brachytherapy of locally advanced cervical cancer. *Radiother Oncol* 2016;120(3):441-446.

(22) Tergas AI, Neugut AI, Chen L, Burke WM, Hershman DL, Wright JD. Radiation duration in women with cervical cancer treated with primary chemoradiation: A population-based analysis. *Cancer Invest* 2016;34(3):137-147.

(23) Bianchi C, Botta F, Conte L, Vanoli P, Cerizza L. Biological effective dose evaluation in gynaecological brachytherapy: LDR and HDR treatments, dependence on radiobiological parameters, and treatment optimisation. *Radiol Med* 2008;113(7):1068-1078.

(24) Beskow C, Ågren-Cronqvist AK, Lewensohn R, Toma-Dasu I. Biological effective dose evaluation and assessment of rectal and bladder complications for cervical cancer treated with radiotherapy and surgery. *J Contemp Brachytherapy* 2012;4(4):205-212.

(25) Huang Z, Mayr NA, Gao M, Lo SS, Wang JZ, Jia G, *et al*. Onset time of tumor repopulation for cervical cancer: First evidence from clinical data. *Int J Radiat Oncol Biol Phys* 2012;84(2):478-484.

(26) Tsang RW, Fyles AW, Li YQ, Rajaraman MM, Chapman W, Pintilie M, *et al*. Tumor proliferation and apoptosis in human uterine cervix carcinoma I: correlations between variables. *Radiother Oncol* 1999;50(1):85-92.

(27) Bolger BS, Cooke TG, Symonds RP, MacLean AB, Stanton PD. Measurement of cell kinetics in cervical tumours using bromodeoxyuridine. *Br J Cancer* 1993;68(1):166-171.

(28) Bolger BS, Symonds RP, Stanton PD, MacLean AB, Burnett R, Kelly P, *et al.* Prediction of radiotherapy response of cervical carcinoma through measurement of proliferation rate. *Br J Cancer* 1996;74(8):1223-1226.

(29) Tsang RW, Fyles AW, Kirkbride P, Levin W, Manchul LA, Milosevic MF, *et al*. Proliferation measurements with flow cytometry Tpot in cancer of the uterine cervix: Correlation between two laboratories and preliminary clinical results. *Int J Radiat Oncol Biol Phys* 1995;32(5):1319-1329.

(30) Symonds P, Bolger B, Hole D, Mao JH, Cooke T. Advanced-stage cervix cancer: rapid tumour growth rather than late diagnosis. *Br J Cancer* 2000;83(5):566-568.

(31) Brenner DJ, Hall EJ. Conditions for the equivalence of continuous to pulsed low dose rate brachytherapy. *Int J Radiat Oncol Biol Phys* 1991;20(1):181-190.

(32) Williams MV, Denekamp J, Fowler JF. A review of ratios for experimental tumors: Implications for clinical studies of altered fractionation. *Int J Radiat Oncol Biol Phys* 1985;11(1):87-96.

(33) Dische S, Saunders MI, Sealy R, Werner ID, Verma N, Foy C, *et al*. Carcinoma of the cervix and the use of hyperbaric oxygen with radiotherapy: a report of a randomized controlled trial. *Radiother Oncol* 1999;52(2):93-98.

(34) Tucker SL, Thames HD, Michalski JM, Bosch WR, Mohan R, Winter K, *et al*. Estimation of α/β for late rectal toxicity based on RTOG 94-06. *Int J Radiat Oncol Biol Phys* 2011;81(2):600-605.

(35) Kutcher GJ, Burman C, Brewster L, Goitein M, Mohan R. Histogram reduction method for calculating complication probabilities for three-dimensional treatment planning evaluations. *Int J Radiat Oncol Biol Phys* 1991;21(1):137-146.

(36) Brenner DJ. Fractionation and late rectal toxicity. *Int J Radiat Oncol Biol Phys* 2004;60(4):1013-1015.

(37) Marzi S, Saracino B, Perongari MG, Arcangeli S, Gomellini S, Arcangeli G, *et al*. Modeling of alpha/beta for late rectal toxicity from a randomized phase II study: conventional versus hypofractionated scheme for localized prostate cancer. *J Exp Clin Cancer Res* 2009;28(1):117.

(38) Halperin E, Perez C, Brady L. Perez and Brady's Principles and Practice of Radiation Oncology. Philadelphia: Wolters Kluwer Lippincott Williams & Wilkins; 2013

(39) Viswanathan AN, Beriwal S, De Los Santos JF, Demanes DJ, Gaffney D, Hansen J, *et al*. American Brachytherapy Society consensus guidelines for locally advanced carcinoma of the cervix. Part II: High-dose-rate brachytherapy. *Brachytherapy* 2012;11(1):47-52.

(40) De Leeuw AAC, van de Kamer JB, Moerland MA, Philippens MEP, Jürgenliemk-Schulz IM. The effect of alternative biological modelling parameters (α/β and half time of repair T1/2) on reported EQD2 values in the treatment of advanced cervical cancer. *Radiother Oncol* 2011;101(2):337-342.

(41) Pötter R, Tanderup K, Kirisits C, de Leeuw A, Kirchheiner K, Nout R, *et al* The EMBRACE II study: The outcome and prospect of two decades of evolution within the GEC-ESTRO GYN working group and the EMBRACE studies. *Clin Transl Radiat Oncol* 2018;9:48-60.

CHAPTER 4
EXPERIMENTAL DETERMINATION OF RADIOBIOLOGICAL PARAMETERS USING A NOVEL *IN VITRO* RADIATION METHODOLOGY

A version of this chapter has been published as: Chow B, Warkentin B, Nanda K, Ghosh S, Huang F, Gamper AM, Menon G. BAIRDA: a novel in vitro setup to quantify radiobiological parameters for cervical cancer brachytherapy dose estimations. Phys Med Biol. 2022;67(4):045012.

4.1 Introduction

Post-EBRT BT boost options (either HDR or PDR) used in locally advance cervical cancer (LACC) treatments vary significantly in both dose fraction size and dose delivery, factors that have been shown to significantly affect radiobiological response (1,2,3,4). Current clinical prescriptions account for this by expressing the combined treatment in units of radiobiological dose (EQD2), which characterizes the cell response through the radiobiological parameters α/β and $T_{1/2}$ (5,6,7,8). Understanding the relative strengths of different prescriptions thus requires an appropriate estimate of both parameters. However, while assumed parameter values have been utilized in clinical cervical cancer dose calculations, these standard values lack direct supporting evidence.

As described in Chapters 2 and 3, there have been attempts to more accurately quantify cervical cancer radiobiological parameters through *in vitro* experiments or the analysis of clinical outcomes data (9,10). However, these studies report a wide range of values (6 to 21 Gy for α/β, and 0.15 to 5.7 hours for $T_{1/2}$), which could result in the significant differences in prescribed tumor doses of up to 13% that were reported in Chapter 3 (11). These differences could result in either the organs at risk receiving higher than necessary doses when striving to achieve a specific tumor control probability, or alternatively, in target underdosing and corresponding reduced rates of tumor control. Therefore, further investigation of the radiobiological parameter values will facilitate a more accurate dosimetric comparison of radiation schedules.

Differences in previous experimental techniques may be a cause for the wide range of reported parameter values. While most *in vitro* experiments utilize clonogenic survival assays, considered the "gold standard" for measuring cell survival, the specifics of radiation delivery (e.g. photon energy, dose rate, radiation schedule) vary significantly between reported BT studies (9,10,12,13). Some studies used Co-60 or 4 MV linac photons, both much higher in average photon energy than Ir-192 (7,9,12). Additionally, most previous research utilized single radiation exposures that do not replicate either the HDR BT or PDR BT delivery schedules and dose rates, which raises concerns about how well these reported parameter values are representative of dose responses to BT.

A first-in-kind **b**rachytherapy **a**fterloader ***i****n vitro* **r**adiation **d**elivery **a**pparatus (BAIRDA) was developed and validated to address these experimental shortcomings. Unlike previously reported experimental studies relevant to BT, which used other radiation sources, this approach eliminates potential confounding factors introduced by photon energy and dose rate differences: cells are irradiated using the Ir-192 sources utilized in clinical HDR and PDR BT afterloaders (9,12). Additionally, clinically relevant treatment schedules (e.g. pulsed and fractionated treatments) were delivered to further reflect real-world contemporary clinical scenarios. The use of multiple cell lines provided a representative cross section of *in vitro* radiation response of cervical cancers. Confirmatory experimental results were obtained through established methodologies using a traditional irradiator. Through a novel methodology that lays the framework for the expanded study of cellular response to BT, radiobiological parameters were established that identify potential uncertainties in BT planning.

4.2 Materials and Methods

4.2.1 Cell Lines and Culture

The *in vitro* experiments were performed with four squamous cell carcinoma (SCC) and three adenocarcinoma (AC) cervical cancer cell lines. The use of both SCC and AC provide a characterization of the two most common cervical cancer types. Table 4.1 provides a summary of the cell lines used, their HPV and p53 gene status, how they were acquired, and the cell culturing media. All cell lines were maintained and used at early passages.

Table 4.1: Summary of SCC and AC cell lines used for *in vit*ro experiments.

Cell Line	Cancer Type	HPV status	p53 status	Acquisition	Culture Medium
CaSki	SCC	HPV 16(+) (14)	Wild-type (15)	ATCC[a]	DMEM[b] + glucose 10% FBS[c] 1% Pen-strep[d]
C-33A	SCC	HPV(-) (15)	Mutated p53 (15)	ATCC	DMEM + glucose 10% FBS 1% Pen-strep
SiHa	SCC	HPV 16(+) (16)	Wild-type (16)	ATCC	DMEM + glucose 10% FBS 1% Pen-strep
SW756	SCC	HPV 18(+) (17)	Wild-type (18)	ATCC	DMEM + glucose 10% FBS 1% Pen-strep
HeLa	AC	HPV 18(+) (19)	Wild-type (19)	Godbout Lab[e]	DMEM + glucose 10% FBS 1% Pen-strep
JHUCS-3	AC[f]	Unknown	Unknown	RIKEN[g]	DMEM/F12[h] + glucose 15% FBS 1% Pen-strep
SiSo	AC	HPV 18(+) (20)	Unknown	DSMZ[i]	RPMI[j] + glucose 10% FBS 1% Pen-strep

[a] American Type Culture Collection, Manassas, VA
[b] Dulbecco's Modified Eagle's Medium
[c] Fetal bovine serum
[d] Penicillin-streptomycin
[e] University of Alberta, Edmonton, AB
[f] JHUCS-3 cells were reported as AC by RIKEN at the time of purchase
[g] RIKEN BioResource Research Center, Tsukuba, Japan
[h] 1:1 mixture of DMEM and Nutrient Mixture F-12
[i] Leibniz Institute DSMZ, Braunschweig, Germany
[j] Roswell Park Memorial Institute 1640 medium

4.2.2 Clonogenic Survival Assays

Cells were irradiated using single or fractionated (hourly "pulses") schedules with Cs-137 (traditional irradiator) or Ir-192 sources (BAIRDA). Subsequently, cells were incubated for 8 to 14 days, depending on the cell line, then stained with 1% crystal violet (70% ethanol) for 10 minutes. The incubation period was empirically determined by pilot experiments for each cell line as the length of time required to establish 50 cell colonies. Each plate was scanned using an Epson Expression 10000XL flatbed scanner (Seiko Epson Corp., Nagano) at 1,200 dpi in tagged image file format (.tif). Colonies, conventionally defined as clusters of ≥50 cells, were manually identified from these scans using Paint.net, an image processing software (21,22). Each

combination of radiation source and irradiation schedule was deployed in at least three independent experiments on different days, with each experiment being conducted in triplicate; i.e., each data point was inferred from at least nine measurements. Details of assay preparation, radiation sources, dose prescriptions, irradiation schedules, and methods for estimating the radiobiological parameters are detailed in the following sections.

4.2.3 Preparation of Cells for Clonogenic Assays

Clonogenic survival assays utilized adherent cells taken from 6 cm tissue culture plates. The cells were incubated at 37°C and 5% CO_2 with their last passaging >24 hours prior to the preparation of the cell culture plates for irradiation (Figure 4.1(a)). The confluency of the tissue culture plates was between 70% and 100% (estimated under microscope) at the time of assay preparation.

Suspension mixtures (an "initial volume") were formed by trypsinizing all cells on the tissue culture plate and suspending them in culture medium (Figure 4.1(b)). Depending on the cell line and initial confluency, the initial volume varied between 4 to 10 mL. This was based on prior experience that ensured a reasonable estimate when measuring the initial volume's cell density using a hemocytometer. A high density mixture would result in cell counting difficultly on the hemocytometer due to overcrowding, whereas low densities can result in inaccurate measurements. A second suspension, referred to as the "diluted mixture", was then prepared to distribute cells for clonogenic survival assays (Figure 4.1(c)). The lower cell density of the diluted mixture allowed for a more consistent seeding distribution for the assays. While the diameters of the tissue culture plates (Sarstedt, Numbrecht, Germany) for the irradiator (6 cm) and BAIRDA (10 cm) were different, the density of the diluted mixture was consistent for both and was determined based on preliminary experiments. The diluted mixture was prepared in a 50 mL flask to contain 1,000 cells/mL. This cell density made the calculation of seeding straightforward: every 1 mL of the suspension added to the assay would seed 1,000 cells. The diluted mixture included a volume of media from the initial mixture and additional culture medium to yield the desired cell density. The suspension was agitated for 10 to 20 minutes to ensure the cells were evenly distributed in the mixture. Cells were then seeded on tissue culture plates by transferring the diluted suspension using a 1 mL micropipette (Brand Tech, Essex,

Connecticut). Additional culture medium was used to fill the plate to 4 mL (6 cm) or 10 mL (10 cm), typical volumes of media for the respective plate sizes. For example, if 1 mL of the diluted solution was transferred to a 6 cm plate, an additional 3 mL of culture media would be added.

For experiments with the Cs-137 irradiator, where cell lines were irradiated to doses from 0 to 6 Gy, it was determined that seeding 1,000 cells on a 6 cm tissue culture plate (approximately 35 cells/cm^2) prevented overcrowding and yielded a large number of colonies. A similar cell seeding density was used for Ir-192 irradiation (3,000 cells per 10 cm plates; approximately 38 cells/cm^2) to prevent variances caused by plate overcrowding. Compared to all other cell lines, preliminary experiments with JHUCS-3 showed that fewer colonies were formed with 1,000 cells seeded on a 6 cm plate. Hence for this cell line, the number of cells was increased to 2,500 and 7,500 cells for the 6 and 10 cm plates, respectively.

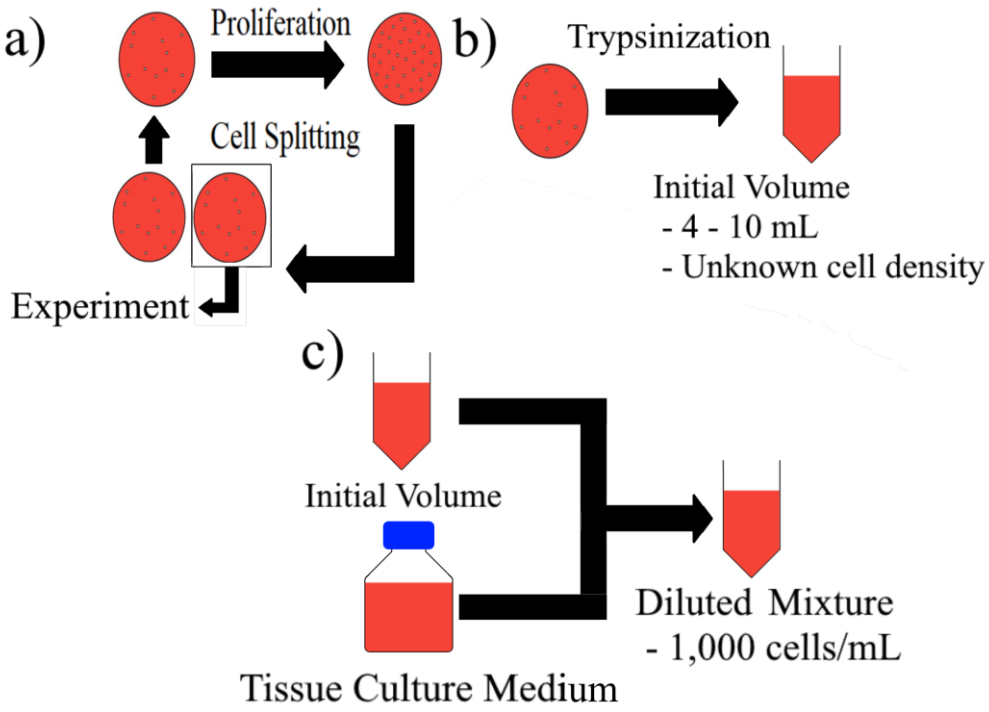

Figure 4.1: The preparation of cells for clonogenic assays. (a) Cells are passaged >24 hours before preparation. (b) Cells from a tissue culture plate are trypsinized and suspended in an "initial volume" of 4 to 10 mL, with the volume selected based on prior experience to ensure a reasonable estimation of the initial volume's cell density via hemocytometer. (c) A portion of the initial volume is mixed with tissue culture medium to create a diluted mixture with a cell density of 1,000 cells/mL. This diluted mixture is then used to seed the tissue culture plates used for experiments.

It was determined that a minimum of 2 hours was necessary for good cell adherence to the plates. However, allowing 8 hours (used only when overnight preparation was necessary) between seeding and radiation delivery did not affect the experimental outcome (further discussion in Section 5.2.1.3). All experiments in this study delivered radiation within 2 to 8 hours after cell seeding.

4.2.4 Irradiation Set Up

4.2.4.1 Cs-137 Irradiation

Radiation biologists have traditionally used Cs-137 irradiators for clonogenic survival assays (23,24,25). Therefore, experiments were performed using a Cs-137 commercial irradiator (JL Shepherd and Associates, San Fernando, CA), to enable comparison to the dose responses observed using Ir-192 sources in clinical BT afterloaders. The Cs-137 irradiator has two Cesium Chloride capsules (collectively called a "Cs-137 source"; source activity of 1,089 Ci at the time of experiments) that are pneumatically raised into position in a shaft, covered with a brass filter, at the back of the irradiation chamber (26). Over the period of the study, the dose rate at the center of the irradiator was 0.74 – 0.77 Gy/min. Tissue culture plates were centrally stacked on the 30 cm diameter turntable (Figure 4.2), rotating at 12 rotations per minute, providing nearly uniform exposure. This was verified by triple-channel dosimetry measurements using Gafchromic EBT3 films (Niagara Falls, NY, Lot # 06201901) by exposing the film to radiation and digitizing the results on the Epson Expression 10000XL scanner (27,28). The maximum relative difference between prescribed and delivered radiation across the irradiated films was 1.2% (details provided in Section 5.2.2.3.4). As prolonged exposures to room temperatures can affect cell response, the plates were irradiated and returned to the incubator within 20 minutes, to ensure that the cells experienced minimal cooling (29).

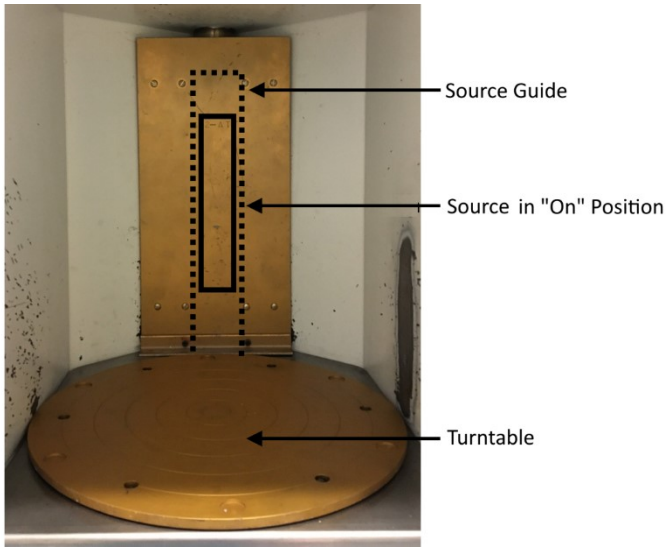

Figure 4.2: The irradiation cavity of the Cs-137 irradiator. The Cs-137 source is raised to the "on" position (solid line) through a source guide (dotted line) behind the brass attenuator to irradiate a 31 x 31 x 37 cm^3 cavity. The tissue culture plates were placed on the 30 cm diameter turntable, set to rotate at 12 rotations per minute.

Two treatment schedules were used for irradiation using the Cs-137 irradiator. Single acute treatments (SATs; similar to HDR treatments), performed to determine α and β values, were delivered using doses from 0.5 to 6 Gy with accompanying unirradiated plates used as controls. An endpoint of 6 Gy was selected since the number of surviving colonies was too low to provide statistically relevant results at higher doses (defined as $\geq$3 colonies). For fractionated schedules, radiation was delivered in 9 hourly pulses (0.23 to 1 Gy/pulse, depending on cell line; similar to PDR treatments) or 5 bihourly pulses (one pulse every two hours; 0.40 to 1.89 Gy/pulse). Doses for the hourly experiments were selected using two approaches, corresponding to a projected survival of either 5% or 15% after 9 hourly pulses, when using the modified LQ model (Equation (2.2)) and the α and β derived from the Cs-137 SAT experiments for each cell line and a conventional $T_{1/2}$ of 1.5 hours (30,31). Details of the application of this model in BT are discussed in Section 4.2.4.1. The selection of two different survival values allowed for adequate characterization of the dose-response relationship, despite a priori uncertainty in the value of $T_{1/2}$. For example, if $T_{1/2}$ was much smaller than the conventional value of 1.5 hours, the plates irradiated for a projected 15% survival would experience less cell death than expected, reducing the range of surviving fractions included in the results. This impact is reduced through the introduction of a second experiment with lower (5%) expected survival when assuming the

conventional value for $T_{1/2}$. Bihourly experiments were conducted to investigate the possibility of non-monoexponential repair, a potential avenue for repair reported in the literature and discussed in Chapter 2 (32). These experiments were performed with a projected survival of 15% after 5 (bihourly) pulses using α and β values from SAT experiments and $T_{1/2}$ = 1.5 hours. If non-monoexponential repair occurs, then the $T_{1/2}$ will vary as the time between pulses changes. For example, if biphasic repair (a biexponential repair model where sublethal damage is divided into two categories: one group of damage that is repaired at a "fast" rate and another at a "slow" rate) occurs, as the time between pulses is varied, the proportion of sublethal damage repaired by the "fast" and "slow" repair processes will also change, resulting in variance in the estimated value of $T_{1/2}$ (32). Therefore, variance in $T_{1/2}$ between experiments using bihourly and hourly pulses would suggest evidence of non-monoexponential repair.

4.2.4.2 Ir-192 Irradiation

Cells were irradiated using clinical microSelectron Ir-192 HDR (nominal activity: 10 Ci) and PDR (nominal activity: 0.5 Ci) afterloaders (Elekta, Stockholm, Sweden) in conjunction with BAIRDA. The selected configuration delivers radiation non-uniformly across a plate (Section 4.3.1). HDR (HDR-BAIRDA) and PDR (PDR-BAIRDA) Ir-192 afterloaders were used for SAT and fractionated radiation deliveries, respectively. Larger plates of 10 cm diameter were used for BAIRDA experiments to facilitate the measurement of a wider range of clonogenic survival generated by the larger dose variation across the bigger plate. A CT scan of the BAIRDA apparatus was imported into the Oncentra Brachy treatment planning software (OcB; v4.5, Elekta, Stockholm, Sweden) for designing the plan for cell irradiation. Doses for the SAT (1.53 to 5.00 Gy at prescription points) and fractionated (0.20 to 0.76 Gy/pulse) Ir-192 experiments were selected to produce approximately 15% survival at the prescription points. Indeed, preliminary experiments using BAIRDA indicated a wide range of survival (approximately 5% to 90%) could be characterized on the irradiated plates using these dose prescriptions.

4.3 BAIRDA: A Novel *in vitro* System for Radiation Delivery Using Brachytherapy Afterloaders

4.3.1 Technical Development

The BAIRDA setup was developed to perform *in vitro* experiments with HDR and PDR afterloaders. During BAIRDA experiments, the tissue culture plate is inserted into a 1 mm deep circular slot made in a 3D printed plastic base (Figure 4.3(a)). The cells are irradiated via movement of the Ir-192 source to 21 dwell positions spaced 5 mm apart within a plastic catheter (ProGuide needle, Elekta, Stockholm) mounted in a tight-fitting groove below the plate (Figure 4.3(b)); alignment of the catheter and plate are confirmed via fixed marks on the apparatus. Dose for 15% survival was prescribed in OcB to points (located 5 mm apart) along lines placed 1 cm on either side of the plastic catheter, emulating an infinite line source (Figure 4.3(c)). Since the irradiation time per pulse using PDR-BAIRDA (4.8 to 17.6 minutes/pulse) was significantly longer compared to the HDR-BAIRDA (1.3 to 4.7 minutes/fraction) exposures, the PDR-BAIRDA plates were placed in a water bath to maintain the cells close to 37°C during radiation delivery (Figure 4.3(a)).

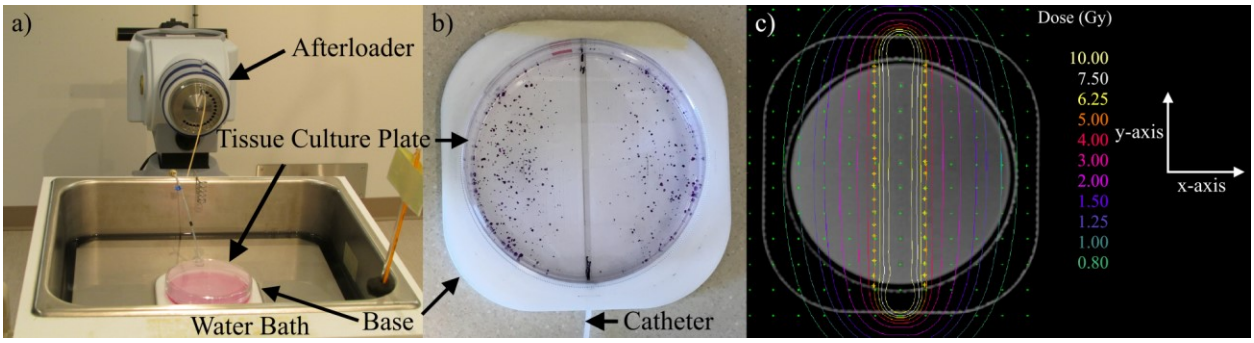

Figure 4.3: (a) Setup for radiation delivery during PDR-BAIRDA (lid not shown). (b) A top-down image of the base with a tissue culture plate irradiated to 5 Gy prescribed to points at 1 cm on either side of the catheter and showing the pattern of colonies (crystal violet stain), (c) Isodose distribution for a dose of 5 Gy prescribed to the same prescription points (yellow crosses).

4.3.2 Dose Delivery Verification

As seen in Figure 4.3(c), there is a dose gradient formed across the plate beyond the prescription lines. The dose gradient across the plates in BAIRDA was verified by exposing 7.5 x 3 cm strips of Gafchromic EBT3 film when 2 Gy is delivered to the prescription points at 1 cm on either side of the catheter. Each film piece was attached to the base of the tissue culture plate and immersed

in 10 mL of water (the amount of culture medium used during experiments); measurements were repeated three times on the HDR afterloader (Figure 4.4(a)). It has been shown that the effects of short-term immersion in water on Gafchromic film (less than 30 minutes) is negligible (33). The films were dried and scanned using the Epson Expression 10000XL scanner. The close agreement (<1%) between the doses measured from a central 3.4 x 1 cm region of the film and the planned dose confirms the accuracy of dose delivery during BAIRDA (Figure 4.4(b)). Details of the Gafchromic film calibration are given in Chapter 5 (see Section 5.2.2.3.3).

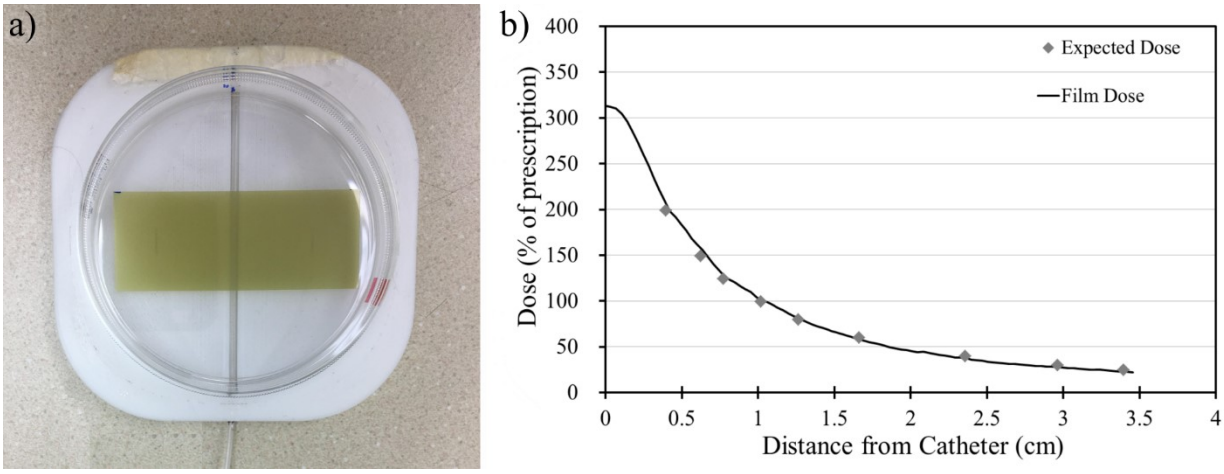

Figure 4.4: (a) Setup for film irradiation to measure dose delivery during HDR-BAIRDA. (b) Dose, as a percent of the prescription, plotted against the distance from the catheter for the planned and film-measured dose, averaged from the three measurements.

4.3.3 Functional Application

The non-uniform dose distribution in BAIRDA allows for a wide range of SF measurements across a single plate. Effective segmentation of a single plate can therefore provide a series of regions of interest (ROIs) with different doses and SF. As a result, characterization of a cell line's dose response can be conducted from just two plates, an irradiated plate (Figure 4.5(a)) and a control (Figure 4.5(b)), unlike in the case of traditional clonogenic assays using a Cs-137 irradiator, where several plates are required for dose-survival relationship estimation (Figure 4.6).

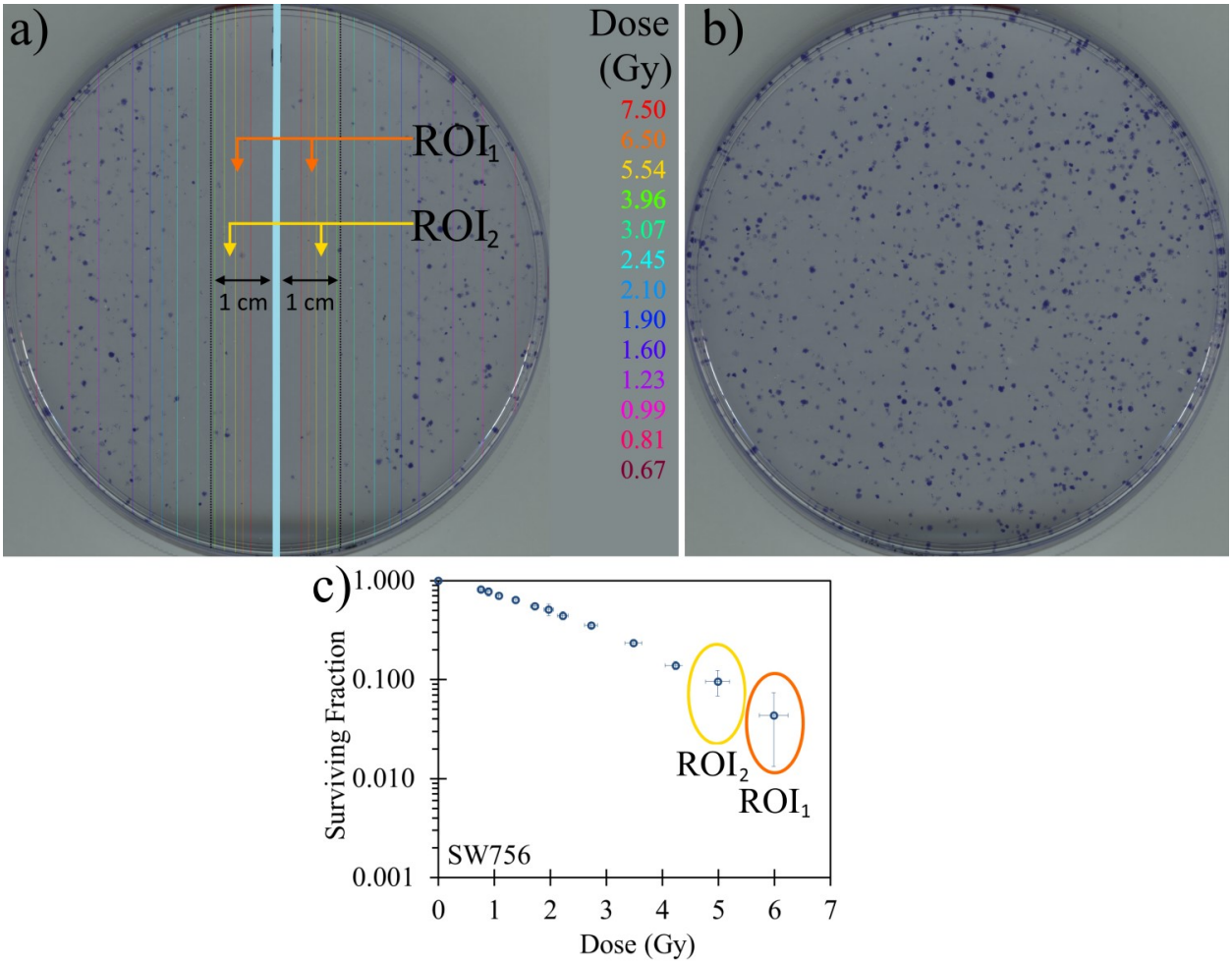

Figure 4.5: (a) Colonies from surviving SW756 cells following irradiation with a single acute exposure (SAT) delivered using HDR-BAIRDA as a line source prescription (3.77 Gy at points 1 cm on either side of the blue line). (b) Colonies from 3,000 SW756 cells plated on a tissue culture plate taken as control (0 Gy). (c) The dose response curve for SW756 cells for a single experiment. The error bars represent the total uncertainties associated with the experiment. Prescription isodoses are shown as black dotted lines in (a).

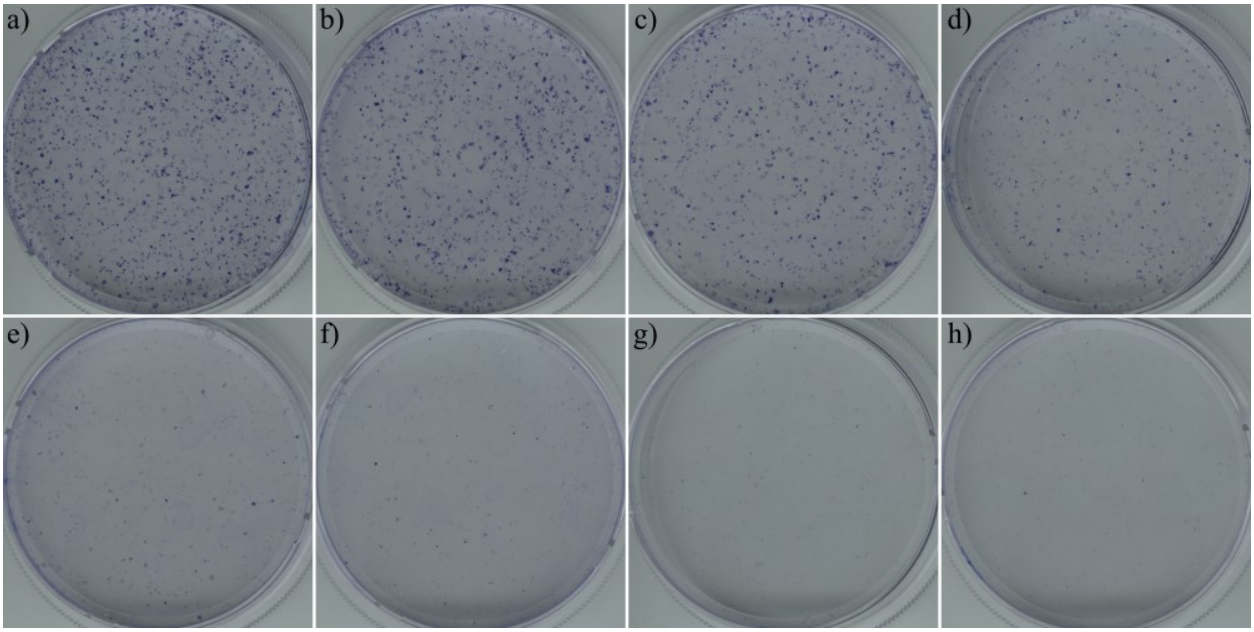

Figure 4.6: (a) SW756 cell colonies in a tissue culture dish used as the control (or 0 Gy exposure). (b) Cell survival after a single fraction of 0.5 Gy, (c) 1 Gy, (d) 2 Gy, (e) 3 Gy, (f) 4 Gy, (g) 5 Gy, and (h) 6 Gy.

For ROI segmentation, each plate was divided into non-overlapping regions running parallel to the catheter (central blue line in Figure 4.5(a)). The widths of the ROIs were selected such that each ROI covered approximately 5% of the plate and would initially contain 150 cells assuming cells are uniformly distributed on the plate. Depending on the cell line, a plating efficiency of 33 to 75% was observed for all cell lines using the control plates, except for JHUCS-3 (plating efficiency of approximately 15%). The corresponding number of estimated colonies in each ROI was thus 50 to 113, before accounting for radiation-induced cell death. With such ROI widths, SFs as low as approximately 4% could be measured. However, for some cell lines with plating efficiencies at the lower end of the range (e.g. SW756), the high dose ROIs (e.g. 6 Gy) had to be enlarged (up to 10% of the plate) for better statistics. The exact dose at which increased ROI sizes were used depended on the cell line's plating efficiency and radiosensitivity (listed in Table 4.2). The average dose and SF in each ROI were estimated using Equations (4.2) and (4.3), respectively (see Section 4.4.1). Survival curves for each cell line were generated using the dose to SF data from all the ROIs on the plate. This approach, particularly using clinical Ir-192 afterloaders, has not been attempted previously.

Table 4.2: Summary of SCC and AC BAIRDA ROIs that were enlarged for better statistics.

Cell Line	Experiment	Prescribed ROI Dose	% of plate
CaSki	HDR-BAIRDA	6 Gy	9.6%
	PDR-BAIRDA	6 Gy	6.3%
C-33A	HDR-BAIRDA	None	-
	PDR-BAIRDA	None	-
SiHa	HDR-BAIRDA	6 Gy	7.9%
	PDR-BAIRDA	None	-
SW756	HDR-BAIRDA	None	-
	PDR-BAIRDA	6 Gy	8.7%
HeLa	HDR-BAIRDA	None	-
	PDR-BAIRDA	7.75 Gy	6.9%
JHUCS-3	HDR-BAIRDA	1.8 Gy 2.5 Gy	7.8% 8.7%
	PDR-BAIRDA	2.0 Gy	7.6%
SiSo	HDR-BAIRDA	None	-
	PDR-BAIRDA	None	-

4.4 Data Analysis

4.4.1 Calculation of Surviving Fraction

The SF is a metric that associates cell survival with the retention of clonogenic capacity after irradiation. To determine clonogenic survival, the number of colonies formed on the irradiated plates was compared to the number formed on a plate seeded in parallel but not exposed to radiation ("control"). Colonies were identified by manual comparison of the size of stained colonies against a reference colony using the image editing software Paint.net. This method of determining survival rate was compared against an Optronix ColCount (Oxford Optronix, Abingdon, UK) automated colony counter, which yielded similar surviving fraction measurements to within 5% (further discussed in Section 5.2.1.6).

For Cs-137 experiments, the uniform dose distribution across each irradiated plate allows for a traditional calculation of the surviving fraction (SF_{Cs}), where each plate provides the cell survival for one dose. The SF_{Cs} for a plate irradiated to dose D will depend on the number of cells seeded on it (N), the colonies they form after radiation (C), as well as the number of cells seeded on a control plate, N_0, that form C_0 colonies.

$$SF_{Cs}(D) = (C/N)/(C_0/N_0) \quad (4.1)$$

Triplicate measurements at each dose D were recorded for all experiments. The SF_{Cs} for a particular dose, D, was calculated using the average C and C_0 values for the triplicate irradiated and control plates in the experiment.

The methodology for calculating surviving fractions for Ir-192-irradiated plates, SF_{Ir}, must be modified from Equation (4.1) as the dose delivered across the plates is non-uniform. This was incorporated by dividing an irradiated plate into multiple ROIs, as shown in Figure 4.5(a). The borders of each ROI were selected to coincide with isodoses generated by an infinite line source of radiation and do not overlap with one another. For example, the area between the orange and yellow lines (isodoses of 6.50 and 5.54 Gy, respectively) represents a single ROI (labeled ROI_1), while the area between the yellow and green lines (5.54 and 4.54 Gy) represents another (ROI_2). For the doses used, 5 to 100 colonies were formed in each ROI, a sufficient number for further analysis.

The average dose delivered to cells in each ROI, D_{ROI}, was calculated using:

$$D_{ROI} = \int D(\vec{r})dA \,/\, \int dA \tag{4.2}$$

where $D(\vec{r})$ is the dose at position $\vec{r}$, and the integration is over the area of the ROI. Using this equation, the D_{ROI} in ROI_1 is 6 Gy and in ROI_2 is 5 Gy, in the example depicted in Figure 4.5(a). D_{ROI} is then taken as the representative dose for the ROI. The surviving fraction for an ROI, SF_{Ir}, can be calculated by modifying Equation (4.1). An ROI of area A_i with N_i cells initially seeded and C_i colonies formed after irradiation was compared against a control plate of area A_0 with N_0 cells that yielded C_0 colonies (Figure 4.5(b)). As the cells were seeded in the same way on the control and irradiated plates, the cells per unit area, ρ, were considered to be the same on both plates. Therefore, SF_{Ir} can be calculated as:

$$SF_{Ir}(D_{ROI}) = (C_i/\rho A_i)/(C_0/\rho A_0) = (C_i/A_i)/(C_0/A_0) \tag{4.3}$$

Thus, a wide range of surviving fractions can be determined following the analysis of the entire plate and all its associated ROIs.

Figure 4.5(c) presents the SF results for the plate irradiated in Figure 4.5(a) for all ROIs on the plate. ROI_1 and ROI_2 provide two surviving fractions at different doses, highlighted in Figure 4.5(c) by orange and yellow ovals, respectively.

4.4.2 Uncertainty Analysis

This section provides a brief overview of the uncertainty analysis, which will be discussed in detail in Chapter 5.

Uncertainties associated with SF estimations and the dose delivered were calculated and represented by error bars in the survival data. SF uncertainty was determined through propagation of errors from Equations (4.1) and (4.3), assuming negligible uncertainty in the selection of the size of the ROI area in Equation (4.3). For these calculations, uncertainty in the colonies formed is taken as the standard deviation in the number of colonies counted in the triplicate experiments for a particular plate (Cs-137) or ROI (Ir-192). For Cs-137 irradiated plates, the measurement uncertainty in SF_{Cs}, ΔSF_{Cs}, included only the uncertainty in the colonies formed, ΔC and ΔC_0, and none in the number of seeded cells, N or N_0. Measurement uncertainty for C and C_0, ΔC and ΔC_0 respectively, was taken as the standard deviation in the number of colonies on the irradiated plates or control plates. Using propagation of errors for Equation (4.1):

$$\Delta SF_{Cs}(D) = SF_{Cs}(D)\sqrt{(\Delta C_0/C_0)^2 + (\Delta C/C)^2} \tag{4.4}$$

For exposures with Ir-192, the measurement uncertainty in SF_{Ir}, ΔSF_{Ir}, was calculated using uncertainties in the number of colonies counted for the ROI, ΔC_i, and the control plate, ΔC_0. The uncertainty was taken as the standard deviation in the number of colonies in the triplicate of ROI or control plates. Therefore, using propagation of errors for Equation (4.3):

$$\Delta SF_{Ir}(D_{ROI}) = SF_{Ir}(D_{ROI})\sqrt{(\Delta C_0/C_0)^2 + (\Delta C_i/C_i)^2} \tag{4.5}$$

Additional uncertainties in survival (6.0% for Cs-137 and 6.3% BAIRDA; including uniformity of cell seeding and subjectivity in the identification of colonies) and dose (<0.8% for Cs-137 and <4.3% for BAIRDA; including source calibration and transit dose) were identified and quantified (represented as error bars from hereon); details are discussed in Chapter 5.

4.4.3 Estimation of α/β Ratio and $T_{1/2}$

For each cell line, the α/β ratio and $T_{1/2}$ were estimated separately using the Cs-137 and Ir-192 sources by fitting the modified LQ model to measured SFs. SAT experiments were used to determine best-fit values of α and β using the following formulation of Equation (2.1) (31,34):

$$-ln(SF_{Cs\ or\ Ir}) = \alpha D + \beta D^2 \tag{4.6}$$

For fractionated experiments, the LQ model relies on $T_{1/2}$ in addition to α and β. The effects of dose rate and fractionation are given by an adaptation of Equation (2.2):

$$-ln(SF_{Cs\ or\ Ir}) = \alpha D + \beta G D^2 \tag{4.7}$$

where G is given by Equation (2.45) (30,31). Simultaneous estimation of all three parameters is sensitive to experimental outliers, which could result in fit values with large uncertainties. To mitigate this, α and β of each cell line were taken to be those found during the SAT experiments of the same cell line, which leaves $T_{1/2}$ as the only adjustable parameter in the fits to the PDR experiments.

Equation (4.6), used to determine the α and β values with SAT, assumes an instantaneous delivery time. As the dose was delivered over the course of a few minutes, for both Cs-137 and HDR-BAIRDA SAT experiments, a more precise estimation would require calculations using Equations (2.45) and (4.7) over the course of a single pulse (N = 1 in Equation (2.45)). The value of G when N = 1 can therefore be calculated to consider the repair of sublethal damage caused by a non-instantaneous delivery, and compared to the value of G = 1 assumed for analysis of the SAT experiments. When using the conventional $T_{1/2}$ value of 1.5 hrs, over the range of irradiation times for Cs-137 and HDR-BAIRDA SAT experiments (1.30 to 8.1 minutes), the value of G would vary from 0.980 to 0.997. The impact of repair within SAT, such as in HDR applications, is therefore minimal.

Radiobiological parameter values were determined from the experimental results using Matlab (vR2016a, The Mathworks Inc, Natick, MA). Fitting of SF data was performed using Matlab's Curve Fitting toolbox to determine best fit parameter values for α and β (SAT experiments) and $T_{1/2}$ (fractionated) using the weighted least squares method, and corresponding 95% Wald confidence intervals (35). For SAT experiments, α and β were estimated by minimizing the X^2 metric in Equation (4.8) (36):

$$X^2(\alpha,\beta) = \sum_{i=1}^{n} \frac{\left([-ln(\alpha D_i + \beta {D_i}^2)] - [-ln(SF_i)]\right)^2}{\left(-\Delta ln(SF_i)\right)^2 + \left((\alpha + 2\beta D_i)\Delta D_i\right)^2} \tag{4.8}$$

where n data points were measured, each reporting an SF (presented as $\ln(SF_i)$) and dose (D_i) with uncertainties of $\Delta\ln(SF_i)$ and ΔD_i, respectively. Calculation of the confidence intervals for

α/β was conducted using propagation of errors from the standard deviation of α and β (36). Fractionated experiments were used to estimate $T_{1/2}$ by minimizing the X^2 metric using:

$$X^2(T_{1/2}) = \sum_{i=1}^{n} \frac{([-ln(\alpha D_i + \beta G(T_{1/2}) D_i{}^2)] - [-ln(SF_i)])^2}{(-\Delta ln(SF_i))^2 + \left((\alpha + 2\beta G(T_{1/2}) D_i)\Delta D_i\right)^2} \quad (4.9)$$

4.5 Results

4.5.1 Validation of the Novel BAIRDA Configuration and Approach

To validate this novel method for radiation delivery, dose responses measured using BAIRDA were compared to the multi-plate approach used in the Cs-137 irradiator. Prescription doses for the HDR-BAIRDA experiments were selected to be 3.4 Gy for C-33A, 5 Gy for CaSki and SiHa, 3.8 Gy for SW756, 4.7 Gy for HeLa, 1.5 Gy for JHUCS-3, and 4.2 Gy for SiSo based on 15% survival at the prescription line. Figures 4.8 (HPV(-) SCC cell line C-33A), 4.9 (HPV(+) SCC cell lines; CaSki, SiHa, SW756), and 4.13 (AC cell lines; HeLa, JHUCS-3, and SiSo) show close agreement between single fraction survival curves generated with Cs-137 and Ir-192 sources. This suggests that differences in photon energy between the sources (average γ energies: 0.662 and 0.380 MeV for Cs-137 and Ir-192, respectively) do not cause substantial differences in dose response and that the experimental procedure using BAIRDA (e.g. configuration, SF assessment) is comparable to traditional approaches. Due to their similar relative biological effectiveness, the difference in photon energies of the two sources was not expected to affect the results significantly. The agreement observed between the two data sets validates the use of the novel method using BAIRDA as an alternative approach for *in vitro* experimental studies.

4.5.2 Considerations using BAIRDA

Due to the non-uniform dose distribution with BAIRDA, the dose and SF are both influenced by the choice of the ROI size: large ROIs reduce the uncertainty in the number of colonies but will encompass a wide dose gradient over the region and vice versa. Since the dose gradient as a function of distance is steepest at higher doses near the catheter, large dose variations are observed in the ROIs in this region. For example, the ROI closest to the catheter in Figure 4.5(a) encompassed a range of 1 Gy (7.50 to 6.50 Gy) across its width, while the dose variance in the ROI farthest away was only 0.14 Gy (0.81 – 0.67 Gy). Low colony counts in the ROIs

experiencing high doses can lead to large relative differences in the number of colonies counted in repeated experiments. For instance, in HDR-BAIRDA for C-33A, the average SF was 0.054 with a standard deviation of 0.016 for the 5 Gy ROI, a relative uncertainty of 31%. However, for the same cell line and experiment, the relative uncertainty in SF for low dose ROIs (e.g. <1 Gy), which bear higher colony counts, was <5%, similar to the variance seen in the control plates.

Although the experiments solely used "infinite line source" plans, multiple alternative configurations of radiation are technically feasible with BAIRDA. The example in Figure 4.7 shows the distribution from an assumed point source approximation resulting from a single source position. Since such a configuration produces extremely small ROIs at high doses, which would result in few, if any, colonies, it would be better suited for evaluating response at lower doses in the outer "rings". Note that the dose profile across the tissue culture plate will not fully match the point source approximation due to an anisotropic dose distribution (37,38).

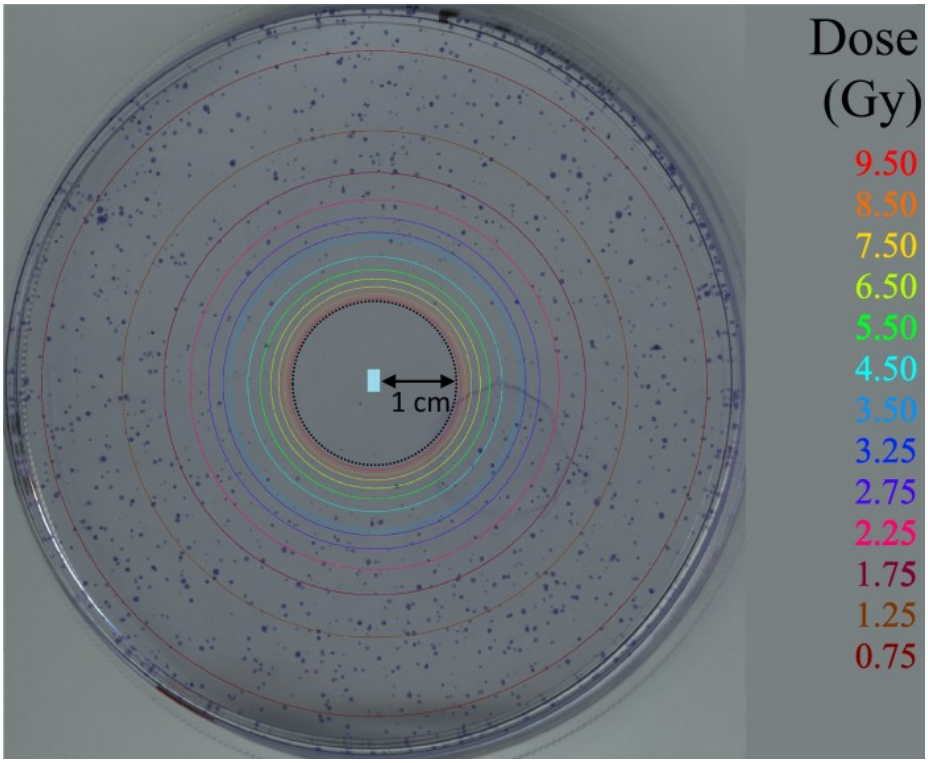

Figure 4.7: Colonies from 3,000 SiHa cells following irradiation with a SAT exposure delivered using HDR-BAIRDA as a point source prescription (10 Gy at points placed on the black dotted circle of 1 cm radius from the blue dot). For all plates, cells were incubated for 10 days following irradiation for colony formation. The isodose lines represent the dose profile assuming a point source approximation.

4.5.3 Estimation of Radiobiological Parameters Utilizing Fractionated Regimens

4.5.3.1 Squamous Cell Carcinoma

With pulsed dose deliveries, the time interval between fractions (pulses) is relatively short, resulting in incomplete repair of sublethal damage. The accumulation of unrepaired sublethal damage and interaction with new damage from subsequent pulses leads to excess cell killing compared to a fractionated regimen with longer breaks between fractions (though the survival is still higher than if the total dose was given acutely). In the LQ model, the β term accounts for the cell killing due to the interaction of sublethal damages. G modulates this term (Equation (4.7)) to incorporate the dependence on the time between pulses, the number of pulses, and $T_{1/2}$ (39,40). To calculate the biological equivalent dose for a given pulsed treatment plan thus requires knowledge of a representative value for $T_{1/2}$.

Results from the single dose experiments used to determine α and β for squamous cell lines are shown in Figures 4.8 and 4.9, and highlight inter-tumoral heterogeneity in radiosensitivity. C-33A, the only HPV(-) cell line in this study (Figure 4.8), is more radiosensitive than the other three (Figure 4.9). For example, at 6 Gy, C-33A has SF values of 0.013 and 0.024 for Cs-137 and Ir-192 experiments, compared to corresponding values of 0.041 and 0.042 for SW756, and values from 0.074 to 0.108 for CaSki and SiHa. This represents an approximate fivefold variation in survival at 6 Gy.

In contrast to SAT deliveries, the time interval between pulses in pulsed dose experiments and the cell line-specific repair capacity determines the extent of repair of sublethal DNA damage. With faster repair rates (smaller $T_{1/2}$), fewer lethal lesions are ultimately formed over the course of treatment. To determine G, and thus $T_{1/2}$, the dose response to pulsed dose treatments was measured by varying the pulse size (compare Figures 4.10(a) and 10(b)) and the time interval (Figure 4.10(c)). Figures 4.10 illustrates the response to different fractionated treatment schedules using the Cs-137 source for SW756. Each data point represents plates irradiated with a different number of pulses.

When compared with the SAT responses in Figure 4.9(c), Figure 4.10 highlights the sparing potential of fractionated treatments using BT. At a total dose of 6 Gy, the SF of SW756 from pulsed dose treatments ranges from 0.062 to 0.065, approximately 60% higher than the corresponding range of 0.038 to 0.042 for SAT. However, a higher SF of 0.19 would be expected for SW756 for daily fractions of 0.68 Gy (Figure 4.11(d)), due to assumed complete sublethal repair between fractions (i.e. G = 1 in Equation (2.44)). This demonstrates the effects of incomplete repair with pulsed deliveries. As expected, a smaller dose per pulse also increases clonogenic survival. This can be seen in Figure 4.11, where SF curves derived from each cell line's hourly pulsed dose experiments are shown against curves of single acute doses (SAT) and daily fractions (calculated; fraction sizes equal to the smaller hourly pulse). Figure 4.11 also highlights the magnitude of increased sparing as a function of increased time between pulses.

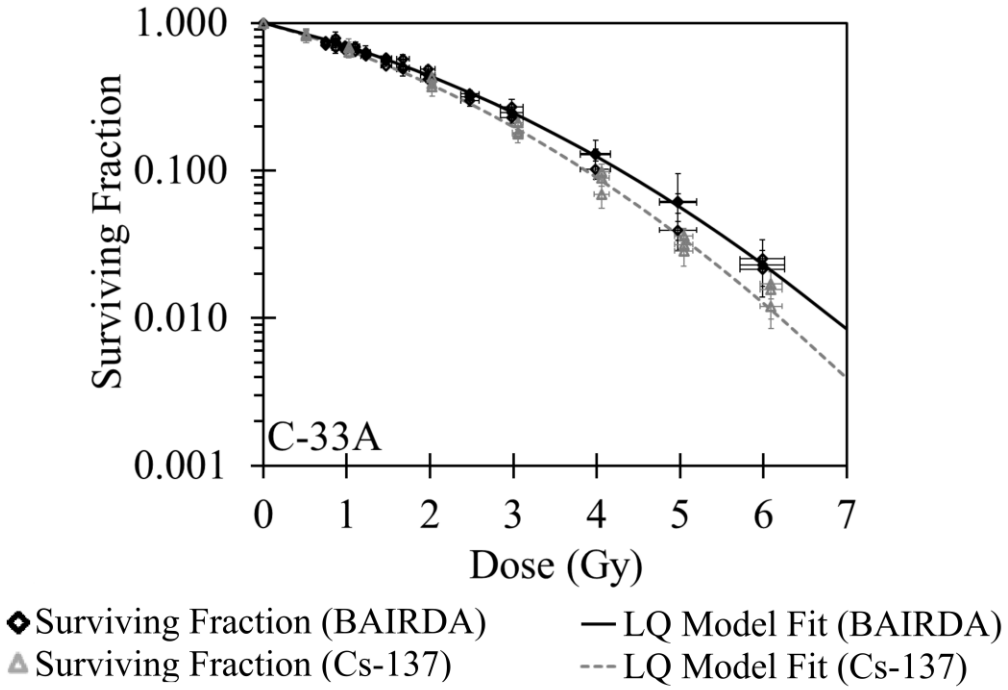

Figure 4.8: Dose response curves for the HPV(-) C-33A cells exposed with a Cs-137 irradiator to single acute doses (SAT) of 0, 0.5, 1, 2, 3, 4, 5, and 6 Gy (gray data points) and HDR-BAIRDA (black), where the doses were prescribed such that an SF of 0.15 was predicted at the prescription points based on the results of the Cs-137 SAT experiments. Each data point represents the average of triplicate experiments performed on the same day (error bars represent uncertainties) and three dose points were acquired for each dose level. The LQ model fit was performed using weighted least squares to estimate α and β (Cs-137 fit shown by the dashed gray line and HDR-BAIRDA in solid black).

PDR-BAIRDA assesses the dose response of several dose fractions on the same plate, and was also used to determine $T_{1/2}$ values. Based on results from the multi-plate Cs-137 experiments for 15% survival, PDR-BAIRDA was delivered using 8 hourly pulses with prescription doses per pulse of 0.49 Gy for C-33A, 0.72 Gy for CaSki, 0.76 Gy for SiHa, and 0.58 Gy for SW756 (AC lines discussed in Section 4.5.3.2). Clonogenic survival curves derived from a plate exposed to 8 hourly pulses (and the respective control) are shown in Figure 4.12. In this case, each data point (i.e. ROI) corresponds to the same number of pulses, but a different dose rate (i.e. dose per pulse). This differs from the multi-plate Cs-137 experiments where the fraction size was constant, but the pulse number varied (Figure 4.10).

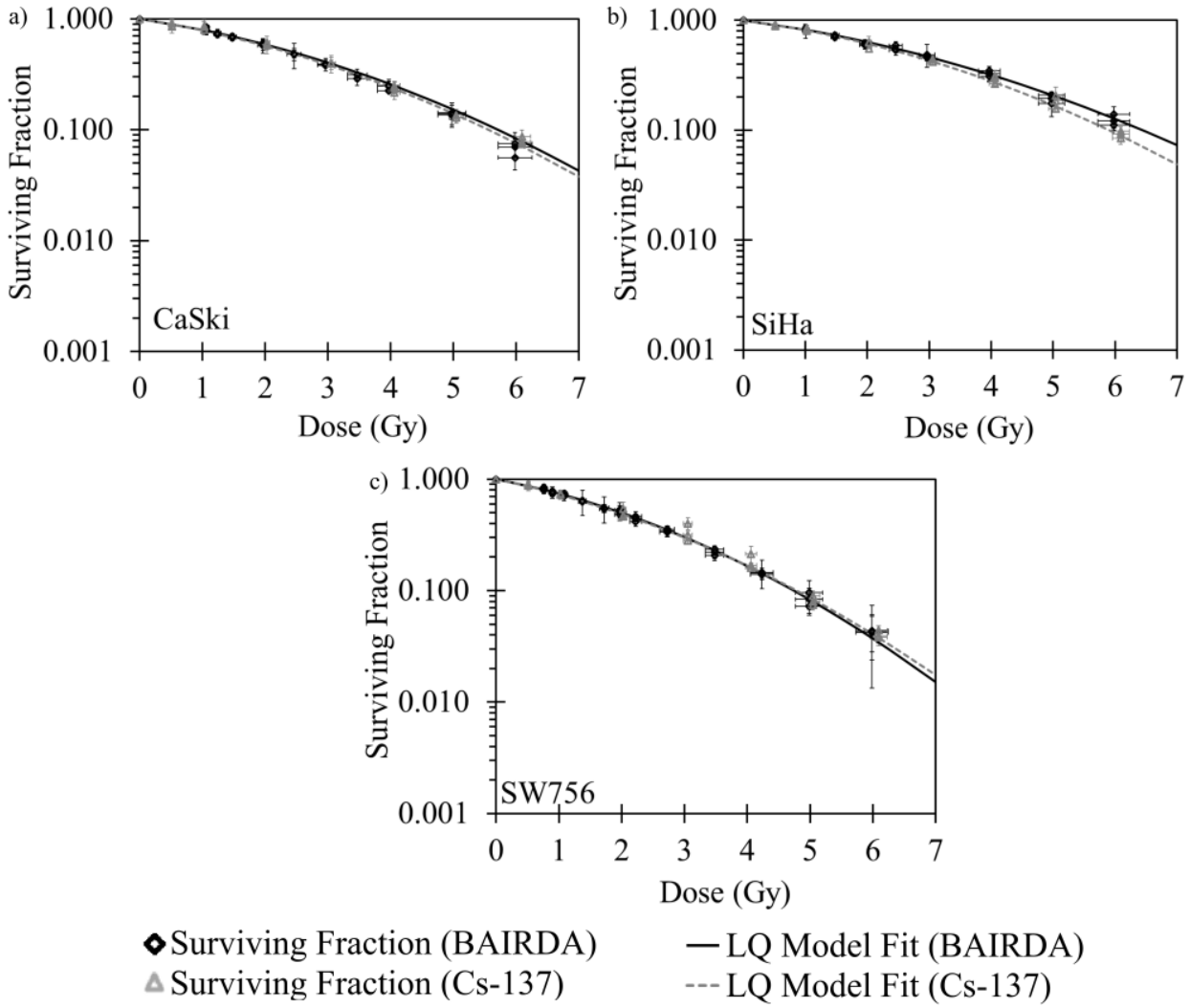

Figure 4.9: Dose response curves for the HPV(+) (a) CaSki, (b) SiHa, and (c) SW756 cells exposed with a Cs-137 irradiator to single acute doses (SAT) of 0, 0.5, 1, 2, 3, 4, 5, and 6 Gy (gray data points) and HDR-BAIRDA (black), where the doses were prescribed such that an SF of 0.15 was predicted at the prescription points based on the results of the Cs-137 SAT experiments for the respective cell lines. Each data point represents the average of triplicate experiments performed on the same day (error bars represent uncertainties) and three dose points were acquired for each dose level. The LQ model fit was performed using weighted least squares to estimate α and β (Cs-137 fit shown by the dashed gray line and HDR-BAIRDA in solid black).

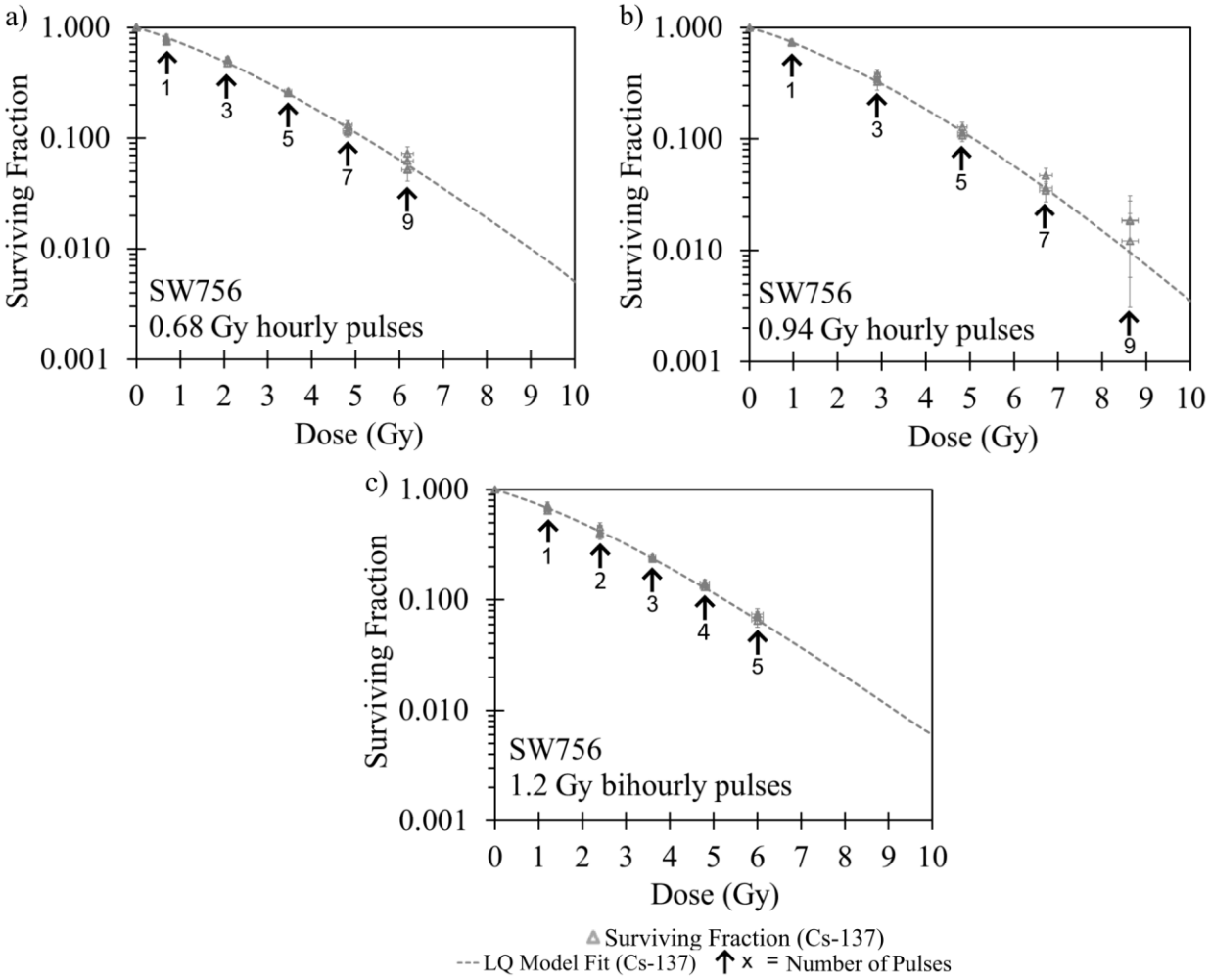

Figure 4.10: Dose response curves from pulsed Cs-137 irradiations fitted to the LQ model using the weighted least squares method to estimate $T_{1/2}$ for the fractionated experiments conducted in triplicate. SW756 cells were irradiated with (a) 9 hourly pulses of 0.68 Gy/pulse, (b) 9 hourly pulses of 0.94 Gy/pulse, or (c) 5 bihourly pulses of 1.2 Gy/pulse. Each data point was derived from a different number of pulses as indicated by the arrows and represents the average of triplicate experiments performed on the same day (error bars represent uncertainties). Three dose points were acquired for each dose level.

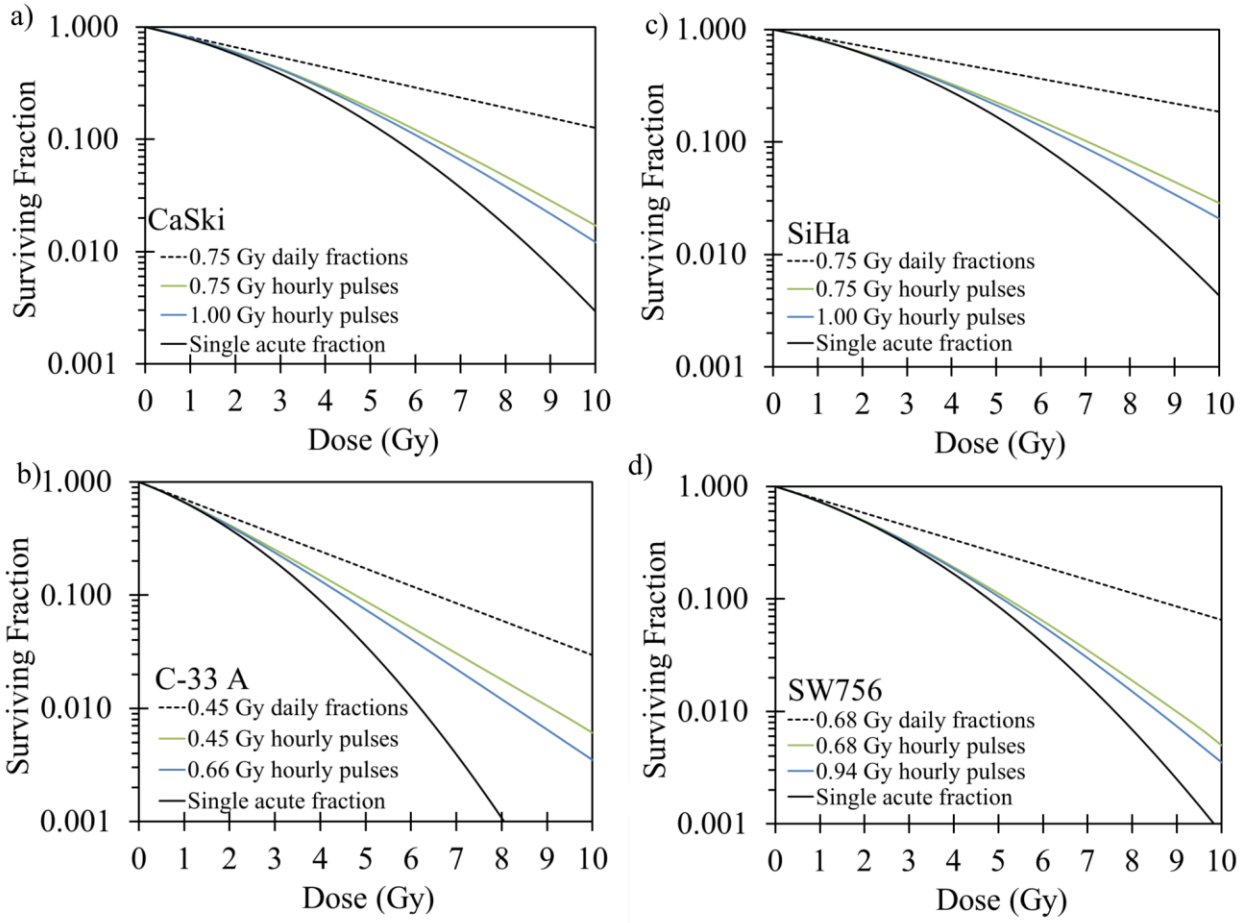

Figure 4.11: Theoretical survival curves for daily fraction, hourly fraction, and SAT irradiations for (a) CaSki, (b) C-33 A, (c) SiHa, and (d) SW756 cells based on radiobiological parameters derived in pulsed dose experiments with the Cs-137 source. The sparing effect of daily fractionation (presumed complete repair of sublethal DNA damage between intervals; dotted black line) compared to SAT (solid black line) or hourly pulses (blue and green lines) is illustrated.

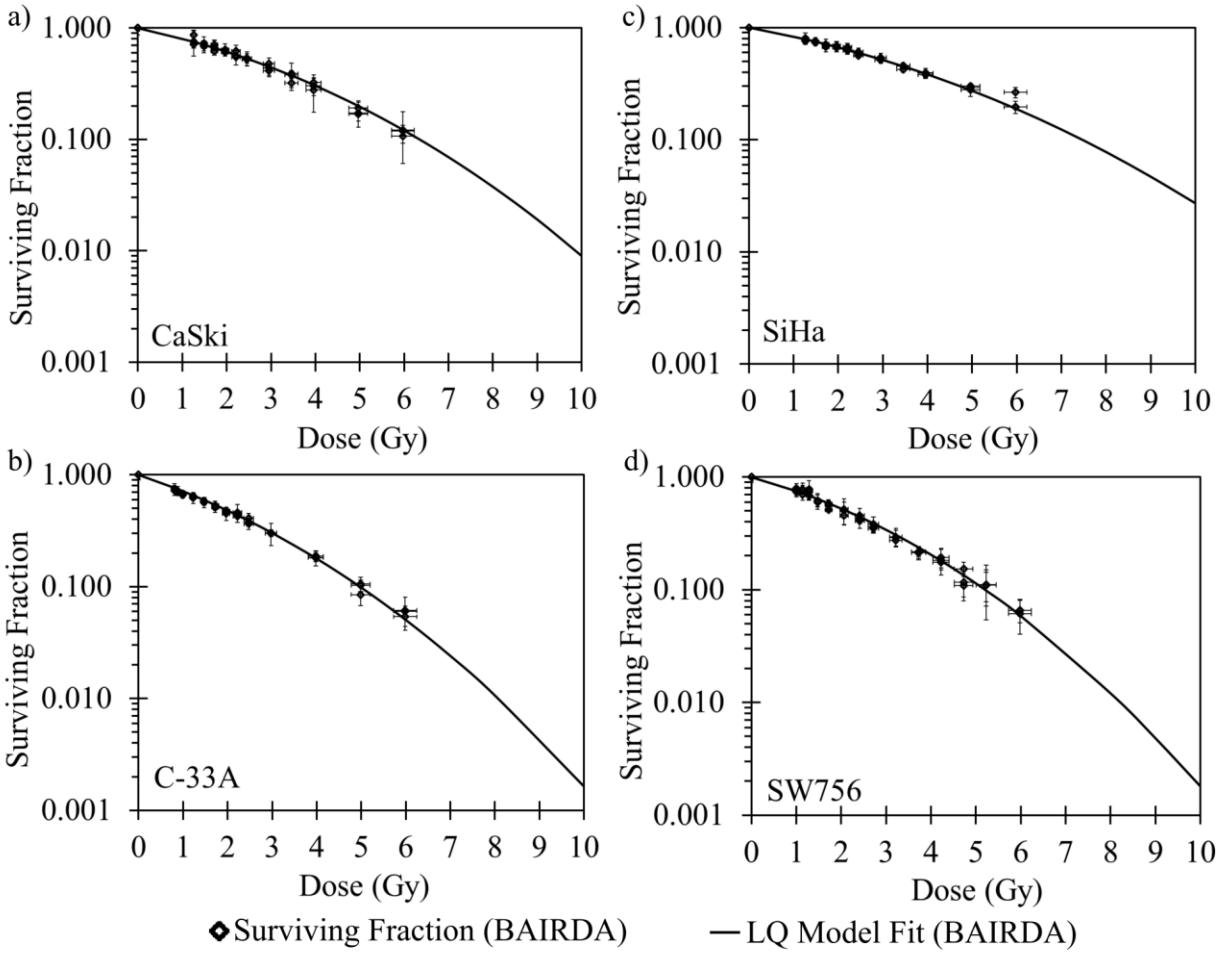

Figure 4.12: Dose response curves from PDR-BAIRDA irradiations for pulsed dose experiments conducted in triplicate for (a) CaSki, (b) C-33A, (c) SiHa, and (d) SW756 cells. Each data point received 8 pulses of radiation and represents the average of triplicate experiments performed on the same day (error bars represent uncertainties). Three dose points were acquired for each dose level. The LQ model fit was performed using the weighted least squares method to estimate $T_{1/2}$. α and β values were derived from HDR-BAIRDA experiments.

Table 4.3 summarizes the radiobiological parameters (α/β ratio and $T_{1/2}$) derived for the four SCC cell lines and the average of the four SCC lines. Welch t-test p-values compare the radiobiological parameters determined by the two radiation sources. To allow for t-test analysis, it is assumed that the α/β and $T_{1/2}$ values are normally distributed and have homogenous variance. Implications for BT dose calculations for treatments aiming to deliver a total dose of 90 Gy EQD2 (including an initial EBRT schedule of 45 Gy delivered in 25 fractions) are illustrated. With the lower α/β ratio and $T_{1/2}$ values determined in this work, the radiobiological doses calculated for both BT techniques (HDR and PDR) differed from those calculated using conventional parameter values. Interestingly, the SCC cell lines studied contained examples of

short and long $T_{1/2}$ values (e.g. C-33A, $T_{1/2} \approx 2$ hrs; SW756, $T_{1/2} \approx 5$ hrs), the clinical implications of which are discussed in Section 4.6.2. These derived $T_{1/2}$ values were consistent between the experimental methods, whether multi-plate Cs-137 or BAIRDA Ir-192 based measurements (Table 4.3).

Table 4.3: Summary of radiobiological parameters determined through single dose and multiple fraction experiments, conducted using a Cs-137 irradiator and BAIRDA (Ir-192 sources) for the squamous cell carcinoma cell lines. α, β, and $T_{1/2}$ were calculated for each experiment, with results presented as a mean (95% confidence interval). p-values were used to compare the radiobiological parameters determined by the two radiation sources. The radiobiological dose of two theoretical treatments is calculated: EBRT delivering 25 fractions of 1.8 Gy followed by a BT boost of either HDR (4 fractions of 7.75 Gy each) or PDR (58 hourly pulses of 0.73 Gy/pulse). These treatments deliver approximately 90 Gy EQD2 with conventional parameter values. Doses were recalculated for both HDR and PDR treatments using α/β ratios and $T_{1/2}$ values determined in this study. The rightmost column shows the resulting dose discrepancy in what would conventionally be assumed to be equivalent HDR and PDR regimens.

	Source	α (Gy^{-1})	β (Gy^{-2})	α/β (Gy)	$T_{1/2}$ (hr)	Radiobiological Dose (Gy EQD2)		
						HDR	PDR	Difference
Clinical assumption	--	--	--	10	1.5	90.1	90.4	-0.3
CaSki	**Cs-137**	0.21 (0.17 - 0.25)	0.036 (0.029 - 0.043)	5.8 (4.2 - 7.3)	3.8 (2.9 - 4.7)	97.7 (94.2 - 103.3)	114.8 (103.2 - 132.0)	-17.1 (-28.7 - -7.8)
	Ir-192	0.20 (0.19 - 0.21)	0.039 (0.035 - 0.042)	5.2 (4.6 - 5.8)	3.3 (2.7 - 3.9)	99.5 (97.7 - 101.6)	112.0 (104.3 - 120.8)	-12.5 (-19.2 - -5.7)
	p-value	0.69	0.28	0.33	0.18	--	--	--
C-33A	**Cs-137**	0.35 (0.31 - 0.39)	0.061 (0.050 - 0.072)	5.7 (4.4 - 6.9)	2.2 (1.5 - 2.8)	98.0 (95.0 - 102.4)	99.4 (91.5 - 109.2)	-1.4 (-8.0 - 9.4)
	Ir-192	0.31 (0.28 - 0.34)	0.056 (0.046 - 0.065)	5.6 (4.5 - 6.6)	2.7 (2.0 - 3.3)	98.3 (95.7 – 102.0)	104.7 (96.3 - 114.6)	-6.4 (-12.6 - 2.8)
	p-value	0.076	0.30	0.82	0.11	--	--	--
SiHa	**Cs-137**	0.16 (0.13 - 0.19)	0.037 (0.032 - 0.043)	4.3 (3.4 - 5.2)	3.6 (3.0 - 4.2)	102.9 (99.5 - 107.3)	119.0 (108.8 - 132.2)	-16.1 (-24.9 - -8.7)
	Ir-192	0.18 (0.16 - 0.20)	0.028 (0.024 - 0.034)	6.3 (4.9 - 7.7)	2.8 (2.4 - 3.1)	96.4 (93.4 - 100.5)	104.2 (98.6 - 110.1)	-7.8 (-10.6 - -2.6)
	p-value	0.17	0.06	0.05	0.06	--	--	--
SW756	**Cs-137**	0.27 (0.23 - 0.31)	0.042 (0.034 - 0.050)	6.5 (4.9 - 8.1)	4.9 (3.9 - 5.8)	95.9 (92.8 - 100.5)	121.5 (109.2 - 138.0)	-25.6 (-37.5 - -16.5)
	Ir-192	0.26 (0.24 - 0.27)	0.048 (0.043 - 0.053)	5.3 (4.7 - 6.0)	4.8 (4.1 - 5.4)	99.2 (97.2 - 101.3)	126.2 (116.8 - 135.7)	-27.0 (-34.4 - -19.6)
	p-value	0.37	0.09	0.13	0.71	--	--	--
All SCC	**Cs-137**	0.25 (0.09 - 0.41)	0.044 (0.021 - 0.067)	5.6 (3.7 - 7.4)	3.6 (1.4 - 5.8)	--	--	--
	Ir-192	0.24 (0.12 - 0.36)	0.043 (0.019 - 0.067)	5.6 (4.6 - 6.6)	3.4 (1.5 - 5.3)	--	--	--
	p-value	0.85	0.89	0.93	0.72	--	--	--

4.5.3.2 Adenocarcinoma

Figure 4.13 shows the results from the single dose experiments for AC cells. As seen in Figures 4.8 and 4.9 for the SCC cell lines, it highlights inter-tumoral heterogeneity in radiosensitivity. JHUCS-3 cells showed significantly higher radiosensitivity than the other cell lines and yielded

no colonies when exposed to >3 Gy. By comparison, both a considerable proportion of HeLa and SiSo cells formed colonies at 4 Gy (SF of approximately 0.25 and 0.18, respectively). Also of interest is the large variance in SF of SiSo cells irradiated using HDR-BAIRDA at 5.75 Gy (in Figure 4.13(c)). The three experiments yielded average SFs of 0.034, 0.058, 0.100, a range of measured SF considerably larger than other cell lines. A possible explanation for this result can be attributed to the small number of colonies formed; an average of 5.3, 9.3, and 12 colonies were identified when calculating the SFs. Therefore, the loss of a small number of colonies would result in large deviations between repeated measurements.

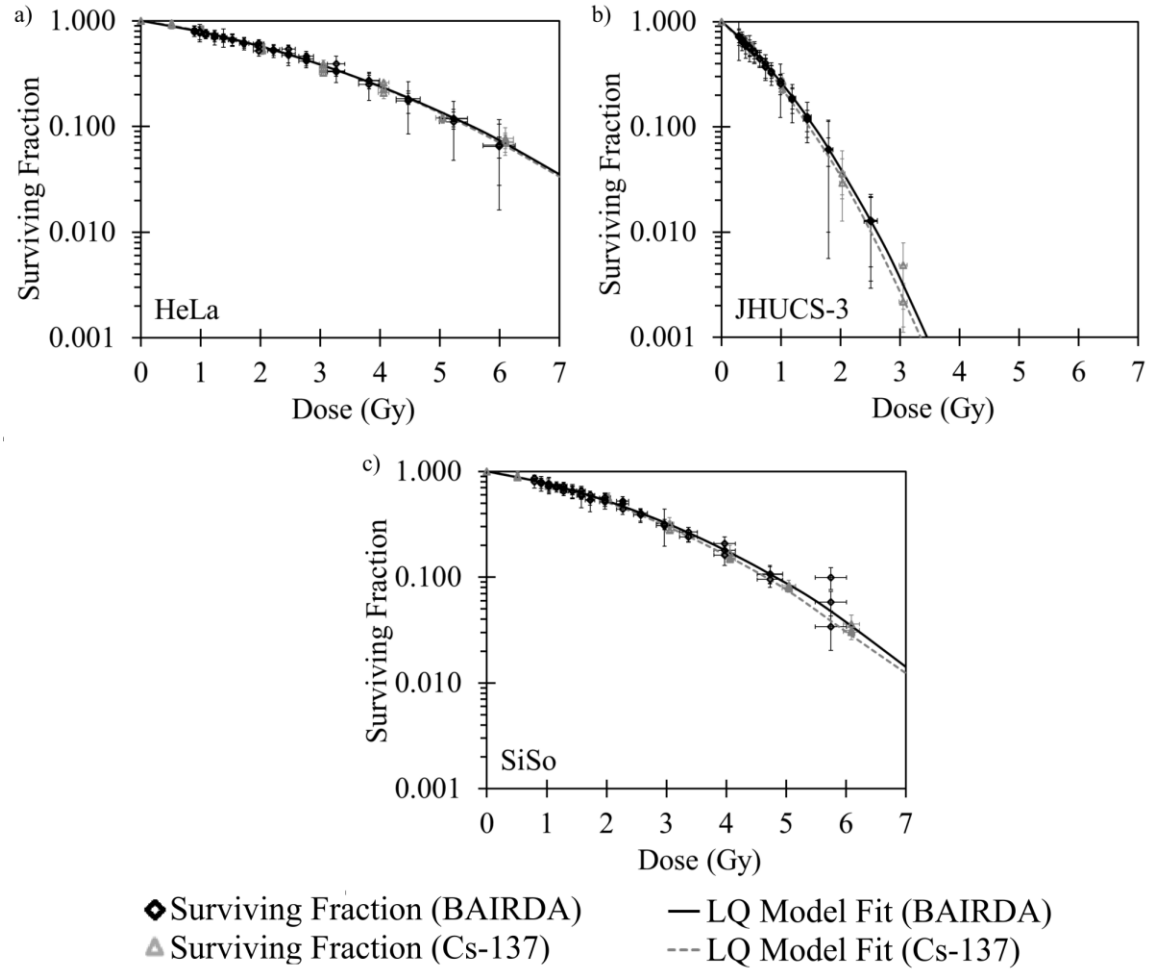

Figure 4.13: Dose response curves for (a) HeLa, (b) JHUCS-3, and (c) SiSo cells exposed with a Cs-137 irradiator to single acute doses (SAT) of 0, 0.5, 1, 2, 3, 4, 5, and 6 Gy (gray data points) and HDR-BAIRDA (black), where the doses were prescribed such that an SF of 0.15 was predicted at the prescription points based on the results of the Cs-137 SAT experiments for the respective cell lines. Each data point represents the average of triplicate experiments performed on the same day (error bars represent uncertainties) and three dose points were acquired for each dose level. The LQ model fit was performed using weighted least squares to estimate α and β (Cs-137 fit shown by the dashed gray line and HDR-BAIRDA in solid black).

Based on results from the multi-plate Cs-137 experiments for 15% survival, PDR-BAIRDA was delivered using 8 hourly pulses with prescription doses per pulse of 0.76 Gy for HeLa, 0.20 Gy for JHUCS-3, and 0.67 Gy for SiSo. The clonogenic survival curves derived from a plate exposed to 8 hourly pulses (and the respective control) are shown in Figure 4.14 for all three AC cells lines. For JHUCS-3, relatively larger uncertainties were measured. This is attributed to the formation of more dispersed cell clusters and greater variability in cell size, increasing the difficulty in colony identification.

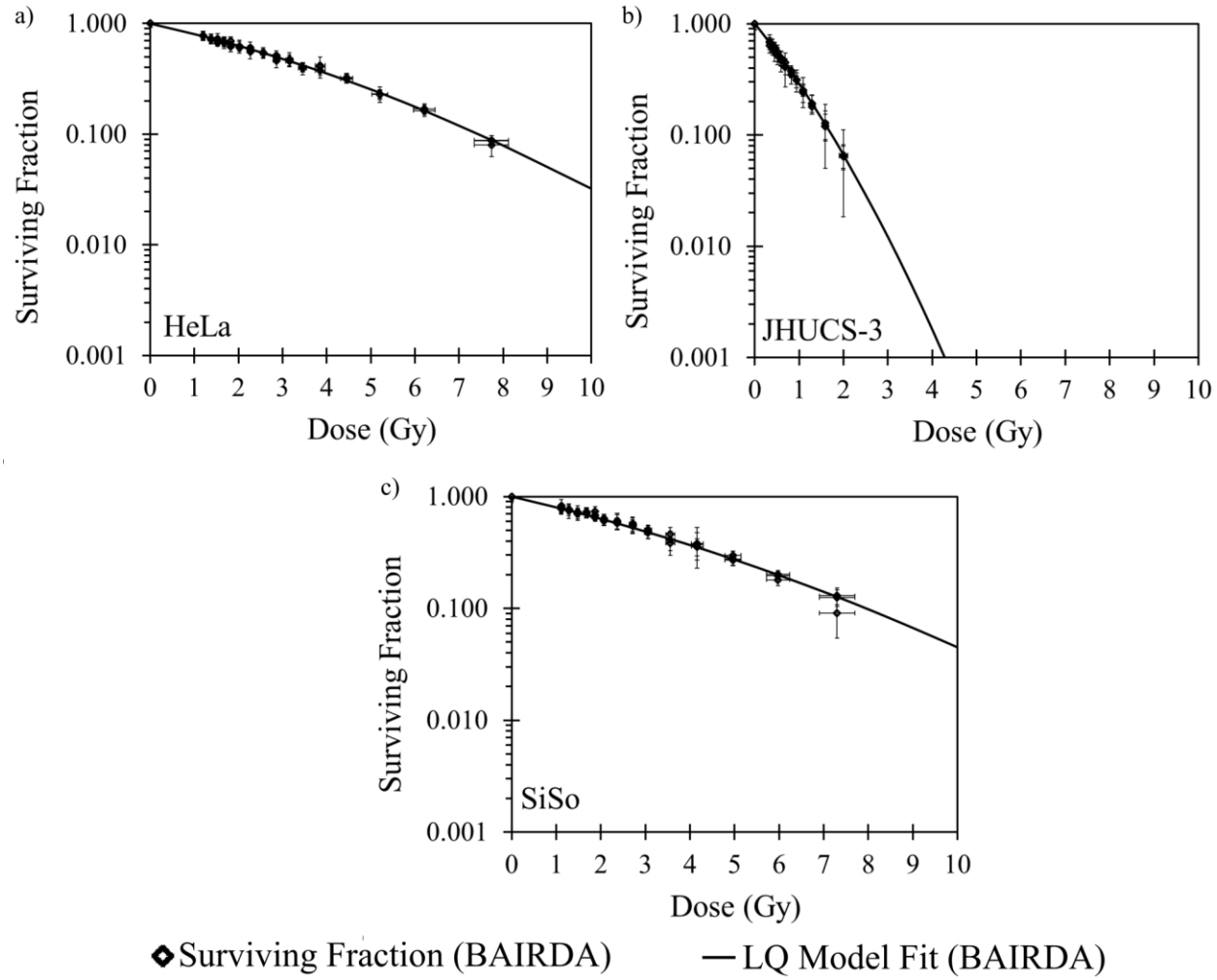

Figure 4.14: Dose response curves from PDR-BAIRDA irradiations for pulsed dose experiments conducted in triplicate for (a) HeLa, (b) JHUCS-3, and (c) SiSo. Each data point received 8 pulses of radiation and represents the average of triplicate experiments performed on the same day (error bars represent uncertainties). Three dose points were acquired for each dose level. The LQ model fit was performed using the weighted least squares method to estimate $T_{1/2}$. α and β values were derived from HDR-BAIRDA experiments.

Table 4.4 summarizes the radiobiological parameters (α/β ratio and $T_{1/2}$ for the three cell lines individually and as an average of the cell lines) derived in this work for the AC cell lines shown in Figures 4.13 and 4.14, and the corresponding effect on the same radiation schedules used in Table 4.3. A Welch t-test (assuming normal distribution and homogenous variance) is used to compare the results of the radiobiological parameters determined using Cs-137 and Ir-192 experiments. Much like the SCC results, AC cell lines exhibit a lower α/β ratio than the conventional assumption. However, the $T_{1/2}$ is lower than the conventionally used 1.5 hour assumption with a range of 0.59 to 1.25 hours.

Table 4.4: Summary of radiobiological parameters determined through single dose and multiple fraction experiments, conducted using a Cs-137 irradiator and BAIRDA (Ir-192 sources) for the adenocarcinoma cell lines. α, β, and $T_{1/2}$ were calculated for each experiment, with results presented as a mean (95% confidence interval). The radiobiological dose of two theoretical treatments is calculated: EBRT delivering 25 fractions of 1.8 Gy followed by a BT boost of either HDR (4 fractions of 7.75 Gy each) or PDR (58 hourly pulses of 0.73 Gy/pulse). These treatments deliver approximately 90 Gy EQD2 with conventional parameter values. Doses were recalculated for both HDR and PDR treatments using α/β ratios and $T_{1/2}$ values determined in this study. The rightmost column shows the resulting dose discrepancy in what would conventionally be assumed to be equivalent HDR and PDR regimens.

	Source	α (Gy^{-1})	β (Gy^{-2})	α/β (Gy)	$T_{1/2}$ (hr)	Radiobiological Dose (Gy EQD2)		
						HDR	PDR	Difference
Clinical assumption	--	--	--	10	1.5	90.1	90.4	-0.3
HeLa	**Cs-137**	0.19 (0.14 - 0.24)	0.042 (0.030 - 0.054)	4.6 (2.8 - 6.4)	1.19 (0.53 - 1.85)	101.6 (96.1 - 111.3)	89.2 (78.1 - 101.8)	12.4 (0.6 - 33.2)
	Ir-192	0.20 (0.19 - 0.22)	0.039 (0.034 - 0.044)	5.2 (4.5 - 6.0)	1.25 (1.17 - 1.34)	99.5 (97.2 - 102.0)	89.6 (88.9 - 90.5)	9.9 (7.2 - 12.8)
	p-value	0.55	0.49	0.39	0.79	--	--	--
JHUCS-3	**Cs-137**	1.14 (1.01 -1.27)	0.264 (0.204 - 0.325)	4.3 (3.2 - 5.4)	1.54 (0.14 - 2.94)	102.9 (98.9 - 108.6)	93.2 (74.1 - 115.7)	9.7 (-8.4 - 34.4)
	Ir-192	1.07 (1.03 -1.11)	0.269 (0.234 - 0.404)	4.0 (3.4 - 4.5)	1.13 (0.88 - 1.38)	104.2 (102.0 – 107.3)	88.0 (84.8 - 92.7)	16.2 (10.3 - 22.3)
	p-value	0.20	0.83	0.42	0.42	--	--	--
SiSo	**Cs-137**	0.21 (0.18 - 0.24)	0.060 (0.053 - 0.067)	3.5 (2.8 - 4.1)	0.55 (0.50 - 0.61)	106.8 (103.7 - 111.3)	80.0 (78.1 - 81.5)	26.8 (22.3 - 33.2)
	Ir-192	0.21 (0.19 - 0.23)	0.057 (0.048 - 0.063)	3.8 (3.1 - 4.4)	0.59 (0.53 - 0.65)	105.2 (102.4 - 109.2)	80.9 (79.1 - 82.2)	24.3 (20.2 - 30.1)
	p-value	0.83	0.24	0.32	0.21	--	--	--
All AC	**Cs-137**	0.51 (-0.55 - 1.57)	0.122 (-0.120 - 0.364)	4.1 (3.0 - 5.2)	1.09 (0.11 - 2.07)	--	--	--
	Ir-192	0.49 (-0.49 - 1.47)	0.121 (-0.130 - 0.372)	4.3 (2.8 - 5.8)	0.99 (0.30 - 1.68)	--	--	--
	p-value	0.96	0.99	0.73	0.79	--	--	--

4.5.3.3 Comparison of Results against Clinical Assumptions

The average SCC and AC radiobiological parameter values are compared against the clinical assumptions in Table 4.5. For each cancer type and each radiation source (Cs-137 and Ir-192), Student t-tests compare the experimentally determined α/β and $T_{1/2}$ against the clinical assumption (10 Gy and 1.5 hr, respectively).

Table 4.5: Summary of the average radiobiological parameters determined through single dose and multiple fraction experiments, conducted using a Cs-137 irradiator and BAIRDA (Ir-192 source) for squamous cell carcinoma and adenocarcinoma cell lines. α/β and $T_{1/2}$ are presented as a mean (95% confidence interval). p-values are shown comparing the experimental results against the conventional clinical assumption using Student t-tests.

	Source	α/β (Gy)	$T_{1/2}$ (hr)
Clinical assumption	--	10	1.5
All SCC	**Cs-137**	5.6 (3.7 - 7.4)	3.6 (1.4 - 5.8)
	p-value vs Clinical Assumption	<0.01	0.03
	Ir-192	5.6 (4.6 - 6.6)	3.4 (1.5 - 5.3)
	p-value vs Clinical Assumption	<0.01	0.03
All AC	**Cs-137**	4.1 (3.0 - 5.2)	1.09 (0.11 - 2.07)
	p-value vs Clinical Assumption	<0.01	0.28
	Ir-192	4.3 (2.8 - 5.8)	0.99 (0.30 - 1.68)
	p-value vs Clinical Assumption	<0.01	0.13

There were statistically significant differences ($p < 0.05$) between the α/β values used clinically and those determined for both SCC and AC. However, the clinically assumed $T_{1/2}$ was statistically different for only SCC. Statistically significant differences in α/β values were not identified when comparing SCC against AC with Welch t-tests for both Cs-137 ($p = 0.20$) and Ir-192 ($p = 0.07$), but were found for $T_{1/2}$ for both Cs-137 ($p = 0.01$) and Ir-192 ($p = 0.01$).

4.5.3.4 Comparison of Estimated $T_{1/2}$ with Hourly and Bihourly Pulses

A comparison of the $T_{1/2}$ values reported with Cs-137 irradiator experiments using both hourly and bihourly fractions for all cell lines is shown in Table 4.6. For each cell line, Welch t-tests (assuming normal distribution and homogenous variance) are used to make the comparisons. Statistically significant differences ($p < 0.05$) were not identified for any cell line.

Table 4.6: Summary of the $T_{1/2}$ values determined through 9 hourly and 5 bihourly fractions using the Cs-137 irradiator for squamous cell carcinoma and adenocarcinoma cell lines. $T_{1/2}$ is presented as a mean (95% confidence interval). p-values are shown comparing the results between the hourly and bihourly experiments of the same cell line using Welch t-tests.

Cell Line	Fractionation Schedule	$T_{1/2}$ (hr)
CaSki	Hourly	3.3 (2.7 - 3.9)
	Bihourly	3.5 (3.0 - 4.0)
	p-value	0.43
C-33A	Hourly	2.7 (2.0 - 3.3)
	Bihourly	2.1 (1.5 - 2.7)
	p-value	0.07
SiHa	Hourly	2.8 (2.4 - 3.1)
	Bihourly	2.9 (2.3 - 3.4)
	p-value	0.68
SW756	Hourly	4.8 (4.1 - 5.4)
	Bihourly	4.5 (3.9 - 5.1)
	p-value	0.32
HeLa	Hourly	1.19 (0.53 - 1.85)
	Bihourly	1.35 (0.58 - 2.12)
	p-value	0.61
JHUCS-3	Hourly	1.54 (0.14 - 2.94)
	Bihourly	1.78 (0.85 - 2.71)
	p-value	0.65
SiSo	Hourly	0.55 (0.50 - 0.61)
	Bihourly	0.49 (0.34 - 0.64)
	p-value	0.30

4.6 Discussion

4.6.1 BAIRDA as a Means to Study BT Radiobiology

By measuring different dose responses on a single plate, and after a single or a series of exposures, BAIRDA is a platform that allows the determination of α, β, and $T_{1/2}$ for a particular cell line in a timely and cost-effective way. The use of BAIRDA in the study of the dose response to SATs allows for a consistent irradiation time, and therefore a standardization of the Lea-Catcheside time factor, for all dose measurements. In SATs where the dose rate is constant for all exposures (such as with the Cs-137 source), irradiation times are varied to deliver different doses. Furthermore, BAIRDA is easily modifiable to integrate environmental changes. Previous studies utilized multi-plate experimentation and were limited to irradiation under atmospheric oxygen concentration. The setup described here can readily be modified to expose cells to conditions of physoxia or hypoxia, thus more closely resembling a tumor microenvironment. Future studies on the influence of combining radiation with systemic therapy agents (cisplatin being the gold standard chemotherapy agent given concurrent with EBRT for LACC) could also make use of BAIRDA to efficiently screen potential novel BT radiosensitizers for efficacy. Besides its utility to investigate clinically relevant questions, the broad and efficient applicability of BAIRDA also provides an ideal tool to deepen the understanding of radiobiological phenomena.

4.6.2 Representative Radiobiological Parameters for the Clinic

Current clinical assumptions used in radiobiological dose prescriptions come with several caveats: tumor heterogeneity is a common feature of most cancers, including cervical cancer. Although established cancer cell lines are not homogenous, the tumor microenvironment has an additional impact on the response to ionizing radiation (41,42). It is therefore imperative to use values for α/β and $T_{1/2}$ in the clinic that, although not knowable for a particular patient's tumor, are representative enough to allow a meaningful estimation of the radiobiological dose. While several previous studies have investigated the dose response of cervical cancer cell lines including sublethal damage repair, the findings reported here are the first to be based on the use of clinical BT sources (9,43,44,45,46,47,48).

4.6.2.1 Comparison of Parameter Values to Previously Published Findings

As mentioned in Chapter 2, previously reported values for α/β and $T_{1/2}$ varied from 6 to 21 Gy and 0.15 to 5.7 hours, respectively, for cervical cancer. Compared to the clinically used value of 10 for α/β, this study reports derived α/β ratios for the SCC lines (4.3 to 6.5 Gy) that are low relative to the previously reported range of values. On the other hand, the derived $T_{1/2}$ values are larger (2.2 to 4.9 hours) than the clinical assumption (1.5 hours) but still within the range previously reported, thus adding confirmatory *in vitro* evidence that the singular value used in clinical practice is probably not sufficiently representative for the treatment population. Decades ago, Kelland and Steel reported α, β, and $T_{1/2}$ values based on a clonogenic survival assay of five SCC cell lines irradiated *in vitro* with a Co-60 source, a source that has also recently found application in BT afterloaders (9). A Welch t-test calculation showed that their results do not differ significantly from our findings, which for the first time were generated in part from a clinical Ir-192 afterloader. However, there is a substantial departure from more contemporary reports, including that of a much larger α/β (95% confidence interval for α/β: 20.83 Gy to an infinitely large value, assuming $T_{1/2}$ of 1.5 hours) and smaller $T_{1/2}$ (95% confidence interval: 0.00 to 0.64 hours, assuming α/β of 10 Gy) by Roberts *et al* (10). A similar comparison cannot be performed for the results with the AC cell lines as no study of the radiobiological parameters for these cells has been reported previously.

4.6.2.2 Monoexponential Repair of Cells

Both hourly and bihourly radiation deliveries were used to investigate repair kinetics. The assumption of a constant halftime of repair implies monoexponential radiation repair kinetics, while previous publications suggest repair kinetics may be biexponential (32). Fractionated hourly and bihourly experiments were utilized with both SCC and AC to check for potential non-exponential repair using Cs-137. Considering a monoexponential repair, both experiments had doses set such that the SF after the maximum number of pulses (9 hourly or 5 bihourly) was 15%. If the repair was non-monoexponential and contained a “slow” and a “fast” component, the repair rate will slow down as the time between pulses increases, and the resulting repair for the bihourly pulses will be less than the more frequently irradiated hourly plates. Fitting the experimental results to the modified LQ model would thus lead to differences in $T_{1/2}$ obtained from hourly and bihourly experiments in the case of non-monoexponential repair. The results

shown in Table 4.6 did not indicate a statistically significant difference between the hourly and bihourly $T_{1/2}$. In addition, the mean R^2 goodness of fit metric value was 0.978 [0.954 - 0.993], suggesting that the monoexponential repair model fit the data very well. The experimental results hence provide no evidence for non-monoexponential repair kinetics within clinically relevant values.

4.6.2.3 Potential Clinical Implications

While additional factors affect the clinical tumor response (e.g. tumor heterogeneity, hypoxia), the radiobiological parameters reported here may have noteworthy clinical implications. For radiobiological dose prescriptions, the current recommendation for curative treatment of LACC is to deliver 90 to 95 Gy EQD2 to HR-CTV D90 (49). Tables 4.3 and 4.4 display the difference in doses calculated using two treatment schedules, delivered with HDR and PDR, that satisfy a 90 Gy EQD2 prescription when calculated using the conventional α/β ratio and $T_{1/2}$ for tumors, for the different combinations of radiobiological parameter values from the experimental results for each cell line.

4.6.2.3.1 Squamous Cell Carcinoma

Though the radiobiological dose from either treatment schedule is nearly equivalent for C-33A, the radiobiological dose of the PDR BT boost is significantly larger than for HDR BT for the other three SCC cell lines. This trend can be understood from the reported parameter values, as it has previously been demonstrated that a lower α/β ratio or $T_{1/2}$, compared to conventional values, results in HDR BT delivering more radiobiological dose than a clinically equivalent PDR BT treatment (11). A small α/β ratio and large $T_{1/2}$ may result in these effects "canceling out" for C-33A while the larger $T_{1/2}$ of other cell lines overwhelm this effect, resulting in a higher radiobiological dose being delivered by PDR BT. Due to the limited inferences that can be made from *in vitro* data, no matter how well designed the assay, further investigations are needed to verify and understand the trend of higher estimated PDR BT dose (up to 27 Gy EQD2 based on the BAIRDA findings). The potential impact of such a large dose variance between standardly calculated and data-informed estimates, in terms of tumor control and organ-specific toxicity, may be profound. Therefore, the concept of using tumor-specific derived radiobiological parameters carries great potential for clinical applicability. It remains to be seen whether PDR

BT may provide clinical benefits over HDR BT. Perhaps, if the *in vitro* derived parameters can be demonstrated to hold true clinically, PDR BT prescriptions may inherently achieve reduced dose to adjacent normal tissue while still delivering the same tumor radiobiological dose as an HDR BT prescription. However, such equivalency also depends on the tissue-dependent dose response of the normal tissue, which is not as well characterized in BT setups. At the very least, for SCC, clinical PDR BT may currently be delivering a higher radiobiological dose than the conventionally equivalent HDR BT and, for the same dose limits to the OAR, PDR BT may be capable of delivering a higher radiobiological dose. Alternatively, the results also suggest that HDR BT may require dose escalation to achieve the same radiobiological dose as the conventional PDR BT equivalent (an escalation that may require delivering additional dose to the OARs).

4.6.2.3.2 Adenocarcinoma

For all three AC cell lines, the radiobiological dose calculated for the HDR BT boost, using the parameters determined in this study, was found to be significantly larger than for PDR BT. While the AC cell lines exhibited a similar α/β ratio to SCC (as differences in the α/β ratio are considered not statistically different, as shown in Table 4.5), the smaller $T_{1/2}$ values compared to SCC decreased the radiobiological dose for a PDR BT boost versus the clinically equivalent HDR BT boost (11). No "canceling out" effect was identified as both findings (smaller α/β and smaller $T_{1/2}$) would result in a higher radiobiological dose from HDR BT relative to PDR BT. These results highlight the potential for improving clinical treatments based on cancer type; should the radiobiological parameters in this chapter represent a trend that is clinically replicable, it may be advantageous to select a BT boost based on the cancer type (i.e. HDR BT for AC and PDR BT for SCC). As many centers only use HDR BT, such findings may identify a potential benefit in the development of afterloaders capable of delivering both HDR and PDR BT.

As with the SCC findings, there are limited inferences that can be made from *in vitro* data. This is further highlighted by the smaller sample size and the large range of reported α values. Further investigation is required *in vivo* to verify a potential variance in $T_{1/2}$ based on cervical cancer type. Alternatively, a review of previous clinical outcomes may help corroborate the *in vitro* findings. If a comparison of AC cervical cancer patients treated with HDR and PDR BT

demonstrates that patients treated with HDR BT have an improved rate of tumor control, it may provide support for these results.

4.6.2.4 Limitation in Findings

It would be premature to adjust dose prescriptions in the clinic as radiobiological parameters identified *in vitro* may not be reflective of clinical parameter values. For example, in a review of previously published α/β and $T_{1/2}$ values for prostate cancer, Carlson *et al* identified that *in vitro* experiments with prostate cancer cells may yield α/β values that are 1.3 to 6.2 times larger and $T_{1/2}$ values that are significantly longer than radiobiological parameters identified *in vivo* using clinical outcomes data (50). Kirsch *et al* highlights the potential importance of metabolism, stem cells, and microenvironments to understand tumor response *in vivo* (51). The heterogeneity in cell populations further complicates interpretation of the relationship between *in vitro* and *in vivo* radiobiological parameters (52).

There are limitations in the experimental methodology. This study mainly included HPV(+) cell lines. Other forms of cervical cancers, such as HPV(-) cancers that represent a minority of clinical cases, have been associated with poor prognosis (7,53,54). While the HPV(-) C-33A included in this study was found to be radiosensitive, generalizations cannot be made with respect to HPV status based on a single cell line. Further investigation, including a larger panel of cervical cancer cells, can provide better insights, with potential applicability to variances observed in clinical outcomes. Indeed, limitations to clinical translatability abound, which will require due consideration to overcome. For example, the clonogenic survival assays were performed under well-oxygenated environments with sufficient nutrients. Cervical cancers frequently develop hypoxic regions, where neither nutrients nor oxygen is abundant, resulting in increased radiation resistance (55,56). Furthermore, the *in vitro* experiments only considered the radiation aspect, while clinical LACC treatment regimens standardly include chemotherapy for radiosensitization. Other mechanisms of cell kill, such as radiation-induced immune responses *in vivo*, are not accounted for in the current methodology (7). Dose prescriptions in these experiments utilize point-based prescriptions while clinical treatments utilize volumetric prescription (e.g. D90) with extreme dose heterogeneities in the volume (49). However, SF measurements have to be performed using discrete doses, precluding the use of more clinically

relevant volume-based prescriptions in such measurements. Extension of the *in vitro* studies to preclinical settings utilizing animal models may be a first step towards establishing transferability of the reported radiobiological parameters to the clinic.

Clinical HDR-BT treatments involve doses higher than the endpoint dose of 6 Gy selected in this study. Modifications to the Cs-137 and BAIRDA experiments, such as the use of larger tissue culture plates or the use of increased cell seeding, could help characterize the response at higher doses. However, for the latter, it should be noted that increasing the number of cells seeded can increase plating efficiency (57) and may result in overcrowding on plates, which affects SF calculations if not properly accounted for (e.g. seeding the same number of cells on each tissue culture plate).

Extrapolation of the findings to high dose levels is limited by the modified LQ model, which has been shown to overestimate cell death at high doses per fraction (58). It should be noted that the precise limitations of the model are still debated (52). For example, in back-to-back commentaries, Brenner suggests that the use of the LQ model is reasonable for fraction sizes up to 18 Gy, while in contrast, Kirkpatrick *et al* highlights inadequacies of the model in describing the response to radiosurgical doses (31,59). Similar to the latter, the assumption of a quadratic component to the SF is not reflected in previous experimental hypofractionated studies. Both Lobrich *et al* and Rydberg *et al* identified decreasing rates of cellular misrepair (leading to decreased cell death compared to the LQ model projection) in fibroblast cells irradiated above 20 Gy (60,61). Such uncertainties in the underlying assumptions of the LQ model motivates future experiments to explore cell survival at high doses of radiation, for improved radiobiological modeling. Further studies could also investigate the accuracy and potential benefits of radiobiological dose calculation using alternative response models to the LQ model (52).

4.7 Conclusion

Radiobiological dose prescription is recommended for clinical treatment planning and comparison of treatments from different BT techniques in cervical cancer. However, previous studies have reported a wide range of α/β ratios and $T_{1/2}$ values based on the results of experiments using different radiation schedules and sources. Four SCC and three AC cell lines were irradiated *in vitro* using a traditional Cs-137 irradiator and a novel system (BAIRDA) developed to mimic HDR and PDR delivery conditions for single acute fractions and fractionated schedules. Validated against Cs-137 techniques, the BAIRDA experiments identified α/β ratio values in the range of 3 to 7 Gy, which are smaller than the conventional value of 10 Gy for cervical cancers, and $T_{1/2}$ values in the range of 2 to 5 hours for SCC (statistically significant difference from the conventional value) and 0.5 to 1.5 hours for AC (not statistically significant from the conventional value). Results using BAIRDA suggest that PDR-BT boosts may deliver more radiobiological dose compared to what is conventionally assumed to be equivalent-dose HDR-BT treatments. These findings highlight the need for further investigation in more clinically relevant scenarios to elucidate any real-world radiobiological differences between PDR-BT and HDR-BT that could lead to improved patient outcomes. In addition, the superior BAIRDA configuration presents potential advantages in multiple fields of *in vitro* investigation.

4.8 References

(1) Kirchheiner K, Nout RA, Lindegaard JC, Haie-Meder C, Mahantshetty U, Segedin B, *et al.* Dose–effect relationship and risk factors for vaginal stenosis after definitive radio(chemo)therapy with image-guided brachytherapy for locally advanced cervical cancer in the EMBRACE study. *Radiother Oncol* 2016;118(1):160-166.

(2) Mazeron R, Fokdal LU, Kirchheiner K, Georg P, Jastaniyah N, Šegedin B, *et al*. Dose–volume effect relationships for late rectal morbidity in patients treated with chemoradiation and MRI-guided adaptive brachytherapy for locally advanced cervical cancer: Results from the prospective multicenter EMBRACE study. *Radiother Oncol* 2016;120(3):412-419.

(3) Sturdza A, Pötter R, Fokdal LU, Haie-Meder C, Tan LT, Mazeron R, *et al*. Image guided brachytherapy in locally advanced cervical cancer: Improved pelvic control and survival in RetroEMBRACE, a multicenter cohort study. *Radiother Oncol* 2016;120(3):428-433.

(4) Tanderup K, Fokdal LU, Sturdza A, Haie-Meder C, Nazeron R, van Limbergen E, *et al*. Effect of tumor dose, volume and overall treatment time on local control after radiochemotherapy including MRI guided brachytherapy of locally advanced cervical cancer. *Radiother Oncol* 2016;120(3):441-446.

(5) Barendsen GW. Dose fractionation, dose rate and iso-effect relationships for normal tissue responses. *Int J Radiat Oncol Biol Phys* 1982;8(11):1981-1997.

(6) Hall EJ, Brenner DJ. The dose-rate effect revisited: Radiobiological considerations of importance in radiotherapy. *Int J Radiat Oncol Biol Phys* 1991;21(6):1403-1414.

(7) International commission on radiation units & measurements. Report 89: Prescribing, recording, and reporting brachytherapy for cancer of the cervix. *Journal of the ICRU* 2013;13:1-258.

(8) Joiner M, van der Kogel A. *Basic clinical radiobiolog*y. 4th ed. Boca Raton:CRC Press/Taylor & Francis Group; 2009.

(9) Kelland LR, Steel GG. Differences in radiation response among human cervix carcinoma cell lines. *Radiother Oncol* 1988;13(2):225-232.

(10) Roberts SA, Hendry JH, Swindell R, Wilkinson JM, Hunter RD. Compensation for changes in dose-rate in radical low-dose-rate brachytherapy: A radiobiological analysis of a randomised clinical trial. *Radiother Oncol* 2004;70(1):63-74.

(11) Chow B, Nanda K, Warkentin B, Huang F, Gamper AM, Menon G. In-vitro determination of radiobiological parameter values used in cervical cancer brachytherapy. *Radiother Oncol* 2020;152(1):S1093-S1094.

(12) Hanisch PH, Furre T, Olsen DR, Pettersen EO. Radiobiological responses for two cell lines following continuous low dose-rate (CLDR) and pulsed dose rate (PDR) brachytherapy. *Acta Oncol* 2007;46(5):602-611.

(13) Mirzayans R, Andrais B, Murray D. Viability assessment following anticancer treatment requires single-cell visualization. *Cancers (Basel)* 2018;10(8):255.

(14) Hsu EM, McNicol PH. Characterization of the HPV-16 E6/E7 transcription in CaSki cells by quantitative PCR. *Mol Cell Probes* 1992;6(6):459-466.

(15) Yaginuma Y, Westphal H. Analysis of the p53 in human uterine carcinoma cell lines. *Cancer Res* 1991;51(24):6506-6509.

(16) Srivastava S, Tong YA, Devadas K, Zou ZQ, Chen Y, Pirollo KF, *et al*. The status of the p53 gene in human papilloma firus positive or negative cervical carcinoma cell lines. *Carcinogenesis* 1992;13(7):1273-1275.

(17) Butz K, Whitaker N, Denk C, Ullmann A, Geisen C, Hoppe-Seyler Fl. Induction of the p53-target gene GADD45 in HPV-positive cancer cells. *Oncogene* 1999;18(14):2381-2386.

(18) COSMIC - Catalogue of Somatic Mutations in Cancer 2021.

(19) Hietanen S, Lain S, Krausz E, Blattner C, Lane DP. Activation of p53 in cervical carcinoma cells by small molecules. *Proc Natl Acad Sci USA* 2000;97(15):8501-8506.

(20) Sonoda K, Nakashima M, Saito T, Amada S, Kamura T, Nakano H, *et al*. Establishment of a new human uterine cervical adenocarcinoma cell-line, SiSo, and its reactivity to anticancer reagents. *Int J Oncol* 1995;6(5):1099-1104.

(21) Puck TT, Markus PI. Action of x-rays on mammalian cells. *J Exp Med* 1956; 103(5):653-666.

(22) Gamper AM, Rofougaran R, Watkins SC, Greenberger JS, Beumer JH, Bakkenist CJ. ATR kinase activation in G1 phase facilitates the repair of ionizing radiation-induced DNA damage. *Nucleic Acids Res* 2013;41(22):10334-10344.

(23) Brady SL, Toncheva G, Dewhirst MW, Yoshizumi TT. Characterization of a 137Cs irradiator from a new perspective with modern dosimetric tools. *Health Phys* 2009;97(3):195-205.

(24) Xu D, Allsop SA, Witherspoon SM, Snider JL, Yeh JJ, Fiordalisi JJ, *et al*. The oncogenic kinase Pim-1 is modulated by K-Ras signaling and mediates transformed growth and radioresistance in human pancreatic ductal adenocarcinoma cells. *Carcinogenesis* 2011;32(4):488-495.

(25) Gomez-Casal R, Bhattacharya C, Ganesh N, Bailey L, Passe P, Gibson M, *et al*. Non-small cell lung cancer cells survived ionizing radiation treatment display cancer stem cell and epithelial-mesenchymal transition phenotypes. *Mol Cancer* 2013;12(1):94.

(26) Brodin NP, Chen Y, Yaparpalvi R, Guha C, Tomé WA. Dosimetry formalism and Implementation of a homogenous irradiation protocol to improve the accuracy of small animal whole-body irradiation using a 137Cs irradiator. *Health Phys* 2016;110(2 Suppl 1):S26-S38.

(27) Devic S, Seuntjens J, Sham E, Podgorsak EB, Schmidtlein CR, Kirov AS, *et al*. Precise radiochromic film dosimetry using a flat-bed document scanner. *Med Physics* 2005;32(7):2245-2253.

(28) Morrison H, Menon G, Sloboda RS. Radiochromic film calibration for low-energy seed brachytherapy dose measurement. *Med Phys* 2014;41(7):072101.

(29) van Rijn J, van den Berg J, Kipp JB, Schamhart DH, van Wijk R. Effect of hypothermia on cell kinetics and response to hyperthermia and x rays. *Radiat Res* 1985;101(2):292-305.

(30) Brenner DJ, Hlatky LR, Hahnfeldt PJ, Huang Y, Sachs RK. The linear-quadratic model and most other common radiobiological models result in similar predictions of time-dose relationships. *Radiat Res* 1998;150(1):83-91.

(31) Brenner DJ. The linear-quadratic model is an appropriate methodology for determining isoeffective doses at large doses per fraction. *Semin Radiat Oncol* 2008;18(4):234-239.

(32) van den Aardweg GJ, Hopewell JW. The kinetics of repair for sublethal radiation-induced damage in the pig epidermis: an interpretation based on a fast and a slow component of repair. Radiother Oncol 1992;23(2):94-104.

(33) Aldelaijan S, Devic S, Mohammed H, Tomic N, Liang L-H, DeBlois F, *et al*. Evaluation of EBT-2 model GAFCHROMIC film performance in water. Med Phys 2010;37(7): 3687-3693.

(34) Dale RG, Huczkowski J, Trott KR. Possible dose rate dependence of recovery kinetics as deduced from a preliminary analysis of the effects of fractionated irradiations at varying dose rates. *Br J Radiol* 1988;61(722):153-157.

(35) Snedecor G, Cochran W. *Statistical methods*. Ames, Iowa: Iowa State Univ. Press; 1992.

(36) Orear J. Least squares when both variables have uncertainties. *Am J Phys* 1982;50(10):912-916.

(37) Nath R, Anderson LL, Luxton G, Weaver KA, Williamson JF, Meigooni AS. Dosimetry of interstitial brachytherapy sources: Recommendations of the AAPM Radiation Therapy Committee Task Group No. 43. *Med Phys* 1995:22(2),209–234.

(38) Rivard MJ, Coursey BM, DeWerd LA, Hanson WF, Huq S, Ibbott GS, *et al*. Update of AAPM Task Group No. 43 Report: A revised AAPM protocol for brachytherapy dose calculations. *Med Phys* 2004;31(3):633-674.

(39) Lea DE, Catcheside DG. The mechanism of the induction by radiation of chromosome aberrations in Tradescantia. *J Genet* 1942;44:216-245.

(40) Kellerer AM, Rossi HH. RBE and the primary mechanism of radiation action. *Radiat Res* 1971;47(1):15-34.

(41) Kidd EA, Grigsby PW. Intratumoral metabolic heterogeneity of cervical cancer. *Clin Can Res* 2008;14(16):5236-5240.

(42) Chong GO, Lee WK, Jeong SY, Park SH, Lee YH, Lee SW *et al*. Prognostic value of intratumoral metabolic heterogeneity on F-18 fluorodeoxyglucose positron emission tomography/computed tomography in locally advanced cervical cancer patients treated with concurrent chemoradiotherapy. *Oncotarget* 2017;8(52):90402-90412.

(43) Allalunis-Turner MJ, Pearcey RG, Barron GM, Buryn DA, Babiak JC, Honoré LH. Inherent radiosensitivity testing of tumor biopsies obtained from patients with carcinoma of the cervix or endometrium. *Radiother Oncol* 1991;22(3):201-205.

(44) Brenner DJ, Hall EJ. Conditions for the equivalence of continuous to pulsed low dose rate brachytherapy. *Int J Radiat Oncol Biol Phys* 1991;20(1):181-190.

(45) West CM, Davidson SE, Roberts SA, Hunter RD. Intrinsic radiosensitivity and prediction of patient response to radiotherapy for carcinoma of the cervix. *Br J Cancer* 1993;68(4):819-823.

(46) Rantanen V, Grénman S, Kulmala J, Grénman R. The intrinsic radiosensitivity and sublethal damage repair capacity of five cervical carcinoma cell lines tested with the 96-well-plate assay. *J Cancer Res Clin Oncol* 1995;121(4):230-234.

(47) Banath JP, MacPhail SH, Olive PL. Radiation sensitivity, H2AX phosphorylation, and kinetics of repair of DNA strand breaks in irradiated cervical cancer cell lines. *Cancer Res* 2004;64(19):7144-7149.

(48) Kim S, Wu HG, Shin JH, Park HJ, Kim IA, Kim IH. Enhancement of radiation effects by flavopiridol in uterine cervix cancer cells. *Can Res Treat* 2005;37(3):191-195.

(49) Pötter R, Tanderup K, Kirisits C, de Leeuw A, Kirchheiner K, Nout R, *et al* The EMBRACE II study: The outcome and prospect of two decades of evolution within the GEC-ESTRO GYN working group and the EMBRACE studies. *Clin Transl Radiat Oncol* 2018;9:48-60.

(50) Carlson DJ, Stewart RD, Li XA, Jennings K, Wang JZ, Guerrero M. Comparison of in vitro and in vivo alpha/beta ratios for prostate cancer. *Phys Med Biol* 2004;49(19):4477-4491.

(51) Kirsch DG, Diehn M, Kesarwala AH, Maity A, Morgan MA, Schwarz JK, *et al*. The future of radiobiology. *J Natl Cancer Inst* 2018;110(4):329-340.

(52) McMahon SJ. The linear quadratic model: usage, interpretation and challenges. *Phys Med Biol* 64:01TR01.

(53) Lei J, Ploner A, Lagheden C, Eklund C, Kleppe SN, Andrae B, *et al*. High-risk human papillomavirus status and prognosis in invasive cervical cancer: A nationwide cohort study. *PLOS Med* 2018;15(10):e1002666.

(54) Nicolás I, Marimon L, Barnadas E, Saco A, Rodríguez-Carunchio L, Fusté P, *et al*. HPV-negative tumors of the uterine cervix. *Mod Pathol* 2019;32(8):1189-1196.

(55) Rofstad EK, Sundfør K, Lyng H, Tropé CG. Hypoxia-induced treatment failure in advanced squamous cell carcinoma of the uterine cervix is primarily due to hypoxia-induced radiation resistance rather than hypoxia-induced metastasis. *Br J Cancer* 2000;83(3):354-359.

(56) Grimes DR, Partridge M. A mechanistic investigation of the oxygen fixation hypothesis and oxygen enhancement ratio. *Biomed Phys Eng Express* 2015;1(4):045209.

(57) Pomp J, Wike JL, Ouwerkerk IJ, Hoogstraten C, Davelaar J, Schrier PI, *et al*. Cell density dependent plating efficiency affects outcome and interpretation of colony forming assays. *Radiother Oncol* 1996;40(2):121-125.

(58) Guerrero M, Carlone M. Mechanistic formulation of a lineal-quadratic-linear (LQL) model: split-dose experimentas and exponentially decaying sources. *Med Phys* 2010;37(8):4173-4181.

(59) Kirkpatrick JP, Meyer JH, Marks LB. The linear-quadratic model is inappropriate to model high dose per fraction effects in radiosurgery. *Semin Radiat Oncol* 2008;18(4):240-243.

(60) Löbrich M, Kühne M, Wetzel J, Rothkamm K. Joining of correct and incorrect DNA double-strand break ends in normal human and ataxia telangiectasia fibroblasts. *Genes Chromosomes Cancer* 2000;27(1):59-68.

(61) Rydberg B, Cooper B, Cooper PK, Holley WR, Chatterjee A. Dose-dependent misrejoining of radiation-induced DNA double-strand breaks in human fibroblasts: experimental and theoretical study for high- and low-LET radiation. *Radiat Res* 2005;163(5):526-534.

CHAPTER 5
UNCERTAINTY ANALYSIS

A version of this chapter is being published as: Chow B, Warkentin B, McEwen M, Huang F, Nanda K, Gamper AM, Menon G. Uncertainties associated with clonogenic assays using a Cs-137 irradiator and Ir-192 afterloader: A comprehensive compilation for radiation researchers. Rad Res. In press 2022.

5.1 Introduction

Clonogenic assays are considered the gold standard for measuring cell clonogenic survival. Common applications include the measurement of a cell line's chemosensitivity or radiosensitivity (1,2,3). Radiosensitivity is measured by counting the number of colonies formed by cells after irradiation to different doses, which establishes the dose dependence of the clonogenic capacity retained by surviving cells ("clonogenic survival"). Clonogenic survival is often described using the LQ model, which includes cell line specific radiobiological parameters (e.g. α/β ratio and $T_{1/2}$) (4,5,6,7). In recent years, radiation oncologists are increasingly acknowledging the need to prescribe treatment doses based on radiobiological considerations by incorporating the α/β and $T_{1/2}$ parameters, which makes the accurate and precise characterization of the parameters crucial.

As discussed in Chapter 4, studies involving *in vitro* clonogenic assays have traditionally utilized irradiators with radioactive sources such as Co-60 or Cs-137, favored because of the practical benefits of their long half-lives (8,9,10). However, these sources are not representative of the source most frequently utilized in cervical cancer brachytherapy (Ir-192) in either photon energy or dose rate. Hence, to more accurately determine radiobiological parameters using clinical Ir-192 afterloaders, Chapter 4 covered the development of BAIRDA for cell irradiation and its application to estimate the α/β ratio and $T_{1/2}$ of cervical cancer cells.

Estimation of radiobiological parameters from *in vitro* cell experiments is inherently influenced by uncertainties affecting both the radiation delivery and the biological response. Several uncertainties, mainly relating to biological response, have been reported for *in vitro* cell

experiments when using irradiators. Biological response uncertainties can arise from differences in cell attachment times (the time between seeding cells and delivery of radiation), effects of hypothermia on cell killing, and variance in the number of cells seeded on a tissue culture plate (11,12). The combined impact of such uncertainties, along with those uncertainties relating to dose delivery by the irradiator, is not known and may have a more significant effect on the reliability and reproducibility of experimental findings than is currently perceived.

A detailed investigation of uncertainties associated with cell survival measurements, including the effect of cell seeding uniformity, source calibration, and differences between planned and delivered doses is presented in this chapter, along with a comprehensive evaluation of the impact of the combined uncertainties on the estimated radiobiological parameters. In a systematic investigation of these uncertainties, specific uncertainties have been identified related to cell experiments using the novel BAIRDA method, the first *in vitro* setup to use clinical afterloaders featuring Ir-192. This provides valuable insights to both the radiation research community, who rely on Cs-137 irradiators for cell-based assays, and those who will use BAIRDA with Ir-192 for cell experiments.

5.2 Uncertainty Analysis and Results

Chapter 4 gives a detailed account of the experimental methods used for the surviving fraction measurements. The following sections report the different uncertainties associated with clonogenic assay experiments performed using the Cs-137 irradiator and BAIRDA. The impact of these uncertainties on the measured SF and dose delivered is quantified.

5.2.1 Uncertainties in SF Associated with Experimental Procedures and Analysis

Uncertainties related to the experimental setup and the analysis of clonogenic assays, including the number of cells seeded, the cell seeding uniformity, and the effect of temperature on the seeded cells when removed from the incubator, were investigated using measurements with SW756 cells. All measurements were performed in triplicate by a single operator and repeated three times to ensure consistency in results.

5.2.1.1 Cell Seeding Density

Calculation of SF assumes that the irradiated and control plates were seeded with the same number of cells. Seeding is performed by pipetting cells from a diluted solution onto the tissue culture plate (13). Finely graduated micropipettes assist in reducing the variation in the volume of solution pipetted for the seeding procedure. Even with this controlled effort, the seeding process could result in some plates being seeded with a slightly different number of cells. The variance in the number of cells seeded in the triplicate plates of the same experiment will affect the SF. For example, Batista and Alberini measured a 1.5 to 2.3% uncertainty when pipetting 100 μL with 1000 μL micropipettes (14). For this analysis, 3,000 cells (in a volume of 3,000 μL dispensed with a 1,000 μL micropipette) were seeded on 10 cm tissue culture plates and incubated without irradiation (similar to control plates). The number of colonies formed was counted following an incubation period of 12 days, the length of time empirically determined by pilot experiments, to establish 50-cell colonies with SW756. Ideally, plates with the same number of seeded cells should form an equal number of colonies. However, the average number of colonies counted was 1096.3 ± 37.5 colonies, indicating a variance of 3.4%.

5.2.1.2 Cell Seeding Uniformity

In BAIRDA, Equation (4.3) calculates SF_{Ir} assuming an initial uniform seeding of cells (same number of cells per unit area) on the tissue culture plate that would result in a uniform distribution of colonies if not irradiated. However, both non-uniform cell seeding and the stochastic nature of colony formation in the ROIs, can affect SF_{Ir}. This uncertainty was estimated by seeding three 10 cm tissue culture plates with 3,000 cells and incubating them without irradiation. The colony density (colonies per unit area) in each of the thirteen ROIs used for HDR-BAIRDA was counted and compared against the average density on the whole plate. The colony density in the ROIs, from triplicate measurements, varied from the average density by ±2.0% [-2.3% - +4.7%]. The average deviation in SF_{Ir} from the expected SF (1.00) in each ROI for the control plate in Figure 5.1 (a) is shown in Figure 5.1(b).

In comparison, for the Cs-137 irradiator measurements, Equation (4.1) calculates SF_{Cs} using the number of colonies counted on an entire plate and therefore will not be affected by cell uniformity (barring extreme cases such as cell clusters).

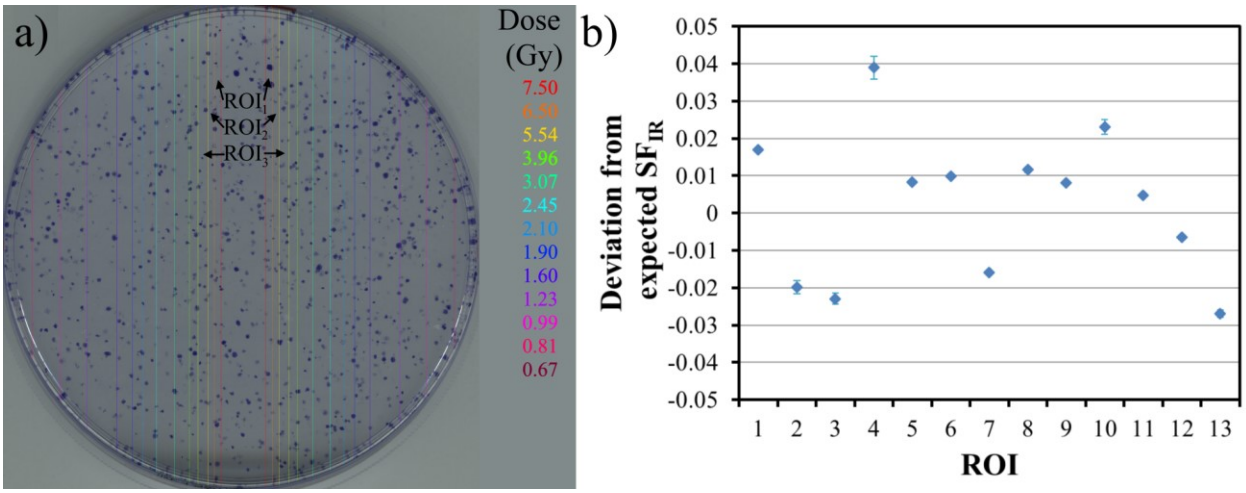

Figure 5.1: (a) A control plate of SW756 cells overlaid with the 13 ROIs used in the corresponding HDR-BAIRDA experiments. (b) The average deviation from the expected SF (1.00) in each ROI shown in (a) from 3 plates. Error bars represent the standard deviation in the values identified for each ROI.

5.2.1.3 Cell Attachment Times

The incubation time from seeding to irradiation (attachment or adherence time) could affect the calculated SF. Depending on the cell line, the time for cells to adhere to the tissue culture plates after seeding varies (13,15,16). Shorter periods may limit maximum cell attachment to the plates while longer periods could result in cell proliferation between seeding and irradiation. Attachment times reported in the literature have a wide range; for the human lung cancer cell line A549, attachment times of 2 to 24 hours have been reported (17,18,19). Despite this, the impact of such variance on clonogenic assays has received limited attention. For this analysis, the effect of using different adherence time intervals was estimated using five triplicate sets of 6 cm tissue culture plates: one set was used as the control and the other four were irradiated with 2 Gy in the Cs-137 irradiator following an attachment time of 2, 4, 6, and 8 hours after seeding. SF_{Cs} for the four attachment times were calculated to be 0.371 ± 0.041, 0.380 ± 0.028, 0.371 ± 0.021, and 0.380 ± 0.025, indicating no discernible trend with increasing attachment times. As the variance in SF (0.006 or 1.5%) is smaller than the uncertainty associated with the number of cells seeded (3.4%), the impact of attachment time was considered to be not significant. This result suggests that an attachment time in the range of 2 to 8 hours does not affect the SF calculated for the SW756 cell line.

5.2.1.4 Cell Hypothermia During Radiation

Cells used for *in vitro* experiments are typically incubated at 37°C, the optimum temperature for the growth of human cells. During the irradiator and HDR-BAIRDA experiments, the tissue culture plates were exposed to room temperature for up to 30 minutes (includes time to transport cells for irradiation and time for irradiation). Studies have reported that mild hypothermia (30 to 33°C) could affect cell metabolism (20,21). van Rijn *et al* noted that cells kept under hypothermic conditions (24 hours at 25°C) were more radiosensitive than cells incubated at 37°C prior to irradiation (11).

To measure the temperature drop, three 6 cm and 10 cm tissue culture plates were filled with 4 mL and 10 mL of tissue culture medium, respectively (the standard volume used during culturing). Each plate was heated to 37°C in the incubator and then exposed to room temperature for up to 45 minutes. A plot of the temperature (measured using a remote-monitoring thermocouple; Cole-Palmer, Vernon Hills IL) against time of exposure to room temperature is shown in Figure 5.2(a). When a plate is left exposed to room temperature, it will asymptotically approach room temperature. The temperature of the medium in the 6 cm and 10 cm plates was observed to drop to 25.0 ± 0.2°C and 25.7 ± 0.6°C, respectively, when the plates were exposed to room temperature for 30 minutes, the maximum time the plates were outside the incubator during the experiments reported in Chapter 4.

To investigate the effect of brief hypothermia, three triplicate sets of 6 cm tissue culture plates were seeded with 1,000 cells - one control and two for irradiation. The latter sets were irradiated to 2 Gy in the Cs-137 irradiator, either (i) as quickly as possible after removal from the incubator (within 5 minutes of removal) or (ii) 30 minutes after removal from the incubator. The SF_{Cs} calculated for the two cooling times were 0.399 ± 0.044 and 0.402 ± 0.055, respectively, suggesting no significant effect on survival when cells are exposed to room temperature for up to 30 minutes.

During PDR-BAIRDA, the tissue culture plates were kept at approximately 37°C using a water bath (Figure 4.3(a)). The temperature of the water bath was monitored hourly over the course of three 8-hour experiments using a mercury thermometer. The deviation of the temperature of the

water bath (used as a surrogate for the temperature of the cell culture media) from the average temperature of the bath over the course of an experiment is presented in Figure 5.2(b). The average temperature for an experiment varied slightly between experiments due to fluctuations in the water bath output on a day-to-day basis (36.1 ± 0.2°C). The water bath also held the temperature relatively constant over the course of an 8-hour experiment: the average deviation for the 8 hourly relative temperature readings (the measurements shown in Figure 5.2(b)) was 0.25°C. This temperature stability over the course of PDR-BAIRDA experiments limits the possibility for potential hypothermia.

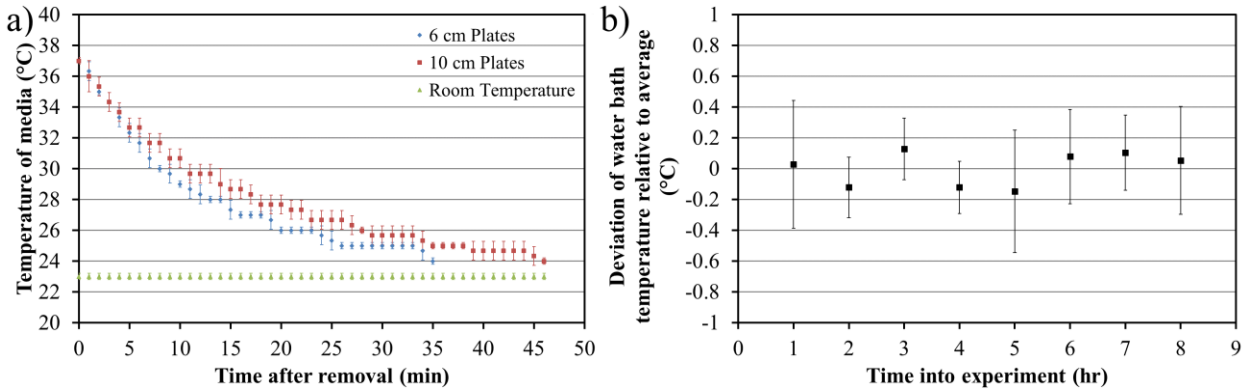

Figure 5.2: (a) Drop in temperature of media in 6 cm and 10 cm tissue culture plates when exposed to room temperature for 35 and 45 minutes, respectively. (b) Deviation in the temperature of the water bath from the average temperature during three 8-hour experiments. Error bars in both represent the standard deviation in the measurement.

5.2.1.5 Colony Definition

A colony has traditionally been defined as a cluster of ≥50 cells (22). This definition is not consistently applied and some studies define colonies as clusters of 100 cells (19,23). A study by Yohem *et al* measured SF of multiple melanoma cell lines with colony size definitions between 25 and 100 cells per cluster and identified a shallower survival curve (lower cell death) for smaller colonies (23). They suggest the length of incubation post-irradiation may be a source of this variance; insufficient incubation time may lead to difficulty distinguishing a slow-growing colony from an abortive colony (a colony unable to continue growth) (23).

To evaluate the sensitivity of colony size definition on radiobiological parameter estimation, 10 cm tissue culture plates seeded with 3,000 cells were irradiated by HDR-BAIRDA. The cells

were stained 12 days after irradiation and SF_{Ir} calculated using colonies defined either as clusters of 50 ("50 cell reference colony") or 100 cells ("100 cell reference colony"). The average deviation in the measured SF_{Ir} was ±2.7% [-6.6% - +5.4%] across all 13 ROIs used in HDR-BAIRDA analysis (Figure 4.5(a)). Both colony definitions yielded similar radiobiological parameters: $\alpha = 0.27$ (95% confidence interval, 0.25 - 0.29) Gy^{-1} and $\beta = 0.050$ (0.043 - 0.059) Gy^{-2} for a 100 cell reference colony, compared to $\alpha = 0.25$ (0.23 - 0.26) Gy^{-1} and $\beta = 0.050$ (0.045 - 0.054) for the 50 cell reference colony.

5.2.1.6 Subjectivity in Colony Counting

Manual colony counting, the most common approach, introduces both intra- and inter-operator subjectivity in the counting process as the process is subject to variances in operator (the individual counting colonies) bias (24). Even though the counting statistics may be improved when multiple operators independently count colonies, it could introduce inter-operator subjectivity. To reduce this variance, a single experienced operator (Braden Chow) performed the colony counting process reported in this thesis.

To identify the extent of intra-operator subjectivity in colony identification, select blinded 10 cm tissue culture plates seeded with 3,000 cells were recounted (Operator 1, Braden Chow). The number of cells counted differed by 0.7 ± 0.1% over the course of three measurements. This low rate of uncertainty suggests that the impact of intra-observer subjectivity may play only a small role in SF calculation. Inter-operator variance was quantified by recounting the number of colonies for a triplicate experiment (Cs-137 SAT irradiation) by two operators (Operator 1 and 2 (Kareena Nanda)) and also using an Oxford Optronix ColCount (Abingdon, United Kingdom) colony counter. The colony counter digitizes 6 cm tissue culture plates with an imager (Figure 5.3(a)) and detects colonies automatically using the ColCount software (Abingdon, United Kingdom) (Figure 5.3(b)).

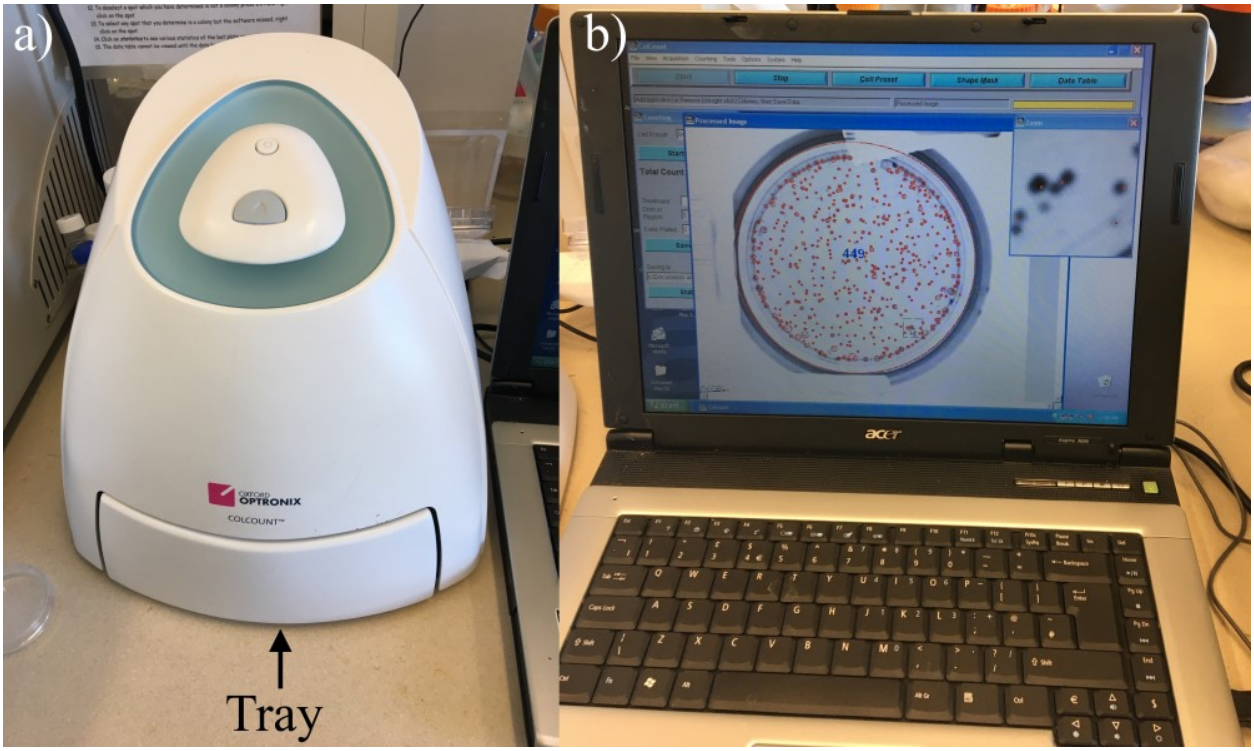

Figure 5.3: (a) The Oxford Optronix Colcount imager. 6 cm tissue culture plates are inserted into the imager's tray, which digitizes the plate for analysis. (b) A screenshot of the ColCount image analysis software measuring the number of colonies identified for a control plate with SiSo cells. Colonies are identified automatically from the scan (red dots) and the total number of colonies is reported in the center of the image.

A higher variation in colony counts was observed between Operator 1 and the colony counter (>20%) than between Operators 1 and 2 (<12%). However, the resulting variance in the SF was much lower than the variance in colonies counted, both between Operator 1 and the colony counter (random uncertainty of 4.6 ± 2.2%) and between Operators 1 and 2 (4.1 ± 2.3%). This indicates internal consistency in the counting: an operator or colony counter that counts a higher number of colonies on a control plate will also count more colonies on an irradiated plate. It should be pointed out that an automated colony counter needs to be trained by an operator to remove false positives and false negatives in the counted colonies, thereby introducing an element of intra-operator subjectivity. Hence, the variance between Operators 1 and 2 was taken as the inter-operator uncertainty.

5.2.2 Dosimetric Uncertainties Associated with the Cs-137 Irradiator

The dose delivered to the tissue culture plates in the Cs-137 irradiator is dependent on the irradiator calibration and associated uncertainties, the uniformity of dose within the irradiator, and the alignment of tissue culture plates during radiation delivery. These uncertainties were quantified either through ion chamber or radiochromic film measurements. All measurements were repeated three times to ensure reliability of the results.

5.2.2.1 Cs-137 Irradiator Calibration

The exposure time required to irradiate the experimental tissue culture plates to the desired dose is estimated from the dose rate specified at the time of irradiator calibration. To confirm the dose rate in the irradiator, which had not been recalibrated since the original installation (November 1992), a PTW 30013 ion chamber and PTW Unidos Webline electrometer (PTW-Freiburg, Freiburg, Germany) pair was used. The equipment pair, calibrated in a Co-60 beam at the National Research Council of Canada in July, 2021, had an air kerma calibration coefficient ($N_{k,Co\text{-}60}$) of 4.956 cGy/nC (with an expanded uncertainty (k = 2) of 1.0%). $N_{k,Cs\text{-}137}$ for the Cs-137 radiation was determined from $N_{k,Co\text{-}60}$ by:

$$N_{k,Cs-137} = k_{Q,Cs-137} N_{k,Co-60} \tag{5.1}$$

The value of $k_{Q,Cs\text{-}137}$, the quality conversion factor for Cs-137 for the PTW 30013 ion chamber was taken to be 1.002 (25). Kang *et al* estimated k_Q using the following equation (25),

$$k_{Q,Q_0} \simeq \frac{[s_{w,air}\, P_Q]_Q}{[s_{w,air}\, P_Q]_{Q_0}} \tag{5.2}$$

where Q is the energy of interest (Cs-137), Q_0 is the mean Co-60 energy, $s_{w,air}$ is the water-to-air stopping power ratio and P_Q the product of correction factors for perturbations related to the cavity and wall of the ion chamber. $s_{w,air}$ was estimated using the relationship between the tissue-phantom ratio in water at depths of 20 and 10 cm in a 10x10 cm^2 field with a source to axis distance of 100 cm ($TPR_{20,10}$) (26). The $TPR_{20,10}$ used by Kang *et al* was not directly measured but determined by using an empirical correlation between $s_{w,air}$ and $TPR_{20,10}$ (25,26):

$$s_{w,air} = 1.3614 - 1.2963 TPR_{20,10} + 2.5302 TPR_{20,10}^2 + 1.6896 TPR_{20,10}^3 \tag{5.3}$$

The values of the correction factors (cavity perturbation factor (p_{cav}), displacement of measuring point (p_{dis}), chamber wall perturbation (p_{wall}), and central electrode effect (p_{cel})) were determined using methodologies recommended in the Technical Report Series (TRS) 277 and 398 protocols

(26,27). For the PTW 30013 ion chamber, Kang *et al* reported a k_Q of 1.002, but did not provide an associated uncertainty. For the uncertainty analysis, k_Q is assumed to have a 0.5% relative uncertainty, which McEwen *et al* estimate based on reported and anecdotal evidence of realistic clinical scenarios (28).

To perform dose measurements, the ion chamber was positioned at the center of the Cs-137 irradiator cavity (Figure 5.4), the calibration point of the irradiator, with a 2 mm acrylic buildup cap to ensure charged particle equilibrium (29). The turntable was kept stationary for these measurements. The dose rate to cells, $\dot{D}_{cells}$, with ~2 mm of medium on top was approximated to be the dose delivered to water, given by:

$$\dot{D}_{cells} = M_{Corr} N_{k,Cs-137} (\mu_{en}/\rho)_{air}^{water} \quad (5.4)$$

where M_{Corr} is the corrected electrometer reading and $(\mu_{en}/\rho)_{air}^{water}$ is the ratio of the mass energy-absorption coefficients for water and air for the photon energy of Cs-137 (662 keV), used to convert the absorbed dose of the detector cavity material to water (25). With the source in the "on" position, the dose rate was measured to be 73.61 cGy/min, which was 0.6% lower than was expected based on the original calibration. This level of agreement is very encouraging given the 30-year time separation between calibrations. A lack of information on the original calibration makes it difficult to further analyze this difference. It should be noted that Equation (5.4) assumes photon attenuation equivalency between water and the tissue culture medium.

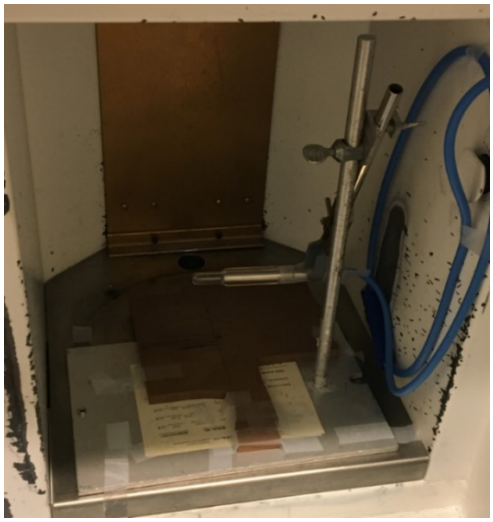

Figure 5.4: Configuration of the ion chamber, with the 2 mm acrylic buildup cap, during calibration in the Cs-137 irradiator. The PTW 30013 ion chamber is held by a retort stand and clamp, which is fastened to the turntable with single-sided and double-sided tape (underneath the stand's base).

5.2.2.2 Irradiator Transit Dose

In a Cs-137 irradiator, transit dose is the additional dose received by the cells as the source moves to the "on" position and returns to the "off" position. However, this transit dose is not included in the calculation of the irradiation dose for a particular experiment, which results in the cells receiving more dose than planned. No study has investigated the transit dose of the Cs-137 irradiator. To estimate this, the ion chamber was positioned at the center of the cavity using the same setup as for calibration measurement (Figure 5.4) and the charge was measured for a predetermined set of exposure times (0.5 to 5 minutes). From a linear least squares fit to the charge versus time data (Figure 5.5), the transit charge was determined to be 0.259 ± 0.006 nC. Using Equation (5.4), this corresponds to a total transit dose of 1.44 ± 0.03 cGy/transit.

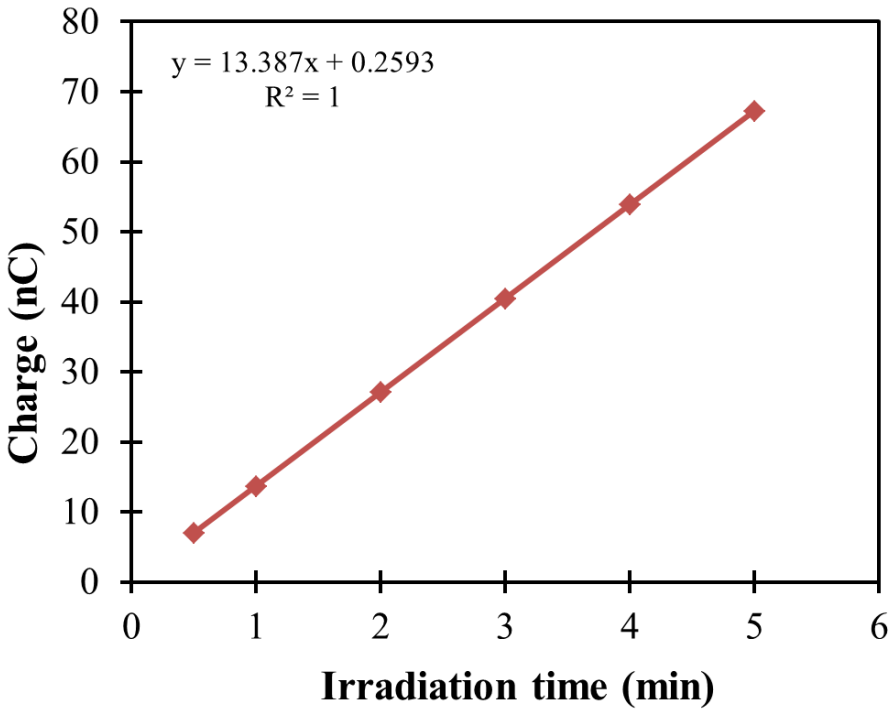

Figure 5.5: A linear regression fit to the charge collected by an ion chamber when exposed for a predetermined set of times in the Cs-137 irradiator. The transit charge corresponds to the intercept from the least squares fit.

5.2.2.3 Dose Non-Uniformity in the Irradiator

During experimentation, multiple tissue culture plates were exposed simultaneously under the assumption that they are all irradiated uniformly. However, there is some regional dose variation in the irradiator cavity. The geometry of the irradiator results in non-uniform irradiation in the

cavity if the turntable is stationary (see Figure 4.2); as the radiation source is on one side of the cavity, plates and cells closer to this side receive higher doses. A rotating turntable is used to reduce this non-uniformity but does not eliminate it. Dose variations inside the Cs-137 irradiator were measured using Gafchromic EBT3 film (Niagara Falls, NY) (30). All films were stored and handled according to the American Association of Physicists in Medicine's Task Group 55 (AAPM TG-55) and TG-235 recommendations (31,32).

.

5.2.2.3.1 Characterization of the Scanner

Film was digitized using an Epson Expression 10000XL flatbed scanner (Figure 5.6(a)) at 72 dpi with 48-bit transmission, color correction features turned off, and with images saved in tagged image file format (.tif). Scans were taken at least 30 minutes after warm up to provide sufficient stabilization of the scanner, and a glass plate was used to hold the films flat during scanning (33).

The uniformity of the scanner was evaluated by performing “empty” scans (no object in the scanner). While these empty scans were relatively uniform, non-uniformities were observed at the edges transverse to the direction of scanning. This is clearly seen in Figure 5.6(b), where the window of the image has been reduced to pixel values between 65,000 and 65,535 (less than 1% of the range of pixel values that can be measured). A central 10 x 20 cm^2 region of the scanner was identified where the pixel values of the scanned film were consistent to within 0.3% (pixel values ranged from 65,350 to 65,535 for the most sensitive color channel (red)). A slightly higher non-uniformity (0.5%; pixel value range of 65,250 to 65,535) was noted when the glass was scanned (Figure 5.6(c)). During film analysis, all films were scanned in this 10 x 20 cm^2 region with glass.

It has been previously noted that there is dose dependent variation along the transverse axis to the scan direction, (M McEwen, personal communication). Therefore, the long axis of the rectangular film pieces was oriented with the scan direction during digitization.

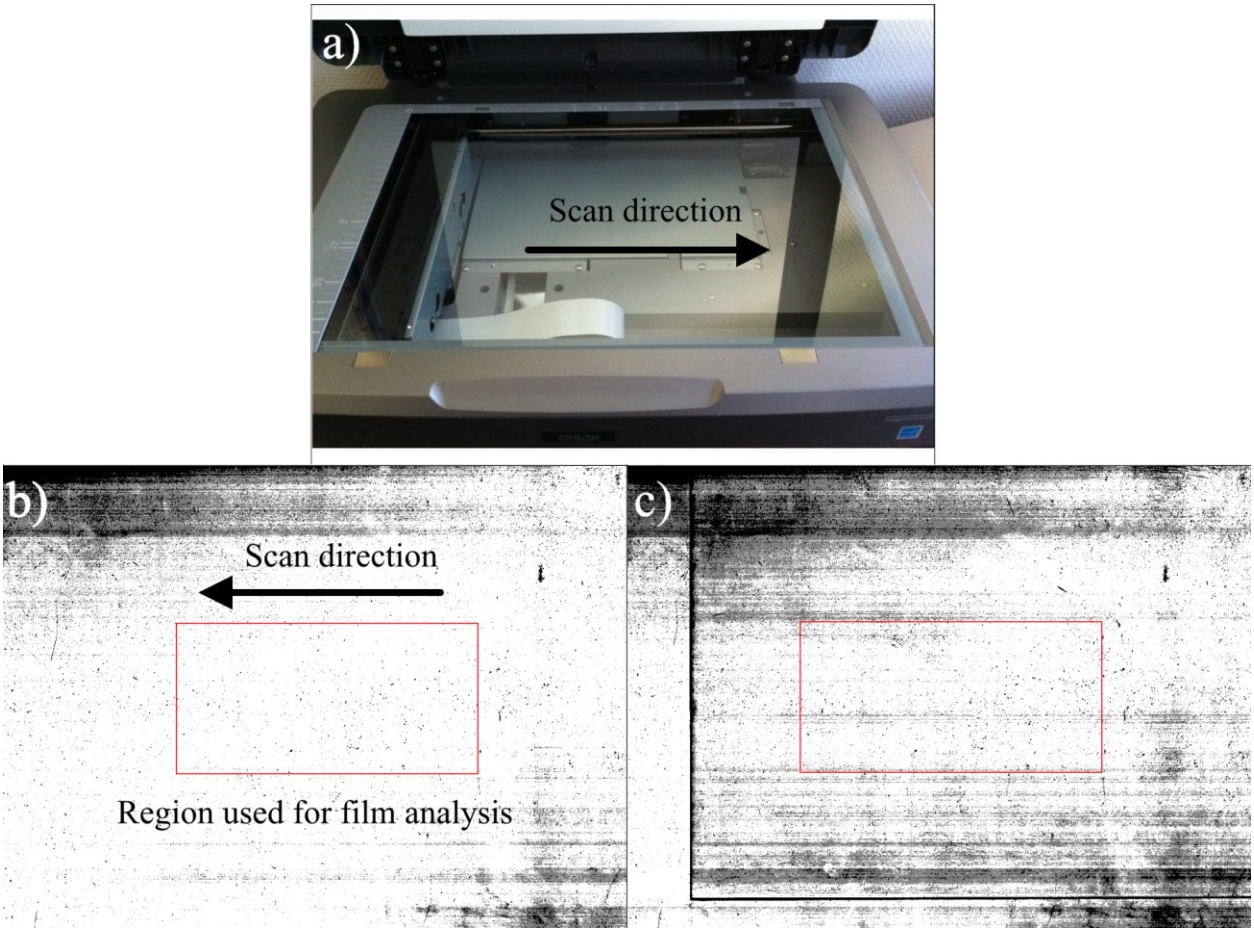

Figure 5.6: (a) The base of an Epson Expression 10000XL flatbed scanner, showing the scan direction. (b) A blank scan of the flatbed scanner with a window of 65,000 to 65,535 pixel values. The direction of the scan is given by the arrow. The red box represents a central 10 x 20 cm^2 region where films were positioned during scanning. (c) A scan with the glass plate. The window was set to 65,000 to 65,535 pixel values and the central 10 x 20 cm^2 region used for analysis is highlighted in red. In this selected region, the pixel values were within 0.5% (65,250 to 65,535).

5.2.2.3.2 Heterogeneity of Film Scans

In addition to scanner uncertainty, film heterogeneity may affect pixel values of the digitized film and result in higher pixel value variance than would be expected with just a characterization of the "empty" scan. To evaluate film heterogeneity, a sheet of unirradiated film (20 x 25 cm^2) was scanned while sandwiched between the glass and scanner (Figure 5.7(a)). In the central 10 x 20 cm^2 region, the average pixel values in the red, green, and blue color channels, measured in ImageJ (Bethesda, MD), were 45,215 ± 110 (0.24% variance), 43,804 ± 120 (0.27%), and 33,000 ± 110 (0.33%), respectively. This is similar to the intra-film uniformity reported by Mizuno *et al* (0.2 to 0.6% for EBT3 film irradiated up to 3 Gy and measured using in-house software that included all three color channels) (34). In addition, the spatial dependence of the uniformity was assessed by measuring the average pixel value in the central 1 cm wide segments of the analyzed

region (blue and green rectangles in (Figure 5.7(a)). The average pixel value was measured every 36 pixels (1.27 cm) in 1 x 1 cm^2 squares. The deviation between the average pixel value in the squares and the average pixel value of the entire 10 x 20 cm^2 region is given for the x-axis in Figure 5.7(b) and for the y-axis in Figure 5.7(c). No trend was identified, which suggests that the film measurement was spatially independent inside the region used for film analysis.

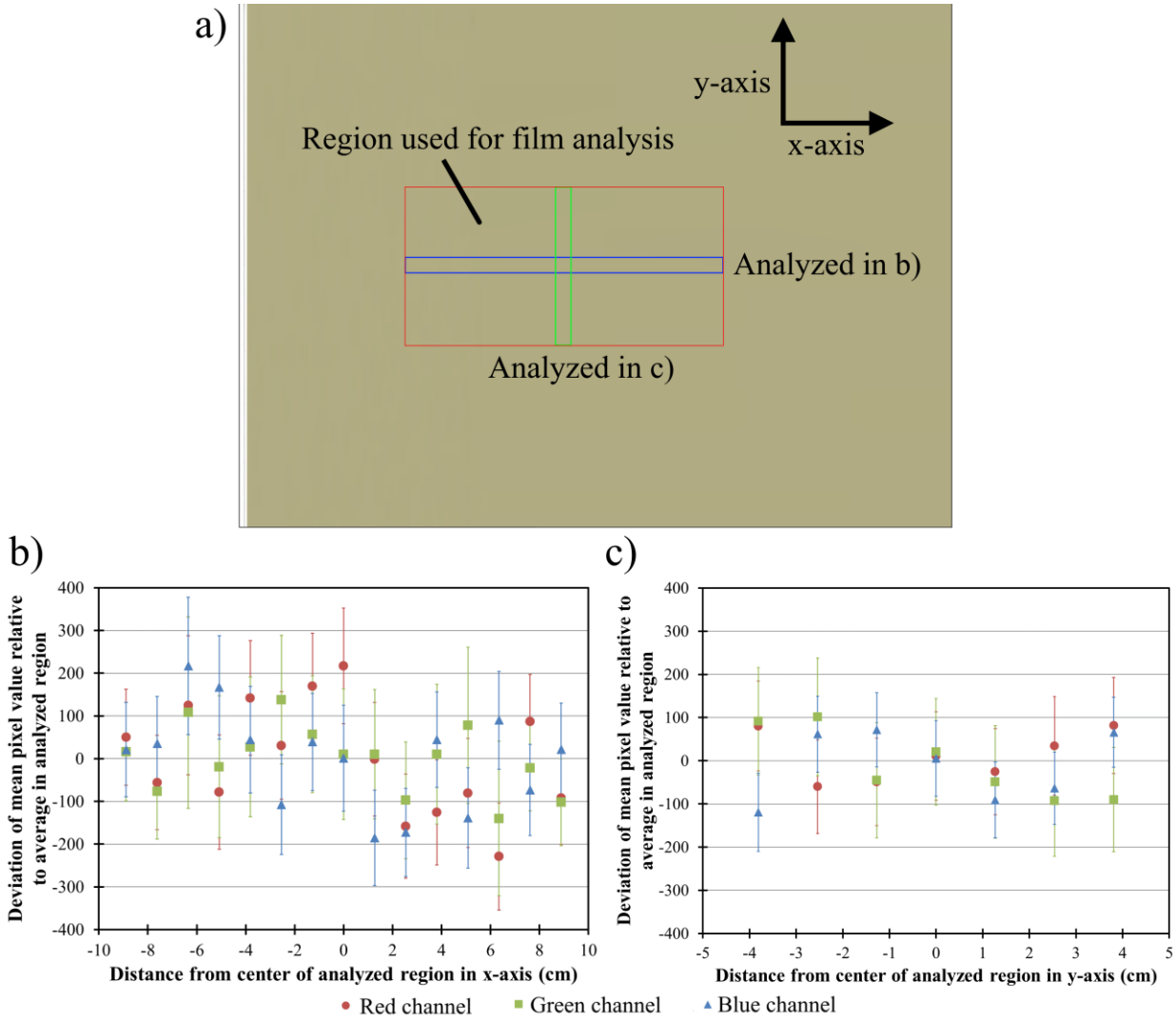

Figure 5.7: (a) The scan of an unirradiated film. The red box represents the region used for film analysis, while the blue and green rectangles represent 1 cm wide segments of the film analyzed to measure spatial dependence of the scanner. (b) Deviation of the red, green, and blue channel along the x-axis in 1 x 1 cm^2 regions from the average pixel value measured in the entire region. (c) Deviation of the red, green, and blue channel along the y-axis. Error bars represent the standard deviation in the measurement.

The dose dependence of film heterogeneity was determined by digitizing 4 x 4 cm^2 film pieces irradiated up to 10 Gy on a linear accelerator (Trilogy, Varian, Palo Alto, CA). The variance in

pixel value in the central 3 x 3 cm^2 region, as a percentage of the mean pixel value in the same 3 x 3 cm^2 region, was measured using ImageJ (Table 5.1). The results closely match the findings of Mizuno *et al*, with an overall variance of <0.7% (34).

Table 5.1: The variance in uniformity for 4 x 4 cm^2 film pieces irradiated from 0.5 to 10 Gy. Each color channel was evaluated independently.

Dose (Gy)	Variance (%)		
	Red	Green	Blue
0.5	0.33	0.34	0.39
1	0.38	0.40	0.38
2	0.42	0.39	0.39
3	0.42	0.37	0.40
4	0.57	0.59	0.45
5	0.61	0.55	0.46
6	0.51	0.59	0.46
7	0.60	0.60	0.47
8	0.63	0.63	0.50
9	0.61	0.60	0.50
10	0.68	0.68	0.52

5.2.2.3.3 Generation of Calibration Curve

For film calibration, a pixel value-to-dose relationship (calibration curve) was generated by irradiating 4 x 4 cm^2 film pieces to doses (D) up to 10 Gy in steps of 1 Gy in the Cs-137 irradiator (Figure 5.8(a)). Film pieces were sandwiched between 2 mm thick pieces of plexiglass to ensure charged particle equilibrium. Each measurement was taken three times and the irradiated films were digitized by scanning each film three times and averaging the three scans. The central 3 x 3 cm^2 region of the digitized film was analyzed using ImageJ. The mean pixel value in the region (PV) was used to determine the optical density (OD) as described by Morrison *et al* (Equation 5.5) (33):

$$OD = -log_{10}(PV/65535) \tag{5.5}$$

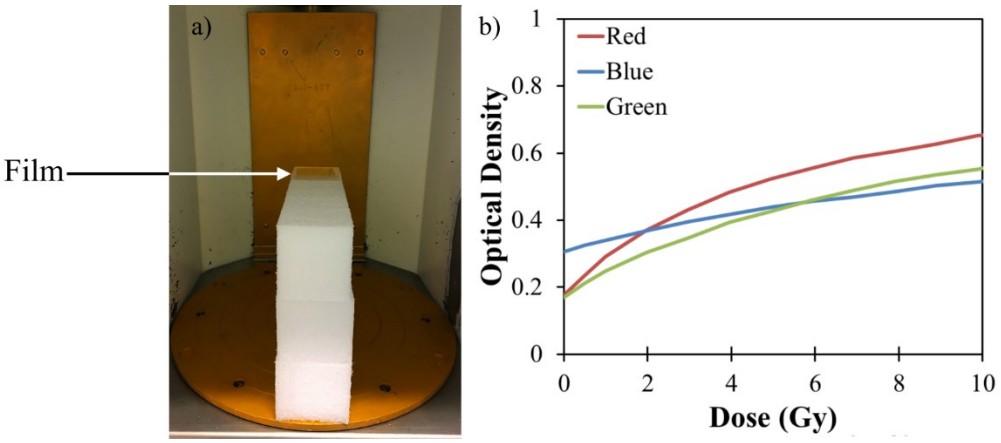

Figure 5.8: (a) Setup for film irradiation to measure dose at the center of the Cs-137 irradiator. The film was sandwiched between 2 mm plexiglass pieces (not shown) for buildup, at a height of 15 cm above the turntable. (b) The calibration curve for the red, blue, and green color channels.

Calculation of OD was conducted using all three color channels independently (triple-channel dosimetry) to take advantage of both the radiosensitivity of the red channel as well as the wider dynamic range of the green and blue channels (35). OD and dose D were correlated through Equation (5.6) (33):

$$D = \frac{A_3\, 10^{-OD} - A_1}{A_2 - 10^{-OD}} \tag{5.6}$$

where A_1 (units of Gy), A_2 (unitless), and A_3 (Gy) are adjustable parameters. The values for A_1, A_2, and A_3 were identified for each color channel using an in-house algorithm created in Matlab to minimize the differences between the three color channels as described by Micke *et al* (35). The relationship between OD and dose is shown in Figure 5.8(b).

5.2.2.3.4 Measurement of Dose Non-uniformity

Dose non-uniformity across the irradiator was estimated by exposing 5 x 17.5 cm^2 film strips (sandwiched between 2 mm pieces of plexiglass) placed 0, 5, 10, 15, and 20 cm above the turntable to 2 Gy (Figure 5.9(a)) using the same turntable rotation speed of 12 rpm as in Chapter 4. Measurements at each height were repeated three times. During scanning, the films were aligned such that the r-axis of the film was parallel to the direction of the scan.

The pixel values in a 1 x 12 cm^2 region were averaged along the y-axis (Figure 5.9(b)) and converted to dose using triple-channel dosimetry. Dose profiles at different elevations,

normalized to the dose delivered to the center of the irradiator at an elevation of 15 cm, are shown as a function of distance away from the center of the turntable (r-axis) in Figure 5.9(c)).

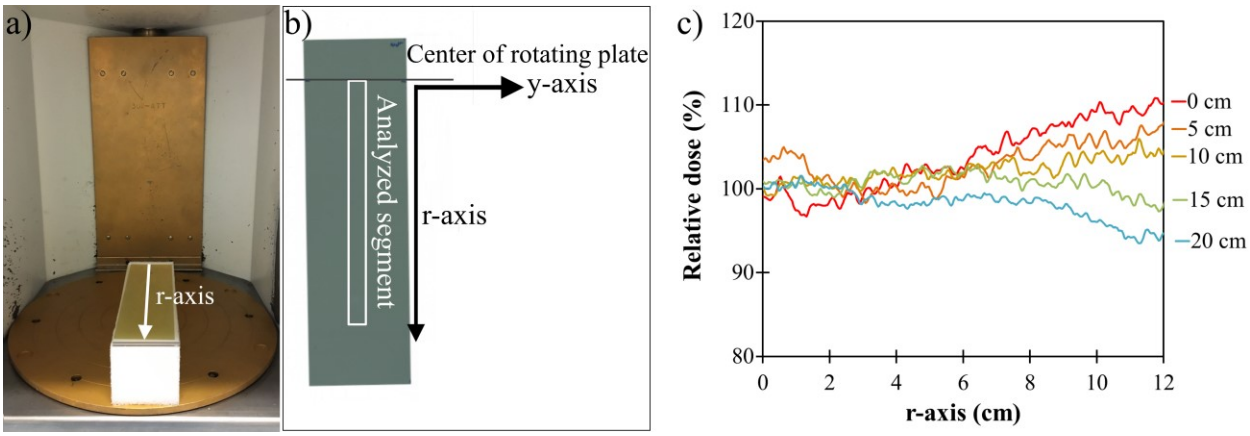

Figure 5.9: (a) Setup for film irradiation to measure dose non-uniformity across the irradiator at different elevations. The film pieces were sandwiched between 2 mm thick plexiglass pieces and irradiated to 2 Gy at elevations up to 20 cm (at 5 cm increments) above the turntable to characterize the radiation profile. (b) An exposed strip of Gafchromic film showing the region analyzed (white rectangle; 1 x 12 cm^2) using triple-channel dosimetry to generate the profiles. The black horizontal line across the film intersects the center of the rotating turntable. (c) The relative dose profiles (as a % of the dose delivered to the center of the irradiator) at different elevations above the turntable as a function of the distance away from the center of the turntable (r-axis).

For both SAT and fractionated experiments, three stacks of tissue culture plates were arranged near the center of the turntable where the dose was most uniform in the r-axis (Figure 5.10). The position of the plates on the stacks was consistent in each triplicate measurement. The stacked arrangement facilitated radiation delivery over a larger dose range in a short timeframe and reduced potential hypothermia in the cells by allowing for multiple plates to be irradiated simultaneously instead of sequentially. Consider SAT experiments, where the cells in the tissue culture plates were irradiated from 0.5 to 6 Gy. After the initial irradiation to 0.5 Gy, triplicate plates on top of the stack (planned to receive 0.5 Gy) were removed from the irradiator. This was followed by another 0.5 Gy irradiation to deliver 1 Gy to the next set of triplicate plates at the top, which were then removed. The process was repeated until all tissue culture plates were irradiated to the planned doses. This method of radiation delivery allows completion of one set of SAT experiments in <15 minutes. On the other hand, when triplicate plates at each dose level are separately irradiated, the experiment requires >28 minutes.

To estimate the effect of dose non-uniformity in such an arrangement, the data represented in Figure 5.9 was used to calculate the relative dose to groups of plates (three plates that represent an experimental triplicate; referred to as a "group" from here on), as depicted in Figure 5.10. Based on the position of the tissue culture plates in each plate group, the dose delivered to a group, $\overline{D}_{plate}$, is calculated using the following equation:

$$\overline{D}_{plate} = D_{presc} \int D(\vec{r}) dA \,/\, \int dA \tag{5.7}$$

where $D(\vec{r})$ is the relative dose at position r, D_{presc} is the prescribed dose at the center of the irradiator (15 cm above the center of the turntable), dA represents an infinitesimal area of the irradiated plate, and the integral is taken over the three plates in a group. The dose as a percentage of the prescribed dose was calculated (Table 5.2), per plate grouping, with a maximum variance of 1.2%.

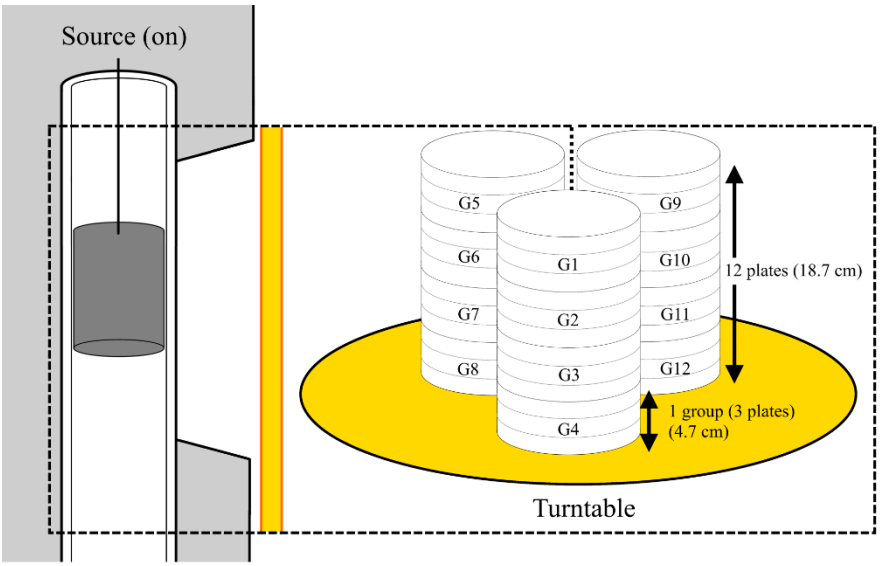

Figure 5.10: Positioning of 6 cm diameter plates for irradiation in the Cs-137 irradiator. Triplicate plates for each experiment were stacked on top of one another as a single "group" of plates, labeled G1 through G12. Each tissue culture plate is 1.53 cm tall and each stack held a maximum of 4 plate groups (18.7 cm).

Table 5.2: The dose delivered, relative to the prescribed dose, as calculated using Equation (5.7). For all experiments, the tissue culture plates were arranged in plate groups (triplicates of plates receiving the same dose) inside the Cs-137 irradiator cavity as shown in Figure 5.10.

Plate Group	G1, G5, G9	G2, G6, G10	G3, G7, G11	G4, G8, G12
Dose (% of prescribed dose)	100.29 ± 0.60	101.15 ± 0.04	100.99 ± 0.13	100.45 ± 0.23

5.2.2.4 Combined Dose Uncertainty

The dose delivered to a plate group, D, is given by:

$$D = \dot{D}_{cells}\left(\frac{\overline{D}_{group}}{D_{presc}}\right)T_{presc} + D_{transit}N = D_{on} + D_{transit}N \quad (5.8)$$

where $\dot{D}_{cells}$ is the dose rate experienced by cells at the center of the irradiator (given by Equation (5.4)), $\overline{D}_{group}/D_{presc}$ accounts for variation in the dose rate based on its location in the irradiator (Table 5.2), T_{presc} is the length of time the source remains in the "on" position, $D_{transit}$ is the transit dose, and N is the number of transit doses experienced by the plate group. The product of $\dot{D}_{cells}\left(\overline{D}_{group}/D_{presc}\right)T_{presc}$ therefore represents the dose delivered while the source is raised (D_{on}).

Assuming no uncertainties in the corrected ion chamber measurement (M_{Corr}), $(\mu_{en}/\rho)^{water}_{acrylic}$, T_{presc}, and N, the uncertainty in D is calculated using the following equation:

$$\frac{\Delta D}{D} \approx \frac{\Delta D_{on}}{D_{on}} + \frac{N\Delta D_{transit}}{D} = \sqrt{\Delta k_{q,Cs-137}{}^2 + \Delta N_{k,Co-60}{}^2 + \Delta\left(\frac{\overline{D}_{group}}{D_{presc}}\right)^2} + \frac{N\Delta D_{transit}}{D} \quad (5.9)$$

Equation (5.9) assumes that that (i) $D_{transit} \ll D_{on}$ and (ii) the transit mechanism is not random, such that the transit uncertainty increases linearly with the number of transits. The components $\Delta k_{q,Cs-137}$, $\Delta N_{k,Co-60}$, $\Delta\left(\overline{D}_{group}/D_{presc}\right)$, and $\Delta D_{transit}$ are the uncertainties of $k_{q,Cs-137}$, $N_{k,Co-60}$, $\left(\overline{D}_{group}/D_{presc}\right)$, and $D_{transit}$, respectively. These components are, in reality, relative uncertainties (i.e. $\Delta k_{q,Cs-137}/k_{q,Cs-137}$) but the denominators have not been shown to simplify the appearance of the equation. The values are as follows: $\Delta k_{q,Cs-137}$ = 0.5%, $\Delta N_{k,Co-60}$ = 0.5% for k = 1, $\Delta\left(\overline{D}_{group}/D_{presc}\right)$ is given by uncertainties of each plate group in Table 1, and $\Delta D_{transit}$ = 0.0003 Gy. Based on Equation (5.9), the uncertainty of D_{on}, ΔD_{on}, ranges from 0.7% to 0.9%, depending on the plate group irradiated. An additional uncertainty component is required to take account of the dosimetry methodology, adopted from an open-field irradiation geometry. Based on an analysis of air-kerma based dosimetry protocol formalisms, a value of 2.0% was adopted.

5.2.2.5 Attenuation by Tissue Culture Plates

In the stacked configuration, attenuation of radiation by the tissue culture plates on the top could reduce the dose delivered to plates below. Dos Santos *et al* showed that EBT3 films placed at the bottom of well plates with 1 mL and 9 mL of media experienced dose variations of +8% and -40% compared to the reference (3 mL), respectively, when exposed to 80 kVp x-rays (36). This impacted the results of the clonogenic assays, where cells in 9 mL of media had a higher SF than cells in 1 mL.

To assess the effect of radiation attenuation in the Cs-137 irradiator, 4 x 4 cm^2 film pieces were placed on the turntable at the position of plate group G4 and irradiated to 2 Gy. During this irradiation, up to nine 10 cm tissue culture plates, each filled with 10 mL of media (~1.4 mm thick, the standard thickness of media used for the experiments in Chapter 4), were placed on the turntable in the same configuration as shown in Figure 5.10. The dose received by the films was determined using Equations (5.5) and (5.6) and the experiment was repeated three times to ensure repeatability. For 1, 3, 5, 7, and 9 plates placed above the film, the doses measured were 1.98 ± 0.04, 1.99 ± 0.03, 2.00 ± 0.04, 1.99 ± 0.04, and 1.98 ± 0.04 Gy, respectively, showing no significant difference. The differences between the measurements are also within the range of uncertainty associated with the film dose calibration curve. Using a comprehensive uncertainty analysis of the calibration process, Bouchard *et al* reported an absolute uncertainty of 0.96% in dose measurements using Gafchromic EBT film (37).

5.2.3 Dosimetric Uncertainties Associated with BAIRDA

The use of BAIRDA introduces several uncertainties that are associated with the afterloader system, experimental setup, and dose calculation.

5.2.3.1 Afterloader related

Uncertainties associated with the afterloader are of clinical interest. As these uncertainties have been extensively investigated previously, this study uses the reported values from previously published literature. Details of each uncertainty, the method of its estimation, and the potential impact on the dose delivered for *in vitro* studies will be discussed below.

5.2.3.1.1 Calibration

As with the irradiator, accurate source calibration for afterloaders is required to reduce differences between the prescribed and delivered dose (38). According to the AAPM TG-138 report, individual source strength calibrations introduce an uncertainty of 1.5% for HDR high energy brachytherapy sources based on an analysis of best practice uncertainties when translating from a primary standards lab to the clinic (39). Based on the TG-138 report and in-house experience performing Ir-192 BT source calibrations, the uncertainty in the calibration of the HDR and PDR sources was taken to be 1.5%.

5.2.3.1.2 Rounding Error

To deliver the required dose at the prescription points with BAIRDA, the Ir-192 source was positioned at 21 dwell positions (5 mm step size) along the catheter for pre-planned dwell times. However, dwell time rounding error can occur when exporting the treatment plan to the afterloader due to differences in the dwell time in the treatment planning software and the time delivered by the afterloader; while OcB can plan dwell positions to 0.01 seconds, dwell times will be rounded to the nearest 0.1 second at the treatment console. The use of dose optimization reduces this error as the different dwell weights will average out dose error, decreasing this uncertainty to less than 1.0% for a dose prescription of 5 Gy through the removal of dwell positions with short dwell times (40). As dose optimization was used in planning BAIRDA deliveries with prescription doses in the range of 3.7 to 6.1 Gy, rounding error uncertainties were taken to be 1.0% of the total dose.

5.2.3.1.3 Transit Dose

In the case of afterloaders, additional dose is contributed when the source travels to and from the catheter and in between dwell positions which is not considered by OcB. It has previously been reported, based on the stationary and integrated charge collected by a well-type ionization chamber while delivering an intracavitary gynecological treatment, that the transit dose generally contributes <2% additional dose for intracavitary PDR and HDR, with PDR treatments adding more transit dose due to their multiple entries and exits during treatment (41). However, a reduction of this effect is possible through “dwell time compensation”, which reduces the dwell times to account for inter-dwell transit dose (40,41). The majority of the transit dose, once inter-

dwell transit dose is effectively compensated for, is due to source entry/exit from the afterloader (<0.5%) (41). Since the microSelectron HDR/PDR afterloaders include inter-dwell transit, a value of 0.5% was added to the uncertainty budget (42).

5.2.3.2 Plate-Base Alignment

The experiments with BAIRDA used prescription to points placed symmetrically on either side of the plastic catheter (source path) such that the dose profile on the tissue culture plate resembles an infinite line source of radiation (Figure 4.3(c)). Variations in geometry can result in differences between the expected and actual dose delivered to the ROI. The placement of the tissue culture plate in the base has to be precise as the dose rate is strongly correlated to the distance from the source.

Plausible uncertainties identified with the plate-base alignment were in the (i) positioning along the axis of irradiation (y-axis in Figures 4.3(c) and 4.5(a)), (ii) positioning perpendicular to the axis of irradiation (x-axis), and (iii) rotation of the plate relative to the base. To estimate the impact of such misalignments, worst-case scenarios were considered by shifting the dwell positions in OcB and recording the dose difference at multiple points on the tissue culture plate (yellow and orange crosses on Figure 5.11(a)) without renormalizing. Dwell positions were moved by +2 mm in the y-axis (representing a scenario where the catheter was displaced along the y-axis), +0.25 mm in the x-axis (representing the maximum shift by the plate or catheter in the x-axis), and 1° clockwise around the center of the tissue culture plate (as a worst-case rotation).

Figure 5.11(b) shows the change in relative dose at the prescription points at 1 cm (along the y-axis) on either side of the catheter due to plate-base misalignment. The average change in dose along the y-axis at different x-axis positions (at the orange crosses) is presented in Figure 5.11(c). y-axis misalignments result in minimal dose uncertainty across the entire tissue culture plate with a mean [range] difference of 0.1 [0.08 - 0.2]% at the orange crosses. This is an expected result as the radiation delivered by the treatment plan is relatively consistent in the y-axis. However, x-axis and rotational misalignment introduce 1.7 [1.1 - 3.0]% and 1.1 [0.4 - 2.5]% uncertainty on average, respectively, to the dose at the orange crosses 1 to 4 cm away

from the catheter (Figure 5.11(c)); their effect is strongest at points closest to the radiation source and decreases at locations further away (e.g. ~1% at 4 cm on the x-axis). While Figures 5.11(b) and 5.11(c) use dose points in the positive x-axis, the effects on the negative x-axis are opposite and equal in magnitude; for example, points on the negative x-axis receive less dose (not shown) after a shift of the source positions in the positive x-axis direction.

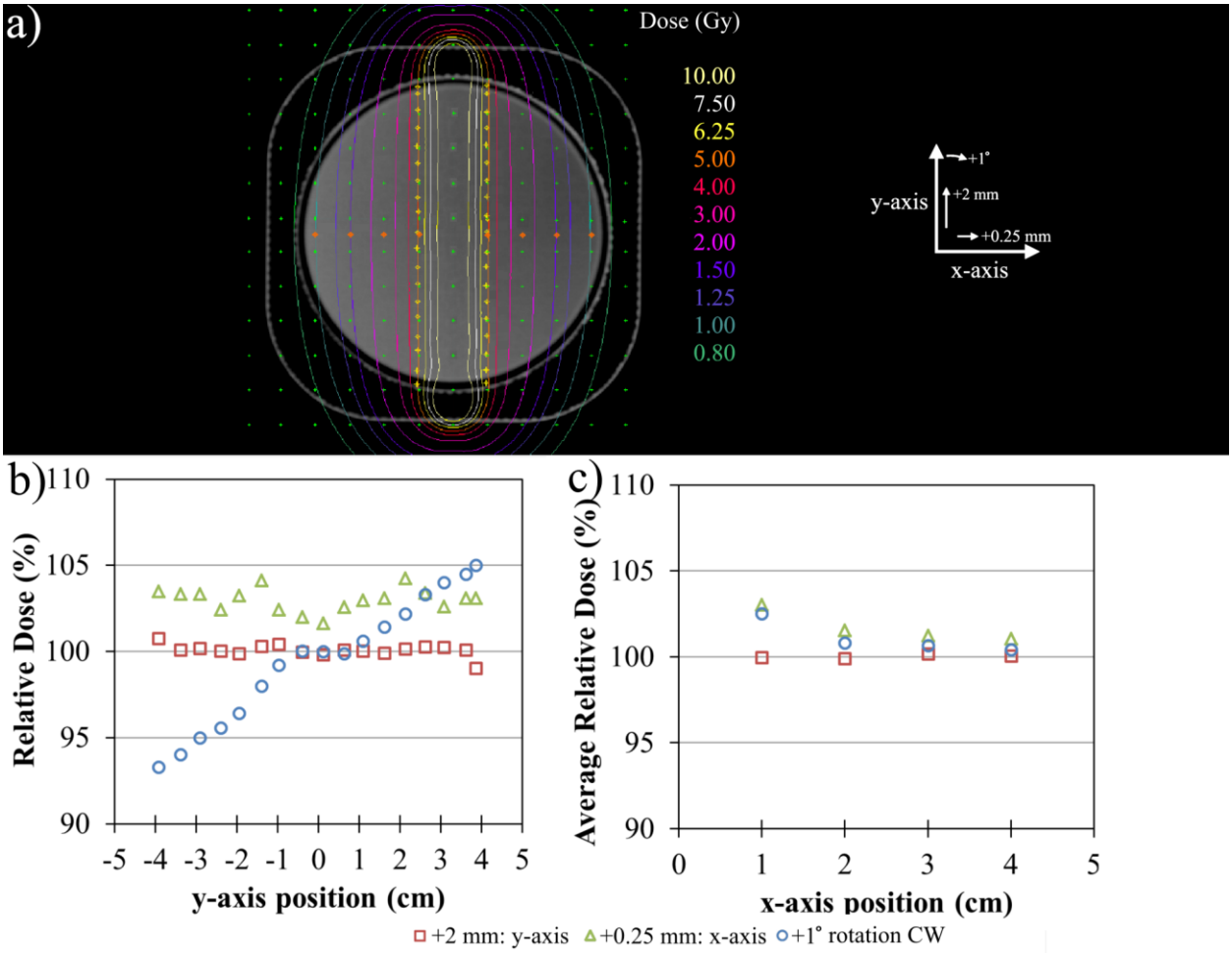

Figure 5.11: (a) Isodose distribution for a dose of 5 Gy prescribed to the prescription points (yellow crosses) at 1 cm on either side of the catheter. Orange crosses along the x-axis represent additional points used to report dose during uncertainty analysis in Figure 5.11(c). (b) The relative change in dose at the prescription points when the dwell positions are shifted +2 mm in the y-axis, +0.25 mm in the x-axis, or 1° clockwise around the center of the plate. These shifts represent the worst-case plate-base misalignment scenarios using BAIRDA. (c) The average relative dose at different x-axis positions for the same dwell position shifts as Figure 5.11(b). For example, the average of the points in Figure 5.11(b) are represented in Figure 5.11(c) at an x-axis position of 1 cm.

5.2.3.3 Effect of Heterogeneity in Dose Calculation

BAIRDA experiments were planned using the TG-43 formalism (Equation (1.1)), which considers the entire dose calculation volume as water with uniform unit density (43,44,45). Though the cell medium is water equivalent, the tissue culture plate and base are less dense than water and may introduce uncertainties in the calculated dose. The AAPM TG-186 report addresses this shortcoming through the recommendation of model based dose calculation algorithms (MBDCA) that can account for differences between absorbed dose in the water and tissue, dose contributions from electrons, and dose heterogeneities resulting from the (non-water) material properties of the applicators (as described in Section 1.10.2) (46,47). The impact of the applicator alone can introduce a significant effect as material selection can result in differences between TG-43 and TG-186 formalisms by up to 2% for metal catheters and 0.7% for plastic catheters (48). In addition, as noted in Chapter 1, the material assignment of rectal tissue can create large differences between TG-43 and TG-186 calculated dose. While the definition of rectal tissue as water only introduces small variances between the two dose calculations (0.81% difference in the calculated rectal D_{2cc}), assignment of rectal tissue as air creates significant differences (11.87% difference) (49). In OcB, the MBDCA used is ACE. To estimate the effect of heterogeneities on the TG-43 calculated doses for experiments performed in Chapter 4, the doses were recalculated using TG-186. The cell culture media and the plastic bottom of the plate were assigned to be water, the base (~ -400 Hounsfield Units (HU)) was assigned physical densities by OcB ACE using the "HU based" option, and all other materials above the base were assigned to be air. The cell culture medium and plastic bottom were manually assigned material properties as their measured physical density in the CT reconstruction was lower than expected (e.g. ~ -200 HU for the water equivalent medium), which occurred due to the blurring of a thin layer of medium (~1.3 mm) and the air layer above it. Water was selected as the representative material for both the medium and the tissue culture plate as the media is primarily water and, based on a series of CT scans by Sande *et al*, the expected HU values for polystyrene (the material for tissue culture plates) are close to water (50).

The dose falloff calculated by the TG-43 formalism, TG-186 formalism, and Gafchromic film measurements from Figure 4.4(b) are shown in Figure 5.12. The dose is symmetric on both sides of the central axis and decreases as the distance from the central axis increases. The TG-186 dose

is 1.3% lower than the TG-43 dose on average (range of -0.6% to -2.1%). The film measurements closely agree with both formalisms: the average relative variance between film and TG-43 dose measurements (as a % of the prescription dose) was 2.3 ± 1.3% (with a maximum variance of 3.9%), while there was a lower average variance between film and TG-186 dose (1.6 ± 1.5%; maximum variance of 3.0%). The similarity in results provides support for the use of both TG-43 and TG-186 dose calculation techniques for BAIRDA.

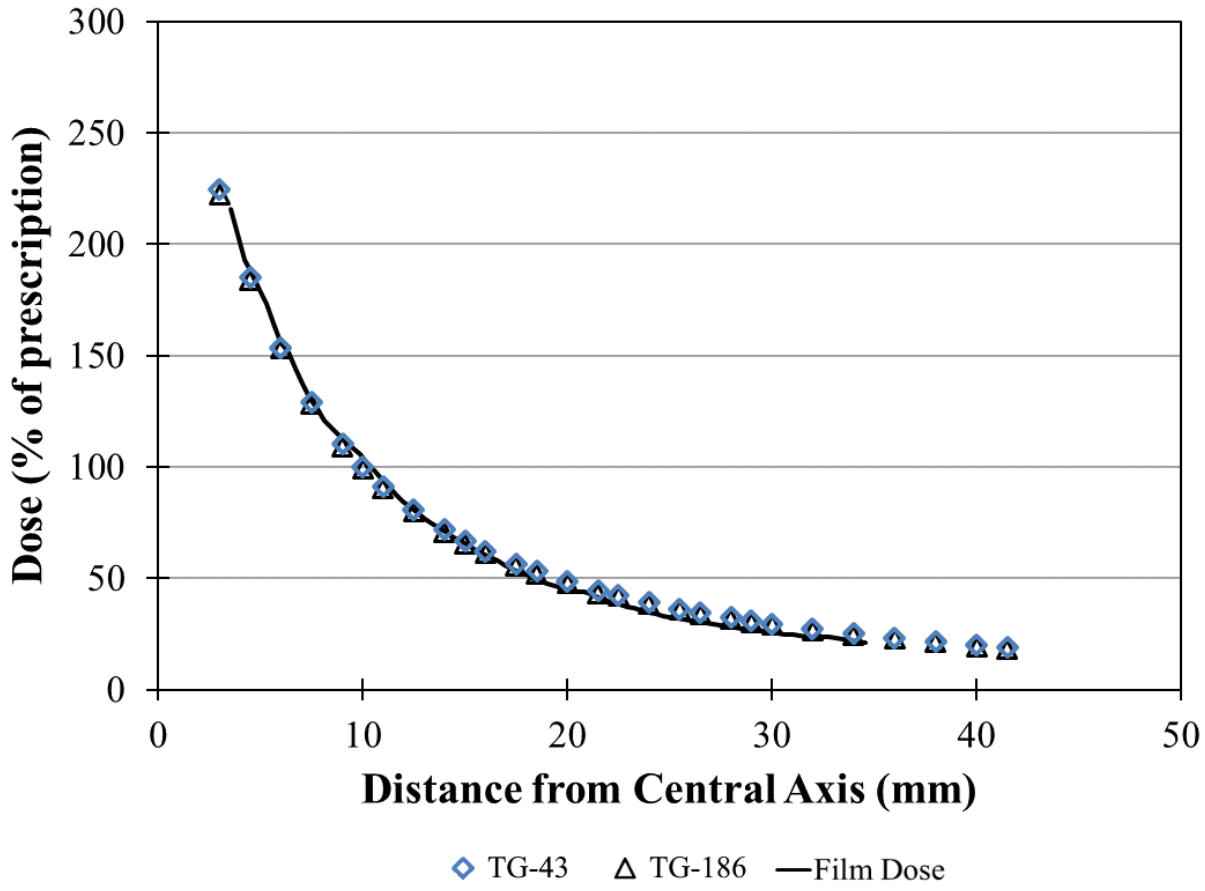

Figure 5.12: Dose, as a percent of the prescription, plotted against the distance from the center of the plate along the x-axis for the TG-43 algorithm, the TG-186 algorithm, and for film measurements.

5.2.3.4 Summary of Uncertainties

The uncertainties identified and their potential impact on SF and dose are given in Tables 5.3 and 5.4, respectively. The measured uncertainties for attachment time and hypothermia were smaller than the uncertainty for the number of cells plated. As these experiments utilized the number of colonies formed on a tissue culture plate to quantify the uncertainty, it is not possible to

distinguish whether the variance measured was the result of the specific uncertainty (attachment time or temperature change), or due to variances in the number of cells plated, or both. Hence, these values are listed as "Not significant", relative to other uncertainties. Similarly, the effect of attenuation of radiation caused by the tissue culture plates on film OD was lower than the standard deviation in the measured OD. With limited possibility to distinguish the effect of attenuation from the heterogeneity of the film/scanner, attenuation-related uncertainty was labeled "Not significant" in Table 5.4. For both tables, the standard and expanded undertainties were calculated using all identified uncertainties.

Table 5.3: Summary of identified uncertainties that affect the measurement of SF. Values are reported assuming a symmetric normal distribution. Uncertainties noted as "Not significant" had values lower than the uncertainty associated with cell seeding density (see text for details).

Source of Uncertainty	**Radiation Source**	
	Cs-137 Irradiator	**BAIRDA**
Cell seeding density	3.4%	
Cell seeding uniformity	-	2.0%
Cell attachment times	Not significant	
Cell hypothermia during radiation	Not significant	
Colony selection (size)	2.7%	
Subjectivity in colony counting		
- Intra-operator	0.7%	
- Inter-operator	4.1%	
Standard uncertainty (k = 1)	6.0%	6.3%
Expanded uncertainty (k = 2)	12.0%	12.6%

The total uncertainty was calculated using a summation in quadrature as no correlation between the uncertainties was identified. Dose uncertainties were divided into two categories: (1) systematic errors which predictably increase or decrease the average dose delivered (e.g. transit dose will increase the dose) and (2) random errors which may be difficult to detect (e.g. phantom-plate alignment may increase or decrease the dose delivered by BAIRDA) (51). The former (arising from factors like irradiator source calibration, transit dose, irradiator non-uniformity, and the incorporation of dose heterogeneity) can be incorporated by using the dose delivered instead of the dose prescribed (e.g. Equation 5.7 for the Cs-137 irradiator experiments) during experimental analysis; the latter (relating to factors like uncertainty in source calibration and transit dose measurement, uncertainty in irradiator non-uniformity within a plate group, dwell time rounding, and phantom-plate alignment) is characterized by uncertainty in the dose

delivered (i.e. error bars). As both systemic and random errors depend on the plate position in the irradiator (Table 5.2) and the distance from the catheter for BAIRDA (Figures 5.11 and 5.12), a range of dose uncertainties are reported in Table 5.4 by calculating the uncertainty for each plate group (for Cs-137 uncertainty) and by distance away from the catheter (for BAIRDA uncertainty).

Table 5.4: Summary of identified uncertainties affecting dose delivered. Values reported with a + or – indicate a systemic uncertainty that is dependent on plate position during irradiation or ROI position on the irradiated plate, and were included in the "Change in average dose" category. All other random uncertainties are assumed to have a normal distribution and were used to determine standard and expanded uncertainty. If both are present, systemic uncertainty is shown first with the random uncertainty in brackets. The phantom-base alignment uncertainties represent the average relative dose uncertainty (Figure 5.11). Note that the tissue culture plate attenuation was measured with EBT3 film and produced uncertainties smaller than the uncertainty in the film's OD measurements (e.g. caused by heterogeneities in film/scanner output). Therefore, the uncertainty due to attenuation was deemed "Not significant" as it could not be isolated from the background noise of the measurement.

Source of Uncertainty	**Radiation Source**	
	Cs-137 Irradiator	**BAIRDA**
Source calibration	-0.6 (0.7)%	1.5%
Source calibration methodology	2.0%	-
Transit dose	+1.4 (0.03) cGy/transit	+0.5%
Dose non-uniformity in the irradiator	+0.3% - +1.2% (0.04% - 0.6%)	-
Attenuation by tissue culture plates	Not significant	-
Dwell time rounding error	-	1.0%
Phantom-base alignment		
- x-axis	-	1.0% - 3.0%
- y-axis	-	0.08% - 0.2%
- Rotational	-	0.4% - 2.5%
Incorporation of dose heterogeneity	-	-2.1% - -0.6%
Change in average dose [a]	-0.3% - +0.6%	-1.6% - 0.1%
Standard uncertainty (k = 1) [b]	2.1 - 2.2%	2.1% - 4.3%
Expanded uncertainty (k = 2)	4.2 - 4.4%	4.2% - 8.6%

[a] Shown by a shift in the dose data points on Figure 5.13
[b] Shown by a change in the error bars on Figure 5.13

5.2.3.5 Potential Impact of Uncertainties on Radiobiological Parameter Estimation

The calculation of a cell line's radiobiological parameters is a common end goal of clonogenic assays (8,52,53). Generally, such studies only include the uncertainty observed in an experimental triplicate (11,54). The introduction of additional uncertainties in either the dose or SF could affect the radiobiological parameter values estimated from clonogenic assays. Figure

5.13(a) overlays the results for SW756 cells exposed with a single fraction of Cs-137 using two different calculation methods: (1) when only the uncertainty in the experimental triplicate is considered and (2) when all identified uncertainties are included. Figure 5.13(b) - (d) presents the same, but with SW756 cells exposed with HDR-BAIRDA, fractionated Cs-137 exposure, and PDR-BAIRDA, respectively.

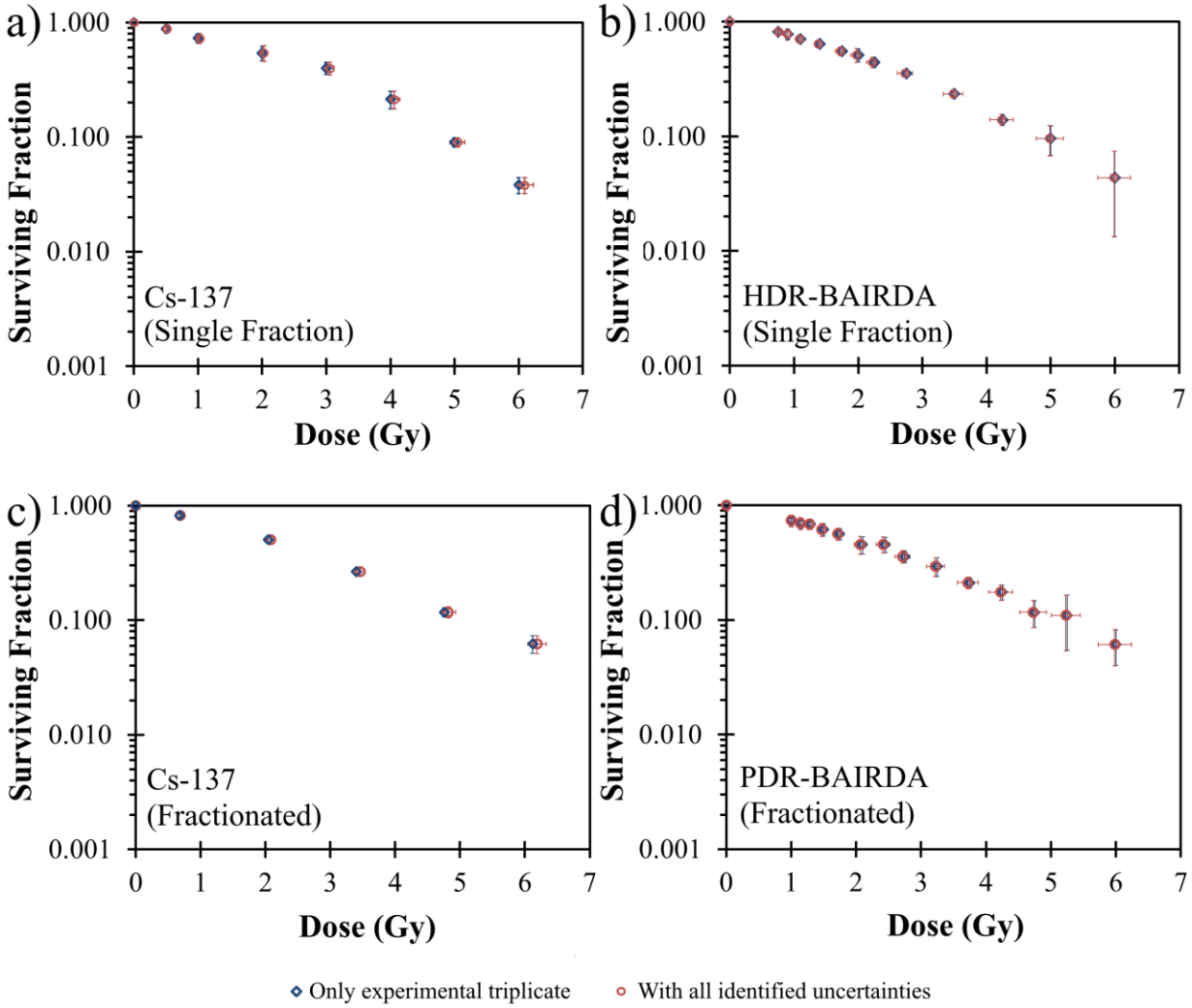

Figure 5.13: Surviving fraction curves for SW756 using (a) single acute exposure in the Cs-137 irradiator, (b) HDR-BAIRDA, (c) hourly fractions of radiation (0.68 Gy/hr) using the Cs-137 irradiator, and (d) PDR-BAIRDA. The error bars in black represent the standard deviation of the SF measurement in an experiment triplicate while the red error bars represent the combination of all identified uncertainties. The addition of all identified uncertainties does not significantly affect the SF error bars in any figure, which suggests that the experiment triplicate uncertainty is dominant.

To assess their impact on radiobiological parameter estimation, the combined uncertainties were applied to revise the α/β and $T_{1/2}$ values for the cells irradiated using both SAT and fractionated schedules, with the Cs-137 irradiator and BAIRDA. The estimation process used weighted least squares fitting. For example, the uncertainty for an SF measurement (ΔSF) is given by:

$$\Delta SF = SF\sqrt{(\Delta C_0/C_0)^2 + (\Delta C/C)^2 + \sum_i \Delta SF_i{}^2} \tag{5.10}$$

where ΔC_0 and ΔC are the standard deviations in the number of colonies measured in a triplicate experiment for the control and irradiated plates, respectively, and ΔSF_i represents the relative uncertainties given in Table 5.3. For this analysis, the variance in the cell seeding density is not included in the ΔSF_i term, since it is already implicit in the $(\Delta C_0/C_0)^2$ term, which was recalculated for each experiment. Similarly, dose uncertainty was calculated by including the uncertainties highlighted in Table 5.4. Radiobiological parameters α and β were estimated from SAT experiments by minimizing the X^2 metric in Equation (4.8) and $T_{1/2}$ was extracted from fractionated experiments using Equation (4.9). These values of α/β and $T_{1/2}$ were compared against best-fit values obtained when considering only uncertainties in the experiment triplicate (Equations (4.4) and (4.5)), the common calculation methodology. Such a comparison is shown in Table 5.5 as an example of the potential impact of the identified uncertainties. An evaluation of the similarity between the results was conducted using a twin tailed Welch t-test with the null hypothesis being equivalence between the radiobiological parameter values determined using the triplicate uncertainty only and that utilizing the full uncertainty analysis. A p-value of 0.05 was assumed to provide statistical significance. For t-test analysis, the α/β and $T_{1/2}$ values are assumed to be normally distributed and have homogenous variance.

While the SF uncertainty analysis was conducted only with SW756 cells, the full analysis shown above was repeated for all cell lines assuming the effect of cell attachment times and hypothermia remained not significant. The results are shown in Tables 5.6 (SCC) and 5.7 (AC).

Table 5.5: Summary of the radiobiological parameters derived for SW756 from SAT and fractionated experiments using (a) a Cs-137 irradiator and (b) BAIRDA (Ir-192). Results are presented as a mean (95% confidence interval) when considering only uncertainties in experimental triplicates, and when all uncertainties identified in this work are included. The results using both uncertainty calculations were compared using p-values.

Source	Uncertainties Included	α (Gy^{-1})	β (Gy^{-2})	α/β (Gy)	$T_{1/2}$ (hr)
(a) Irradiator	**Experiment triplicate**	0.27 (0.24 - 0.31)	0.044 (0.036 - 0.052)	6.3 (4.9 - 7.6)	5.3 (4.1 - 6.4)
	All identified	0.27 (0.23 - 0.31)	0.042 (0.034 - 0.050)	6.5 (4.9 - 8.1)	4.9 (3.9 - 5.8)
	p-value	0.94	0.57	0.91	0.53
(b) BAIRDA	**Experiment triplicate**	0.25 (0.23 - 0.26)	0.050 (0.045 - 0.054)	5.0 (4.5 - 5.5)	4.9 (4.2 - 5.8)
	All identified	0.26 (0.24 - 0.27)	0.048 (0.043 - 0.053)	5.3 (4.7 - 6.0)	4.8 (4.1 - 5.4)
	p-value	0.18	0.29	0.29	0.76

Table 5.6: Summary of the radiobiological parameters derived for (a) CaSki, (b) C-33A, and (c) SiHa from SAT and fractionated experiments using a Cs-137 irradiator and BAIRDA (Ir-192). Results are presented as a mean (95% confidence interval) considering only uncertainties in experimental triplicates, and when all uncertainties are included. The results using both uncertainty calculations were compared using p-values.

Source		Uncertainties Included	α (Gy^{-1})	β (Gy^{-2})	α/β (Gy)	$T_{1/2}$ (hr)
(a) CaSki	**Irradiator**	**Experiment triplicate**	0.21 (0.17 - 0.24)	0.037 (0.031 - 0.044)	5.5 (4.1 - 6.9)	3.9 (3.0 - 4.9)
		All identified	0.21 (0.17 - 0.25)	0.036 (0.029 - 0.043)	5.8 (4.2 - 7.3)	3.8 (2.9 - 4.7)
		p-value	0.95	0.74	0.65	0.81
	BAIRDA	**Experiment triplicate**	0.19 (0.18 - 0.21)	0.040 (0.036 - 0.043)	4.9 (4.3 - 5.4)	3.4 (2.8 - 4.0)
		All identified	0.20 (0.19 - 0.21)	0.039 (0.035 - 0.042)	5.2 (4.6 - 5.8)	3.3 (2.8 - 3.9)
		p-value	0.27	0.57	0.29	0.64
(b) C-33A	**Irradiator**	**Experiment triplicate**	0.35 (0.31 - 0.40)	0.063 (0.052 - 0.074)	5.6 (4.4 - 6.8)	2.2 (1.7 - 2.8)
		All identified	0.35 (0.31 - 0.39)	0.061 (0.050 - 0.072)	5.7 (4.4 - 6.9)	2.2 (1.5 - 2.8)
		p-value	0.77	0.70	0.90	0.79
	BAIRDA	**Experiment triplicate**	0.31 (0.29 - 0.33)	0.054 (0.050 - 0.057)	5.7 (5.2 - 6.3)	2.5 (2.2 - 2.8)
		All identified	0.31 (0.28 - 0.34)	0.056 (0.046 - 0.065)	5.6 (4.5 - 6.6)	2.7 (2.0 - 3.3)
		p-value	0.85	0.57	0.67	0.50
(c) SiHa	**Irradiator**	**Experiment triplicate**	0.17 (0.14 - 0.19)	0.038 (0.033 - 0.043)	4.5 (3.6 - 5.4)	3.5 (2.8 - 4.2)
		All identified	0.16 (0.13 - 0.19)	0.037 (0.032 - 0.043)	4.3 (3.4 - 5.2)	3.6 (3.0 - 4.2)
		p-value	0.53	0.97	0.66	0.65
	BAIRDA	**Experiment triplicate**	0.17 (0.15 - 0.19)	0.029 (0.024 - 0.035)	5.8 (4.5 - 7.1)	2.9 (2.6 - 3.3)
		All identified	0.18 (0.16 - 0.20)	0.028 (0.024 - 0.034)	6.3 (4.9 - 7.7)	2.8 (2.4 - 3.1)
		p-value	0.42	0.70	0.40	0.31

Table 5.7: Summary of the radiobiological parameters derived for (a) HeLa, (b) JHUCS-3, and (c) SiSo from SAT and fractionated experiments using a Cs-137 irradiator and BAIRDA (Ir-192). Results are presented as a mean (95% confidence interval) when considering only uncertainties in experimental triplicates, and when all uncertainties identified in this work are included. The results using both uncertainty calculations were compared using p-values.

Source		Uncertainties Included	α (Gy^{-1})	β (Gy^{-2})	α/β (Gy)	$T_{1/2}$ (hr)
(a) HeLa	Irradiator	Experiment triplicate	0.19 (0.14 - 0.24)	0.044 (0.031 - 0.056)	4.4 (2.7 - 6.0)	1.22 (0.42 - 2.02)
		All identified	0.19 (0.14 - 0.24)	0.042 (0.030 - 0.054)	4.6 (2.8 - 6.4)	1.19 (0.53 - 1.85)
		p-value	0.96	0.73	0.78	0.93
	BAIRDA	Experiment triplicate	0.20 (0.18 - 0.21)	0.040 (0.035 - 0.044)	5.0 (4.3 - 5.6)	1.28 (1.19 - 1.38)
		All identified	0.20 (0.19 - 0.22)	0.039 (0.034 - 0.044)	5.2 (4.5 - 6.0)	1.25 (1.17 - 1.34)
		p-value	0.32	0.61	0.41	0.46
(b) JHUCS-3	Irradiator	Experiment triplicate	1.17 (1.04 - 1.31)	0.256 (0.197 - 0.313)	4.6 (3.4 - 5.8)	1.59 (0.09 - 3.94)
		All identified	1.14 (1.01 - 1.27)	0.264 (0.204 - 0.325)	4.3 (3.2 - 5.4)	1.54 (0.14 - 2.94)
		p-value	0.56	0.73	0.57	0.94
	BAIRDA	Experiment triplicate	1.04 (1.00 - 1.08)	0.281 (0.248 - 0.314)	3.7 (3.2 - 4.2)	1.53 (0.86 - 2.20)
		All identified	1.07 (1.03 - 1.11)	0.269 (0.234 - 0.404)	4.0 (3.4 - 4.5)	1.13 (0.88 - 1.38)
		p-value	0.20	0.45	0.28	0.10
(c) SiSo	Irradiator	Experiment triplicate	0.21 (0.17 - 0.24)	0.062 (0.054 - 0.069)	3.4 (2.8 - 4.1)	0.56 (0.50 - 0.63)
		All identified	0.21 (0.18 - 0.24)	0.060 (0.053 - 0.067)	3.5 (2.8 - 4.1)	0.55 (0.50 - 0.61)
		p-value	0.85	0.65	0.89	0.66
	BAIRDA	Experiment triplicate	0.20 (0.17 - 0.22)	0.057 (0.050 - 0.065)	3.4 (2.8 - 4.0)	0.54 (0.47 - 0.61)
		All identified	0.21 (0.19 - 0.23)	0.057 (0.048 - 0.063)	3.8 (3.1 - 4.4)	0.59 (0.53 - 0.65)
		p-value	0.23	0.64	0.27	0.12

5.3 Discussion

Uncertainties associated with clonogenic assays using a Cs-137 irradiator and BAIRDA have been presented, quantifying the impact of each uncertainty. The uncertainties identified were categorized based on the type of outcome measured. Uncertainties associated with the experimental procedure and analysis of clonogenic assays affect the SF, while uncertainties

associated with the radiation sources affect the dose delivered. Based on this framework, the largest uncertainties were associated with SF measurements. For the Cs-137 irradiator, total dose-related uncertainties were within 2.2%, while the determination of SF led to several uncertainties that individually exceeded 2%. The number of colonies formed is affected by both human error (e.g. cell seeding density) and the biological response of the cells. Heterogeneities in the plated cells (e.g. phase in the cell cycle, genetic background) can lead to differences in dose response (55). As such, even perfect plating free of human error will be subject to SF uncertainty for both Cs-137 and BAIRDA irradiation experiments.

While the SF uncertainty is similar for both Cs-137 and BAIRDA, the dose uncertainties is larger for BAIRDA. This is mainly due to plate-base misalignment, which is the dominant term for BAIRDA in Table 5.4. Without it, BAIRDA's standard uncertainty (1.8%) would be comparable to that of the irradiator.

SF uncertainty assessments were conducted using clonogenic assays of a single cell line (SW756), which is a limitation of this study as some parameters (temperature changes, seeding time, etc.) are likely cell line-dependent. Exploration of these uncertainties using additional cell lines would improve the general applicability of the findings. For example, potential inter-cell line differences in attachment time would warrant a thorough investigation of each cell line used in an experiment, to ensure that variances in attachment times do not affect the experimental findings. Even mild hypothermia can impact cellular responses *in vitro*, such as the propensity for neuronal apoptosis, which may influence measured SF values after radiation (56,57,58). It is therefore important to consider cell line characteristics.

The calibration of the Cs-137 irradiator presents an additional limitation due to the method used to determine the ion chamber's N_k (utilizing the findings of Kang *et al*) (25). Kang *et al*'s estimated $TPR_{20,10}$ (0.46), used to estimate $s_{w,air}$ via Equation (5.3), is lower than values reported using Monte Carlo calculations (0.476 to 0.488). In addition, extrapolation was required for the mass energy absorption coefficient of the wall ($(\bar{\mu}_{en}/\rho)_{wall}$) as TRS 398 tables report $TPR_{20,10}$ values only to a minimum of 0.50. These differences motivate the need for an accurate determination of k_Q for PTW-30013 ion chambers for Cs-137.

5.3.1 Recommendations for Reducing Uncertainties

5.3.1.1 Clonogenic Assays

The largest uncertainties identified during clonogenic assays are associated with the experimental procedure and analysis. As such, efforts to minimize uncertainties in these steps will be most effective in reducing overall uncertainty.

The largest source of error was identified to be inter-operator subjectivity in colony counting, which is mainly due to differences in counting techniques used by operators. If this variability were eliminated, possible when using a single experienced operator for colony identification, the total SF uncertainty for the irradiator experiments can be reduced to 4.4%. As colony identification is a time-intensive process, it is important to consider the potential time investment required to minimize this specific uncertainty, especially in larger-scale studies. The trade-off between accuracy and precision should also be considered; the use of a single operator could reduce uncertainties but may not provide a more accurate measurement of the SF. Conversely, measurement by multiple experienced operators will provide an accurate measurement but will introduce inter-operator subjectivity.

Plating efficiency (number of colonies/number of cells seeded) also introduced an uncertainty of larger magnitude (3.4%). This may relate to both human error (e.g. calibration of the pipette) and the stochastic nature of cell suspension, cell adherence, and cell clonogenicity. Routine calibration of pipettes can accurately control the volume of medium dispensed and therefore the number of cells used for seeding (59). Batista *et al* have reported on refinements for accurate calibration of micropipettes to reduce uncertainties during volume measurements (60). The use of sensors has also been investigated as a method for preventing pipetting errors (61,62). It should be noted that SF is influenced by the variance in the number of cells seeded on different plates rather than the absolute number of cells seeded on each plate of the same experiment. Hence, ensuring a homogenous single cell “stock solution” by repeated resuspension during seeding is recommended.

Variance due to reference colony definition introduces an uncertainty of 2.7%. In this analysis, there were 8.1 ± 3.0% fewer colonies counted in each ROI when using a 100 cell reference colony instead of a 50 cell reference colony. Colony counting using the same plate with a 100 cell reference colony biases the counting procedure to faster growing colonies. As a single cell must grow more quickly to become identifiable as a colony when using a 100 cell reference (7 doublings in 12 days), compared to a 50 cell reference (6 doublings), slower growing colonies will potentially be affected more so by this uncertainty. This was not a significant factor in this study as the SFs for both reference colonies were similar. However, it could be significant for a cell line that has a substantial delay in proliferation after irradiation due to a longer cell cycle arrest/DNA repair time.

Uniformity in cell seeding, one of the smaller uncertainties associated with clonogenic assays (2.0%, only applied to BAIRDA irradiated plates), can occur because of variances in the seeding distribution between operators. Reynolds *et al* found significant non-uniformity in the distribution of cells when 12-well plates were seeded with human embryonic stem cells by different operators, suggesting the use of a uniform cell seeder to improve uniformity in cell seeding (63).

Though the intra-operator variance in colony counting was the smallest detected uncertainty in the SF measurements, factors such as fatigue following continuous counting may affect the counting procedure, whereby a cluster of cells that would not be identified as a colony at the start of a counting session may be classified as one towards the end. Furthermore, uncertainties associated with hypothermia of the cells and cell attachment times were found to be negligible in this study. The lack of a discernible effect for either may be due to the range of the times explored and the cell line utilized for quantification. It is therefore recommended to thoroughly characterize each cell line, for even less well studied uncertainty factors, to mitigate potential impact on the experimental measurements.

5.3.1.2 Cs-137 Irradiator

For the Cs-137 irradiator, plates placed in the center of the turntable experience minimal dose variance (≤1.2% using the configuration shown in Figure 5.10). The primary source of this

variation comes from plate elevation; plates closer to the lower capsule (7 cm above the floor of the irradiator) than where the ion chamber is usually placed during calibration (placed at the center of the cavity; 15 cm above the floor) did experience a higher dose rate. Routine characterization of an irradiator to determine dose rate and uniformity can improve the accuracy of planned dose delivery. Further reduction in dose variance can be achieved by positioning the tissue culture plates at ~15 cm above the center of the turntable, the height at which the calibration measurements were made.

The transit dose should be taken into consideration when plates are exposed to multiple irradiations. The increase in dose due to transit (1.4 cGy/transit) would be 1.6% for 6 Gy delivered in 7 fractions but would be 0.2% if the 6 Gy was delivered as a SAT. Therefore, experiments with a large number of fractions should consider the additional dose from the several transits.

5.3.1.3 BAIRDA

The greatest source of uncertainty for BAIRDA was due to plausible plate-to-base misalignments. These had the largest impact near the catheter because of the sharp dose falloff from the brachytherapy source path; the dose falloff from a single source position is close to the inverse-square law at larger distances. However, with precise alignment of the plate-to-base using visual markers, this uncertainty can be mitigated.

The base was printed with poly(lactic acid) (PLA) and included pockets of air. This resulted in its attenuation properties being in-between water and air. The dose calculated using the TG-186 formalism was on average 1.3% lower than the TG-43 dose measurement. This may be attributed to the reduced backscatter from the air above the media. As the distance from the plastic catheter increases, a greater amount of dose expected in the TG-43 calculation would be delivered from backscatter off water, decreasing the dose relative to the TG-43 calculation. Another potential rationale for the differences in calculated dose is the accuracy of ACE. When comparing I-125 dose calculations for Collaborative Ocular Melanoma Study (COMS) eye plaques, Morrison *et al* found ACE and Monte Carlo (MCNP6 v.1) disagreed significantly in the penumbral shadow of an ocular plaque (64). Some of the potential sources of uncertainty in their ACE calculations

(e.g. intra-voxel presence of materials, angular discretization) may limit the accuracy of ACE. Regardless, the use of a base with properties closer to water can reduce this effect by reducing the differences between the experimental configuration and the assumptions made in TG-43.

5.3.1.4 Summary of Recommendations

Table 5.8: Summary of the uncertainties identified in this study, the method used for their identification, and recommendations for reducing uncertainties in dose delivery and measurement of SF.

Source of Uncertainty	Method of Identification	Recommendations
Cell seeding density	Clonogenic assay	Use calibrated pipettes
Cell seeding uniformity	Clonogenic assay	Experiments performed by trained and experienced operators; Use of a cell seeder (63)
Cell attachment times	Clonogenic assay	Investigate prior to use for each cell line
Cell hypothermia during radiation	Clonogenic assay	Investigate prior to use for each cell line mimicking experimental methodology
Colony selection	Clonogenic assay	Investigate appropriate time for cell proliferation between irradiation and staining
Intra-operator subjectivity	Re-counting results (single operator)	Colony counting performed by trained and experienced operators
Inter-operator subjectivity	Re-counting results (multiple operators)	Separately compile results from each operator prior to averaging results
Source calibration	Cs-137: Ion chamber BAIRDA: Previous findings (39)	Calibration of sources prior to experiments
Transit dose	Cs-137: Ion chamber BAIRDA: Previous findings (41)	Inclusion of transit dose in dose prescription
Dose non-uniformity in the irradiator	Cs-137: Film measurement	Characterize irradiator prior to experiments
Dwell time rounding error	BAIRDA: Previous findings (40)	Account in dose calculation
Phantom-base alignment	BAIRDA: OcB calculations	Ensure accurate, repeatable alignment
Incorporation of dose heterogeneity	BAIRDA: OcB ACE calculations	Utilize a base with water-equivalent properties

5.3.2 Differences in Uncertainty between the Cs-137 Irradiator and BAIRDA

The development of BAIRDA as an alternative to well-established irradiator techniques encourages comparison between the two. Dose uncertainties identified for the irradiator were smaller than for BAIRDA. In particular, BAIRDA's dose uncertainties are large in the ROIs close to the catheter, with uncertainties from x-axis misalignment alone being greater than the total uncertainty for a Cs-137 irradiator. Nevertheless, this uncertainty is a worst-case scenario and can be mitigated by ensuring a precise alignment of the setup during experimentation. In

combination with large SF_{Ir} uncertainties in this region, BAIRDA's high dose ROIs exhibit larger uncertainties in dose. For example, the dose uncertainty in ROI_1 of Figure 4.5(c) (6 Gy) was 4.5% but was 2.1% for the ROI between the 0.81 and 0.67 Gy isodoses. If all of the alignment uncertainties were corrected and only dose uncertainties (in source strength and dwell time rounding) were included, BAIRDA's total dosimetric uncertainty would be 1.8%. As such, BAIRDA may have similar dose uncertainty to that of the Cs-137 irradiator. The relative advantages of the irradiator (e.g. lower uncertainty in dose) and BAIRDA (e.g. acquisition of experimental results on a single plate) must be weighed when selecting a method of radiation to suit the intended experimental application.

5.3.3 Impact on Radiobiological Parameters

Recalculation of α/β and $T_{1/2}$ with the additional uncertainties would be unlikely to affect trends in the experimentally identified radiobiological parameter values. For example, in Tables 5.5 to 5.7, α/β varied by a maximum of 0.5 Gy and $T_{1/2}$ by a maximum of 0.4 hr. In addition, the 95% confidence intervals did not change significantly, with a maximum change to the interval of 0.6 Gy for α/β and a general decrease in the $T_{1/2}$ 95% confidence interval. This limited impact of the additional uncertainties may be explained by the dominance of uncertainties created by the experimental triplicate. For SW756 cells, the average relative uncertainty in the SF measurements from experimental triplicates was 9.2 ± 3.9% and 16.6 ± 12.7% for the irradiator and BAIRDA, respectively. Application of the additional uncertainties identified in this Chapter will only increase the uncertainties modestly to 9.8% and 17.8%, respectively. Therefore, the addition of the identified uncertainties did not significantly affect the parameter fit.

The results of the irradiator and BAIRDA measurements also remain in agreement with each other, despite consideration of additional uncertainties, further validating the application of BAIRDA as a method for delivering radiation *in vitro*.

There are no statistically significant differences in the impact of the complete uncertainty analysis between SCC (Tables 5.5 and 5.6) and AC (Table 5.7) cell lines. For SCC, the average change in the best fit α/β and $T_{1/2}$ was 0.18 ± 0.2 Gy and -0.06 ± 0.2 hr compared to the scenario where only the experimental triplicate was considered. In comparison, the AC cell lines

experienced an average difference of 0.15 ± 0.2 Gy and -0.09 ± 0.2 hr. A similar trend was identified in the 95% confidence interval, where the addition of a full uncertainty analysis did not yield statistically significant differences in SCC (increase in the 95% confidence interval of 0.3 ± 0.3 Gy for α/β and decrease of 0.0 ± 0.3 hr for the $T_{1/2}$ on average compared to the scenario of including only the uncertainty of the experimental triplicate) and AC (decrease in the 95% confidence interval of -0.1 ± 0.3 Gy for α/β and decrease of -0.2 ± 0.4 hr for the $T_{1/2}$ on average), which suggests the identified uncertainties do not affect one cancer type uniquely.

5.4 Conclusion

Clonogenic assays are a standard technique for measuring cell radiosensitivity. The uncertainties associated with both surviving fraction measurement and dose were suspected to have a measurable influence on the experimental findings. Comprehensive quantification of uncertainties associated with the use of a Cs-137 Shepherd irradiator and Ir-192 brachytherapy afterloaders (using BAIRDA, both HDR and PDR) in clonogenic assay measurements was therefore performed. This study determined ±6.0% and ±6.3% uncertainty in SF measurements and up to ±2.2% and ±4.3% for dose measurements, using the Cs-137 irradiator and BAIRDA, respectively. These uncertainties introduced minimal effect on the calculation of radiobiological parameters (a maximum difference of 0.5 Gy and 0.4 hours in α/β and $T_{1/2}$, respectively for all cell lines) and did not yield statistically significant differences in the response of SCC and AC cell lines with the consideration of the complete uncertainty analysis. Regardless, a better understanding of uncertainties and their impact, in both clonogenic assays and the delivery of radiation, is encouraged to improve the accuracy and reproducibility of experimental analyses, and to provide greater confidence in experimental findings.

5.5 References

(1) Azmi AS, Aboukameel A, Banerjee S, Wang Z, Mohammad M, Wu J, *et al*. MDM2 inhibitor MI-319 in combination with cisplatin is an effective treatment for pancreatic cancer independent of p53 function. *Eur J Cancer* 2010;46(6):1122-1131.

(2) Mirzayans R, Andrais B, Murray D. Viability assessment following anticancer treatment requires single-cell visualization. *Cancers (Basel)* 2018;10(8):255.

(3) Matsui T, Nuryadi E, Komatsu, S, Hirota Y, Shibata A, Oike T, *et al*. Robustness of clonogenic assays as a biomarker for cancer cell radiotherapy. *Int J Mol Sci* 2019;20(17);4148.

(4) International commission on radiation units & measurements. Report 89: Prescribing, recording, and reporting brachytherapy for cancer of the cervix. *J of the ICRU* 2013; 13:1-258.

(5) Joiner M, van der Kogel AJ. Basic clinical radiobiology. 4th ed. Boca Raton: CRC Press/Taylor & Francis Group; 2009.

(6) Kellerer AM, Rossi HH. RBE and the primary mechanism of radiation action. *Radiat Res* 1971;47(1):15-34.

(7) Dale RG, Huczkowski J, Trott KR. Possible dose rate dependence of recovery kinetics as deduced from a preliminary analysis of the effects of fractionated irradiations at varying dose rates. *Br J Radiol* 1988;61(722):153-157.

(8) Kelland LR, Steel GG. Differences in radiation response among human cervix carcinoma cell lines. *Radiother Oncol* 1988;13(2):225-232.

(9) Tang J, Inoue T, Matsumura S, Fukushima S, Koizumi M, Ozeki S, *et al*. Differences in repair of potentially lethal damage in Chinese hamster ovary cells exposed to 65 MeV proton beams and (137)Cesium gamma-rays. *Oncol Rep* 1997;4(2):407-412.

(10) Kamen, J, Hsu WY, Boswell B, Hill C. Successful migration from radioactive irradiators to x-ray irradiators in one of the largest medical centers in the US. *Health Phys* 2019;117(5):558-570.

(11) van Rijn J, van den Berg J, Kipp JB, Schamhart DH, van Wijk R. Effect of hypothermia on cell kinetics and response to hyperthermia and x rays. *Radiat Res* 1985;101(2):292-305.

(12) Gupta N, Lamborn K, Deen DF. A statistical approach for analyzing clonogenic survival data. *Radiat Res* 1996;145(5):636-640.

(13) Franken NAP, Rodermond HM, Stap J, Haveman J, van Bree C. Clonogenic assay of cells in vitro. *Nat Protoc* 2006;1(5):2315-2319.

(14) Batista E, Alberini M. Results of the supplementary comparison (bilateral) of a fixed volume micropipette of 50 µl and a variable volume micropipette of 1000 µl. *Metrologia* 2018;55:07009-07009.

(15) Villalona GA, Udelsman B, Duncan DR, McGillicuddy E, Sawh-Martinez RF, Hibino N, *et al*. Cell-seeding techniques in vascular tissue engineering. *Tissue Eng Part B Rev* 2010;16(3):341-350.

(16) Twentyman PR. Timing of assays: An important consideration in the determination of clonogenic cell survival both in vitro and in vivo. *Int J Radiat Oncol Biol Phys* 1979;5(8):1213-1220.

(17) Okada S, Ono K, Hamada N, Inada T, Kubota N. A low-pH culture condition enhances the radiosensitizing effect of wortmannin. *Int J Radiat Oncol Biol Phys* 2001;49(4):1149-1156.

(18) Choi EK, Terai K, Ji IM, Kook YH, Park KH, Oh ET *et al*. Upregulation of NAD(P)H:quinone oxidoreductase by radiation potentiates the effect of bioreductive β-lapachone on cancer cells. *Neoplasia* 2007;9(8):634-642.

(19) Kim BM, Won J, Maeng KA, Han YS, Yun YS, Hong SH. Nimesulide, a selective COX-2 inhibitor, acts synergistically with ionizing radiation against A549 human lung cancer cells through the activation of caspase-8 and caspase-3. *Int J Oncol* 2009;34(5):1467-1473.

(20) Rieder CL, Cole RW. Cold-shock and the mammalian cell cycle. *Cell Cycle* 2002;1(3):169-175.

(21) Vergara M, Becerra S, Berrios J, Osses N, Reyes J, Rodriguez-Moyá M, *et al*. Differential effect of culture temperature and specific growth rate on CHO cell behavior in chemostat culture. *PLOS One* 2014;9(4):e93865.

(22) Puck TT, Markus PI. Action of x-rays on mammalian cells. *J Exp Med* 1956; 103(5):653-666.

(23) Yohem KH, Bregman MD, Meysken Jr FL. Effect of tumor colony definition on ionizing radiation survival curves of melanoma-colony forming cells. *Int J Radiat Oncol Biol Phys* 1987;13(11):1725-1733.

(24) Militello C, Rundo L, Minafra L, Cammarata FP, Calvaruso M, Conti V, *et al*. MF2C3: Multi-feature fuzzy clustering to enhance cell colony detection in automated clonogenic assay evaluation. *Symmetry* 2020;12(5):773.

(25) Kang SK, Rhee DJ, Kang YR, Kim JK, Jeong DH. Determination of TRS-398 quality factors for Cs-137 gamma rays in reference dosimetry. *Prog Med Phys* 2014;25(3):123-127.

(26) Absorbed dose determination in external beam radiotherapy: An international code of practice for dosimetry based on standards of absorbed dose to water. Vienna: International Atomic Energy Agency; 2000.

(27) Absorbed dose determination in photons and electron beams: An international code of practice. Vienna: International Atomic Energy Agency; 1997.

(28) McEwen M, DeWerd L, Ibbott G, Followill D, Rogers DWO, Seltzer S, *et al*. Addendum to the AAPM's TG-51 protocol for clinical reference dosimetry of high-energy photon beams. *Med Phys* 2014;41(4):041501.

(29) Brady SL, Toncheva G, Dewhirst MW, Yoshizumi TT. Characterization of a 137Cs irradiator from a new perspective with modern dosimetric tools. *Health Phys* 2009;97(3):195-205.

(30) Lewis D, Micke A, Yu X, Chan MF. An efficient protocol for radiochromic film dosimetry combining calibration and measurement in a single scan. *Med Phys* 2012; 39(10):6339–6350.

(31) Niroomand-Rad A, Blackwell CR, Coursey BM, Gall KP, Galvin JM, McLaughlin WL. Radiochromic film dosimetry: Recommendations of AAPM Radiation Therapy Committee Task Group 55. American Association of Physicists in Medicine. *Med Phys* 1998;25(11):2093–2115.

(32) Niroomand-Rad A, Chiu-Tsao S, Grams MP, Lewis DF, Soares CG, Van Battum LJ, *et al*. Report of AAPM Task Group 235 Radiochromic film dosimetry: An update to TG-55. *Med Phys* 2020;47(12):5986-6025.

(33) Morrison H, Menon G, Sloboda RS. Radiochromic film calibration for low-energy seed brachytherapy dose measurement. *Med Phys* 2014;41(7):072101.

(34) Mizuno H, Sumida I, Tanaka A, Ogawa K. Comparing homogeneity between Gafchromic film EBT2 and EBT3. *Med Phys* 2014;41(6):239.

(35) Micke A, Lewis DF, Yu X. Multichannel film dosimetry with nonuniformity correction. *Med Phys* 2011;38(5):2523-2534.

(36) Dos Santos M, Paget V, Kacem MB, Trompier F, Benadjaoud MA, Francois A, *et al*. Importance of dosimetry protocol for cell irradiation on a low x-rays facility and consequences for the biological response. *Int J Radiat Biol* 2018; 94(6):597-606.

(37) Bouchard H, Lacroix F, Beaudoin G, Carrier JF, Kawrakow I. On the characterization and uncertainty analysis of radiochromic film dosimetry. *Med Phys* 2009;36(6):1931-1946.

(38) Strohmaier S, Zwierzchowski G. Comparison of 60Co and 192I sources in HDR brachytherapy. *J Contemp Brachytherapy* 2011;3(4):199-208.

(39) DeWerd LA, Ibbott GS, Meigooni AS, Mitch MG, Rivard MJ, Stump KE, *et al*. A dosimetric uncertainty analysis for photon-emitting brachytherapy sources: Report of AAPM Task Group No. 138 and GEC-ESTRO. *Med Phys* 2011;38(2):782-801.

(40) Kirisits C, Rivard MJ, Baltas D, Ballester F, De Brabandere M, van der Laarse R, *et al*. Review of clinical brachytherapy uncertainties: Analysis guidelines of GEC-ESTRO and the AAPM. *Radiother Oncol* 2014;110(1):199-212.

(41) Menon GV, Carlone MC, Sloboda RS. Transit dose contributions to intracavitary and interstitial PDR brachytherapy treatments. *Phys Med Biol* 2008;53(13):3447-3462.

(42) van der Laarse R, Niatsetki Y, Henning J, van der Meer E. Flexitron® and microSelectron® HDR/PDR afterloaders' transit time and dose. Stockholm, Sweden: Elekta AB;2018 12 p. Report No.: 888.00645 MKT_1.0

(43) Nath R, Anderson LL, Luxton G, Weaver KA, Williamson JF, Meigooni AS. Dosimetry of interstitial brachytherapy sources: Recommendations of the AAPM Radiation Therapy Committee Task Group No. 43. *Med Phys* 1995:22(2),209–234.

(44) Rivard MJ, Coursey BM, DeWerd LA, Hanson WF, Huq S, Ibbott GS, *et al*. Update of AAPM Task Group No. 43 Report: A revised AAPM protocol for brachytherapy dose calculations. *Med Phys* 2004;31(3):633-674.

(45) White SA, Landry G, Fonseca GP, Holt R, Rusch T, Beaulieu L, *et al*. Comparison of TG-43 and TG-186 in breast irradiation using a low energy electronic brachytherapy source. *Med Phys* 2014;41(6):061701.

(46) Rivard MJ, Venselaar JLM, Beaulieu L. The evolution of brachytherapy treatment planning. *Med Phys* 2009;36(6):2136-2153.

(47) Beaulieu L, Tedgren AC, Carrier J-F, Davis SD, Mourtada F, Rivard MJ, *et al*. Report of the Task Group 186 on model-based dose calculation methods in brachytherapy beyond the TG-43 formalism: Current status and recommendations for clinical implementation. *Med Phys* 2012;39(10):6208-6236.

(48) Hofbauer J, Kirisits C, Resch A, Xu Y, Sturdza A, Pötter R, *et al*. Impact of heterogeneity-corrected dose calculation using a grid-based Boltzmann solver on breast and cervix cancer brachytherapy. *J Contemp Brachytherapy* 2016;8(2):143-149.

(49) Abe K, Kadoya N, Sato S, Hashimoto S, Nakajima Y, Miyasaka Y, *et al*. Impact of a commercially available model-based dose calculation algorithm on treatment planning of high-dose-rate brachytherapy in patients with cervical cancer. *J Radiat Res* 2018;59(2):198-206.

(50) Sande EPS, Martinsen ACT, Hole EO, Olerud HM. Interphantom and interscanner variations for Houndsfield units-establishment of reference values for HU in a commercial QA phantom. *Phys Med Biol* 2010;55(17):5123-5135.

(51) Joint committee for guides in metrology. Evaluation of measurement data - Guide to the expression of uncertainty in measurement. 2008.

(52) Chapman JD, Nahum AE. Radiotherapy treatment planning. Baton Rouge: CRC Press; 2016.

(53) Chow B, Nanda K, Warkentin B, Huang F, Gamper AM, Menon G. In-vitro determination of radiobiological parameter values used in cervical cancer brachytherapy. *Radiother Oncol* 2020;152(1):S1093-S1094.

(54) Gamper AM, Rofougaran R, Watkins SC, Greenberger JS, Beumer JH, Bakkenist CJ. ATR kinase activation in G1 phase facilitates the repair of ionizing radiation-induced DNA damage. *Nucleic Acids Res* 2013;41(22):10334-10344.

(55) Pawlick TM, Keyomarsi K. Role of cell cycle in mediating sensitivity to radiotherapy. *Int J Radiat Oncol Biol Phys* 2004;59(4):928-942.

(56) Popovic R, Liniger R, Bickler PE. Anesthetics and mild hypothermia similarly prevent hippocampal neuron death in an in vitro model of cerebral ischemia. *Anesthesiology* 2000;92(5):1343-1349.

(57) Xu L, Yenari MA, Steinberg GK, Giffard RG. Mild hypothermia reduces apoptosis of mouse neurons in vitro early in the cascade. *J Cereb Blood Flow Metab* 2002;22(1):21-28.

(58) Tanaka T, Wakamatsu T, Daijo H, Oda S, Kai S, Adachi T, *et al*. Persisting mild hypothermia suppresses hypoxia-inducible factor-1α protein synthesis and hypoxia-inducible factor-1-mediated gene expression. *Am J Physiol Regul Integr Comp Physiol* 2010;298(3):R661-R671.

(59) Batista E, Almeida N, Filipe E. A study of factors that influence micropipette calibrations. *NCSLI Measure 2015*;10(1):60-66.

(60) Batista E, Pinto L, Filipe E, van der Veen AMH. Calibration of micropipettes: Test methods and uncertainty analysis. *Measurement* 2007;40:338-342.

(61) Lee D, Chang L. Development of the pipetting error sensor. *Sensor Actuat B-Chem* 2006;119(1):150-158.

(62) Kyle L, Daniel F, Ye H, Chetkovich DM. A novel method for reducing human pipetting errors. *J Med Lab Diagn* 2015;6(6):36-40.

(63) Reynolds PM, Rasmussen CH, Hansson M, Dufva M, Riehle MO, Gadegaard N. Controlling fluid flow to improve cell seeding uniformity. *PLOS One* 2018;13(11):e0207211.

(64) Morrison H, Menon G, Larocque MP, van Veelen B, Niatsetski Y, Weis E, *et al*. Initial evaluation of Advanced Collapsed cone Engine dose calculations in water medium for I-125 seeds and COMS eye plaques. *Med Phys* 2018;45(3):1276-1286.

CHAPTER 6
SUMMARY, CONCLUSIONS, AND FUTURE WORK

6.1 Summary

Cervical cancer remains the fourth most common cancer worldwide (1). However, the prevalence of cervical cancer is significantly lower in high income countries (HIC) compared to low and middle income countries (LMIC) due to vaccine programs and routine screening (2). This has resulted in an 18-fold increase in mortality from cervical cancer in LMIC than in HIC (2). In Canada, there has been a decrease in the annual percent change in age-standardized incidence rates of cervical cancer (3). Further vaccination and screening are currently planned by institutes like the Canadian Partnership Against Cancer such that cervical cancer is eliminated in Canada by 2040 (4). Despite these efforts, there are still currently about 1,350 cervical cancer patients being diagnosed annually (5). For locally advanced cervical cancer, the standard of care is concurrent chemotherapy and EBRT with a BT boost (6,7). The use of BT facilitates the delivery of highly localized boost doses to the tumor and provides higher patient survival rates compared to alternative treatments (8,9).

The dose prescription for the combined EBRT and BT boost dose is commonly given in units of EQD2, which requires assumptions about the irradiated tissue's (tumor and OAR) α/β ratio and $T_{1/2}$ to compare different treatment schedules (e.g. HDR vs PDR BT). The assumed radiobiological parameter values have been selected without definitive supporting evidence beyond a lack of contradicting clinical evidence (10). However, a wide range of potential parameter values have been previously reported in the literature (11). The use of radiobiological dose prescriptions thus demands a fuller understanding of the underlying radiobiological model and its current limitations. Deviations in either the α/β ratio or $T_{1/2}$ from their conventionally used values can affect assumed equivalencies in treatment and could result in variances in the radiobiological dose delivered to tumor and OARs (and therefore, may affect clinical outcome). Therefore, investigating the potential uncertainties in the dose delivered, through large-scale outcome studies, *in vitro* cell experiments, or *in vivo* animal models, may help clinical teams design superior radiation treatment regimens that can improve outcomes in locally advanced cervical cancer (LACC) patients.

There have been no previously published compilations of reported radiobiological parameters for cervical cancer and the surrounding normal tissue. Therefore, an exhaustive search was completed for these parameter values. This included values reported for α/β, $T_{1/2}$, and those related to post-irradiation tumor proliferation ($T_{kickoff}$, T_{pot}, and α of tumor cells). As shown in Tables 3.1 to 3.5, a wide range of parameter values have been identified in previous studies using different methods of estimation, including *in vitro* studies and analysis of patient outcomes. For example, the α/β ratio and $T_{1/2}$ for cervical cancer have been reported to range between 5.9 to 21 Gy and 0.15 to 5.7 hours, respectively (11). There is also variation in values for the surrounding normal tissues (e.g. rectum, bladder, sigmoid colon): 2.5 to 5.4 Gy for α/β and 0.20 to 2.5 hours for $T_{1/2}$. While limited research has been conducted to determine $T_{kickoff}$, there is significant variance in the reported T_{pot} (4 to 42.1 days) and α (0.06 to 0.74 Gy^{-1}) (12,13,14,15).

The large variances in reported parameters, should they be representative of *in vivo* tumor and OAR values, may affect the assumed equivalency of treatments planned using conventional radiobiological parameter values. The implications in the reported parameter values for theoretical radiobiological dose calculations was presented in Chapter 3. Hypothetical treatments were generated from EBRT (25 fractions of 1.8 Gy each) followed by different BT boost options that are equivalent when assuming conventional tumor α/β and $T_{1/2}$ values (10 Gy and 1.5 hours, respectively) and deliver 90 Gy EQD2 (meeting the EMBRACE II targets for dose to the HR-CTV D90) (16). Variations in α/β or $T_{1/2}$ alone, within the range reported in Chapter 3, could result in variances between conventionally equivalent HDR and PDR BT boosts of up to 10% or 13%, respectively. Varying additional parameters in PDR BT that characterize the pulse delivery (number of pulses, duration, and frequency of pulses) was investigated for their individual impact on the radiobiological dose delivered by (*cf.* parameter q in Equation (3.1)). Of all the parameters, only the interval between pulses had a significant effect. However, radiation is traditionally delivered hourly during PDR (17). Therefore, under this assumption, the crucial factor that affects the equivalence of HDR and PDR BT treatments is the difference between the assumed and actual radiobiological parameter values.

While not generally included as part of radiobiological dose calculations, the impact of proliferation parameters is a potentially important consideration for cervical cancer. The range of

reported proliferation parameters was considered by calculating the effective loss of radiobiological dose (ΔD) after extending a treatment by 15 days (from an overall treatment time of 40 days to 55 days). ΔD was found to vary from 3.5 Gy EQD2 to 10.8 Gy EQD2 depending on the assumed values of T_{pot} and α. However, ΔD was not affected by the reported range of $T_{kickoff}$. Therefore, variances in overall treatment time, T_{pot}, and α may affect the radiobiological dose delivered while, for the range of overall treatment times investigated, $T_{kickoff}$ will not.

The potential impact of the current range of reported radiobiological parameter values highlights the necessity for further investigation of the clinical radiobiological parameters to better understand pitfalls in the current approach to dose calculation. Such analysis could make treatment planning more accurate and improve cervical cancer patient outcomes. Previous studies determining radiobiological parameter values *in vitro* vary significantly in the specifics of radiation delivery (e.g. photon energy, dose rate, radiation schedule), which raises concerns about how well these reported parameter values are representative of dose responses to brachytherapy. Therefore, while irradiators are traditionally utilized for estimating radiobiological parameters *in vitro*, experimental investigations with clinically relevant sources and schedules were deemed necessary. A novel radiation delivery apparatus (brachytherapy afterloader *in vitro* radiation delivery apparatus; BAIRDA) was developed to irradiate tissue culture plates *in vitro* while utilizing clinically relevant photon energies and radiation schedules.

BAIRDA was used to estimate the radiobiological parameters of cervical cancer cells through clonogenic assays. A panel of seven cervical cancer cell lines (4 SCC and 3 AC), selected to provide a representative sample of the two most common cervical cancer cell histologies, were irradiated using both HDR (delivering a single acute fraction of radiation) and PDR BT (hourly pulses of radiation) sources. The dose delivered using the different radiation schedules was calculated using the OcB treatment planning system. The accuracy of the OcB calculated dose was verified by comparing it to the dose estimated by exposing Gafchromic EBT3 films using the BAIRDA setup. The OcB ACE calculated and film measured doses agreed to within 3% (maximum difference). By dividing irradiated tissue culture plates into multiple ROIs, the resulting SF for a range of doses can be measured from the clonogenic assays. Analysis of the plates irradiated in a single acute fraction of radiation yielded similar α/β ratios for the SCC and

AC cell lines (p-value = 0.07), in the range of 3.8 to 6.3 Gy, which was significantly smaller than the conventional assumption (p-value ≈ 0.0004 and 0.006, respectively). However, the $T_{1/2}$ of SCC (2.8 to 4.8 hours) was significantly larger than for AC (0.59 to 1.25 hours) (p-value ≈ 0.01). The findings using BAIRDA were validated by comparing the α/β and $T_{1/2}$ results to comparable experiments performed with a traditional Cs-137 irradiator. No significant differences were observed between the two, thereby providing support for the BAIRDA-determined findings.

In addition, a comparison of the $T_{1/2}$ determined by hourly and bihourly pulsed fractions of radiation was conducted to explore the assumption of monoexponential repair. For both SCC and AC cell lines, the $T_{1/2}$ values were found to be similar for the hourly and bihourly schedules (p-value ≥0.07), providing no evidence of non-monoexponential repair.

Several uncertainties were identified for *in vitro* studies using either the traditional irradiator or BAIRDA experiments. While the dose uncertainty is typically not considered and surviving fraction uncertainty limited to variances in the experimental triplicate, it was determined that these additional uncertainty factors could affect the experimental findings presented in Chapter 4. A comprehensive analysis was therefore performed to quantify these uncertainties to (a) compare the SF and dose uncertainties for BAIRDA against the established irradiator method and (b) quantify the uncertainties against the variance in measured SF from an experimental triplicate. To accommodate both analyses, uncertainties were divided based on the measurement they affected: SF, dose delivered by BAIRDA, or dose delivered by the irradiator.

Uncertainties that affected the measurement of SF included cell seeding density, cell seeding uniformity, cell attachment times, colony definition, cell hypothermia during radiation, and subjectivity in colony counting. Except for the uncertainty in colony counting subjectivity (done by recounting the assay plates), all other uncertainties were determined through additional clonogenic assays. A relative uncorrelated uncertainty of 6.3% and 6.0% (k = 1) was determined for BAIRDA and Cs-137 experiments, respectively, in addition to the uncertainty in an experimental triplicate (measured using only the standard deviation in the number of colonies identified on the control plate and irradiated plate/ROI, as shown in Equation (5.9)). For both radiation sources, the dominant uncertainty was the variance in colony counting between

different operators (4.1%). BAIRDA and Cs-137 experiments have similar overall SF uncertainty since, aside from cell seeding uniformity, the other SF uncertainty components are identical.

BAIRDA dose uncertainties result from afterloader source calibration and positioning uncertainties, plate-base misalignments during experimental setup, and exclusion of material heterogeneities during dose calculation. As uncertainties associated with afterloaders, such as source calibration, rounding error in the dwell time, and transit dose delivered, are of great importance in clinical treatments, they have been previously studied and reported in the literature. Of the BAIRDA related dose uncertainties identified in this study, the largest was associated with potential plate-base misalignment. Assuming the worst-case scenario, analysis conducted in OcB showed that there could be a relative dose uncertainty of up to 3.0% due to misalignments in the x-axis and plate rotation. However, this uncertainty can be eliminated by accurately aligning the tissue culture plate with the base. Comparisons were also made in OcB using TG-43 and ACE to quantify the effects of material heterogeneity in the dose calculation. Overall, the dose was reduced by an average of 1.3% (range of 0.6% at points close to the catheter to 2.1% at points 2 to 3 cm away from the catheter), which may be attributed to reduced backscatter from the air above the media. OcB dose calculations for BAIRDA-irradiated plates have a total dose uncertainty of 2.1% to 4.3%, which is the largest for ROIs closest to the catheter.

A dose uncertainty analysis was also performed for the Cs-137 irradiator and was divided into two categories: dose delivered at the center, and dose away from the center of the irradiator. The dose rate at the center of the irradiator was measured using a PTW 30013 ion chamber and yielded a dose rate 0.6% lower than was expected using the original calibration. The non-uniformity of the dose profile inside the irradiator was quantified via exposure of EBT3 Gafchromic films placed across the cavity at different elevations above the turntable. It was observed that points towards the outside of the irradiator's turntable received doses 10% higher than that at the center of the irradiator. However, when compared against BAIRDA, the Cs-137 irradiator had lower overall dose uncertainty (2.1% to 2.2%).

The α/β and $T_{1/2}$ values calculated with the uncertainties identified in Chapter 5 and those estimated with only the uncertainty related to experimental triplicates, were comparable (difference of 0.5 Gy and 0.5 hours, respectively). Therefore, the uncertainty analysis in Chapter 5 did not strongly affect the findings of Chapter 4. The results of this analysis indicate that the dominant uncertainty is the variance in the measurement of SF within an experimental triplicate.

Should the results from this thesis hold clinically, the reported parameter values present theoretical advantages of both HDR and PDR BT: HDR BT will deliver a higher radiobiological dose than the conventionally equivalent PDR BT for AC and vice versa for SCC. This may allow for delivery of higher radiobiological doses to AC and SCC through the selection of HDR and PDR BT, respectively. Hence, these findings highlight the possibility of personalizing BT boost based on cancer histologic type to improve patient outcome through dose escalation.

6.2 Future Work

The findings of this thesis present a comprehensive effort to better identify tumor radiobiological parameter values for cervical cancer BT. Further research building upon the conclusions of this thesis is needed for translation allowing improved cervical cancer BT treatments.

The experimental findings were determined using only 4 SCC and 3 AC cell lines. For each cervical cancer histology, this may provide limited statistical strength to the findings when transferring the results to a clinical environment. Therefore, increasing the number of cervical cancer cell lines investigated with BAIRDA would provide greater confidence in the identified parameters. However, at present, the availability of AC cell lines is quite limited compared to SCC cell lines. After a thorough search through multiple international cell banks, only three AC cell lines (HeLa, JHUCS-3, and SiSo) were available. The vast majority of AC cells currently available are derivatives of HeLa and therefore do not characterize the original tumor as their biological properties have been adapted (e.g. HeLa S3 cells can effectively grow colonies in suspension). The use of HeLa cells is also subject to deviation from the original tumor due to the cell line's genomic instability. In a study of 4 HeLa cell lines procured from different laboratories, Frattini *et al* showed that an indeterminate number of different HeLa cell lines may exist due to large genomic differences observed between each of the cell lines characterized in

their study (18). Hence, there is a need to establish more AC cell lines to allow for a more thorough investigation of AC cervical cancer radiosensitivity. An increase in the number of cell lines investigated would provide support to the Welch t-tests, which assume a normal distribution for the α/β ratio and $T_{1/2}$ values. While such a distribution for radiobiological parameters is commonly assumed, there is no direct supporting evidence for this assumption (19,20).

Currently, few studies have investigated radiobiological parameter values for the OARs, such as bladder, rectum, bowel, and sigmoid, relevant to cervical cancer treatments. An α/β of 3 Gy and $T_{1/2}$ of 1.5 hours have been conventionally used for these tissues. Similar to differences in tumor dose resulting from deviations from the conventional radiobiological parameters, there could also be variances in the dose delivered to OARs. For example, the variance in α/β for OARs (2.5 to 5 Gy) may result in differences of up to 5% in the dose delivered by an HDR and an (assumed) equivalent PDR BT boost (Table 3.7). Therefore, further investigation of normal tissue response to radiation is warranted. A similar configuration using BAIRDA with the same methodology from Chapter 4 could be employed for such measurements.

The uncertainty of the dose delivered by BAIRDA (2.1 to 4.3%) was much larger than that of the irradiator (0.7% to 0.9%). However, further refinements to BAIRDA would reduce the dose uncertainty considerably. For example, the diameter of the groove that fits the tissue culture plate to BAIRDA's base is approximately 0.5 mm larger than the outer diameter of the tissue culture plate (and results in the ±0.25 mm uncertainty in the x-axis that was quantified in Chapter 5). The dose uncertainty could thus be reduced by using a base with a smaller groove. If all potential plate-base misalignments were eliminated, the dose uncertainty from BAIRDA (1.8%) would be comparable to that of the irradiator.

While OcB ACE was used to more accurately calculate dose delivered to the tissue culture plate, accuracy of the simpler TG-43 calculation would be improved by using a different material to make the base. The current PLA base has hollow areas inside, with PLA columns to improve structural integrity. The use of a water-equivalent material for the base would result in a more accurate TG-43 dose calculation (within 0.5% of TG-186).

The experiments in Chapter 4 have been conducted under ideal conditions, providing the cells with ample nutrients, room for growth, and an oxygenated environment. However, cervical cancers frequently develop hypoxic regions and standard treatments include chemotherapy for radiosensitization, neither of which are considered in the procedure discussed in Chapter 4 (21,22). Hypoxic conditions will result in an effective lower radiosensitivity: Pajonk *et al* measured an SF of 0.10 for SiHa cells *in vitro* at 5.26 Gy under oxic conditions and 8.5 Gy under hypoxic conditions (23). Conversely, the introduction of a radiosensitizer (e.g. cisplatin) will induce heightened radiosensitivity. Słonina *et al* observed decreased survival of CaSki and SiHa cells *in vitro* when treated with cisplatin and a low dose fractionated schedule (4 fractions of 0.125 Gy/fraction) (24). Exploration of the cell response to hypoxic conditions and radiosensitizers would better characterize the clinical environment experienced by cells during BT boosts. This may be approached through a modified BAIRDA configuration (e.g. one that allows tissue culture plates to be kept hypoxic during the radiation delivery).

Translation of *in vitro* findings to the clinical setting will require further research as it is infrequent for findings in a laboratory setting to translate successfully to clinical trials (25). The use of animal model studies could act as the next step to better replicate the multiple complex mechanisms that affect tumor control. For example, Nakano *et al* reported that infiltration of Langerhans cells was a predictor of an increase in the 5-year survival after radiation therapy for both stage III SCC (78% with infiltration vs 60% without) and AC (49% vs 25%) patients (26). Based on the result, they suggested that Langerhans cells may induce T-cell-mediated antitumor response and improve patient outcome (26). Such a response is not replicated in these experiments and would require animal models. Another possibility for further exploration is the analysis of patient outcomes with respect to the radiobiological parameters identified in this research. The results from Chapter 4 suggest that, for SCC, the tumor cells receiving PDR BT will experience a higher dose (and will therefore have a higher rate of tumor control) than those which received conventionally equivalent HDR BT. Comparative analyses are being performed to investigate if the conventionally recommended α/β and $T_{1/2}$ values for tumor and normal tissue fit with clinical outcomes as observed in the EMBRACE study (K. Tanderup and C. Kirisits, personal communication). Conclusions could then be drawn by relating the *in vivo* findings to the outcomes studies.

6.3 References

(1) Sung H, Ferlay J, Siegel RL, *et al*. Global cancer statistics 2020: GLOBOCAN estimates of incidence and mortality worldwide for 36 cancers in 185 countries. *CA Cancer J Clin* 2021;71(3):209-249.

(2) Vu M, Yu J, Awolude OA, Chuang L. Cervical cancer worldwide. *Curr Probl Cancer* 2018;42(5):457-465.

(3) Canadian Cancer Statistics. Canadian Cancer Society; 2021.

(4) Canadian Partnership against Cancer. Action Plan for the Elimination of Cervical Cancer in Canada 2020–2030. Available online: https://s22438.pcdn.co/wp-content/uploads/2020/11/Elimination-cervical-cancer-action-plan-EN.pdf (accessed on 28 Nov 2021).

(5) Brenner DR, Weir HK, Demers AA, Ellison LF, Louzado C, Shaw A, et al. Projected estimates of cancer in Canada in 2020. *CMAJ* 2020;192(9):E199-E205.

(6) International commission on radiation units & measurements. Report 89: Prescribing, recording, and reporting brachytherapy for cancer of the cervix. *J of the ICRU* 2013; 13:1-258.

(7) Cibula D, Pötter R, Planchamp F, Avall-Lundqvist E, Fischerova D, Haie-Meder C, *et al*. The European Society of Gynaecological Oncology/European Society for Radiotherapy and Oncology/European Society of Pathology guidelines for the management of patients with cervical cancer. *Virchows Arch* 2018;472(6):919-936.

(8) Georg D, Kirisits C, Hillbrand M, *et al*. Image-guided radiotherapy for cervix cancer: High-tech external beam therapy versus high-tech brachytherapy. *Int J Radiat Oncol Biol Phys* 2008;71:1272-1278

(9) Han K, Milosevic M, Fyles A, *et al.* Trends in the Utilization of Brachytherapy in Cervical Cancer in the United States. *Int J Radiat Oncol Biol Phys* 2013;87:111-119.

(10) Fowler J. Dose reduction factors when increasing dose rate in LDR or MDR brachytherapy of carcinoma of the cervix. *Radiother Oncol* 1997;45:49-54.

(11) Chow B, Nanda K, Warkentin B, Huang F, Gamper AM, Menon G. In-vitro determination of radiobiological parameter values used in cervical cancer brachytherapy. Radiother Oncol 2020;152(1):S1093-S1094.

(12) Roberts SA, Hendry JH, Swindell R, Wilkinson JM, Hunter RD. Compensation for changes in dose-rate in radical low-dose-rate brachytherapy: A radiobiological analysis of a randomised clinical trial. *Radiother Oncol* 2004;70(1):63-74.

(13) Bolger BS, Symonds RP, Stanton PD, MacLean AB, Burnett R, Kelly P, *et al.* Prediction of radiotherapy response of cervical carcinoma through measurement of proliferation rate. *Br J Cancer* 1996;74(8):1223-1226.

(14) Tsang RW, Fyles AW, Kirkbride P, Levin W, Manchul LA, Milosevic MF, *et al*. Proliferation measurements with flow cytometry Tpot in cancer of the uterine cervix: Correlation between two laboratories and preliminary clinical results. *Int J Radiat Oncol Biol Phys* 1995;32(5):1319-1329.

(15) Brenner DJ, Hall EJ. Conditions for the equivalence of continuous to pulsed low dose rate brachytherapy. *Int J Radiat Oncol Biol Phys* 1991;20(1):181-190.

(16) Pötter R, Tanderup K, Kirisits C, de Leeuw A, Kirchheiner K, Nout R, *et al*. The EMBRACE II study: The outcome and prospect of two decades of evolution within the GEC-ESTRO GYN working group and the EMBRACE studies. *Clin Transl Radiat Oncol* 2018;9:48-60.

(17) Banerjee R, Kamrava M. Brachytherapy in the treatment of cervical cancer: a review. *Int J Women's Health* 2014;6:555-564.

(18) Frattini A, Fabbri M, Valli R, De Paoli E, Montalbano G, Gribaldo L, *et al*. High variability of genomic instability and gene expression profiling in different HeLa clones. *Sci Rep* 2015;5;15377.

(19) Jones B, Dale RG. Mathematical models of tumour and normal tissue response. *Acta Oncol* 1999;38(7);883-893.

(20) Barazzuol, Burnet NG, Jena R, Jones B, Jefferies SJ, Kirkby NF. A mathematical model of brain tumour response to radiotherapy and chemotherapy considering radiobiological aspects. *J Theor Biol* 2010;262(3):553-565.

(21) Rofstad E, Sundfor K, Lyng H, *et al*. Hypoxia-induced treatment failure in advanced squamous cell carcinoma of the uterine cervix is primarily due to hypoxia-induced radiation resistance rather than hypoxia-induced metastasis. *Br J Cancer* 2000;83:354-359.

(22) Grimes D, Partridge M. A mechanistic investigation of the oxygen fixation hypothesis and oxygen enhancement ratio. *Biomed Phys Eng Express* 2015;1:045209.

(23) Pajonk F, Grumann T, McBride WH. The proteasome inhibitor MG-132 protects hypoxic SiHa cervical carcinoma cells after cyclic hypoxia/reoxygenation from ionizing radiation. *Neoplasia* 2006;8(12):1037-1041.

(24) Słonina D, Kabat D, Biesaga B, Janecka-Wiłda A, Szatkowski W. Chemopotentiating effects of low-dose fractionated radiation on cisplatin and paclitaxel in cervix cancer cell lines and normal fibroblasts from patients with cervix cancer. DNA Repair (Amst) 2021;103;103113.

(25) Mak IW, Evaniew N, Ghert M. Lost in translation: animal models and clinical trials in cancer treatment. *Am J Transl Res* 2014;5(2):114-118.

(26) Nakano T, Oka K, Takahashi T, Morita S, Arai T. Roles of Langerhans' cells and T-lymphocytes infiltrating cancer tissues in patients treated by radiation therapy for cervical cancer. *Cancer* 1992;70(12):2839-2844.

BIBLIOGRAPHY

Abe K, Kadoya N, Sato S, Hashimoto S, Nakajima Y, Miyasaka Y, *et al*. Impact of a commercially available model-based dose calculation algorithm on treatment planning of high-dose-rate brachytherapy in patients with cervical cancer. *J Radiat Res* 2018;59(2):198-206.

Absorbed dose determination in external beam radiotherapy: An international code of practice for dosimetry based on standards of absorbed dose to water. Vienna: International Atomic Energy Agency; 2000.

Absorbed dose determination in photons and electron beams: An international code of practice. Vienna: International Atomic Energy Agency; 1997.

Akpochafor MO, Aweda MA, Durosinmi-Etti FA, Adeneye SO, Omojola AD. Simulation of the Linear Boltzmann transport equation in modelling of photon beam data. *IOSR J Appl Phys* 2014;5(6):72-86.

Aldelaijan S, Devic S, Mohammed H, Tomic N, Liang L-H, DeBlois F, *et al*. Evaluation of EBT-2 model GAFCHROMIC film performance in water. Med Phys 2010;37(7): 3687-3693.

Allalunis-Turner MJ, Pearcey RG, Barron GM, Buryn DA, Babiak JC, Honoré LH. Inherent radiosensitivity testing of tumor biopsies obtained from patients with carcinoma of the cervix or endometrium. *Radiother Oncol* 1991;22(3):201-205.

Arbyn M, Weiderpass E, Bruni L, de Sanjosé Sm Saraiya M, Ferlay J, *et al*. Estimates of incidence and mortality of cervical cancer in 2018: a worldwide analysis. *Lancet Glob Health 2020*;8(2):e191-e203.

Arezzo F, Cormio G, Loizzi V, Cazzato G, Cataldo V, Lombardi C, *et al*. HPV-negative cervical cancer: A narrative review. *Diagnostics (Basel)* 2021;11(6):952.

Azmi AS, Aboukameel A, Banerjee S, Wang Z, Mohammad M, Wu J, *et al*. MDM2 inhibitor MI-319 in combination with cisplatin is an effective treatment for pancreatic cancer independent of p53 function. *Eur J Cancer* 2010;46(6):1122-1131.

Balgobind BV, Koedooder K, Ordonez Zuniga DO, Fajardo RD, Rasch CRN, Pieters BR. A review of the clinical experience in pulsed dose rate brachytherapy. *Br J Radiol* 2015;88(1055):20150310.

Banahene JO, Darko EO, Awuah B. Low dose rate caesium-137 implant time of intracavitary brachytherapy source of a selected oncology center in Ghana. *Clin Cancer Investig J* 2015;4(2):158-164.

Banath JP, MacPhail SH, Olive PL. Radiation sensitivity, H2AX phosphorylation, and kinetics of repair of DNA strand breaks in irradiated cervical cancer cell lines. *Cancer Res* 2004;64(19):7144-7149.

Banerjee R, Kamrava M. Brachytherapy in the treatment of cervical cancer: a review. *Int J Women's Health* 2014;6:555-564.

Bansal N, Herzog TJ, Shaw RE, Burke WM, Deutsch I, Wright JD. Primary therapy for early-stage cervical cancer: radical hysterectomy vs radiation. *Am J Obstet Gynecol* 2009;201(5):485.e1-9.

Barazzuol, Burnet NG, Jena R, Jones B, Jefferies SJ, Kirkby NF. A mathematical model of brain tumour response to radiotherapy and chemotherapy considering radiobiological aspects. *J Theor Biol* 2010;262(3):553-565.

Barendsen GW. Dose fractionation, dose rate and iso-effect relationships for normal tissue responses. *Int J Radiat Oncol Biol Phys* 1982;8(11):1981-1997.

Batista E, Alberini M. Results of the supplementary comparison (bilateral) of a fixed volume micropipette of 50 µl and a variable volume micropipette of 1000 µl. *Metrologia* 2018;55:07009-07009.

Batista E, Almeida N, Filipe E. A study of factors that influence micropipette calibrations. *NCSLI Measure 2015*;10(1):60-66.

Batista E, Pinto L, Filipe E, van der Veen AMH. Calibration of micropipettes: Test methods and uncertainty analysis. *Measurement* 2007;40:338-342.

Beaulieu L, Tedgren AC, Carrier J-F, Davis SD, Mourtada F, Rivard MJ, *et al*. Report of the Task Group 186 on model-based dose calculation methods in brachytherapy beyond the TG-43 formalism: Current status and recommendations for clinical implementation. *Med Phys* 2012;39(10):6208-6236.

Beskow C, Ågren-Cronqvist AK, Lewensohn R, Toma-Dasu I. Biological effective dose evaluation and assessment of rectal and bladder complications for cervical cancer treated with radiotherapy and surgery. *J Contemp Brachytherapy* 2012;4(4):205-212.

Bhatla N, Aoki D, Sharma DN, Sankaranarayanan R. Cancer of the cervix uteri. *Int J Gynaecol Obstet* 2018;143 Supple 2:22-36.

Bhatla N, Berek JS, Fredes MC, Denny LA, Grenman S, Karunaratne K, *et al*. Revised FIGO staging for carcinoma of the cervix uteri. *Int J Gynecol Obstet* 2019;145(1):129-135.

Bianchi C, Botta F, Conte L, Vanoli P, Cerizza L. Biological effective dose evaluation in gynaecological brachytherapy: LDR and HDR treatments, dependence on radiobiological parameters, and treatment optimisation. *Radiol Med* 2008;113(7):1068-1078.

Bidmead M, Briot E, Burger J, Ferreira I, Grusell E, Kirisits C, *et al*. A practical guide to quality control of brachytherapy equipment [booklet]. Brussels: The European SocieTy for Radiotherapy and Oncology; 2004.

Bolger BS, Cooke TG, Symonds RP, MacLean AB, Stanton PD. Measurement of cell kinetics in cervical tumours using bromodeoxyuridine. *Br J Cancer* 1993;68(1):166-171.

Bolger BS, Symonds RP, Stanton PD, MacLean AB, Burnett R, Kelly P, *et al.* Prediction of radiotherapy response of cervical carcinoma through measurement of proliferation rate. *Br J Cancer* 1996;74(8):1223-1226.

Bosch FX, Lorincz A, Muñoz N, Meijer CJLM, Shah KV. The causal relation between human papillomavirus and cervical cancer. *J Clin Pathol* 2002;55(4):244-265.

Bouchard H, Lacroix F, Beaudoin G, Carrier JF, Kawrakow I. On the characterization and uncertainty analysis of radiochromic film dosimetry. *Med Phys* 2009;36(6):1931-1946.
Bourgioti C, Chatoupis K, Moulopous LA. Current imaging strategies for the evaluation of uterine cervical cancer. *World J Radiol* 2016;8(4):342-354.
Brady S, Yaeger T. Encyclopedia of radiation oncology. Springer, Heidelberg, Dordrecht London, New York: Springer-Verlag Berlin, Heidelberg; 2013.
Brady SL, Toncheva G, Dewhirst MW, Yoshizumi TT. Characterization of a 137Cs irradiator from a new perspective with modern dosimetric tools. *Health Phys* 2009;97(3):195-205.
Bray F, Lortet-Tieulent J, Znaor A, Brotons M, Poljak M, Arbyn M. Patterns and trends in Human Papillomavirus-related diseases in central and eastern Europe and central Asia. *Vaccine* 2013;31:H32-H45.
Brenner DJ, Hall EJ. Conditions for the equivalence of continuous to pulsed low dose rate brachytherapy. *Int J Radiat Oncol Biol Phys* 1991;20(1):181-190.
Brenner DJ, Hlatky LR, Hahnfeldt PJ, Huang Y, Sachs RK. The linear-quadratic model and most other common radiobiological models result in similar predictions of time-dose relationships. *Radiat Res* 1998;150(1):83-91.
Brenner DJ. Fractionation and late rectal toxicity. *Int J Radiat Oncol Biol Phys* 2004;60(4):1013-1015.
Brenner DJ. Radiation biology in brachytherapy. *J Surg Oncol* 1997;65(1):66-70.
Brenner DJ. The linear-quadratic model is an appropriate methodology for determining isoeffective doses at large doses per fraction. *Semin Radiat Oncol* 2008;18(4):234-239.
Brenner DR, Weir HK, Demers AA, Ellison LF, Louzado C, Shaw A, *et al*. Projected estimates of cancer in Canada in 2020. *CMAJ* 2020;192(9):E199-E205.
Brierley J, Gospodarowicz MK, Wittekind C. Cervix Uteri. *TNM Online* 2017:166-170.
Brodin NP, Chen Y, Yaparpalvi R, Guha C, Tomé WA. Dosimetry formalism and Implementation of a homogenous irradiation protocol to improve the accuracy of small animal whole-body irradiation using a 137Cs irradiator. *Health Phys* 2016;110(2 Suppl 1):S26-S38.
Butz K, Whitaker N, Denk C, Ullmann A, Geisen C, Hoppe-Seyler Fl. Induction of the p53-target gene GADD45 in HPV-positive cancer cells. *Oncogene* 1999;18(14):2381-2386.
Canadian Cancer Statistics. Canadian Cancer Society; 2021.
Candelaria M, Garcia-Arais A, Centina L, Cetina L, Dueñas-Gonzalez A. Radiosensitizers in cervical cancer. Cisplatin and beyond. *Radiat Oncol* 2006;1:15.
Carlone M, Wilkins D, Raaphorst P. The modified linear-quadratic model of Guerrero and Li can be derived from a mechanistic basis and exhibits linear-quadratic-linear behaviour. *Phys Med Biol* 2005;50(10):L9-L13.
Carlson DJ, Stewart RD, Li XA, Jennings K, Wang JZ, Guerrero M. Comparison of in vitro and in vivo alpha/beta ratios for prostate cancer. *Phys Med Biol* 2004;49(19):4477-4491.
Chadwick KH, Leenhouts HP. A molecular theory of cell survival. *Phys Med Biol* 1973;18(1):78-87.

Chang HHY, Pannuzio NR, Adachi N, Lieber MR. Non-homologous DNA end joining and alternative pathways to double-strand break repair. *Nat Rev Mol Cell Biol* 2017;18(8):495-406.

Chapman JD, Nahum AE. Radiotherapy treatment planning. Baton Rouge: CRC Press; 2016.

Chassagne D, Dutreix A, Almond P, Burgers HMV, Busch M, Joslin CA. Report 38: Dose and volume specification for reporting intracavitary therapy in gynecology. *J of the ICRU* 1985;1(1):1-23.

Chen JLY, Huang CY, Huang YS, Chen RJ, Wang CW, Chen YH, *et al*. Differential clinical characteristics, treatment response and prognosis of locally advanced adenocarcinoma/adenosquamous carcinoma and squamous cell carcinoma of cervix treated with definitive radiotherapy. *Acta Obstet Gynecol Scand* 2014;93(7):661-668.

Chen SW, Liang JA, Yang SN, Ko HL, Lin FJ. The adverse effect of treatment prolongation in cervical cancer by high-dose-rate intracavitary brachytherapy. *Radiother Oncol* 2003;67(1):69-76.

Cheng HY, Liang JA, Hung YC, Yeh LS, Chang WC, Lin WC, *et al*. Stereotactic body radiotherapy for pelvic boost in gynecological cancer patients with local recurrence or unsuitable for intracavitary brachytherapy. *Taiwan J Obstet Gynecol* 2021;60(1):111-118.

Cho O, Chun M. Management for locally advanced cervical cancer: new trends and controversial issues. *Radiat Oncol J* 2018;36(4):254–264.

Choi EK, Terai K, Ji IM, Kook YH, Park KH, Oh ET *et al*. Upregulation of NAD(P)H:quinone oxidoreductase by radiation potentiates the effect of bioreductive β-lapachone on cancer cells. *Neoplasia* 2007;9(8):634-642.

Chong GO, Lee WK, Jeong SY, Park SH, Lee YH, Lee SW *et al*. Prognostic value of intratumoral metabolic heterogeneity on F-18 fluorodeoxyglucose positron emission tomography/computed tomography in locally advanced cervical cancer patients treated with concurrent chemoradiotherapy. *Oncotarget* 2017;8(52):90402-90412.

Chow B, Nanda K, Warkentin B, Huang F, Gamper AM, Menon G. In-vitro determination of radiobiological parameter values used in cervical cancer brachytherapy. *Radiother Oncol* 2020;152(1):S1093-S1094.

Cibula D, Pötter R, Planchamp F, Avall-Lundqvist E, Fischerova D, Haie-Meder C, *et al*. The European Society of Gynaecological Oncology/European Society for Radiotherapy and Oncology/European Society of Pathology guidelines for the management of patients with cervical cancer. *Virchows Arch* 2018;472(6):919-936.

COSMIC - Catalogue of Somatic Mutations in Cancer 2021.

Curtis SB. Lethal and potentially lethal lesions induced by radiation--a unified repair model. *Radiat Res* 1986;106(2):252-270.

Dale RG, Huczkowski J, Trott KR. Possible dose rate dependence of recovery kinetics as deduced from a preliminary analysis of the effects of fractionated irradiations at varying dose rates. *Br J Radiol* 1988;61(722):153-157.

Dale RG, Jones B. The clinical radiobiology of brachytherapy. *Br J Radiol* 1998;71(845):465-483.

Dale RG. The application of the linear-quadratic dose-effect equation to fractionated and protracted radiotherapy. *Br J Radiol* 1985;58(690):515-528.

Dale RG. The application of the linear-quadratic model to fractionated radiotherapy where there is incomplete normal tissue recovery between fractions, and possible implications for treatments involving multiple fractions per day. *Br J Radiol* 1986;59(705):919-927.

Dale R. Use of the linear-quadratic radiobiological model for quantifying kidney response in targeted radiotherapy. *Cancer Biother Radiopharm* 2004;19(3):363-370.

De Leeuw AAC, van de Kamer JB, Moerland MA, Philippens MEP, Jürgenliemk-Schulz IM. The effect of alternative biological modelling parameters (α/β and half time of repair T1/2) on reported EQD2 values in the treatment of advanced cervical cancer. *Radiother Oncol* 2011;101(2):337-342.

Devlin PM, Cormack RA, Holloway CL, Stewart AJ. Brachytherapy: Applications and techniques. Springer Publishing Company; 2015.

Denekamp J. Cell kinetics and radiation biology. *Int J Radiat Biol Relat Stud Phys Chem Med* 1986;49(2):357-380.

Derks K, Steenhuijsen JLG, van den Berg HA, Houterman S, Cnossen J, van Haaren P, *et al*. Impact of brachytherapy technique (2D versus 3D) on outcome following radiotherapy of cervical cancer. *J Contemp Brachytherapy* 2018;10(1):17-25.

Dische S, Saunders MI, Sealy R, Werner ID, Verma N, Foy C, *et al*. Carcinoma of the cervix and the use of hyperbaric oxygen with radiotherapy: a report of a randomized controlled trial. *Radiother Oncol* 1999;52(2):93-98.

Devic S, Seuntjens J, Sham E, Podgorsak EB, Schmidtlein CR, Kirov AS, *et al*. Precise radiochromic film dosimetry using a flat-bed document scanner. *Med Physics* 2005;32(7):2245-2253.

DeWerd LA, Ibbott GS, Meigooni AS, Mitch MG, Rivard MJ, Stump KE, *et al*. A dosimetric uncertainty analysis for photon-emitting brachytherapy sources: Report of AAPM Task Group No. 138 and GEC-ESTRO. *Med Phys* 2011;38(2):782-801.

Dos Santos M, Paget V, Kacem MB, Trompier F, Benadjaoud MA, Francois A, *et al*. Importance of dosimetry protocol for cell irradiation on a low x-rays facility and consequences for the biological response. *Int J Radiat Biol* 2018; 94(6):597-606.

Enger SA, Vijande J, Rivard MJ. Model-based dose algorithms for brachytherapy dosimetry. *Semin Radiat Oncol* 2020;30(1):77-86.

Follen M, Levenback CF, Iyer RB, Grigsby PW, Boss EA, Delpassand ES, *et al*. Imaging in cervical cancer. Cancer 2003;98(9 Suppl):2028-2038.

Fonseca KA, Koskinas MF, Dias MS. Disintegration rate measurement of a 192Ir solution. *Appl Radiat Isotopes* 2001;54(1):141-145.

Fowler JF. 21 years of biologically effective dose. *Br J Radiol* 2010;83(991):554-568.

Fowler JF. Dose reduction factors when increasing dose rate in LDR or MDR brachytherapy of carcinoma of the cervix. *Radiother Oncol* 1997;45(1):49-54.
Fowler JF. Repair between dose fractions: A simpler method of analyzing and reporting apparently biexponential repair. *Radiat Res* 2002;158(2):141-151.
Fowler JF. Sensitivity analysis of parameters in linear-quadratic radiobiologic modeling. *Int J Radiat Oncol Biol Phys* 2009;73(5):1532-1537.
Fowler JF. The linear-quadratic formula and progress in fractionated radiotherapy. *Br J Radiol* 1989;62(740):679-694.
Franken NAP, Rodermond HM, Stap J, Haveman J, van Bree C. Clonogenic assay of cells in vitro. *Nat Protoc* 2006;1(5):2315-2319.
Frattini A, Fabbri M, Valli R, De Paoli E, Montalbano G, Gribaldo L, *et al*. High variability of genomic instability and gene expression profiling in different HeLa clones. *Sci Rep* 2015;5;15377.
Gamper AM, Rofougaran R, Watkins SC, Greenberger JS, Beumer JH, Bakkenist CJ. ATR kinase activation in G1 phase facilitates the repair of ionizing radiation-induced DNA damage. *Nucleic Acids Res* 2013;41(22):10334-10344.
Gasinska A, Fowler JF, Lind BK, Urbanski K. Influence of overall treatment time and radiobiological parameters on biologically effective doses in cervical cancer patients treated with radiation therapy alone. *Acta Oncol* 2004;43(7):657-666.
Georg D, Kirisits C, Hillbrand M, Dimopoulos J, Pötter R. Image-guided radiotherapy for cervix cancer: High-tech external beam therapy versus high-tech brachytherapy. *Int J Radiat Oncol Biol Phys* 2008;71(4):1272-1278.
Ghim SJ, Basu PS, Jenson AB. Cervical cancer: Etiology, pathogenesis, treatment, and future vaccines. *Asian Pac J Cancer Prev* 2002;3(3):207-214.
Ghorbani M, Salahshour F, Haghparast A, Moghaddas TA, Knaup C. Effect of tissue composition on dose distribution in brachytherapy with various photon emitting sources. *J Contemp Brachytherapy* 2014;6(1):54-67.
Gomez-Casal R, Bhattacharya C, Ganesh N, Bailey L, Passe P, Gibson M, *et al*. Non-small cell lung cancer cells survived ionizing radiation treatment display cancer stem cell and epithelial-mesenchymal transition phenotypes. *Mol Cancer* 2013;12(1):94.
Grigsby PW,Williamson JF, Perez CA. Source configuration and dose rates for the Selectron Afterloading equipment for gynecologic applicators. *Int J Radiat Oncol Biol Phys* 1992;24(2):321-327.
Grimes DR, Partridge M. A mechanistic investigation of the oxygen fixation hypothesis and oxygen enhancement ratio. *Biomed Phys Eng Express* 2015;1(4):045209.
Grover S, Longo J, Einck J, Pri P, Brown D, Chino J, *et al*. The unique issues with brachytherapy in low- and middle-income countries. *Semin Radiat Oncol* 2019;27(2):136-142.

Guerrero M, Carlone M. Mechanistic formulation of a lineal-quadratic-linear (LQL) model: split-dose experimentas and exponentially decaying sources. *Med Phys* 2010;37(8):4173-4181.

Guerrero M, Carlson DJ. A radiobiological model of reoxygenation and fractionation effects. *Med Phys* 2017;44(5):2002-2010.

Guerrero M, Li XA. Halftime for repair of sublethal damage in normal bladder and rectum: an analysis of clinical data from cervix brachytherapy. *Phys Med Biol* 2006;51(16):4063-4071.

Gupta N, Lamborn K, Deen DF. A statistical approach for analyzing clonogenic survival data. *Radiat Res* 1996;145(5):636-640.

Haie-Meder C, Pötter R, Van Limbergen E, Briot E, De Brabandere M, Dimopoulos J, *et al*. Recommendations from gynaecological (GYN) GEC-ESTRO working group (I): concepts and terms in 3D image based 3D treatment planning in cervix cancer brachytherapy with emphasis on MRI assessment of GTV and CTV. *Radiother Oncol* 2005;74(3):235-245.

Hall EJ, Brenner DJ. The dose-rate effect revisited: Radiobiological considerations of importance in radiotherapy. *Int J Radiat Oncol Biol Phys* 1991;21(6):1403-1414.

Hall E, Giaccia A. Radiobiology for the radiologist. 7th ed. Philadelphia PA: Williams & Wilkins; 2012.

Han K, Milosevic M, Fyles A, Pintilie M, Viswanathan AN. Trends in the utilization of brachytherapy in cervical cancer in the United States. *Int J Radiat Oncol Biol Phys* 2013;87(1):111-119.

Hanisch PH, Furre T, Olsen DR, Pettersen EO. Radiobiological responses for two cell lines following continuous low dose-rate (CLDR) and pulsed dose rate (PDR) brachytherapy. *Acta Oncol* 2007;46(5):602-611.

Hietanen S, Lain S, Krausz E, Blattner C, Lane DP. Activation of p53 in cervical carcinoma cells by small molecules. *Proc Natl Acad Sci USA* 2000;97(15):8501-8506.

Hofbauer J, Kirisits C, Resch A, Xu Y, Sturdza A, Pötter R, *et al*. Impact of heterogeneity-corrected dose calculation using a grid-based Boltzmann solver on breast and cervix cancer brachytherapy. *J Contemp Brachytherapy* 2016;8(2):143-149.

Hsu EM, McNicol PH. Characterization of the HPV-16 E6/E7 transcription in CaSki cells by quantitative PCR. *Mol Cell Probes* 1992;6(6):459-466.

Huang Z, Mayr NA, Gao M, Lo SS, Wang JZ, Jia G, *et al*. Onset time of tumor repopulation for cervical cancer: First evidence from clinical data. *Int J Radiat Oncol Biol Phys* 2012;84(2):478-484.

Hyer DE, Sheybani A, Jacobson GM, Kim Y. The dosimetric impact of heterogeneity corrections in high-dose-rate 192Ir brachytherapy for cervical cancer: Investigation of both conventional Point-A and volume-optimized plans. *Brachytherapy* 2012;11(6):515-520.

International commission on radiation units & measurements. Report 89: Prescribing, recording, and reporting brachytherapy for cancer of the cervix. *J of the ICRU* 2013; 13:1-258.
Jhingran A, Eifel P. Radiation therapy for cervical carcinoma. *Glob Libr Women Med* 2009.
Joiner M, van der Kogel AJ. Basic clinical radiobiology. 4th ed. Boca Raton: CRC Press/Taylor & Francis Group; 2009.
Joint committee for guides in metrology. Evaluation of measurement data - Guide to the expression of uncertainty in measurement. 2008.
Jones B, Dale RG. Mathematical models of tumour and normal tissue response. *Acta Oncol* 1999;38(7);883-893.
Kamen, J, Hsu WY, Boswell B, Hill C. Successful migration from radioactive irradiators to x-ray irradiators in one of the largest medical centers in the US. *Health Phys* 2019;117(5):558-570.
Kang SK, Rhee DJ, Kang YR, Kim JK, Jeong DH. Determination of TRS-398 quality factors for Cs-137 gamma rays in reference dosimetry. *Prog Med Phys* 2014;25(3):123-127.
Kelland LR, Steel GG. Differences in radiation response among human cervix carcinoma cell lines. *Radiother Oncol* 1988;13(2):225-232.
Kellerer AM, Rossi HH. RBE and the primary mechanism of radiation action. *Radiat Res* 1971;47(1):15-34.
Kemikler, G. History of brachytherapy. *Turk J Oncol* 2019;34(Supp 1):1-10.
Khan F. The physics of radiation therapy. Philadelphia: Lippincott Williams & Wilkins; 2010.
Khazaei Z, Sohrabivafa M, Mansori K, Naemi H, Goodarzi E. Incidence and mortality of cervix cancer and their relationship with the human development index in 185 countries in the world: An ecology study in 2018. *Adv Hum Biol* 2019;9(3):222-227.
Kidd EA, Grigsby PW. Intratumoral metabolic heterogeneity of cervical cancer. *Clin Can Res* 2008;14(16):5236-5240.
Kim BM, Won J, Maeng KA, Han YS, Yun YS, Hong SH. Nimesulide, a selective COX-2 inhibitor, acts synergistically with ionizing radiation against A549 human lung cancer cells through the activation of caspase-8 and caspase-3. *Int J Oncol* 2009;34(5):1467-1473.
Kim S, Wu HG, Shin JH, Park HJ, Kim IA, Kim IH. Enhancement of radiation effects by flavopiridol in uterine cervix cancer cells. *Can Res Treat* 2005;37(3):191-195.
Kim YJ, Kang HC, Kim YS. Impact of intracavitary brachytherapy technique (2D vs 3D) on outcomes of cervical cancer: a systematic review and meta-analysis. *Strahlenther Onkol* 2020;196(11):973-982.
Kirchheiner K, Nout RA, Lindegaard JC, Haie-Meder C, Mahantshetty U, Segedin B, *et al.* Dose–effect relationship and risk factors for vaginal stenosis after definitive radio(chemo)therapy with image-guided brachytherapy for locally advanced cervical cancer in the EMBRACE study. *Radiother Oncol* 2016;118(1):160-166.
Kirsch DG, Diehn M, Kesarwala AH, Maity A, Morgan MA, Schwarz JK, *et al*. The future of radiobiology. *J Natl Cancer Inst* 2018;110(4):329-340.

Kirisits C, Rivard MJ, Baltas D, Ballester F, De Brabandere M, van der Laarse R, *et al*. Review of clinical brachytherapy uncertainties: Analysis guidelines of GEC-ESTRO and the AAPM. *Radiother Oncol* 2014;110(1):199-212.

Kirkpatrick JP, Meyer JH, Marks LB. The linear-quadratic model is inappropriate to model high dose per fraction effects in radiosurgery. *Semin Radiat Oncol* 2008;18(4):240-243.

Koskela P, Anttila T, Bjørge T, Brunsvig A, Dillner J, Hakama M, *et al*. Chlamydia trachomatis infection as a risk factor for invasive cervical cancer. *Int J Cancer* 2000;85(1):35-39.

Kumar P, Sharma DN, Kumar S, Gandhi AK, Rath GK, Julka PK. Pulsed-dose-rate vs. high-dose-rate intracavitary radiotherapy for locally advanced carcinoma of cervix: A prospective randomized study. *Brachytherapy* 2016;15(3):327-332.

Kutcher GJ, Burman C, Brewster L, Goitein M, Mohan R. Histogram reduction method for calculating complication probabilities for three-dimensional treatment planning evaluations. *Int J Radiat Oncol Biol Phys* 1991;21(1):137-146.

Kyle L, Daniel F, Ye H, Chetkovich DM. A novel method for reducing human pipetting errors. *J Med Lab Diagn* 2015;6(6):36-40.

Lang S, Nulens A, Briot E, Kirisits C, De Brabandere M, Dumas I, *et al*, Intercomparison of treatment concepts for MR image assisted brachytherapy of cervical carcinoma based on GYN GEC-ESTRO recommendations. *Radiother Oncol* 2006;78(2):185-193.

Lea DE, Catcheside DG. The mechanism of the induction by radiation of chromosome aberrations inTradescantia. *J Genet* 1942;44:216-245.

Lee D, Chang L. Development of the pipetting error sensor. *Sensor Actuat B-Chem* 2006;119(1):150-158.

Lee SI, Atri M. 2018 FIGO staging system for uterine cervical cancer: Enter cross-sectional imaging. *Radiology* 2019;292(1):15-24.

Lee YY, Choi CH, Kim TJ, Lee JW, Kim BG, Lee JH, *et al*. A comparison of pure adenocarcinoma and squamous cell carcinoma of the cervix after radical hysterectomy in stage IB-IIA. *Gynecol Oncol* 2011;120(3):439-443.

Lei J, Ploner A, Lagheden C, Eklund C, Kleppe SN, Andrae B, *et al*. High-risk human papillomavirus status and prognosis in invasive cervical cancer: A nationwide cohort study. *PLOS Med* 2018;15(10):e1002666.

Levin D, Menhel J, Rabin T, Pfeffer R, Symon Z. Dosimetric comparison of tandem and ovoids vs tandem and ring for intracavitary gynecologic applications. *Med Dosim* 2008;33(4):315-320.

Lewis D, Micke A, Yu X, Chan MF. An efficient protocol for radiochromic film dosimetry combining calibration and measurement in a single scan. *Med Phys* 2012; 39(10):6339–6350.

Li X, Heyer WD. Homologous recombination in DNA repair and DNA damage tolerance. *Cell Res* 2008;18(1):99-113.

Lindblom E, Dasu A, Beskow C, Toma-Dasu I. High brachytherapy doses can counteract hypoxia in cervical cancer—a modelling study. *Phys Med Biol* 2016;62(2):560-572.

Löbrich M, Kühne M, Wetzel J, Rothkamm K. Joining of correct and incorrect DNA double-strand break ends in normal human and ataxia telangiectasia fibroblasts. *Genes Chromosomes Cancer* 2000;27(1):59-68.

Lockhart SP, Down JD, Steel GG. The effect of low dose-rate and cyclophosphamide on the radiation tolerance of the mouse lung. *Int J Radiat Oncol Biol Phys* 1986;12(8):1437-1440.

Marchant KJ, Sadikov E. The evolving practice of intrauterine cervix brachytherapy in Canada: A medical physics perspective. *Brachytherapy* 2013;12(4):324-330.

Mak IW, Evaniew N, Ghert M. Lost in translation: animal models and clinical trials in cancer treatment. *Am J Transl Res* 2014;5(2):114-118.

Marzi S, Saracino B, Perongari MG, Arcangeli S, Gomellini S, Arcangeli G, *et al*. Modeling of alpha/beta for late rectal toxicity from a randomized phase II study: conventional versus hypofractionated scheme for localized prostate cancer. *J Exp Clin Cancer Res* 2009;28(1):117.

Matsui T, Nuryadi E, Komatsu, S, Hirota Y, Shibata A, Oike T, *et al*. Robustness of clonogenic assays as a biomarker for cancer cell radiotherapy. *Int J Mol Sci* 2019;20(17);4148.

Mazeron R, Fokdal LU, Kirchheiner K, Georg P, Jastaniyah N, Šegedin B, *et al*. Dose–volume effect relationships for late rectal morbidity in patients treated with chemoradiation and MRI-guided adaptive brachytherapy for locally advanced cervical cancer: Results from the prospective multicenter EMBRACE study. *Radiother Oncol* 2016;120(3):412-419.

McEwen M, DeWerd L, Ibbott G, Followill D, Rogers DWO, Seltzer S, *et al*. Addendum to the AAPM's TG-51 protocol for clinical reference dosimetry of high-energy photon beams. *Med Phys* 2014;41(4):041501.

McMahon SJ. The linear quadratic model: usage, interpretation and challenges. *Phys Med Biol* 64:01TR01.

McNeil C. New standard of care for cervical cancer sets stage for next questions. *J Natl Cancer* Inst 1999;91(6):500-501.

Meadows JL, Bichay TJ. Low dose-rate brachytherapy for the treatment of cervix cancer is outdated and should be discontinued. *Med Phys* 2016;43(9):4963.

Menon GV, Carlone MC, Sloboda RS. Transit dose contributions to intracavitary and interstitial PDR brachytherapy treatments. *Phys Med Biol* 2008;53(13):3447-3462.

Micke A, Lewis DF, Yu X. Multichannel film dosimetry with nonuniformity correction. *Med Phys* 2011;38(5):2523-2534.

Mikkel JK, Klopp AH, Gonzalez GMN, Kisling KD, Price MJ, Berner PA, *et al*. Impact of heterogeneity-based dose calculation using a deterministic grid-based Boltzmann equation solver for intracavitary brachytherapy. *Int J Radiat Oncol Biol Phys* 2012;83(3):e417-422.

Militello C, Rundo L, Minafra L, Cammarata FP, Calvaruso M, Conti V, *et al*. MF2C3: Multi-feature fuzzy clustering to enhance cell colony detection in automated clonogenic assay evaluation. *Symmetry* 2020;12(5):773.

Millar WT, Jen YM, Hendry JH, Canney PA. Two components of repair in irradiated kidney colony-forming cells. *Int J Radiat Biol* 1994;66(2):189-196.

Mirzayans R, Andrais B, Murray D. Viability assessment following anticancer treatment requires single-cell visualization. *Cancers (Basel)* 2018;10(8):255.

Mizuno H, Sumida I, Tanaka A, Ogawa K. Comparing homogeneity between Gafchromic film EBT2 and EBT3. *Med Phys* 2014;41(6):239.

Momenimovahed Z, Ghoncheh M, Pakzad R, Hasanpour H, Salehiniya H. Incidence and mortality of uterine cancer and relationship with Human Development Index in the world. *Cukurova Med J* 2017;42:233-233.

Morrison H, Menon G, Larocque MP, van Veelen B, Niatsetski Y, Weis E, *et al*. Initial evaluation of Advanced Collapsed cone Engine dose calculations in water medium for I-125 seeds and COMS eye plaques. *Med Phys* 2018;45(3):1276-1286.

Morrison H, Menon G, Sloboda RS. Radiochromic film calibration for low-energy seed brachytherapy dose measurement. *Med Phys* 2014;41(7):072101.

Muñoz N, Castellsagué X, de González AB, Gissmann L. Chapter 1: HPV in the etiology of human cancer. *Vaccine* 2006;24 Suppl 3:1-10.

Nag S. High dose rate brachytherapy: Its clinical applications and treatment guidelines. *Technol Cancer Res Treat* 2004;3(3):269-287.

Nakano T, Oka K, Takahashi T, Morita S, Arai T. Roles of Langerhans' cells and T-lymphocytes infiltrating cancer tissues in patients treated by radiation therapy for cervical cancer. *Cancer* 1992;70(12):2839-2844.

Narisawa-Saito M, Kiyono T. Basic mechanisms of high-risk human papillomavirus-induced carcinogenesis: roles of E6 and E7 proteins. *Cancer Sci* 2007;98(10):1505-1511.

Nath R, Anderson LL, Luxton G, Weaver KA, Williamson JF, Meigooni AS. Dosimetry of interstitial brachytherapy sources: Recommendations of the AAPM Radiation Therapy Committee Task Group No. 43. *Med Phys* 1995:22(2),209–234.

Nath R, Bice WS, Butler WM, Chen Z, Meigoni AS, Narayana V, *et al* AAPM recommendations on dose prescription and reporting methods for permanent interstitial brachytherapy for prostate cancer: Report of Task Group 137. *Med Phys* 2009;36(11):5310-5322.

Nicolás I, Marimon L, Barnadas E, Saco A, Rodríguez-Carunchio L, Fusté P, *et al*. HPV-negative tumors of the uterine cervix. *Mod Pathol* 2019;32(8):1189-1196.

Niroomand-Rad A, Blackwell CR, Coursey BM, Gall KP, Galvin JM, McLaughlin WL. Radiochromic film dosimetry: Recommendations of AAPM Radiation Therapy Committee Task Group 55. American Association of Physicists in Medicine. *Med Phys* 1998;25(11):2093–2115.

Niroomand-Rad A, Chiu-Tsao S, Grams MP, Lewis DF, Soares CG, Van Battum LJ, *et al*. Report of AAPM Task Group 235 Radiochromic film dosimetry: An update to TG-55. *Med Phys* 2020;47(12):5986-6025.

Okada S, Ono K, Hamada N, Inada T, Kubota N. A low-pH culture condition enhances the radiosensitizing effect of wortmannin. *Int J Radiat Oncol Biol Phys* 2001;49(4):1149-1156.

Oliver R. A comparison of the effects of acute and protracted gamma-radiation on the growth of seedlings of Vicia Faba. Part II Theroetical Calcualtions. *Int J Radiat Biol Relat Stud Phys Chem Med* 1964;8:475-499.

Orear J. Least squares when both variables have uncertainties. *Am J Phys* 1982;50(10):912-916.

Orton CG. High and low dose-rate brachytherapy for cervical cancer. *Acta Oncol* 1998;37(2):117-125.

Pajonk F, Grumann T, McBride WH. The proteasome inhibitor MG-132 protects hypoxic SiHa cervical carcinoma cells after cyclic hypoxia/reoxygenation from ionizing radiation. *Neoplasia* 2006;8(12):1037-1041.

Pappas EP, Peppa V, Hourdakis CJ, Karaiskos P, Papagiannis P. On the use of a novel Ferrous Xylenol-orange gelatin dosimeter for HDR brachytherapy commissioning and quality assurance testing. *Phys Medica* 2018;45(1):162-169.

Park C, Papiez L, Zhang S, Story MM, Timmerman RD. Universal survival curve and single fraction equivalent dose: useful tools in understanding potency of ablative radiotherapy. *Int J Radiat Oncol Biol Phys* 2008;70(3):847-852.

Patankar SS, Tergas AI, Deutsch I, Burke WM, Hou JY, Ananth CV, *et al*. High verse low-dose rate brachytherapy for cervical cancer. *Gynecol Oncol* 2015;136(3):534-541.

Pavithra V, Sai Shalini CN, Priya S, Rani U, Rajendiran S, Joseph LD. Small cell neuroendocrine carcinoma of the cervix: A rare entity. *J Clin Diagn Res* 2014;8(2):147-148.

Pawlick TM, Keyomarsi K. Role of cell cycle in mediating sensitivity to radiotherapy. *Int J Radiat Oncol Biol Phys* 2004;59(4):928-942.

Perez-Calatyud J, Ballester F, Das RK, Dewerd LA, Ibbott GS, Meigooni AS, *et al*. Dose calculation for photon-emitting brachytherapy sources with average energy higher than 50 keV: report of the AAPM and ESTRO. *Med Phys* 2012;39(5):2904-2929.

Phan T, Mula-Hussain L, Pavamani S, Pearce A, D'Souza D, Patil NG, *et al*. The changing landscape of brachytherapy for cervical cancer: a Canadian practice survey. *Curr Oncol* 2015;22(5):356-360.

Pomp J, Wike JL, Ouwerkerk IJ, Hoogstraten C, Davelaar J, Schrier PI, *et al*. Cell density dependent plating efficiency affects outcome and interpretation of colony forming assays. *Radiother Oncol* 1996;40(2):121-125.

Pop LA, Millar WT, van der Plas M, van der Kogel AJl. Radiation tolerance of rat spinal cord to pulsed dose rate (PDR) brachytherapy: the impact of differences in temporal dose distribution. *Radiother Oncol* 2000;55(3):301-315.

Popovic R, Liniger R, Bickler PE. Anesthetics and mild hypothermia similarly prevent hippocampal neuron death in an in vitro model of cerebral ischemia. *Anesthesiology* 2000;92(5):1343-1349.

Pötter R, Haie-Meder C, Van Limbergen E, Barillot I, De Brabandere M, Dimopoulos J, *et al*. Recommendations from gynaecological (GYN) GEC ESTRO working group (II): concepts and terms in 3D image-based treatment planning in cervix cancer brachytherapy-3D dose volume parameters and aspects of 3D image-based anatomy, radiation physics, radiobiology. *Radiother Oncol* 2006;78(1):67-77.

Pötter R, Tanderup K, Kirisits C, de Leeuw A, Kirchheiner K, Nout R, *et al* The EMBRACE II study: The outcome and prospect of two decades of evolution within the GEC-ESTRO GYN working group and the EMBRACE studies. *Clin Transl Radiat Oncol* 2018;9:48-60.

Puck TT, Markus PI. Action of x-rays on mammalian cells. *J Exp Med* 1956; 103(5):653-666.

Rantanen V, Grénman S, Kulmala J, Grénman R. The intrinsic radiosensitivity and sublethal damage repair capacity of five cervical carcinoma cell lines tested with the 96-well-plate assay. *J Cancer Res Clin Oncol* 1995;121(4):230-234.

Reynolds PM, Rasmussen CH, Hansson M, Dufva M, Riehle MO, Gadegaard N. Controlling fluid flow to improve cell seeding uniformity. *PLOS One* 2018;13(11):e0207211.

Rieder CL, Cole RW. Cold-shock and the mammalian cell cycle. *Cell Cycle* 2002;1(3):169-175.

Rivard MJ, Coursey BM, DeWerd LA, Hanson WF, Huq S, Ibbott GS, *et al*. Update of AAPM Task Group No. 43 Report: A revised AAPM protocol for brachytherapy dose calculations. *Med Phys* 2004;31(3):633-674.

Rivard MJ, Venselaar JLM, Beaulieu L. The evolution of brachytherapy treatment planning. *Med Phys* 2009;36(6):2136-2153.

Roberts SA, Hendry JH, Swindell R, Wilkinson JM, Hunter RD. Compensation for changes in dose-rate in radical low-dose-rate brachytherapy: A radiobiological analysis of a randomised clinical trial. *Radiother Oncol* 2004;70(1):63-74.

Roden RBS, Stern PL. Opportunities and challenges for human papillomavirus vaccination in cancer. *Nat Rev Cancer* 2018;18(4):240-254.

Rodriguez-Carunchio L, Soveral I, Steenbergen RDM, Torné A, Martinez S, Fusté P, *et al*. HPV-negative carcinoma of the uterine cervix: a distinct type of cervical cancer with poor prognosis. *BJOG* 2015;112(1):119-127.

Rofstad EK, Sundfør K, Lyng H, Tropé CG. Hypoxia-induced treatment failure in advanced squamous cell carcinoma of the uterine cervix is primarily due to hypoxia-induced radiation resistance rather than hypoxia-induced metastasis. *Br J Cancer* 2000;83(3):354-359.

Rosen R, Sapra A. TNM Classification. NCBI 2021.

Rydberg B, Cooper B, Cooper PK, Holley WR, Chatterjee A. Dose-dependent misrejoining of radiation-induced DNA double-strand breaks in human fibroblasts: experimental and theoretical study for high- and low-LET radiation. *Radiat Res* 2005;163(5):526-534.

Sande EPS, Martinsen ACT, Hole EO, Olerud HM. Interphantom and interscanner variations for Houndsfield units-establishment of reference values for HU in a commercial QA phantom. *Phys Med Biol* 2010;55(17):5123-5135.

Schiffman M, Castle PE, Jeronimo J, Rodriguez AC, Wacholder S. Human papillomavirus and cervical cancer. *Lancet* 2007;370(9590):890-907.

Sharma BA, Signh TT, Singh LJ, Singh YI, Devi YS. Biological effective doses in the intracavitary high dose rate brachytherapy of cervical cancer. *J Contemp Brachytherapy* 2011;3(4):188-192.

Shrivastava S, Mahantshetty U, Engineer R, Chopra S, Hawaldar R, Handre V, *et al*. Cisplatin chemostherapy vs radiotherapy in RIGO stage IIIB squamous cell carcinoma of the uterine cervix: A randomized clinical trial. *JAMA Oncol* 2018;4(4):506-513.

Shukla AK, Jangid PK, Rajpurohit VS, Verma A, Dangayach SK, Gagrani V, *et al*. Dosimetric comparison of 60Co and 192Ir high dose rate source used in brachytherapy treatment of cervical cancer. *J Cancer Res Ther* 2019;15(6):1212-1215.

Singh GK, Azuine RE, Siapush M. Global inequalities in cervical cancer incidence and mortality are linked to deprivation, low socioeconomic status, and human development. *Int J MCH AIDS* 2012;1(1);17-30.

Skowronek J, Malicki J, Piotrowski T. Values of biologically equivalent doses in healthy tissues: Comparison of PDR and HDR brachytherapy techniques. *Brachytherapy* 2010;9(2):165-170.

Sloboda RS, Morrison H, Cawston-Grant B, Menon GV. A brief look at model-based dose calculation principles, practicalities, and promise. *J Contemp Brachytherapy* 2017;9(1):79-88.

Słonina D, Kabat D, Biesaga B, Janecka-Wiłda A, Szatkowski W. Chemopotentiating effects of low-dose fractionated radiation on cisplatin and paclitaxel in cervix cancer cell lines and normal fibroblasts from patients with cervix cancer. DNA Repair (Amst) 2021;103;103113.

Snedecor G, Cochran W. Statistical methods. Ames, Iowa: Iowa State Univ. Press; 1992.

Song CW, Cho LC, Yuan J, Dusenbery KE, Griffin RJ, Levitt SH. Radiobiology of stereotactic body radiation therapy/stereotactic radiosurgery and the linear-quadratic model. *Int J Radiat Oncol Biol Phys* 2013;87(1):18-19.

Song S, Rudra S, Hasselle MD, Dorn PL, Mell LK, Mundt AJ, *et al*. The effect of treatment time in locally advanced cervical cancer in the era of concurrent chemoradiotherapy. *Cancer* 2013;119(2):325-331.

Sonoda K, Nakashima M, Saito T, Amada S, Kamura T, Nakano H, *et al*. Establishment of a new human uterine cervical adenocarcinoma cell-line, SiSo, and its reactivity to anticancer reagents. *Int J Oncol* 1995;6(5):1099-1104.

Srivastava A, Datta NR. Brachytherapy in cervical cancer: Time to move ahead from point A? *World J Clin Oncol* 2014;5(4):764-774.

Srivastava S, Tong YA, Devadas K, Zou ZQ, Chen Y, Pirollo KF, *et al*. The status of the p53 gene in human papilloma firus positive or negative cervical carcinoma cell lines. *Carcinogenesis* 1992;13(7):1273-1275.

Stewart AJ, Viswanathan AN. Current controversies in high-dose-rate versus low-dose-rate brachytherapy for cervical cancer. *Cancer* 2006;107(5):908-915.

Stewart RD. Two-lesion kinetic model of double-strand break rejoining and cell killing. *Radiat Res* 2001;156(4):365-378.

Strohmaier S, Zwierzchowski G. Comparison of 60Co and 192I sources in HDR brachytherapy. *J Contemp Brachytherapy* 2011;3(4):199-208.

Sturdza A, Pötter R, Fokdal LU, Haie-Meder C, Tan LT, Mazeron R, *et al*. Image guided brachytherapy in locally advanced cervical cancer: Improved pelvic control and survival in RetroEMBRACE, a multicenter cohort study. *Radiother Oncol* 2016;120(3):428-433.

Subramanya D, Grivas PD. HPV and cervical cancer: updates on an established relationship. *Postgrad Med* 2008;120(4):7-13.

Sudhyadhom A. On the molecular relationship between Hounsfield unit (HU), mass density, and electron density in computed tomography (CT). *PLoS One* 2020;15(12): e0244861.

Sung H, Ferlay J, Siegel RL, Laversanne M, Soerjomataram I, Jemal A, *et al*. Global cancer statistics 2020: GLOBOCAN estimates of incidence and mortality worldwide for 36 cancers in 185 countries. *CA Cancer J Clin* 2021;71(3):209-249.

Symonds P, Bolger B, Hole D, Mao JH, Cooke T. Advanced-stage cervix cancer: rapid tumour growth rather than late diagnosis. *Br J Cancer* 2000;83(5):566-568.

Szostak JW, Orr-Weaver TL, Rothstein RJ, Stahl FW. The double-strand-break repair model for recombination. *Cell* 1983;33(1):25-35.

Taggar AS, Martell K, Leung E, Banerjee R, Fortin I, Doll CM. Changing landscape of radiation therapy for advanced cervical cance with a focus on interstitial brachytherapy: A Canadian practice patterns survey. *Pract Radiat Oncol* 2021;S1879-8500(21)00283-6.

Taggar AS, Phan T, Traptow L, Banerjee R, Doll CM. Cervical cancer brachytherapy in Canada: A focus on interstitial brachytherapy utilization. *Brachytherapy* 2017;16(1):161-166.

Tanaka T, Wakamatsu T, Daijo H, Oda S, Kai S, Adachi T, *et al*. Persisting mild hypothermia suppresses hypoxia-inducible factor-1α protein synthesis and hypoxia-inducible factor-1-mediated gene expression. *Am J Physiol Regul Integr Comp Physiol* 2010;298(3):R661-R671.

Tanderup K, Fokdal LU, Sturdza A, Haie-Meder C, Nazeron R, van Limbergen E, *et al*. Effect of tumor dose, volume and overall treatment time on local control after radiochemotherapy including MRI guided brachytherapy of locally advanced cervical cancer. *Radiother Oncol* 2016;120(3):441-446.

Tang J, Inoue T, Matsumura S, Fukushima S, Koizumi M, Ozeki S, *et al*. Differences in repair of potentially lethal damage in Chinese hamster ovary cells exposed to 65 MeV proton beams and (137)Cesium gamma-rays. *Oncol Rep* 1997;4(2):407-412.

Tantivatana T, Rongsriyam K. Treatment outcomes of high-dose-rate intracavitary brachytherapy for cervical cancer: a comparison of Ir-192 vs Co-60 sources. *J Gynecol Oncol* 2018;29(5):e86.

Tarbell NJ, Amato DA, Down JD, Mauch P, Hellman S. Fractionation and dose rate effects in mice: a model for bone marrow transplantation in man. *Int J Radiat Oncol Biol Phys* 1987;13(7):1065-1069.

Tergas AI, Neugut AI, Chen L, Burke WM, Hershman DL, Wright JD. Radiation duration in women with cervical cancer treated with primary chemoradiation: A population-based analysis. *Cancer Invest* 2016;34(3):137-147.

Thames HD, Bentzen SM, Turesson I, Overgaard M, Van den Bogaert W. Time-dose factors in radiotherapy: A review of the human data. *Radiother Oncol* 1990;19(3):219-235.

Thames HD. An 'incomplete-repair' model for survival after fractionated and continuous irradiations. *Int J Radiat Biol Relat Stud Phys Chem Med* 1985;47(3):319-339.

Tjalma WAA. HPV negative cervical cancers and primary HPV screening. *Facts Views Vis Obgyn* 2018;10(2):107-113.

Tobias CA. The Repair-misrepair model in radiobiology: comparison to other models. *Radiat Res Suppl* 1985;8:S77-95.

Tod M, Meredith WJ. Treatment of cancer of the cervix uteri, a revised Manchester method. *Br J Radiol* 1953;26(305):252-257.

Travis EL, Tucker SL. Isoeffect models and fractionated radiation therapy. *Int J Radiat Oncol Biol Phys* 1987;13(2):283-287.

Tsang RW, Fyles AW, Kirkbride P, Levin W, Manchul LA, Milosevic MF, *et al*. Proliferation measurements with flow cytometry Tpot in cancer of the uterine cervix: Correlation between two laboratories and preliminary clinical results. *Int J Radiat Oncol Biol Phys* 1995;32(5):1319-1329.

Tsang RW, Fyles AW, Li YQ, Rajaraman MM, Chapman W, Pintilie M, *et al*. Tumor proliferation and apoptosis in human uterine cervix carcinoma I: correlations between variables. *Radiother Oncol* 1999;50(1):85-92.

Tucker SL, Thames HD, Michalski JM, Bosch WR, Mohan R, Winter K, *et al*. Estimation of α/β for late rectal toxicity based on RTOG 94-06. *Int J Radiat Oncol Biol Phys* 2011;81(2):600-605.

Twentyman PR. Timing of assays: An important consideration in the determination of clonogenic cell survival both in vitro and in vivo. *Int J Radiat Oncol Biol Phys* 1979;5(8):1213-1220.

van den Aardweg GJ, Hopewell JW. The kinetics of repair for sublethal radiation-induced damage in the pig epidermis: an interpretation based on a fast and a slow component of repair. Radiother Oncol 1992;23(2):94-104.

van der Horst J, Siebers AG, Bulten J, Massuger LF, de Kok IMCM. Increasing incidence of invasive and in situ cervical adenocarcinoma in the Netherlands during 2004-2013. *Cancer Med* 2017;6(2):416-423.

van der Laarse R, Niatsetki Y, Henning J, van der Meer E. Flexitron® and microSelectron® HDR/PDR afterloaders' transit time and dose. Stockholm, Sweden: Elekta AB;2018 12 p. Report No.: 888.00645 MKT_1.0.

van Rijn J, van den Berg J, Kipp JB, Schamhart DH, van Wijk R. Effect of hypothermia on cell kinetics and response to hyperthermia and x rays. *Radiat Res* 1985;101(2):292-305.

Vergara M, Becerra S, Berrios J, Osses N, Reyes J, Rodriguez-Moyá M, *et al*. Differential effect of culture temperature and specific growth rate on CHO cell behavior in chemostat culture. *PLOS One* 2014;9(4):e93865.

Villa LL, Schlegel R. Differences in transformation activity between HPV-18 and HPV-16 map to the viral LCR-E6-E7 region. *Virology* 1991;181(1):374-377.

Villalona GA, Udelsman B, Duncan DR, McGillicuddy E, Sawh-Martinez RF, Hibino N, *et al*. Cell-seeding techniques in vascular tissue engineering. *Tissue Eng Part B Rev* 2010;16(3):341-350.

Viswanathan AN, Beriwal S, De Los Santos JF, Demanes DJ, Gaffney D, Hansen J, *et al*. American Brachytherapy Society consensus guidelines for locally advanced carcinoma of the cervix. Part II: High-dose-rate brachytherapy. *Brachytherapy* 2012;11(1):47-52.

Viswanathan AN, Creutzberg CL, Craighead P, McCormack M, Toita T, Narayan K, *et al*. International brachytherapy practice patterns: A survey of the gynecologic cancer intergroup (GCIC). *Int J Radiat Oncol Biol Phys* 2012;82(1):250-255.

Viswanathan A, Dimopoulos J, Kirisits C, Berger D, Pötter R. Computed tomography versus magnetic resonance imaging-based contouring in cervical cancer brachytherapy: results of a prospective trial and preliminary guidelines for standardized contours. *Int J Radiat Oncol Biol Phys* 2007; 68(2):491-498.

Viswanathan AN, Thomadsen B. American Brachytherapy Society consensus guidelines for locally advanced carcinoma of the cervix. Part I: General principles. Brachytherapy 2012;11(1):33-46.

Vu M, Yu J, Awolude OA, Chuang L. Cervical cancer worldwide. *Curr Probl Cancer* 2018;42(5):457-465.

Wang X, Liu R, Ma B, Yang K, Tian J, Jiang L, *et al*. High dose rate versus low dose rate intracavity brachytherapy for locally advanced uterine cervix cancer. *Cochrane Database Syst Rev*;2014;7(7):CD007563.

Wang Y, Ye WJ, Du LH, Li AJ, Ren YF, Cao XP. Dose-volume parameters and clinical outcome of CT-guided free-hand high-dose-rate interstitial brachytherapy for cervical cancer. *Chin J Cancer* 2012;31(12):598-604.

West CM, Davidson SE, Roberts SA, Hunter RD. Intrinsic radiosensitivity and prediction of patient response to radiotherapy for carcinoma of the cervix. *Br J Cancer* 1993;68(4):819-823.

White SA, Landry G, Fonseca GP, Holt R, Rusch T, Beaulieu L, *et al*. Comparison of TG-43 and TG-186 in breast irradiation using a low energy electronic brachytherapy source. *Med Phys* 2014;41(6):061701.

Williams MV, Denekamp J, Fowler JF. A review of ratios for experimental tumors: Implications for clinical studies of altered fractionation. *Int J Radiat Oncol Biol Phys* 1985;11(1):87-96.

Winter 3rd WE, Maxwell GL, Tian CC, Sobel E, Rose GS, Thomas G, *et al*. Association of hemoglobin level with survival in cervical carcinoma patients treated with concurrent cisplatin and radiotherapy: a gynecologic oncology group study. *Gynecol Oncol* 2004;94(2):495-501.

Withers HR, Thames Jr HD, Peters LJ. A new isoeffect curve for change in dose per fraction. *Radiother Oncol* 1983;1(2):187-191.

Xu D, Allsop SA, Witherspoon SM, Snider JL, Yeh JJ, Fiordalisi JJ, *et al*. The oncogenic kinase Pim-1 is modulated by K-Ras signaling and mediates transformed growth and radioresistance in human pancreatic ductal adenocarcinoma cells. *Carcinogenesis* 2011;32(4):488-495.

Xu L, Yenari MA, Steinberg GK, Giffard RG. Mild hypothermia reduces apoptosis of mouse neurons in vitro early in the cascade. *J Cereb Blood Flow Metab* 2002;22(1):21-28.

Xu Y, Qiu Y, Yan S, Wang H. Prognostic implication of human papillomavirus types in cervical cancer patients: a systemic review and meta-analysis. *Infect Agent Cancer* 2020;15(1):66.

Yaginuma Y, Westphal H. Analysis of the p53 in human uterine carcinoma cell lines. *Cancer Res* 1991;51(24):6506-6509.

Yohem KH, Bregman MD, Meysken Jr FL. Effect of tumor colony definition on ionizing radiation survival curves of melanoma-colony forming cells. *Int J Radiat Oncol Biol Phys* 1987;13(11):1725-1733.

Zhu L, Lu Z, Zhao H. Antitumor mechanisms when pRb and p53 are genetically inactivated. *Oncogene* 2015;34(35);4547-4557.